Characterising the interaction between (p)ppGpp and ribosome-associated GTPases in *Staphylococcus aureus*

Daniel J Bennison

A thesis submitted in partial fulfilment of the requirements for the degree of Doctor of Philosophy

The University of Sheffield
Faculty of Science
Department of Molecular Biology and Biotechnology

June 2021

Abstract

Staphylococcus aureus is an important human pathogen, responsible for a range of superficial and invasive infections worldwide. During invasion and colonisation of the host, the ability of *S. aureus* to adapt to stressful conditions is paramount for survival and the success and continuation of infection. These stresses trigger production of two small nucleotide alarmones, guanosine 3',5'-bis(diphosphate) and guanosine 3'-diphosphate 5'-triphosphate, known as ppGpp and pppGpp respectively, which function as the effector molecules of the highly conserved signalling network known as the stringent response to enable cell adaptation and survival. Previously, screening for (p)ppGpp interacting proteins in *S. aureus* identified four Ribosome Associated (RA)-GTPases, RsgA, Era, RbgA and HflX, each of which are cofactors in ribosome assembly where they cycle between the GTP-bound ON state and the GDP-bound OFF state to govern their function. While bound to (p)ppGpp, the GTPase activity of these proteins is inhibited.

In this study, we sought to determine the mechanistic effect of (p)ppGpp on RA-GTPase interactions with the ribosome by examining the affinity and kinetics of this binding in different nucleotide-bound states. We show that RA-GTPases bind with higher affinity to 5'-diphosphate-containing nucleotides GDP and ppGpp over GTP, which is likely exploited as a mechanism of regulation of RA-GTPase activity within the cell. (p)ppGpp binding also reduced stable complex formation between RA-GTPases and the ribosomal subunits when compared to GTP binding. Structural studies of RsgA revealed that the ppGpp-bound state is conformationally reflective of the GDP-bound OFF state in which the switch I loop necessary for catalysis adopts a conformation which is incompatible with ribosome association and enzymatic activity, leading to a decrease in 70S ribosome biogenesis, translation rate and growth. Altogether, we characterise and highlight the inhibition of RA-GTPase activity by (p)ppGpp as a major mechanism of control of ribosome biogenesis and cell growth during the stringent response in *S. aureus*.

Publications

Bennison, D.J., Nakamoto, J.A., Craggs, T.C., Milón, P., Rafferty, J.B., Corrigan, R.M. (2021) (p)ppGpp inhibits 70S ribosome formation in *Staphylococcus aureus* by impeding GTPase-ribosome interactions. BioRχiv 2021.01.19.427108. https://doi.org/10.1101/2021.01.19.427108

Bennison, D.J., Irving, S.E., Corrigan, R.M. (2019) The Impact of the Stringent Response on TRAFAC GTPases and Prokaryotic Ribosome Assembly. Cells 8(11):1313. https://doi.org/10.3390/cells8111313

Wood, A., Irving, S.E., Bennison, D.J., Corrigan, R.M. (2019) The (p)ppGpp-binding GTPase Era promotes rRNA processing and cold adaptation in *Staphylococcus aureus*. PLOS Genetics 15(8): e1008346. https://doi.org/10.1371/journal.pgen.1008346

Acknowledgements

Table of Contents

List of Figures

List of Tables

List of Abbreviations

Abbreviation	Definition
(p)ppGpp	Guanosine 3',5'-bis(diphosphate) and Guanosine 3'-diphosphate 5'-triphosphate
°	Degrees
°C	Degrees Celsius
A	Absorbance
Å	Ångström
A-site	Aminoacyl site
aa-tRNA	Aminoacyl transfer ribonucleic acid
ABC	ATP-binding cassette
ACME	Arginine catabolic mobile element
ACT	aspartate kinase, chorismate and TyrA
AD	Atopic dermatitis
AIP	Autoinducing peptide
ANOVA	Analysis of variance
AnP	Antarctic phosphatase
ANTAR	AmiR and NasR transcription anti-termination regulator
Atet	Anhydrotetracycline
ATP	Adenosine triphosphate
ATPase	Adenosine triphosphate hydrolase
AU	Arbitrary Units
B	Bridge
BHI	Brain-heart infusion
B_{max}	Maximum ligand occupancy
BSA	Bovine serum albumen
CA-MRSA	Community-acquired methicillin-resistant *Staphylococcus aureus*
CC	Conserved cysteine
CD	Circular dichroism
cm	Centimetre
CNS	Coagulase negative staphylococci
cpGTPase	Circularly permuted guanosine triphosphate hydrolase
CPS	Coagulase positive staphylococci
cryo-EM	Cryoelectron microscopy
c.v.	Column volume
CWA	Cell wall anchored
D-Ala	D-Alanine

D-Lac	D-Lactate
DNA	Deoxyribonucleic acid
DNase	Deoxyribonuclease
DRaCALA	Differential Radial Capillary Action of Ligand Assay
E-site	Exit site
ECL	Enhanced chemiluminescence
EDTA	Ethylenediaminetetraacetic acid
EF	Elongation factor
fMet	N-formylmethionine
FRET	Förster Resonance Energy Transfer
g	Gravity
G+C	Guanine-cytosine
GAP	GTPase activating protein
gDNA	Genomic deoxyribonucleic acid
GDP	Guanosine diphosphate
GEF	Guanosine exchange factor
GMP	Guanosine monophosphate
GMPPNP	5'-guanylyl imidodiphosphate
GTP	Guanosine triphosphate
GTPase	Guanosine triphosphate hydrolase
h	Helix
HA-MRSA	Hospital-acquired methicillin resistant-*Staphylococcus aureus*
HAS-GTPase	Hydrophobic amino acid substituted for catalytic glutamine
His	Histidine
HPF	Hibernation promoting factor
hr	Hour
HRP	Horseradish peroxidase
IC	Initiation complex
IF	Initiation factor
IMAC	Immobilised metal affinity chromatography
IMP	Inosine monophosphate
IP	Photostimulable phosphor imaging plate
IPTG	Isopropyl β-d-1-thiogalactopyranoside
K	Rate constant
k_{app}	Apparent reaction rate
kb	Kilobase
K_D	Dissociation constant
kDa	Kilodalton

KH	K-homology
kHz	Kilohertz
kV	Kilovolts
LB	Lysogeny broth
LED	Light emitting diode
M	Molar
mA	Milliamps
MBq	Megabequerels
MDR	Multidrug resistant
MGE	Mobile genetic element
min	Minute
ml	Millilitre
mM	Millimolar
mm	Millimetre
mqH$_2$O	MilliQ water
mRNA	Messenger ribonucleic acid
MRSA	Methicillin-resistant *Staphylococcus aureus*
ms	Millisecond
MSSA	Methicillin-sensitive *Staphylococcus aureus*
N-state	Classical state of the ribosome
NADPH	Nicotinamide adenine dinucleotide phosphate
NAG	N-acetylglucosamine
NAM	N-acetylmuramic acid
ND1	HflX N-terminal domain
ng	Nanogram
nM	Nanomolar
NTP	Nucleotide triphosphate
NTPase	Nucleotide triphosphate hydrolase
NuDiX	Nucleoside diphosphate linked to any moiety 'X'
OB-fold	Oligonucleotide/oligosaccharide binding fold
ORF	Open reading frame
p	Probability
P-loop	Phosphate-binding loop
P-site	Peptidyl site
PBP	Penicillin-binding protein
PBS	Phosphate buffered saline
PCR	Polymerase chain reaction
PDBe	Protein data bank in Europe

PG	Peptidoglycan
pGp	Guanosine 3',5'-bis(monophosphate)
pGpp	Guanosine 3'-diphosphate 5'-monophosphate
pH	Potential of hydrogen
P_i	Inorganic phosphate
pmol	Picomoles
PNK	Polynucleotide kinase
ppApp	Adenosine 3',5'-bis(diphosphate)
ppGpp	Guanosine 3',5'-bis(diphosphate)
pppGpp	Guanosine 3'-diphosphate 5'-triphosphate
pre-IC	Preinitiation complex
PSM	Phenol-soluble modulin
PTC	Peptidyl transferase centre
PVDF	Polyvinyl fluoride
PVL	Panton-Valentine Leukocidin
r-protein	Ribosomal protein
R-state	Hybrid state of the ribosome
RA-GTPase	Ribosome-associated guanosine triphosphate hydrolase
RBS	Ribosome binding site
RF	Release factor
RMF	Ribosome modulation factor
RNA	Ribonucleic acid
RNAP	Ribonucleic acid polymerase
RNase	Ribonuclease
rpm	Revolutions per minute
RRM	RNA recognition motif
rRNA	Ribosomal ribonucleic acid
RSH	RelA/SpoT homologue
S	Svedberg units
s	Second
SAgs	Superantigens
SAH	Small alarmone hydrolase
SAS	Small alarmone synthetase
SCC*mec*	Staphylococcal cassette chromosome *mec*
SCV	Small colony variant
SD	Shine-Dalgarno
SDS-PAGE	Sodium dodecyl sulphate polyacrylamide gel electrophoresis
SIMIBI	Signal recognition particle, MinD and BioD

SNP	Single nucleotide polymorphism
SOC	Super optimal media with catabolite repression
TA	Toxin-antitoxin
TBS	Tris buffered saline
TCA	Trichloroacetic acid
TEMED	Tetramethylethylenediamine
TGS	ThrRS, GTPase and SpoT
TLC	Thin layer chromatography
Tn	Transposon
ToxSAS	Toxic small alarmone synthetase
TRAFAC	Translation factor associated
Tfb	Transformation buffer
tRNA	Transfer ribonucleic acid
tRNAi	Initiating transfer ribonucleic acid
TSA	Tryptic soy agar
TSB	Tryptic soy broth
U	Units
UV	Ultraviolet light
V	Volts
VISA	Vancomycin-intermediate *Staphylococcus aureus*
VRSA	Vancomycin-resistant *Staphylococcus aureus*
ZNF	Zinc-finger domain
μCi	Microcuries
μF	Microfaradays
μg	Microgram
μl	Microlitre
μM	Micromolar
Ω	Ohms

Chapter 1 – Introduction

1.1 *Staphylococcus aureus*, an overview

Staphylococcus aureus is a non-motile, Gram-positive bacterium, responsible for a wide array of human infections worldwide (Feng *et al.*, 2008). Etymologically, the binomen of this species is derived from the Greek *staphyl* and *kokkus*, translating to 'grapes' and 'berry' respectively in reference to the propensity of *S. aureus* to form clusters of near-spherical cells, and the Latin *aurum* referring to the golden hue of *S. aureus* stationary phase cultures due to the presence of the antioxidant carotenoid staphyloxanthin (Clauditz *et al.*, 2006). The *Staphylococcus* genus was traditionally divided into two major clades, the coagulase positive staphylococci (CPS), which exhibit the capacity to clot blood plasma during virulence (McAdow *et al.*, 2012), and the coagulase negative staphylococci (CNS) (Foster, 1996). *S. aureus* constitutes the sole species within the CPS clade, whereas the CNS comprises over 30 species identified to date based on their presumed lack of pathogenicity – although this classification approach has since been considered redundant due to the discovery that commensal CNS such as *Staphylococcus epidermidis* and *Staphylococcus haemolyticus* were capable of opportunistic infection (Becker *et al.*, 2014), and that not all pathogenic strains of *S. aureus* were capable of producing coagulases (Matthews *et al.*, 1997). Nowadays, the 38 known species of staphylococci can be placed into one of three major groups based on their genetic orthologues, in accordance with comparative genomics studies (Coates-Brown *et al.*, 2018). Group A, a large group dominated by those capable of colonising and causing infection in humans, includes such species as *S. aureus, S. epidermidis* and *S. haemolyticus*. Group B comprises species with similar cell wall structure and propensity to infect animal hosts, such as *Staphylococcus equorum* and *Staphylococcus cohnii*, and Group C is comprised of species such as *Staphylococcus pseudointermedius* and *Staphylococcus delphini* associated with the infection of domesticated animals.

The genome of *S. aureus*, for example strain USA300 (accession number: CP000255) consists of a single circular chromosome, which contains on average between 2.7 Mbp and 2.8 Mbp with a guanine-cytosine (G+C) content of around 32% (Młynarczyk *et al.*, 1998). Due to this relatively low G+C content, *S. aureus* and all staphylococci are members of the Firmicutes phylum. In addition to the single chromosome, the genome of *S. aureus* comprises myriad extrachromosomal elements including transposons, prophage, mobile genetic elements (MGEs) and both conjugative and nonconjugative plasmids. These extrachromosomal elements often encode antibiotic resistance cassettes and other important virulence factors.

1.1.1 Epidemiology of *S. aureus*

S. aureus was first identified as a pathogen in 1880 by Sir Alexander Ogston, following the observation that the fluid from donor abscesses was capable of inducing abscess formation in a healthy host (Ogston, 1881; 1882). Over the course of the following century, this organism was understood to be a major human pathogen, and the cause of many distinct infections worldwide including subclinical skin abscesses and inflammation, and invasive bacteraemia, endocarditis and necrotising pneumonia (Chalmers and Wylam, 2020). As a member of the Group A staphylococci, *S. aureus* is found as a natural commensal on the skin and in the nares of around 5% and 30% of humans respectively (Tong *et al.*, 2015) where it remains asymptomatic in the majority of immunocompetent hosts. However there is a correlation between colonisation of the skin and recurrent skin infection such as atopic dermatitis (AD) and eczema, with 76% and 100% of AD patients colonised on the skin in healthy regions and lesions respectively (Abeck and Mempel, 1998). The incidence of AD in this highly colonised patient group is thought to be associated with an above average IgE response to staphylococcal toxins, indicative of a heightened inflammatory immune response (Tomczak *et al.*, 2019). As with any opportunistic pathogen, the risk of *S. aureus* infection increases when immunosuppressed or when presenting an open wound, and as such screening for colonisation before medical treatments including surgery has become routine (Rao *et al.*, 2008). It is estimated that preoperative decolonisation reduces the incidence of nosocomial infection by over 60% (Rao *et al.*, 2008).

Multilocus sequence typing analyses of seven housekeeping genes (*arcC, aroE, glpF, gmk, pta, tpi and yqiL*) from multiple *S. aureus* strains (Enright *et al.*, 2000; Feil *et al.*, 2004) has enabled grouping of distinct lineages into clonal complexes, which has enabled tracking of hypervirulent lineages which may require more stringent medical intervention, as well as monitoring the transmission of said lineages. In the UK, the prevalence of *S. aureus* bacteraemia increased by 3.7% between 2017 and 2018 (Public Health England, 2018). In 2017, there were 120,000 recorded cases of nosocomial *S. aureus*-related bacteraemia in the U.S. alone, with 20,000 associated deaths (Kourtis *et al.*, 2019), representing a mortality rate of 17% and highlighting this organism as both a leading cause of morbidity and a heavy financial burden on the healthcare institution.

1.1.2 Virulence factors of *S. aureus*

As previously stated, *S. aureus* is capable of causing a wide variety of infections in humans, ranging from subclinical skin and soft tissue infections to severe invasive infections. The ability of this organism to occupy such a wide range of niches is in part due to the arsenal of tightly regulated virulence factors

available which facilitate host invasion, tissue degradation, immune evasion and antimicrobial resistance.

1.1.2.1 MRSA and the SCCmec cassette

In 1961, the first instance of methicillin-resistant *S. aureus* (MRSA) was recorded which demonstrated insensitivity to the engineered β-lactam methicillin through acquisition of the *mecA* gene encoding an alternate penicillin-binding protein (PBP), namely PBP2a. This variant has a decreased affinity for nearly all β-lactam antibiotics (Chambers, 1997) with the exception of next-generation cephalosporins including ceftaroline (Saravolatz *et al.*, 2011), and therefore a greatly increased resistance to most broad-spectrum frontline antibiotics traditionally used to treat *S. aureus* infection. Nowadays, around 10% of those colonised by *S. aureus* harbour MRSA strains (Tong *et al.*, 2015), and infection by these strains is associated with a higher rate of morbidity than methicillin-sensitive *S. aureus* (MSSA) due to a combination of more potent virulence factors and a lower success rate of antibiotic therapy (Cosgrove *et al.*, 2003; Li *et al.*, 2021), leading to the coinage of the term 'superbug' to refer to MRSA infection. *mecA* is encoded within a large (40 kb – 60 kb) MGE termed the staphylococcal cassette chromosome *mec* (SCC*mec*) (Kwon *et al.*, 2005), responsible for the horizontal and vertical transmission of methicillin resistance. SCC*mec* cassettes consist of two major components, the *ccr* gene complex and the *mec* gene complex, the former of which encodes two site-specific recombinases *ccrA* and *ccrB* to enable the mobility of this genetic element (Moosavian *et al.*, 2018). The *mec* gene complex encodes *mecA*, the regulatory genes of *mecA* including *mecR1* and *mecI*, as well as any additional resistance determinants (Kwon *et al.*, 2005). Interestingly, *mecR1* and *mecI* exhibit very high sequence homology when compared to the regulators of β-lactamase expression *blaR1* and *blaI*, indicating that the *mec* system may have adapted these β-lactam-sensing regulators during its evolution (Kuwahara-Arai *et al.*, 1996; Stapleton and Taylor, 2002).

SCC*mec* cassettes can be typed based on their *ccrAB* allotype and the class of the *mec* gene complex, with 13 types being recognised to date (Singh-Moodley *et al.*, 2019). Hospital-acquired strains of MRSA (HA-MRSA) typically encode types I - III SCC*mec* cassettes (Ito *et al.*, 2001; Ito *et al.*, 1999), whereas community-acquired (CA-MRSA) strains typically encode types IV – VIII (Oliveira *et al.*, 2006; Shore and Coleman, 2013; Zhang *et al.*, 2009a). The most common CA-MRSA SCC*mec* typing is IV, often associated with hypervirulent strains (Baba *et al.*, 2002), and encodes no accessory resistance determinants in the *mec* cluster. This 'short' cassette is thought to impose less severe fitness costs upon strains harbouring it, both due to the lack of additional resistance markers and the altered ribosome binding site (RBS) present in type IV, which leads to lower PBP2a production and more

efficient growth during the absence of methicillin stress (Lee *et al.*, 2007). Furthermore, this potentially enables greater tolerance to the fitness cost of producing further virulence factors such as Panton-Valentine Leukocidin (PVL) and the arginine catabolic mobile element (ACME) which facilitates the skin-to-skin transmission indicative of many hypervirulent strains such as those within sequence type 8 such as the CA-MRSA USA300 (Strauß *et al.*, 2017).

1.1.2.2 Cell-well anchored proteins

The cell wall of Gram-positive organisms consists of an inner phospholipid bilayer surrounded by a tens of nanometres thick mesh of crosslinked peptidoglycan (PG), lipoteichoic acids, teichoic acids and cell wall anchored (CWA) proteins (Figure 1.1.2.2), imparting chemical and mechanical resistance to a variety of stresses and functioning to balance the intracellular turgor (Pasquina-Lemonche *et al.*, 2020). As this layer forms the outermost surface of the bacterial cell, it is the primary point of contact between the bacterium and host tissue, and as such is responsible for much of the initial adhesion and interaction with the host immune system (Sukhithasri *et al.*, 2013). *S. aureus* contains up to 25 CWA proteins which have been covalently linked to the cell wall peptidoglycan by enzymes in the sortase family, primarily sortase A, which form amide bonds between threonine residues and the cell wall amine groups (Mazmanian *et al.*, 1999). The presence of these CWA proteins is essential for virulence, and sortase-deficient mutants were found to lack the ability to cause abscess formation in murine models (Mazmanian *et al.*, 2000).
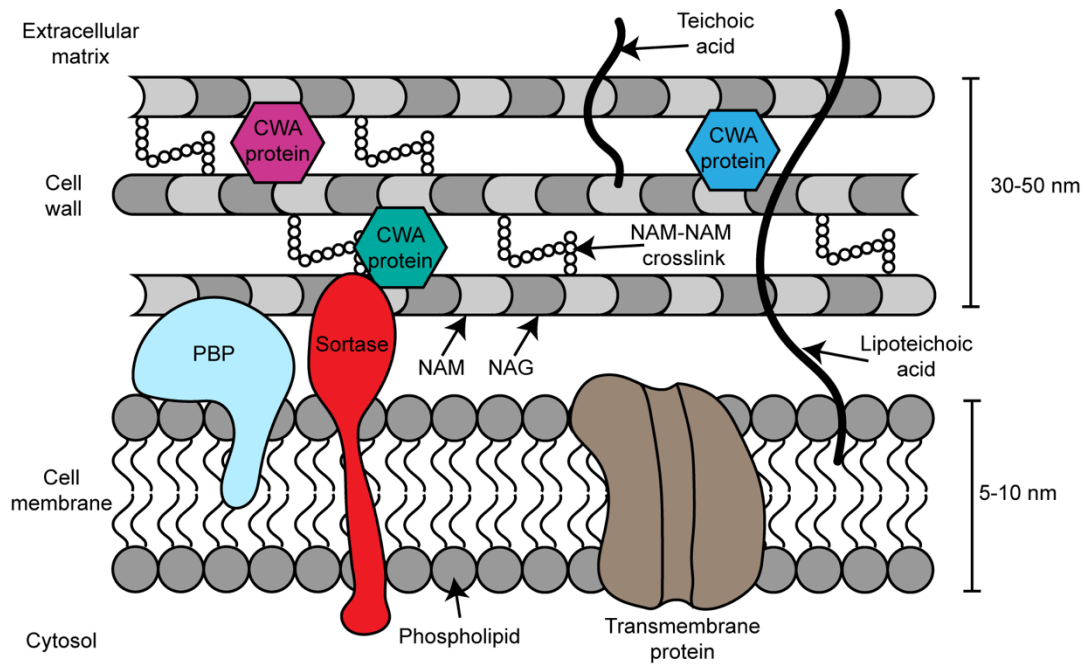
Figure 1.1.2.2: The *S. aureus* cell wall. The cell wall structure of Gram-positive organisms such as *S. aureus* is complex, with a thick layer of crosslinked peptidoglycan constituting alternating N-acetylglucosamine (NAG) and N-acetylmuramic acid (NAM) units. Crosslinks in *S. aureus* are made up of L-Ala – D-Glu – L-Lys – D-Ala, with pentaglycine crosslinks forming between D-Ala and L-Lys of adjacent strands (Srisuknimit *et al.*, 2017), with PBPs catalysing crosslink formation between nascent lipid II-linked PG components. Lipoteichoic acids and teichoic acid polymers are anchored to the phospholipid bilayer and cell wall PG respectively. The 25 different CWA proteins of *S. aureus*, such as ClfA, ClfB, Protein A, and SasX are covalently linked to cell wall amino groups, where they carry out a range of functions including those crucial for virulence.

Initial adhesion is an important stage of colonisation, and is mediated by several CWA proteins in the case of *S. aureus* including clumping factor A and B (ClfA, ClfB) which enable clumping of bacteria in plasma through binding to the fibrinogen, fibronectin-binding proteins A and B which enables adhesion to and invasion of the host epithelium, endothelium and fibroblasts, and SasX which enhances the ability of bacterial cells to adhere to the epithelium (Lacey *et al.*, 2016). In terms of immune evasion, Protein A (*spa*) is a major virulence factor which can bind to the F_c fragment of immunoglobulin, the TNFR1 receptor and von Willebrand factor (Foster *et al.*, 2014) to downregulate the host immune response. Furthermore, protein A has been shown to induce an immunomodulatory effect through activation of IL-10 and TGFβ production by regulatory T-cells (Uebele *et al.*, 2020). Additionally, the iron-regulated surface (*isd*) proteins contain a haem-binding motif in order to circumvent nutritional immunity in the case of ferrous ions (Foster *et al.*, 2014). While it has never been shown, these CWA proteins are hypothesised to play an important role in recognition of *S. aureus* by the adaptive immune system and as such form part of the complex host-pathogen interaction.

1.1.2.3 Secreted toxins

In addition to the exterior display of CWA proteins, *S. aureus* is capable of producing a wide array of secreted virulence factors which fall into three major groups: the exfoliative toxins, the pore-forming toxins and superantigens (SAgs) (Oliveira *et al.*, 2018). Exfoliative toxins are highly specific serine proteases secreted by 5% of clinical *S. aureus* in order to hydrolyse the cadherins which anchor keratinocytes together in human skin, enabling invasion and the development of superficial infections such as impetigo and staphylococcal scalded skin syndrome (Hisatsune *et al.*, 2013; Lee *et al.*, 1987). SAgs are proteins secreted by some bacteria, primarily members of the *Streptococcus* and *Staphylococcus* genera, which stimulate an intense, non-localised adaptive immune response (Xu and McCormick, 2012) which is both qualitatively and quantitatively distinct from normal T-cell activation due to induction of a pro-inflammatory cytokine storm including IFN-γ, TNF$_\alpha$ and IL-2 (Fleischer and Schrezenmeier, 1988; Holtfreter *et al.*, 2006), leading to host symptoms such as fever, desquamation, diarrhoea, hypotension, and in severe cases multiple organ failure and toxic shock syndrome . While this may seem counterintuitive given the quantity of virulence factors dedicated to immune evasion, immune-mediated tissue damage may provide alternate routes of dissemination of bacterial cells, as well as leading to the release of intracellular contents as a source of nutrition. Approximately 80% of clinical MRSA strains encode at least one SAg gene of the 23 currently described (Oliveira *et al.*, 2018), however the majority encode several (Xu and McCormick, 2012). The propensity of superantigens to be encoded and maintained on MGEs in clinically relevant strains of *S. aureus* suggests that these secreted toxins have a productive effect on fitness while invading the host tissue.

The success or failure of infection depends primarily on the ability of *S. aureus* to evade immune clearance. The hypervirulent CA-MRSA strains of sequence type 8 have significantly increased capacity for destroying host neutrophils, which are the major leukocyte involved in initial clearance of bacterial infections (Voyich *et al.*, 2005). While not strictly limited to mononuclear phagocytes, staphylococcal pore-forming toxins such as haemolysin-α, haemolysin-β, phenol soluble modulins (PSMs) and leukotoxins including PVL (Baba *et al.*, 2002; Oliveira *et al.*, 2018; Otto, 2010) are involved in host cell lysis through oligomerisation to form open pores in cell membranes, facilitating leakage of the intracellular matrix, collapse of the proton motive force and ultimately cell death (Los *et al.*, 2013; Verma *et al.*, 2021). The precise significance of these toxins in the outcome of *S. aureus* infection is the subject of ongoing research, however studies have shown that the prevalence of PVL in CA-MRSA strains infection is 85%, compared to 5% of HA-MRSA strains (Lina *et al.*, 1999; Naimi *et al.*, 2003). This implicates increased pore-forming toxin production in virulence within the immunocompetent host,

and indeed PVL-producing strains are more likely to inflict invasive, systemic infections than non-PVL producing MRSA strains (Gillet *et al.*, 2002). The leukotoxins LukED and γ-haemolysin have potent activity against human erythrocytes, forming a key source of ferrous iron when in conjunction with the haem scavenging ISD CWA, and it is estimated that 99% of MRSA strains worldwide carry erythrocidal pore-forming toxins (Liu *et al.*, 2015a).

1.1.2.4 Regulation of virulence factors

The breadth of niches capable of infiltration by *S. aureus* is facilitated mainly by the vast array of available virulence factors. However suboptimal expression of these virulence factors comes at a cost to growth and fitness (Lee *et al.*, 2007) and may compromise successful infection. Due to this, regulation of virulence factor production has evolved to be extremely stringent transcriptionally in response to growth phase or cellular energy availability (Coleman, 1983). Two component systems are the major regulators of virulence in *S. aureus*, including the *agr*, *arlSR*, *lytRS* and *sae* operons (Bronner *et al.*, 2004). Other regulators include SigB and other DNA-binding repressors such as Rot and SarA. The overall regulatory network in this organism is highly complex and interlinked, with multiple factors feeding into the overall control of virulence factor expression, which often leads to indirect activation or repression of genes through accessory regulator interactions. This enables a high degree of specificity and control over virulence factor production depending on the real-time requirements and conditions of the immediate environment of the bacterium.

Two component systems are generally sensitive to exogenous, extracellular signals. The signal is recognised by a sensory histidine kinase, either through direct binding or through recognition of a primary receptor, which triggers homodimerization and subsequent autophosphorylation or transphosphorylation of a histidine residue of the intracellular domain (Tiwari *et al.*, 2017). Following priming of the histidine kinase, the cytoplasmic response regulator docks and catalyses aspartyl autophosphorylation using the phosphohistidine as a donor, which enables DNA binding and transcriptional up- or downregulation (Zschiedrich *et al.*, 2016). The most well-understood staphylococcal two component system is the accessory gene regulator (*agr*) system, which is involved in a quorum sensing network culminating in the downregulation of CWA proteins and upregulation of secreted toxins when cell density reaches a threshold (Bronner *et al.*, 2004), with 104 genes being upregulated and 34 downregulated in total (Dunman *et al.*, 2001). This locus consists of five genes, *agrA*, *agrC*, *agrD*, *agrB* and *hld*, and is transcribed as two divergent transcripts RNAII and RNAIII under the control of two promoters P2 and P3 (Le and Otto, 2015). P1 triggers polycistronic transcription of RNAII, including *agrA*, *agrC*, *agrD* and *agrB*. *agrD* encodes the precursor peptide to the major quorum

sensing autoinducing peptide (AIP), which is processed into mature AIP by AgrB. AgrC and AgrA constitute the two component signalling system responsible for detecting the threshold level of AIP, representing the histidine kinase and response regulator respectively (Koenig *et al.*, 2004). Upon homodimerization and autophosphoryation of AgrC, aspartyl phosphorylation of AgrA, this protein can bind to the P2 and P3 promoters and the promoters controlling PSM transcription to promote expression of RNAII, RNAIII and exogenous PSMs (Queck *et al.*, 2008). RNAIII encodes the haemolysin-δ exotoxin, however prior to translation it also functions as the intracellular effector of the *agr* system, regulating transcription of many genes directly, or indirectly through interaction with other regulatory factors and messenger RNAs (mRNAs) (Goerke *et al.*, 2001; Schmidt *et al.*, 2001), ultimately repressing CWA virulence factors (Huntzinger *et al.*, 2005) and upregulating exotoxin production (Boisset *et al.*, 2007). This is achieved in a manner independent of other toxin-controlling two component systems such as *sae* (Liu *et al.*, 2016), highlighting the functional redundancy within the regulatory machinery of *S. aureus* virulence factors.

In *S. aureus*, the sigma factor A (σ^A) is responsible for promoting transcription of housekeeping genes during proliferative growth when in complex with RNA polymerase (RNAP) (Deora and Misra, 1996). However, *S. aureus* encodes several alternative sigma factors to further regulate the transcriptome under specific conditions. σ^B is responsible for modulating the stress response in response to heat shock, oxidative stress and antibiotic stress, σ^S is responsible for adaptation to conditions of nutrient limitation and σ^H has been shown to be involved in competence and prophage regulation (Tao *et al*., 2010; Tuchscherr *et al*., 2015). σ^B expression peaks during late exponential phase, and positively regulating *sarA* expression and many virulence determinants including α-and β-haemolysin, catalase (Kullik *et al.*, 1998) and staphyloxanthin production (Shaw *et al.*, 2006) while indirectly decreasing transcription of the regulatory *agr*-associated factor RNAIII (Bischoff *et al.*, 2001).

1.1.3 Current treatment options for *S. aureus* infection

As with all bacterial infections, the predominant methods of treating *S. aureus* infection are through the use of broad-spectrum antibiotics such as cephalexin, dicloxacillin and clindamycin for MSSA strains and cotrimoxazole, doxycycline, vancomycin, mupirocin, linezolid and ciprofloxacin in the case of multidrug resistant (MDR) MRSA strains. These are used in combination with culture diagnostics which aim to establish the resistance profile of any given strain to enable efficient treatment and epidemiological tracking. Naturally, *S. aureus* is susceptible to nearly every antibiotic used to date, however this organism exhibits an extraordinary capacity to develop resistance to antibiotics. This is primarily achieved through horizontal gene transfer, often facilitated through conjugation and phage,

yet other mechanisms such as selection pressure and random mutation remain important (Chambers and Deleo, 2009).

Treatment of hypervirulent MDR strains of MRSA often involves the use of antibiotics of last resort, which commonly cause an array of side effects. One such antibiotic is the glycopeptide vancomycin, which has been the preferred treatment for MDR Gram-positive infections since their emergence. Continued use of antibiotics exerts a strong selection pressure to encourage the maintenance of resistance markers, and the first vancomycin-intermediate *S. aureus* (VISA) strains emerged in 1997 (Hiramatsu *et al.*, 1997) following extended use of vancomycin during the 1980s, and exhibit a range of genetic elements which decrease sensitivity to vancomycin (Rishishwar *et al.*, 2014). VISA strains were followed shortly by vancomycin-resistant *S. aureus* (VRSA) in the early 21st century (CDC, 2002). The true vancomycin-resistant phenotype is imparted through the *vanA* operon, acquired by *S. aureus* from vancomycin-resistant enterococci, in which the *vanA* operon is encoded on transposon (Tn)*1546* as part of a conjugative plasmid (Arthur *et al.*, 1993). This gene can be maintained in *S. aureus* either through plasmid maintenance or through integration of Tn*1546* into the acceptor genome. Vancomycin is a glycopeptide antibiotic which prevents the correct assembly of the peptidoglycan cell wall through specific binding to the D-Ala-D-Ala terminus of lipid II (van der Aart *et al.*, 2016). The *vanA* operon comprises seven genes, which modify the lipid II stem to constitute a C-terminal D-Ala-D-Lac and decreasing the affinity of vancomycin binding by three orders of magnitude (Howden *et al.*, 2010; van der Aart *et al.*, 2016). VRSA is particularly rare, in part due to the tightly regulated prescription of vancomycin throughout the Western world, with only 2.4% of clinical isolates of *S. aureus* encoding the *vanA* operon (compared to 4.3% classed as VISA) between 2010 and 2019 (Shariati *et al.*, 2020). Concerningly, *S. aureus* has recently exhibited resistance to many major antibiotics of last resort, that is to say those which have been reserved for use in the absence of other effective antimicrobial therapy, including daptomycin (Pader *et al.*, 2016; Sabat *et al.*, 2018), clindamycin (Dorneanu *et al.*, 2016) and fifth-generation cephalosporins such as ceftaroline (Morroni *et al.*, 2018). Thus, the requirement for novel antistaphylococcal therapies is extremely urgent, sparking much research into this topic.

Within nosocomial environments, the prevalence of *S. aureus* infection is greater in patients following the insertion of an exogenous medical device such as a catheter or prosthetic, with up to 37.7% of MRSA-related bacteraemia being catheter associated (Cuervo *et al.*, 2015). Removal of the catheter and the associated biofilm often enables successful treatment, however in the case of prosthetic implants removal is often not a viable option due to risk and cost, and to this end prophylactic

impregnation of antimicrobials into the prosthetic has proved an effective solution, reducing infection rates by 50% (Parvizi *et al.*, 2008; Romanò *et al.*, 2019). The development of antimicrobial polymers is a topic of ongoing research, using such mechanisms as heavy metal impregnation (Quintero-Quiroz *et al.*, 2020) and nanostructured polymers based on the antimicrobial properties of insect wings (Jenkins *et al.*, 2020). The adoption of systematic disinfection protocols within hospital environments has also proven successful in reducing MRSA cases by over 50% (Garvey *et al.*, 2018), as well as a range of other nosocomial infections. Considering the increasing difficulty in treating MDR infections, stringent disinfection and sterility protocols in combination with routine decolonisation of patients and hospital staff has become an important frontline prophylactic solution to increasing MRSA prevalence.

Arguably the most important tool of humanity against microbial infection is the vaccine, however research into potential vaccines against *S. aureus* has so far proved unsuccessful upon reaching human clinical trials despite several candidates showing promising preliminary data in animal models (Daum and Spellberg, 2012; Dayan *et al.*, 2016). The diminished effectiveness of SAgs and pore-forming toxins in the non-human model is theorised to render clearance of infection more effective, especially in the murine host (Bubeck Wardenburg *et al.*, 2008; Salgado-Pabón and Schlievert, 2014). Surprisingly, PVL was ineffective at augmenting CA-MRSA infection in non-human primate models (Olsen *et al.*, 2010), leading to the suggestion that vaccine development may be impossible prior to the establishment of a representative model system, and following the harmful effect of a seemingly promising vaccine first-in-human trial (Fowler *et al.*, 2013) it was suggested that focus should shift to novel prophylactics and post-infection treatments rather than general vaccines. Despite this, research into vaccine development is ongoing and now focusing primarily on T-cell activation rather than improvement of opsonisation (O'Brien and McLoughlin, 2019).

1.2 Translation in prokaryotes

1.2.1 The prokaryotic 70S ribosome

Ribosomes are a fundamental requirement of cellular life, and no known living organism to date has been identified which does not require ribosomes (Root-Bernstein and Root-Bernstein, 2015). Similar to the eukaryotic 80S ribosome, the 70S prokaryotic ribosome is a large, yet incredibly precise macromolecular machine responsible for facilitating the second step of the central dogma – translation of mRNA into primary amino acid sequence during *de novo* protein synthesis. Around 50% of the dry mass of an *E. coli* cell can be attributed to the ribosomes, and the intracellular concentration of ribosomes is the major determinant of growth rate, with *E. coli* containing between 7,000 per cell during stationary phase and 70,000 per cell (around 70 μM) during rapid growth (Nierhaus, 2014).

Here, specific details unless stated otherwise are based on the most complete and well-understood model of translation – *E. coli*. The mature 70S complex comprises two subunits, the small 30S and the large 50S subunits, the functions of which together enable translational fidelity via accurate decoding of mRNA and specific peptidyl transfer respectively (Leung *et al.*, 2011). The 50S contains three distinct sites which constitute the peptidyl transferase centre (PTC): the Aminoacyl (A) site, the Peptidyl (P) site and the Exit (E) site, which facilitate the mRNA ratchet during elongation (Jomaa *et al.*, 2011). The 30S contains cognate sites which form at the subunit interface to yield the functional combination of the mRNA decoding centre and the mature PTC. In *E. coli*, the 30S subunit is made up of 21 ribosomal proteins (r-proteins) and a single 16S ribosomal RNA (rRNA), and the 50S subunit consists of 34 r-proteins and two rRNAs, the 23S and 5S (Jomaa *et al.*, 2011), leading to the 70S particle mass being around 60% rRNA and 40% protein respectively. The PTC of the 50S ribosome is encoded within domain V of the 23S rRNA. Despite evolutionary drift towards the usage of proteins as catalytic machinery (enzymes) due to the enhanced functional spectrum due to the 20 commonly employed amino acid residues, there as yet exists no proteinaceous enzyme capable of peptidyl transfer (Leung *et al.*, 2011). The ribosome is thus a ribozyme, a relic of the RNA world, in which chemical catalysis was carried out using the four canonical RNA bases before the evolution of amino acid-based machinery. This has been hypothesised to have been self-replicating and self-governing prior to the development of cellular life (Root-Bernstein and Root-Bernstein, 2015).

1.2.2 The translation elongation cycle

The fidelity of translation is the keystone upon which all life is built, with single amino acid substitutions, deletions or insertions often leading to decreased viability of the cell, and the control of the polypeptide elongation process is highly conserved between all organisms (Rodnina and Wintermeyer, 2009). This is split into four distinct phases: initiation, elongation, termination and recycling (Figure 1.2.2), which together enable the efficient translation of mRNA.
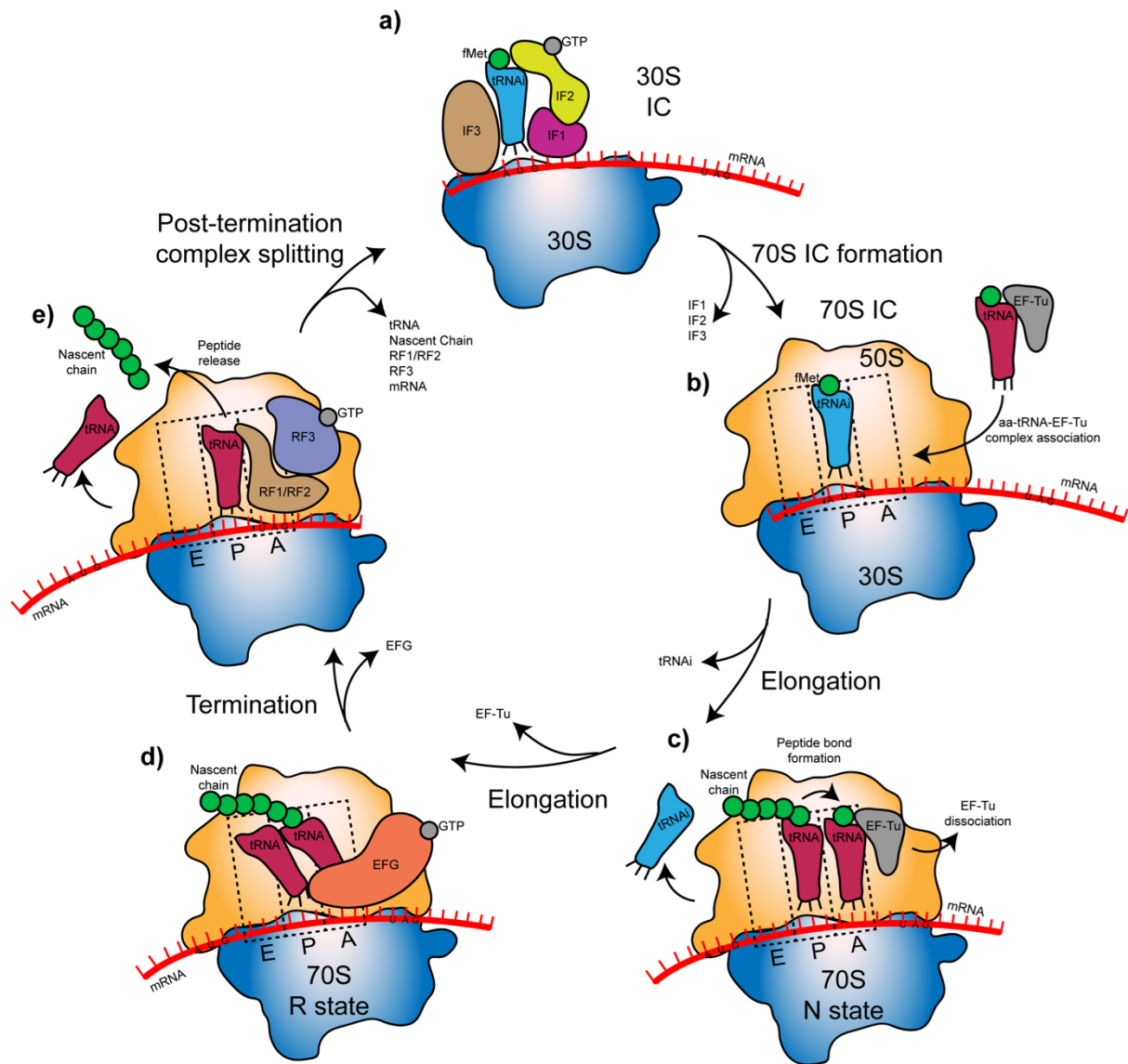
Figure 1.2.2: The translation elongation cycle – a schematic. a) Initial formation of the 30S IC occurs following the kinetically limiting association of the mRNA template containing the initiating AUG codon, the initiating fMet-tRNA[fMet], IF1, IF2-GTP and IF3. b) Association of the 50S subunit triggers release of the initiation factors sequentially, and in a GTPase-dependent manner in the case of IF2, forming the 70S IC. c) Elongation occurs following delivery of the correct aa-tRNA by EF-Tu-GTP, which dissociates via GTP hydrolysis enabling peptidyl transfer to occur between the P and A-site amino acids, subsequently hydrolysing the ester bond linking the nascent chain to the P-site tRNA. d) Peptidyl-tRNA translocation occurs following EF-G-GTP association, which leads to isomerisation of the 70S into the hybrid R-state in which the P and A-site tRNAs contacts the adjacent binding site. GTP hydrolysis by EF-G leads to return to the N-state and release of the newly translocated E-site tRNA. e) The elongation cycle terminates upon recognition of an mRNA STOP codon (usually UAG), which is recognised by either RF1 or RF2 to facilitate release of the nascent chain. RF3-GTP then associates and displaces RF1/RF2, then dissociates in a GTPase dependent manner. Following RRF and EF-G mediated subunit recycling, the translation cycle can begin anew. Information drawn from (Gualerzi and Pon, 2015; Moore, 2005; Noller, 1984).

1.2.2.1 Initiation

Initiation of translation is the process during which the 30S pre-initiation complex (pre-IC) forms around the mature 30S ribosomal subunit (Figure 1.2.2a, b). This is controlled kinetically by three initiation factors (IF) in bacteria, namely IF1, the guanosine triphosphate hydrolase (GTPase) IF2 and IF3. The complex equilibrium between these factors, as well as the initiating N-formylmethionine conjugated fMet-tRNA[fmet] (tRNAi), the objective mRNA and the 30S ribosomal subunit facilitates the rapid and accurate 30S pre-IC formation (López-Alonso *et al.*, 2017a). Initially, there is no Watson-Crick base pairing between the initiator codon AUG (occasionally UUG or GUG in *S. aureus* (McLaughlin *et al.*, 1981)) and the initiator anticodon present on the anticodon loop of fMet-tRNA[fmet]; the 30S pre-IC formation is facilitated via Shine-Dalgarno (SD) interactions with the anti-SD sequence on the 3' end of the 16S rRNA (Shine and Dalgarno, 1974). A first-order structural rearrangement of the 30S pre-IC following association of all factors positions the mRNA such that codon-anticodon recognition can occur within the 30S P-site (López-Alonso *et al.*, 2017a). This conformational change matures the 30S pre-IC into the 30S initiation complex (IC), and capable of complexing with the 50S ribosomal subunit, followed by dissociation of IF1 and IF3 to form the 70S IC. IF2 remains associated until the acceptor arm of fMet-tRNA[fmet] is delivered into the 30S A-site, triggering hydrolysis of guanosine triphosphate (GTP) and subsequent dissociation of IF2 (Tomsic *et al.*, 2000). As the primary stage of translation, initiation is often the target of regulation to control the rate of translation within cells. Should the P-site be occupied by a nonconventional initiator codon, IF1 and IF3 will sterically prevent the maturation of the 30S pre-IC to the 30S IC, and hence inhibit association with the 50S (La Teana *et al.*, 1993). Furthermore, translational repressor proteins often occlude the RBS of specific mRNAs to regulate translation (Jenner *et al.*, 2005), an effect which can also be mediated through small antisense RNA interference, although this is thought to have a greater effect on mRNA stability than the formation of the 30S pre-IC (Watkins and Arya, 2019).

1.2.2.2 Elongation

The elongation cycle of the prokaryotic ribosome is capable of incorporating six amino acids into the nascent chain per second, with the 30S/50S interface ratcheting the distance of precisely three nucleotides along the mRNA template following each peptidyl transfer event (Lareau *et al.*, 2014). In the cytoplasm, elongation factor (EF)-Tu forms a high-affinity ternary complex with GTP and the aminoacyl (aa)-tRNA in the case of the 20 canonical amino acids (Figure 1.2.2c,d). In rare cases, the modified amino acid selenocysteine forms a ternary complex in the cytosol with the alternative translation factor SelB (Forchhammer *et al.*, 1989). Decoding occurs following delivery of the aa-tRNA to the A-site to form a complex with the ribosome and EF-Tu, and upon correct recognition of the

tRNA anticodon with the mRNA template codon, but not just high affinity association of near-cognate anticodons, allosteric activation of EF-Tu leads to GTP hydrolysis and dissociation (Zhang *et al.*, 2009b). Peptidyltransfer can then occur following nucleophilic displacement of the carboxyl carbon of the ester bond of polypeptidyl-tRNA within the P-site, and formation of a peptide bond between the nascent chain and the aa-tRNA within the A-site. This GTPase activity of EF-Tu, dependent on the Watson-Crick pairing between cognate codons and anticodons, confers a degree of translational fidelity which would be lacking if near-cognate codons and anticodons could trigger peptidyl transfer simply by associating with the ribosome. The peptide bond formation occurs between the A- and P-site of the PTC, and following this event complex conformational changes of the ribosome itself on both small and large scales, including a 6° rotation of the 30S relative to the 50S, facilitate the passage of the A- and P-site residues to the P and E sites respectively in order to accommodate the next aa-tRNA within the A site (Noller *et al.*, 2017). Crucially, this process cannot allow any template slippage, which would cause a reading frame shift and either premature termination or aberrant protein synthesis (Noller *et al.*, 2017). This rotation causes the ribosome to leave the 'classical' (N)-state and enter the 'hybrid' (R)-state, in which the associated tRNA molecules are angled such that the tRNA anticodon loop remains in the initial site whereas the acceptor tail of the tRNA moves to the next site (Moazed and Noller, 1989). The N and R-states can be fluctuated between before the association of GTP-bound EF-G to the A-site, which structurally mimics tRNA binding (Chen *et al.*, 2016). The R ribosomal state allosterically triggers the GTPase activity of EF-G, which undergoes a large conformational change upon entry into the guanosine diphosphate (GDP)-bound state which stimulates a further intra-subunit conformational change, leading to mRNA translocation, E-site tRNA dissociation and EF-G dissociation to enable association of the subsequent aa-tRNA within the A-site (Chen *et al.*, 2016). The nascent polypeptide chain is fed through the exit tunnel, which can prevent premature peptide hydrolysis by peptidases that target unfolded proteins, and the quaternary conformation of the exit tunnel can aid in correct folding before entry into the cytosol (Kudva *et al.*, 2018).

Each mRNA template can often be occupied by multiple actively translating ribosomes, raising translational efficiency by producing multiple functional proteins per mRNA molecule transcribed (Brandt *et al.*, 2009). During *E. coli* exponential growth, 70% of ribosomes at any given time participate in polysomes, with an average density of occupation of 1.3 ribosomes per 100 nucleotides (Andreeva *et al.*, 2018). In addition to cytosolic free polysomes, membrane associated polysomes are often responsible for the co-translational export of periplasmic or secreted proteins (Smith *et al.*, 1978). Overpacking of translating ribosomes may lead to collisions or queuing, reducing the overall

translation rate in a manner similar to traffic. Recently, it has been observed via disome-sequencing that certain mRNA sequences promote ribosomal stalling and encourage disome formation, although this phenomenon can also be attributed to mRNA sequences which encode primary α-helix translation (Zhao *et al.*, 2021). It has been proposed that monitoring of disome complexes by chaperone proteins may facilitate correct folding of *de novo* peptide chains with unfavourable folding dynamics (Collart and Weiss, 2020). This offers insight into an intriguing mechanism of elongation-mediated regulation of protein synthesis (Nürenberg-Goloub and Tampé, 2019; Zhao *et al.*, 2021) and demonstrating that regulation can occur at the elongation level as well as during initiation.

1.2.2.3 Termination

Upon completion of the nascent polypeptide production, termination occurs following recognition of a nonsense STOP codon within the mRNA template (Figure 1.2.2e), namely UAG/UGA/UAA in prokaryotes (Martin *et al.*, 1988). Release Factor (RF) 1 and 2 are responsible for reading the UAG/UAA and UGA/UAA stop codons respectively, using the highly conserved PVT and SPF recognition motifs, with both stabilising the ribosome in the N-state (Ma *et al.*, 2017), although RF2 complexes confer a greater degree of rotational flexibility between the N- and R-states. Hydrolysis of the ester bond linking the nascent chain and P-site tRNA is achieved by the 50S P-site and the conserved RF1 and RF2 GGQ motif, which features a universally methylated glutamine residue in order to increase the rate of peptide release (Rodnina, 2018). The reaction progresses via a tetrahedral intermediate due to nucleophilic attack and proton transfer by an activated water molecule, yielding free peptide and deacylated tRNA (Rodnina, 2018). Release of RF1 and RF2 from the terminated ribosome is facilitated by RF3, a GTPase which constitutes one of the rare prokaryotic cases of a guanosine exchange factor (GEF) being utilised to encourage GTP binding – with the ribosome itself serving to enhance nucleotide exchange (Peske *et al.*, 2014). The relative 5 nM and 20 nM affinity of free RF3 to GDP and GTP respectively however suggests that under most circumstances where cellular GTP concentrations are an order or magnitude higher than GDP (Varik *et al.*, 2017), RF3 will freely enter the GTP-bound state. This GEF activity may be an adaptation to enable the essential process of translation even under nutrient-limiting conditions where GTP concentrations plummet. Peptide release results in the stabilisation of the RF3-GTP-RF1/2-ribosome complex shifted into the R-state, and facilitates RF1 or RF2 release, followed by GTP hydrolysis and dissociation of RF3-GDP from the ribosome (Adio *et al.*, 2018).

1.2.2.4 Recycling

Both mRNA and tRNA remain in the post-termination ribosome, and removal of these factors is necessary before a second round of initiation and elongation can occur. Prokaryotic ribosome splitting is facilitated by ribosome recycling factor (RRF) and EF-G, during which RRF binds to the A-site of the ribosome and stabilises the rotated R-state, such that the P-site tRNA adopts a hybrid conformation between the P- and E-sites (Gao *et al.*, 2005). Subsequent hydrolysis of GTP by EF-G promotes steric clashing between the elongated domain I of RRF and the crucial intersubunit bridges B2a and B3 due to a 60° rotation of RRF about its own longitudinal axis (Gao *et al.*, 2005). mRNA is capable of stochastic exchange, however association of the IF3-containing 30S IC with the 50S subunit triggers release of the associated deacylated-tRNA from the P-site (Gualerzi *et al.*, 1971), although the precise temporal occurrence of this has proven controversial (Borg *et al.*, 2016). Following splitting, 30S pre-IC formation can occur in preparation for a downstream elongation cycle. In *E. coli*, depletion of RRF decreases the recycling of 3'-untranslated region associated ribosomes, however this protein was not essential (Saito *et al.*, 2020) suggesting the presence of other less efficient mechanisms of ribosome recycling. Indeed, the heat-shock associated GTPase HflX is known to be capable of dissociating 70S ribosomes independently of GTPase hydrolysis (Zhang *et al.*, 2015), and this has been hypothesised to represent a parallel mechanism of splitting terminated ribosomes under different upstream conditions.

1.2.3 The 100S ribosome complex

Protein synthesis as a whole is one of the most energy-intensive processes within the cell, and *de novo* ribosome biogenesis alone can account for up to 40% of total energy usage during exponential phase growth (Strunk and Karbstein, 2009). During growth limiting conditions, transcription of the rRNA-encoding *rrn* operon is often repressed to prevent cell growth and enable long-term survival (Durfee *et al.*, 2008), however the mature ribosomes represent a huge energy investment and therefore are converted to inactive hibernating forms referred to as 100S complexes. In γ-Proteobacteria such as *E. coli*, this complex formation is achieved through the activity of two proteins, ribosome modulation factor (RMF) and short hibernation promoting factor (short-HPF) (Beckert *et al.*, 2018). RMF binds within a cleft adjacent to helix 28 (h28), h37 and h40 of the 16S rRNA, upon which bS1 usually associates (Beckert *et al.*, 2018). A cluster of positively charged residues mediates this binding between α-helix 1 (α1) of RMF and the 3' of the 16S rRNA, positioning the anti-SD sequence in such a manner that it is incompatible with the cognate SD of mRNAs. Short-HPF binds within the 30S A and P-sites, adjacent to h30 and h44 of the 16S rRNA, rendering the ribosome inactive due to occlusion of the tRNA binding sites (Beckert *et al.*, 2018). Together, these proteins indirectly stabilise 100S dimer

formation indirectly through stabilisation of bS1 and uS2 on the 30S ribosome, initiating a productive point of interface. These proteins on particle 1 form inter-particle bridges with uS4 and uS3, granting 2-fold rotational symmetry to the complete 100S particle (Beckert *et al.*, 2018).

In Gram-positive bacteria such as *S. aureus*, a long-HPF homologue is the sole factor involved in 100S formation, via an unrelated mechanism in which homodimerization of the extended CTD of long-HPF is the major stabilising factor (Matzov *et al.*, 2017), with some interaction between 30S rRNA augmenting this. Moreover, while in organisms containing both RMF and short-HPF, 100S complexes are strictly formed during stationary phase. In organisms containing long-HPF however, 100S complexes can be isolated from exponential phase cultures also, albeit at a lower concentration than during stationary phase (Akanuma *et al.*, 2016; Ueta *et al.*, 2013). While the precise reason for this is unknown, it is thought to contribute to translational regulation and the overall bacterial bet-hedging strategy (Basu and Yap, 2016) which leads to increased antimicrobial tolerance. Deletion of long-HPF in both *S. aureus* and *Bacillus subtilis* leads to mass breakdown of 70S ribosomes upon entry to stationary phase, ultimately leading to cell death via loss of translational machinery and the inability of cells to resume growth (Akanuma *et al.*, 2016; Basu and Yap, 2016).

The precise events leading to the disassembly of the 100S complex upon resumption of growth remains the subject of investigation, although several factors capable of this disassembly have been identified. Canonically, the 100S must be split firstly into two 70S monomers, and then into constituent 30S and 50S subunits to enable initiation of translation. HflX is an universally conserved GTPase shown to the be capable of 70S disassembly in a GTPase-independent manner (Coatham *et al.*, 2016) during repair of heat-shock related rRNA damage (Dey *et al.*, 2018), however this protein is also capable of GTPase-dependent dissociation of the 100S complex (Basu and Yap, 2017). Recently, the 100S ribosome has been identified as a target of EF-G and RRF-mediated splitting in a GTPase-dependent manner through the conformational change of EF-G displacing long-HPF in *S. aureus* rather than via N-R-state transition of the 70S (Basu *et al.*, 2020; Feaga *et al.*, 2020). Thus, it has been suggested that during standard outgrowth conditions, the highly abundant (20 μM each) EF-G and RRF function to recycle 100S complexes into active ribosomes, whereas HflX may function under more specific heat-shock related conditions, and *in trans* expression of HflX can complement RRF deficiency, supporting two parallel disassembly pathways regulated on a transcriptional level (Basu *et al.*, 2020).

1.2.4 The ribosome as an antimicrobial target

The universally conserved overall structure and mechanism of action of the ribosome has led to the evolution and rational development of many antibiotics which target the process of translation through binding to both the large and small subunit. These include commonly used antibiotics such as aminoglycosides, chloramphenicol, lincosamides, macrolides, mupirocin and tetracycline, in addition to many more. For recent reviews on this extremely broad antibiotic class, see (Arenz and Wilson, 2016), (Lin *et al.*, 2018) and (Wilson *et al.*, 2020). The majority of clinically used antibiotics target either the 30S decoding centre, often causing slippage to yield premature nonsense codons or nonfunctional protein variants, or the 50S P-site to inhibit peptidyl transfer (Wilson, 2014). Some less commonly used antibiotics prevent aa-tRNA synthesis or association, or by sterically blocking the nascent chain from passing through the exit tunnel (Wilson, 2014). The breadth of activity and efficacy of these antibiotics has led to the ribosome-targeting class as the most common antibiotic target in terms of quantity (Kavčič *et al.*, 2020), and these are often used in conjunction or as part of an antibiotic cocktail to help curtail the development of antimicrobial resistance in an effort to prolong the effectiveness of these valuable broad-spectrum antibiotics (Kavčič *et al.*, 2020).

The development of resistance to ribosome-targeting antibiotics is testament to the ability of microorganisms to adapt even the most fundamental process due to the overwhelming selection pressure of extensive antibiotic usage. Mycobacteria and Gram-negative bacteria have an innate resistance to some antibiotics with large structures, such as macrolides (Vaara, 1993), although some innately susceptible organisms have developed resistance to a wide variety of antibiotics through the use of multidrug efflux pumps (van Veen, 2010). Aside from this efflux approach, one of the more commonly employed mechanisms of resistance is modification of target motifs and sites within the ribosome. Most ribosome targeting antibiotics specifically target the rRNA sequences, and providing that the integrity of the rRNA helices or catalytically active sites are not compromised, either single nucleotide polymorphisms (SNP) or single-copy r-protein deletions which influence rRNA structure can confer almost total resistance (Gomez *et al.*, 2017). For example, mutation of the 50S proteins bL4 and bL5 in *S. aureus* and *S. epidermidis* isolates confer resistance to linezolid in combination with the commonly described SNP C2534U (LaMarre *et al.*, 2013). An alternative but highly effective mechanism of resistance arises following methylation of rRNA bases by methyltransferases including KamA, KsgA and KgmA (Gupta *et al.*, 2013). Notably, the common determinant of resistance to the macrolide erythromycin, *erm*, functions by specifically methylating the highly conserved adenine nucleotide within the A-site to prevent binding of erythromycin and confer high levels of resistance to a range of macrolides, lincosamides and streptogramins (Choi *et al.*, 2018). Methylation of active site

residues leads to diminished translational efficiency, and so to avoid the fitness cost associated with antibiotic resistance, genes such as *ermB* are often induced by the presence of the antibiotic in question (Rosato *et al.*, 1999) or as a general post-transcriptional response to ribosome stalling (Dzyubak and Yap, 2016).

The functional redundancy between classes of ribosome-targeting antibiotics is a subject of concern, as resistance determinants frequently confer resistance to a range of antibiotics (Wilson, 2014). Due to this, the development of novel ribosome-targeting broad spectrum antimicrobials is a priority for worldwide medical research, and to this end, many novel therapeutic approaches currently in the research and developmental phase are focused on targeting the exceedingly complex ribosome assembly process (Nikolay *et al.*, 2016).

1.3 Ribosome assembly

1.3.1 The current model of ribosome assembly

The innate complexity of the 70S ribosome requires an extremely well organised assembly process, owing to the fact that aberrant ribosome conformation can lead to catastrophic errors in translation (Rodnina, 2018), and involves a high level of coordination between several concurrent steps. These include the transcription and post-transcriptional modification of rRNA, which can entail both methylation and pseudouridylation, correct post-translational modification and folding of primary, secondary and tertiary r-proteins, and the precisely timed association and dissociation of myriad ribosome assembly cofactors (Connolly and Culver, 2009). The bacterial cell employs two major tactics for correct preliminary assembly, firstly co-transcriptional assembly of rRNA during which the nascent rRNA transcript is immediately processed by endoribonucleases, then bound and stabilised by constitutively expressed primary r-proteins to induce correct folding (Figure 1.3.1.1) (Davis and Williamson, 2017). Secondly, this folding of the nascent rRNA forms the epitopes required for further r-protein association, and as such the assembly of the ribosomal subunit is both limited and guided by the conformational state of the newly transcribed rRNA (Mougey *et al.*, 1993; Ramakrishnan, 1986). In agreement with this, cryoelectron microscopy (cryo-EM) studies of multiple 30S assembly intermediates show that assembly occurs from the 5'-3' of the 16S rRNA, from the head domain to the lower body domain, in line with the orientation of rRNA transcription (Razi *et al.*, 2019).
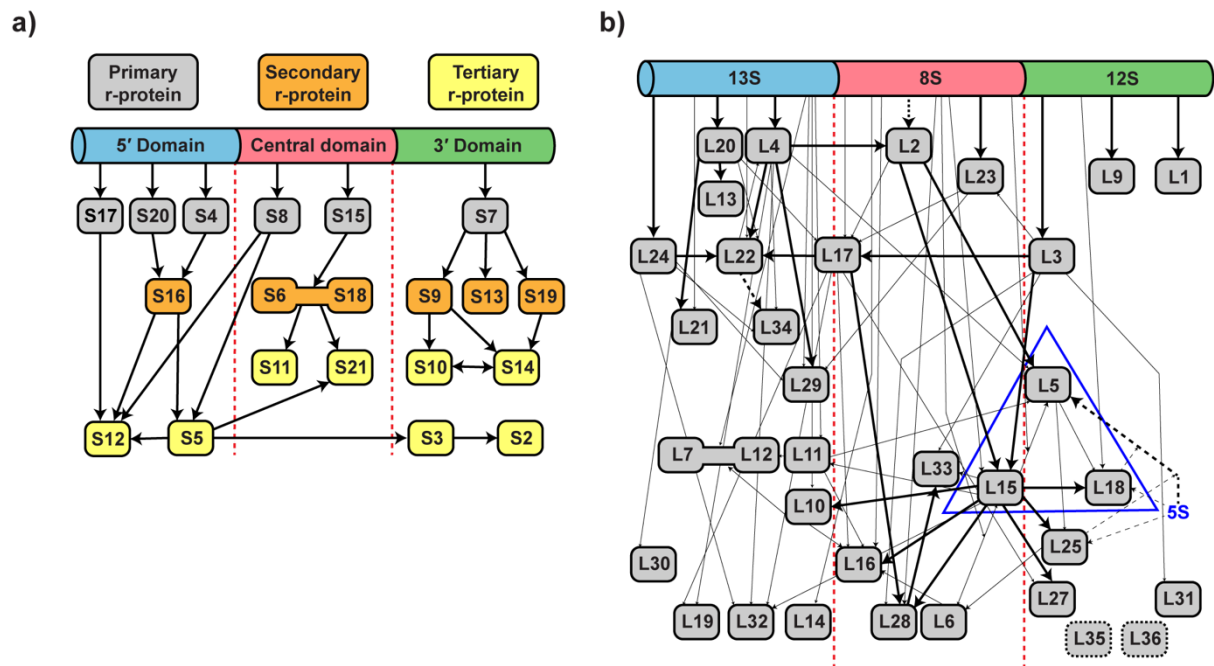
Figure 1.3.1.1: Mapping r-protein association during ribosomal subunit assembly. a) The updated Nomura map (Grondek and Culver, 2004; Held *et al.*, 1974; Mizushima and Nomura, 1970) based on thermodynamic dependencies of r-protein binding to the 16S rRNA during assembly of the 30S subunit in *E. coli*. The clear hierarchy of primary, secondary and tertiary protein binding is represented here as grey, orange and yellow boxes respectively, and interprotein interactions are shown with thick black arrows. The 16S rRNA is split into three domains, the 5', central and 3', to depict the geography of r-protein association relative to the 16S. S1 only transiently associates with the 30S complex and as such is omitted from this figure. b) The updated Nierhaus map (Herold and Nierhaus, 1987; Röhl and Nierhaus, 1982), based on thermodynamic dependencies of protein binding to the 23S and 5S rRNA during 50S subunit assembly in *E. coli*. The 23S rRNA is split into three domains, the 13S, 8S and 12S, which demonstrates the geography of 50S assembly. The hierarchy of r-proteins is not clear due to the plethora of minor interactions (small black arrows) which contribute to the modularity of 50S assembly. The 5S rRNA is represented by a blue triangle, and relies of L5, L15 and L18 to associate with the pre-50S subunit. Dashed black arrows represent interactions considered transient during the assembly process. Figure drawn by the author using Adobe Illustrator.

Despite the absolute requirement of correct rRNA conformation for translational efficacy, the subunit assembly process is known to be highly modular in terms of r-protein association (Davis *et al.*, 2016). rRNA is encoded on the genome by the multicopy *rrn* operon, with *E. coli* encoding seven copies, *B. subtilis* encoding 10 and *S. aureus* encoding either five or six (Fluit *et al.*, 2016). Depending on the copy number of a particular species, these operons can comprise up to 1% of the total genomic DNA (Farrelly *et al.*, 1995). During transcription, the polycistronic precursor rRNA is processed by ribonuclease (RNase) III, yielding the monocistronic rRNA precursor 5S, 17S, 25S and tRNA sequences (Figure 1.3.1.2) (Apirion and Miczak, 1993). Protein-independent folding of these precursors recruits r-proteins in a hierarchical manner, with primary r-proteins initially binding to naked rRNA (Figure 1.3.1.1), and 'locking in' the productive conformation as a checkpoint towards the mature state (Davis and Williamson, 2017). This conformation facilitates secondary r-protein binding to the primary factors (Napper and Culver, 2015). Finally, tertiary r-proteins can associate with the secondary r-

proteins (Razi *et al.*, 2019), with each subsequent binding event further stabilising and remodelling the rRNA fold (Jomaa *et al.*, 2011; Talkington *et al.*, 2005). The processing of 17S rRNA during 30S subunit assembly is thought to occur following association of primary and secondary r-proteins during relatively late-stage assembly. The enzymes involved in 16S maturation differ greatly between the Firmicutes and γ-Proteobacteria; in *E. coli*, 115 nucleotides are removed from the 5' terminus by RNase E and G, and 33 nucleotides from the 3' terminus by the functionally redundant 3'-5' exoribonucleases RNase R, PH, II and polynucleotide phosphorylase in conjunction with the endoribonuclease activity of YbeY (Kaczanowska and Ryden-Aulin, 2007; Tamaru *et al.*, 2018). In the Firmicutes, rRNA processing is less well understood but is thought to involve initial processing by RNase Y and potential downstream processing by the poorly understood ribosome-dependent endoribonucleases Rae1 and YacP (Clouet-d'Orval *et al.*, 2018). Increased size, complexity and modularity of the 50S subunit has led to increased difficulty in modelling assembly efficiently (Davis *et al.*, 2016; Seffouh *et al.*, 2019), however the general mechanism by which the 5S and 25S rRNA precursor molecules are decorated by primary, secondary and tertiary r-proteins prior to processing, although the precise RNases involved in this processing remain unknown in prokaryotes.
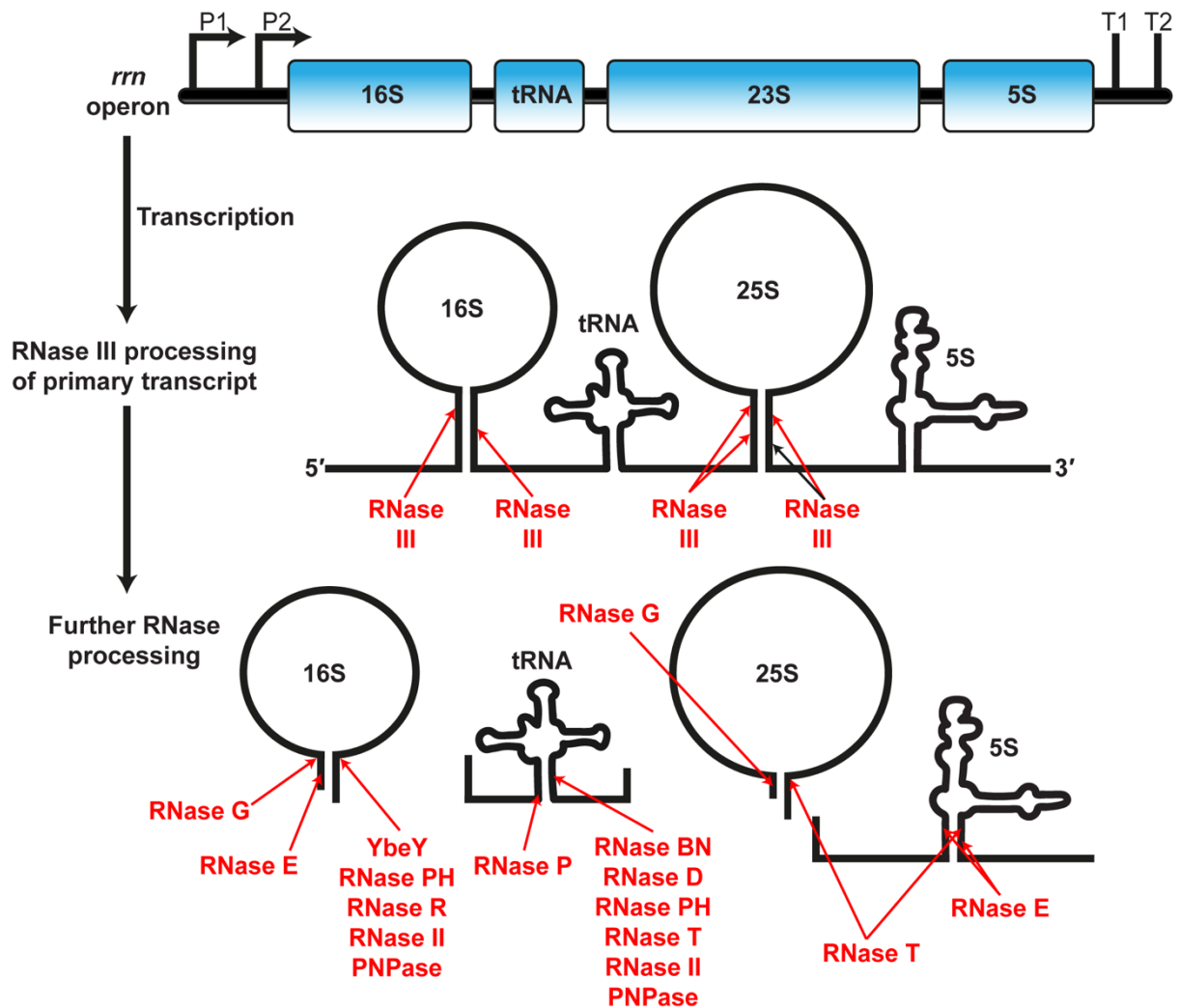
Figure 1.3.1.2: A schematic overview of rRNA processing in prokaryotes. Initial transcription of the multi-copy *rrn* operon by RNAP from one of two promoters yields a polycistronic transcript containing the 16S, 23S, 5S and in many cases multiple tRNAs. Endoribonuclease processing by RNase III begins concomitantly with transcription, cleaving the transcript into pre-16S (17S), pre-23S (25S), pre-5S and pre-tRNA following secondary stem loop recognition. R-proteins associate continuously throughout this process, encouraging secondary structure formation, stability and processing factor recruitment. A range of exo- and endoribonucleases facilitate further processing (as indicated) during subunit biogenesis to produce mature 16S, 23S, 5S and tRNAs. *E. coli* RNases were included here, as the process of rRNA processing is best understood in this organism (Apirion and Miczak, 1993; Li and Deutscher, 1996; Roy-Chaudhuri *et al.*, 2010).

tRNA transcripts require both 3' and 5' processing, with the conserved RNase P removing precursor-specific nucleotides from the 5' terminus (Li and Deutscher, 1996) depending on the specific tRNA precursor sequence – each tRNA anticodon variant is encoded separately with different precursors, often with multiple differing copies of each anticodon variant encoded within the same genome (Fujishima and Kanai, 2014). *E. coli* contains 86 tRNA genes, with like-for-like tRNAs such as the seven valine-binding variants frequently encoded within several polycistronic operons (Agrawal *et al.*, 2014). The 3' terminus of tRNA precursors is processed by a complex and poorly understood network of

exoribonucleases, including RNase BN, D, PH, T, II and polynucleotide phosphorylase (Agrawal *et al.*, 2014).

1.3.2 Ribosome assembly cofactors

The accuracy of h44 folding at the 3' of the 30S 16S rRNA, specifically that of the decoding centre, has been implicated in downstream translational fidelity, and as such maintaining this accuracy during biogenesis of *de novo* ribosomes is crucial for the function of every translated protein and the viability of the cell as a whole (Razi *et al.*, 2017). h69 of the 23S rRNA forms a late-stage maturation step during 50S biogenesis, being located towards the 3' terminus. This helix interacts extensively with h44 of the 30S to form the crucial intersubunit bridge, B2a, during 70S IC formation, as well as directly contacting the P-site tRNA during elongation. Δh69 *E. coli* variants exhibit a dominant lethal phenotype due to a drastically slowed rate of initiation (Liu and Fredrick, 2015), and assembly defects in this helix recapitulate this lethal phenotype. Non-optimal pseudouridylation, Mg^{2+} coordination and secondary conformation can reduce translational efficiency (Sakakibara and Chow, 2011; 2012), accentuating the necessity for stringent quality control during assembly. Many protein families contribute towards the assembly process, including endo/exoribonucleases, GTPases, helicases, methyltransferases, kinases and several more (Apirion and Miczak, 1993; Bennison *et al.*, 2019; Martin *et al.*, 2013; Pletnev *et al.*, 2020). The focus of this section will be on the four ribosome-associated GTPases (RA-GTPases) used in this study, which directly contribute to the correct assembly of the ribosomal subunits. For information regarding other RA-GTPases involved in ribosome assembly such as the highly conserved anti-association factor ObgE (Feng *et al.*, 2014), the 50S associated BipA (Kumar *et al.*, 2015) and the tandem 50S assembly factor Der (Hwang and Inouye, 2006; 2010), see (Bennison *et al.*, 2019; Britton, 2009; Verstraeten *et al.*, 2011).

1.3.2.1 The conserved GTPase domain

As the major currency of energy within the cell due to their high-energy β,γ-phosphodiester bond, nucleotide triphosphates (NTPs) such as adenosine triphosphate (ATP) and GTP have a variety of proteins dedicated to their hydrolysis (Romero Romero *et al.*, 2018). The phosphate-binding loop (P-loop) NTPases constitute the most abundant class of proteins within *E. coli*, representing up to 18% of all translated protein under exponential conditions. ATPases are regularly involved in the storage and transfer of energy within the cell, whereas GTPases are more heavily implicated in signal transduction, where they may function as monomeric small GTPase switches or within signalling complexes such as two-component systems. The monophyletic GTPase superclass can be further divided into two major subclasses which differ in their functional components and role in the cell. First are the SIMIBI (Signal

Recognition Particle, MinD and BioD) GTPases, involved in chromosomal segregation, protein trafficking and membrane transport, and second are the TRAFAC (Translation Factor Associated) GTPases involved in intracellular transport, motility and translation (Leipe *et al.*, 2002). The TRAFAC subclass is much more functionally diverse and well-studied than the SIMIBI class, with many TRAFAC GTPases being involved in translation or ribosome assembly and thus further classified as RA-GTPases. The correct organisation and timing of both early and late-stage r-protein association onto precursor rRNA is often regulated and facilitated by RA-GTPases, which act as checkpoints of ribosome assembly through the binding of immature sections of the rRNA while in the GTP-bound ON state, sterically preventing the premature association of r-proteins or rRNA maturation factors (Britton, 2009). RA-GTPases each contain at least one accessory rRNA-binding domain, unlike small GTPases such as Ras which exist in the cytosol as an isolated GTPase domain (Verstraeten *et al.*, 2011). Upon correct folding of the target rRNA, the GTPase activity of the assembly factor is activated, GTP is hydrolysed to GDP and the RA-GTPase enters the GDP-bound OFF state – enabling dissociation from the ribosome and association of downstream r-proteins or maturation factors (Britton, 2009).

The universally conserved GTPase domain is a globular arrangement of a central β-sheet surrounded by α-helices, with the presence of either four or five highly conserved functional motifs (G1-G5) involved in the recognition, binding and hydrolysis of GTP (Figure 1.3.2.1a) (Bennison *et al.*, 2019; Verstraeten *et al.*, 2011). The G1 motif, also referred to as the Walker A motif or the P-loop, is present in the vast majority of identified NTP-binding proteins – both ATP and GTP binding. The [GxxxxGKS/T] consensus sequence facilitates orientation of the α and β-phosphate of NTPs in such a way to allow nucleophilic attack of the γ-phosphate by the primary R_1 amino group of the conserved G1 lysine residue (Deltoro *et al.*, 2016) during hydrolysis. The G2 motif, also referred to as switch I, is characterised by a conserved threonine in the TRAFAC GTPases [xTx], which can bind and coordinate the essential Mg^{2+} cofactor responsible for activating the hydrolytic water molecule while simultaneously stabilising the γ-phosphate leaving group of GTP (Carvalho *et al.*, 2015). The G3 motif, also referred to as the Walker B motif or switch II, is situated adjacent to the Mg^{2+} cofactor and plays a similar role in activation of the hydrolytic water molecule and stabilisation of the γ-phosphate as the G2 motif. The G3 consensus sequence is [DxxG]. Both switch I and switch II undergo large conformational rearrangements during the transition from the GTP-bound ON state and GDP-bound OFF state, which contribute to the role of the GTPase as a molecular switch through alteration of binding specificity to target proteins in order to regulate activity (Verstraeten *et al.*, 2011). The G4 motif is characterised by four large hydrophobic and often aromatic amino acids followed by the consensus [(N/T)(K/Q)xD], within which the conserved lysine/glutamine residues form π-stacking

interactions with the guanine ring. The aspartate residue is crucial for the specific binding of guanine over alanine nucleotides, with the R-group carboxylate forming bifurcated hydrogen bonds (H-bonds) with the guanine 1' and 2' primary and secondary amines but not the 1' tertiary amine or 2' methine group of the adenine ring (Daumke and Praefcke, 2016), thus representing a selectivity barrier against the latter. The G5 motif is poorly conserved and not strictly ubiquitous, however is hypothesised to interact with the guanine nucleobase via a water-mediated hydrogen bonding network. Hydrolysis of the β,γ-phosphodiester proceeds via an S_N2-like $A_N D_N$ pathway, in which formation of a single pentavalent transition state facilitates bond formation between an active hydroxyl group and inorganic phosphate (P_i) leaving group and bond cleavage to release the leaving group occurs via a single intermediate (Carvalho *et al.*, 2015).
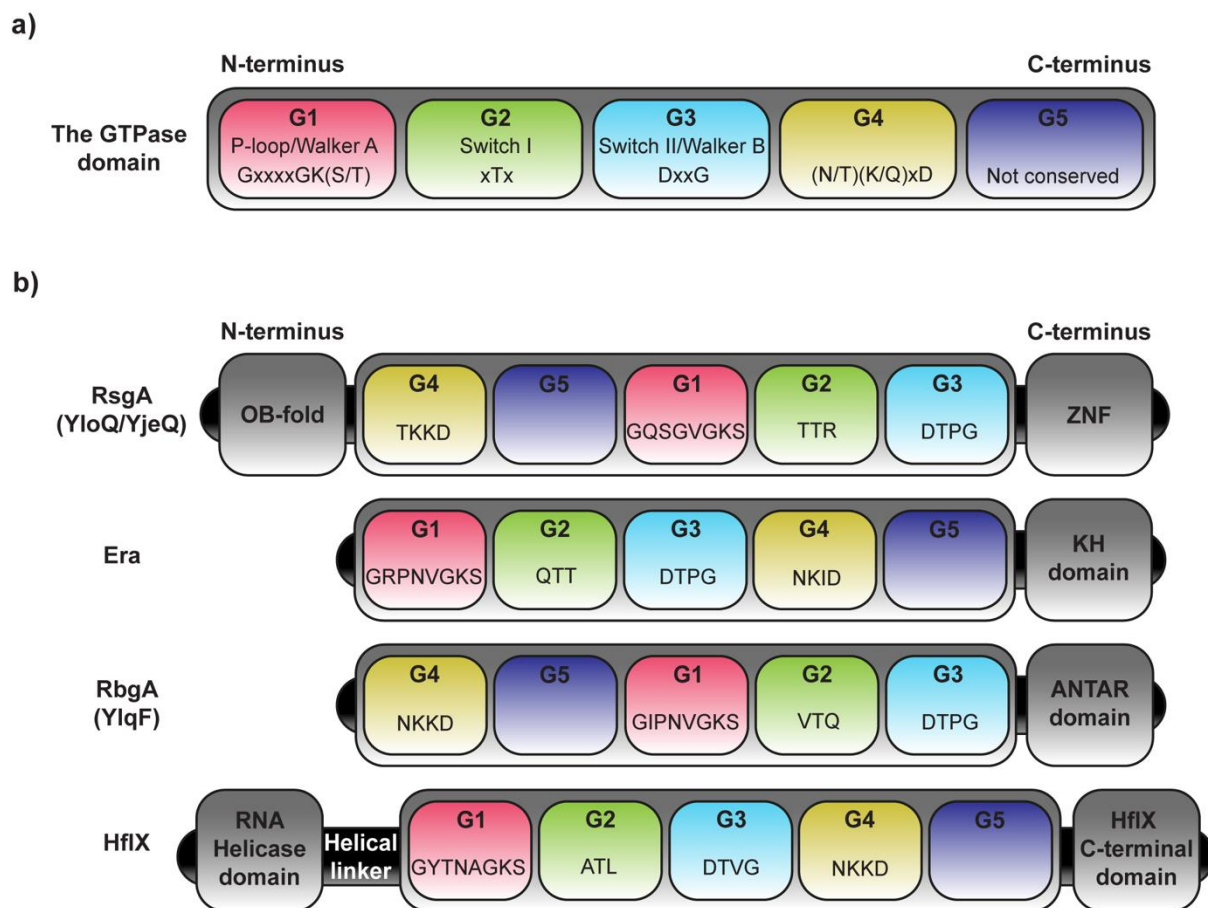
Figure 1.3.2.1: The domain structure of the RA-GTPases RsgA, RbgA and HflX. a) A schematic representation of the highly conserved domain structure and functional motifs of the canonical GTPase domain. These motifs include the G1 (P-loop/Walker A) motif, responsible for recognising the α and β-phosphate of the GTP substrate. The G2 (Switch I) and G3 (Switch II) motifs coordinates an essential Mg^{2+} cofactor, which in turn contacts the γ-phosphate leaving group of the GTP substrate and also activates a water molecule in order to facilitate hydrolysis. The G4 motif grants highly selective binding of nucleotides containing guanine rings relative to adenine rings via specific π-stacking interactions and bifurcated hydrogen bonding to amines specific to guanine. The G5 motif is also thought to enhance binding specificity to guanine rings, however this motif is not highly conserved and therefore difficult to identify. b) Specific domain structure of the four TRAFAC GTPases discussed

in Section 1.3.2.2, including the G1, G2, G3 and G4 consensus motifs as per the *S. aureus* USA300 homologues. Note the presence of accessory domains in all four cases, and the circular permutation of the RsgA and RbgA GTPase domain (Bennison *et al.*, 2019; Verstraeten *et al.*, 2011).

1.3.2.2 GTPases involved in 30S subunit assembly

1.3.2.2.1 RsgA (YloQ, YjeQ)

The tri-domain GTPase RsgA (YjeQ in *E. coli*, YloQ in *B. subtilis*) is a late-stage 30S assembly factor that is widely distributed and highly conserved among bacteria, although nonessential for proliferative growth (Guo *et al.*, 2011). The G-motifs of RsgA adopt a different permutation than the canonical GTPase domain, arranged as G4-G5-G1-G2-G3 (Figure 1.3.2.1b), and as such this protein is a member of the Circularly Permuted (cp)GTPase family alongside other RA-GTPases such as RbgA, YawG and YqeH. Despite the sequential permutation, the spatial orientation of the G-motifs is consistent with that of canonical GTPase domains and so GTP binding and hydrolysis occurs in an identical manner (Levdikov *et al.*, 2004). One structural consequence of the circular permutation is that the highly flexible switch II loop is located at the extreme C-terminus of the cpGTPase domain, and as such a C-terminal domain is required for stabilisation, which may be functional or purely serve to stabilise the cpGTPase (Anand *et al.*, 2006). RsgA has two accessory RNA-binding domains, the β-barrel N-terminal oligonucleotide/oligosaccharide-binding fold (OB-fold) domain and a C-terminal Zinc-finger (ZNF) domain (Figure 1.3.2.2.1a) (Levdikov *et al.*, 2004). The most commonly accepted model for GTP hydrolysis by P-loop GTPases features the use of a catalytic glutamine residue which resides within the switch II loop (Mishra *et al.*, 2005), however RsgA and all RA-GTPases exhibit a substitution of this catalytic glutamine residue for a non-catalytic hydrophobic amino acid, and as such members of the Hydrophobic Amino Acid Substituted for Catalytic Glutamine (HAS)-GTPase subclass and therefore the hydrolysis of GTP is triggered via a different mechanism. Despite the availability of several high-resolution crystallographic and cryo-EM structures of RsgA homologues, the precise means of catalysis has yet to be elucidated due to the innate flexibility and low resolution of the switch I region (Levdikov *et al.*, 2004; López-Alonso *et al.*, 2017a; Razi *et al.*, 2017). It has been suggested that a highly conserved switch I histidine residue, located slightly upstream of the G2 threonine, facilitates the hydrolysis of GTP following correct maturation of the h44 binding site on the 30S subunit (López-Alonso *et al.*, 2017a).
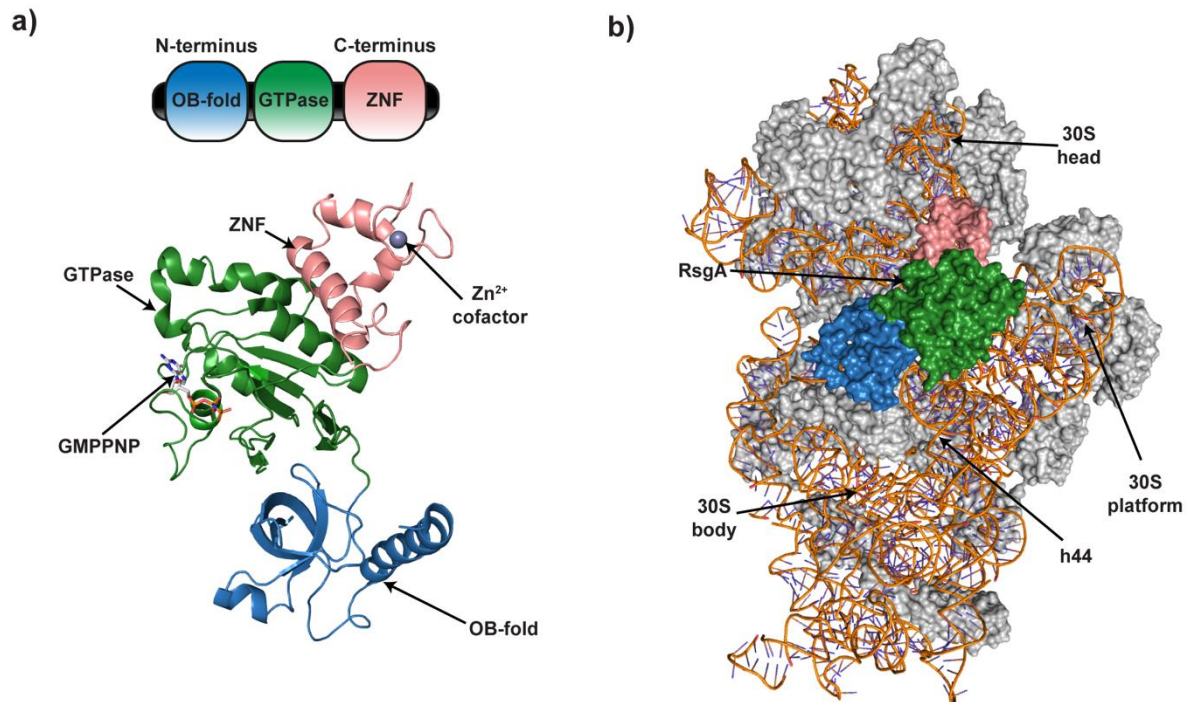
Figure 1.3.2.2.1: The structure and binding site of RsgA. a) Cartoon representation of *E. coli* RsgA (PDB: 5UZ4). The model is coloured according to domain, with the N-terminal OB-fold coloured blue, the central GTPase domain coloured green and the C-terminal ZNF coloured pink. The associated Zn^{2+} cofactor is represented by a grey sphere, and the bound GMPPNP ligand is represented by a stick model and coloured by atom as follows: carbon, white; nitrogen, blue; oxygen, red; phosphorous, orange. b) The cryo-EM structure of *E. coli* RsgA associated with the *E. coli* 30S ribosomal subunit (PDB: 5UZ4) (Razi *et al.*, 2017). The RsgA model is coloured as in (a), and the 30S r-proteins are shown as a grey surface. The rRNA has been coloured as an orange helix. Figure drawn by author using PyMOL.

The affinity of RsgA binding to the 30S subunit is extremely high (66.7± 7.7 nM) (Thurlow *et al.*, 2016), and cryo-EM models have identified the RsgA binding site towards the 3' of h44 (Figure 1.3.2.2.1b), adjacent to the 30S decoding centre (López-Alonso *et al.*, 2017a). The 30S body is contacted by the OB-fold, with residues 49-51 inserted into the minor groove of h44 A-site. The 30S head is contacted by the ZNF, in a position involved in interactions between aa-tRNA and the ribosomal P-site, leading to positioning of the GTPase domain adjacent to the decoding site of h44 to generate a tripartite interaction interface (López-Alonso *et al.*, 2017a). In the case of *E. coli* YjeQ binding to the 30S, h44 is clamped between the switch I loop and a β_6-β_7 extension while in the ON-conformation (Razi *et al.*, 2017), although this extension is lacking in the Firmicutes homologues (Levdikov *et al.*, 2004). The localisation of the binding sites of RsgA suggests that this protein can monitor the maturation state of the rRNA of the P-site and 30S decoding centre. *In vitro*, an excess of RsgA has been shown to dissociate 70S complexes into the constitutive 30S and 50S subunits while destabilising the r-proteins uS2, uS3, uS7, uS12 and bS21 (Himeno *et al.*, 2004), implying that under very specific physiological conditions, RsgA may be capable of rescuing kinetically trapped 30S and 70S ribosomes by

encouraging dissociation of incorrectly bound r-proteins. Further studies into the cytosolic concentration of RsgA are required to lend weight to this hypothesis.

RsgA also directly contributes to the function of a non-GTPase 30S assembly cofactor, RbfA, which is thought to bind strongly to the 5' end of the 17S pre-rRNA prior to encourage maturation via temporary destabilisation to enable RNase activity (Datta *et al.*, 2007). RbfA consists of a singular type-II K-homology (KH) domain, characteristic of nucleic acid binding proteins, and is constitutively expressed in prokaryotes under proliferative conditions. Association of RbfA to the 16S rRNA facilitates correct secondary structure formation of h1 and dramatic alterations in the tertiary structure of h44 and h45, which abolishes the 30S-50S interface and prohibits 70S formation (Datta *et al.*, 2007). RsgA association to the 30S subunit can sterically displace RbfA in a GTPase-independent manner, followed by RsgA-mediated positioning of h44 and h45 in a manner amenable to subunit joining. This suggests that a primary function of RsgA may be to cease RbfA-mediated maturation events and remodel the 16S rRNA into a 70S-compatible conformation during late-stage 30S assembly, immediately prior to 30S pre-IC formation (Goto *et al.*, 2011; López-Alonso *et al.*, 2017a) as a final quality control checkpoint.

1.3.2.2.2 Era

Era is one of the most well-studied bacterial GTPases, in part due to the universal conservation and pleiotropic roles across eukaryotic and prokaryotic organisms including ribosome assembly, apoptosis and cell cycle control (Ji, 2016; Sharma *et al*., 2005; Verstraeten *et al.*, 2011). Era consists of two domains, an N-terminal GTPase domain and a C-terminal RNA-binding KH domain (Figure 1.3.2.1b). Crystallographic studies have identified that the KH domain of Era specifically binds the 3' of the 16S rRNA adjacent to the anti-SD, recognising the highly conserved GAUCA motif (Figure 1.3.2.2.2a), which is universally conserved as part of h45 (Tu *et al.*, 2011; Tu *et al.*, 2009) and forms part of the intersubunit interface (Figure 1.3.2.2.2b). An excess of Era *in vitro* has been shown to inhibit 30S and 50S joining in a similar manner to most intersubunit interface-associated factors (Sharma *et al.*, 2005). When the *Aquifex aeolicus* homologue of Era is bound to the non-hydrolysable GTP analogue GMPPNP, a slight rotation in the KH domain and rearrangement of the switch II loop leads to Era adopting a closed conformation, forming a tight binding pocket around the bound ligand (Figure 1.3.2.2.2a) (Tu *et al.*, 2009). In the *E. coli* Era GDP-bound state, the relative domain positioning opens by between 10 Å and 15 Å to enable stochastic nucleotide exchange, while simultaneously altering the binding interface between Era and the 30S subunit to control association depending on the nucleotide bound (Figure 1.3.2.2.2a) (Tu *et al.*, 2009). While the target binding rRNA sequence is

undoubtably the GAUCA motif, the 12-fold optimum GTPase stimulation relies on the correctly ordered anti-SD sequence (CCUCC), and so in *E. coli*, Era functions to monitor the maturation and correct ordering of the $_{1530}$GAUCACCUCC$_{1539}$ sequence which is crucial for efficient 30S pre-IC formation (Tu *et al.*, 2011). In the mature 30S IC, the Era binding site is occupied by the final r-protein to associate, namely bS1; the association of Era and bS1 on the 30S particle is mutually exclusive. Therefore, Era sterically prevents association of bS1 prior to complete maturation of the anti-SD motif (Himeno *et al.*, 2004). During formation of the 30S pre-IC, IF3 associates with the $_{1532}$UCA$_{1534}$ (Pioletti *et al.*, 2001), which when considered in the context of Era occluding IF3, and bS1 recruitment and mRNA binding to the 30S subunit could feasibly suggest that Era dissociation from the mature 30S subunit could be the final quality-control stage before formation of the 30S pre-IC and initiation of translation.
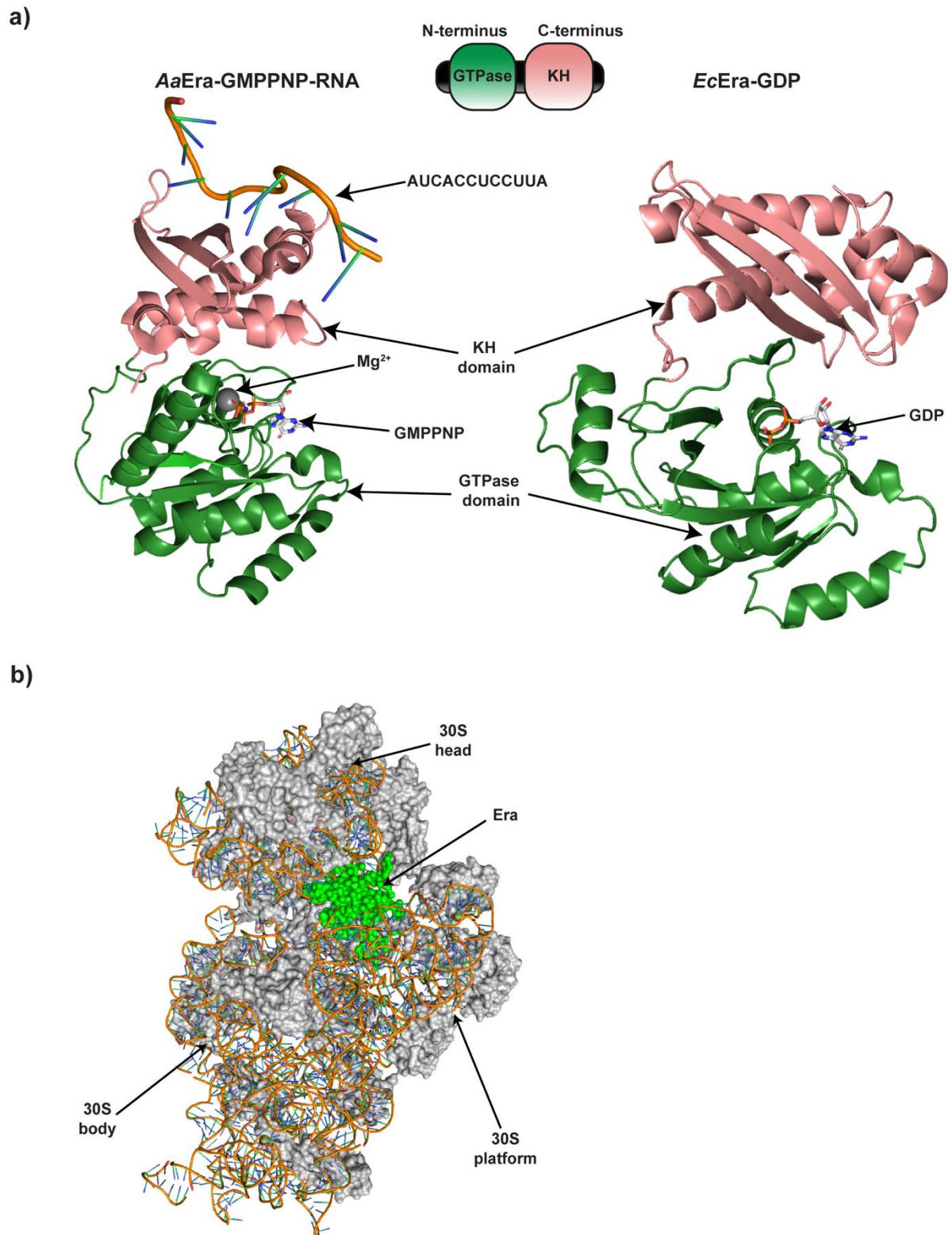
Figure 1.3.2.2.2: The structure and ribosome association site of Era. a) Structural models of the *A. aeolicus* Era bound to GMPPNP and the 12 bp RNA recognition motif AUCACCUCCUAA (PDB: 3IEV) and *E. coli* Era bound to GDP (PDB: 3IEU) (left and right panel respectively). The models are coloured by domain, with the N-terminal GTPase domain coloured green and the C-terminal KH domain coloured pink. The associated ligands are coloured by atom as follows: carbon, white; nitrogen, blue; oxygen, red; phosphorous, orange, and the Mg^{2+} cofactor is represented by a grey sphere. Note the alternate conformations, with the GMPPNP-bound model adopting the open conformation and the GDP-bound model adopting the closed conformation. b) The *E. coli* Era binding site on the *E. coli* 30S ribosome. The cryo-EM structure of the *E. coli* Era 30S association site (PDB: 1X18)

(Sharma *et al.*, 2005) was aligned with the cryo-EM structure of the *E. coli* 30S ribosomal subunit (PDB: 5UZ4) (Razi *et al.*, 2017). The 30S r-proteins are coloured as grey surfaces, and the rRNA is coloured as orange helices. The density assigned to Era is coloured green, although lack of structural detail makes it impossible to identify specific domains, cofactors or ligands.

Until recently, Era was considered essential for prokaryotic growth, however Δ*era* mutations in *S. aureus* have been shown to be viable despite a profound growth defect, at least in part due to a reduction in 70S ribosome content (Wood *et al.*, 2019). An increase in free 50S subunits and a decrease in 30S subunits was also observed, further corroborating that Era is implicated in 30S assembly. Analysis of pre-30S intermediates from Era-depleted *E. coli* cells through use of cryo-EM and quantitative mass spectrometry revealed accumulation of a plethora of both early and late-stage assembly intermediates (Razi *et al.*, 2019). The only consistency between these intermediates was lack of structure of the 30S platform domain (Razi *et al.*, 2019), with electron density relating to uS2, uS5, bS21, h44 and h45 entirely lacking. Furthermore, density for h23 and h24 in the platform region was fragmented, leading the authors to postulate that correct assembly of the platform region relies heavily on overcoming the kinetic barrier associated with h23 and h24 folding, and that Era may directly or indirectly facilitate this folding (Razi *et al.*, 2019).

Overexpression of Era can partially suppress the growth phenotype associated with Δ*rsgA* strains, indicating some functional redundancy (Goto *et al.*, 2011; Guo *et al.*, 2011; Wood *et al.*, 2019), although Era may be involved in a downstream assembly step as destabilisation of h44 by Era decreases the affinity of RsgA binding to the 30S from 58.4 nM to 2.3 µM (Razi *et al.*, 2019). In many bacteria, including *E. coli*, the *era* gene is encoded within the same operon as the *ybeXYZ* cluster. YbeY is a highly conserved endoribonuclease with pleiotropic effects of cellular RNA processing (Davies *et al.*, 2010), deletion of which in *E. coli* leads to 5' processing defects and accumulation of both 17S and semi-processed 16S (16S*) rRNA (Jacob *et al.*, 2013), leading to the formation of defective 70S ribosomes and a slowing of growth. Sharing an operon is often an indication of a biological relationship, and indeed bacterial two-hybrid assays using YbeY as bait have identified that this endoribonuclease interacts directly with both Era via the GTPase domain, and the r-protein uS11 which binds the 30S subunit adjacent to Era (Vercruysse *et al.*, 2016). Overexpression of Era in Δ*ybeY* strains can partially recover the 16S processing defect, implicating other exoribonucleases such as RNase PH, RNase R and RNase II in 16S processing although the precise details of this are unclear (Jacob *et al.*, 2013; Vercruysse *et al.*, 2016). *S. aureus* Era has also been shown to interact directly with the cold-shock DEAD-box RNA helicase CshA (Wood *et al.*, 2019), which has previously been implicated in 50S rRNA processing via direct subunit binding (Giraud *et al.*, 2015). Deletion of this helicase in *S. aureus* led to 16S processing defects at 25°C, suggesting that while unable to directly associate with

the 30S, CshA is important in 30S rRNA processing under cold-shock conditions (Wood *et al.*, 2019) – potentially via unwinding of kinetically trapped non-functional secondary structures. No direct link between CshA activity and 16S processing has been observed however, and as such the possibility of these processing defects being indirect cannot be overlooked especially considering that CshA has been implicated in general metabolic processes such as fatty acid homeostasis (Khemici *et al.*, 2020) and mRNA decay (Ingle *et al.*, 2020). Taken together with the direct interaction between Era and YbeY, this has led to the proposal that Era may function as a scaffold protein, enabling the association of 16S rRNA processing factors to their target sites, and triggering dissociation of both Era and the processing enzymes upon correct processing and maturation of the 16S binding site of Era.

1.3.2.3 GTPases involved in 50S subunit assembly

1.3.2.3.1 RbgA (YlqF)

The late-stage 50S assembly cofactor RbgA is an essential protein in the Firmicutes but is completely absent from all clades of the Proteobacteria, and constitutes an N-terminal cpGTPase domain featuring an unusual K-loop, and a C-terminal AmiR and NasR transcription anti-termination regulator (ANTAR) RNA binding/remodelling domain (Figures 1.3.2.1b and 1.3.2.3.1a) (Do *et al.*, 2008). Interactions between the ANTAR domain and 23S rRNA helices h38, h81 and h85 position RbgA adjacent to the bL5 protein implicated in mediating the interaction between aa-tRNA and the ribosomal P-site (Figure 1.3.2.3.1b) (Do *et al.*, 2008), suggesting that RbgA may be implicated in monitoring the P-site rRNA prior to bL5 association. This interaction places the GTPase domain in close proximity to the conserved peptidyl transferase-implicated nucleotides C928, C942, A2301 and A2354 (Seffouh *et al.*, 2019). GTP hydrolysis upon detection of the correctly conformed rRNA would facilitate entry of RbgA into the GDP-bound OFF state, followed by dissociation and subsequent bL5 association to form the functional 50S P-site (Seffouh *et al.*, 2019).
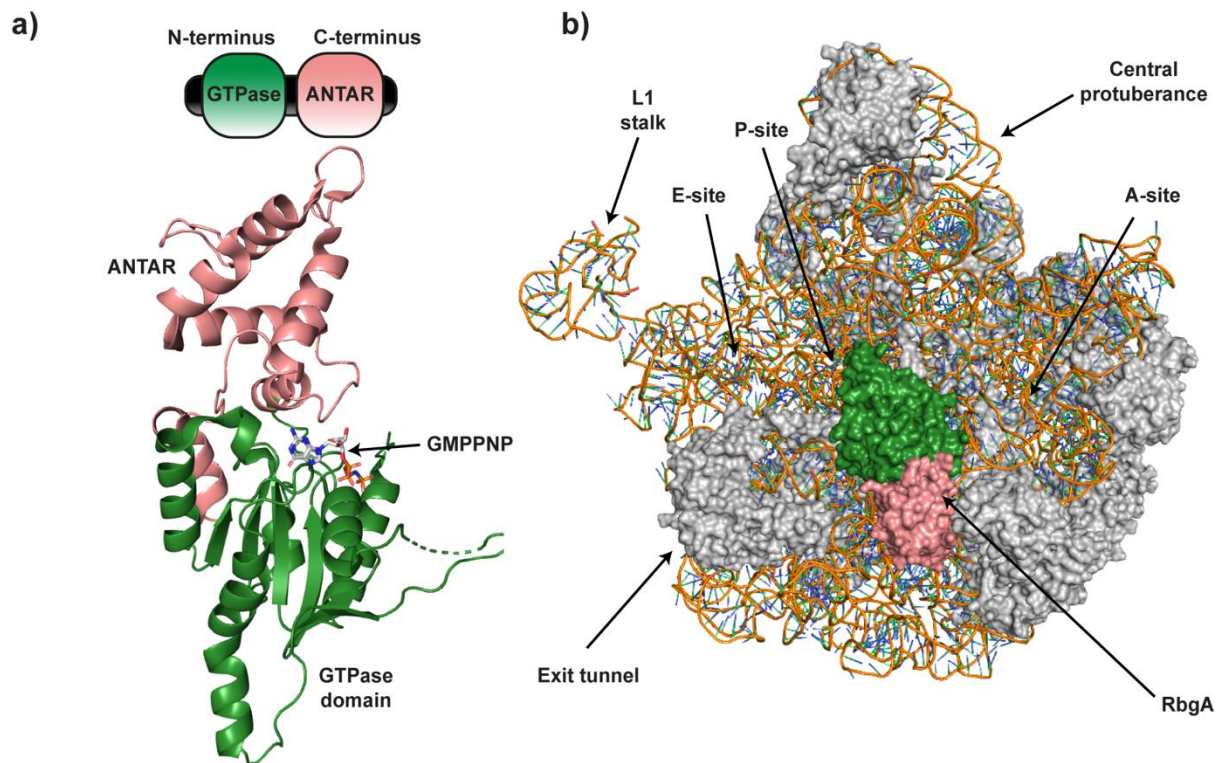
Figure 1.3.2.3.1: The structure and 45S association site of RbgA. a) Crystallographic structure of *S. aureus* RbgA bound to GMPPNP (PDB: 6G12) (Pausch *et al.*, 2018). The N-terminal GTPase domain is coloured green, and the C-terminal ANTAR domain is coloured pink. The GMPPNP ligand is coloured by atom as follows: carbon, white; nitrogen, blue; oxygen, red; phosphorous, orange. b) The cryo-EM structure of *B. subtilis* RbgA associated with the immature 45S ribosomal subunit (PDB: 6PPK) (Seffouh *et al.*, 2019). The 50S r-proteins are coloured as grey surfaces, and the rRNA is shown as an orange helix. RbgA is coloured as in part (a), and the rough positions of the ribosomal A, P and E-sites are indicated.

Mutation of the ANTAR domain of RbgA in *B. subtilis* has been shown to completely abrogate the ribosomal interaction, with a deleterious phenotype *in vivo* (Matsuo *et al.*, 2006), and depletion of this protein through the use of RNA interference results in the formation of 45S intermediates, although it is unclear whether these are kinetically trapped dead-end complexes or whether the presence of RbgA could provoke correct maturation (Uicker *et al.*, 2006). These intermediates were found to be lacking uL16, bL27 and bL36, each of which contribute to ribosomal A-site and P-site integrity to enable efficient aa-tRNA association (Uicker *et al.*, 2006). Both uL16 and bL27 interact with 16S helices implicated in RbgA binding, h38 and h81 respectively, further implicating this RA-GTPase in cofactor recruitment following correct maturation of the ribosomal aa-tRNA binding sites. In the presence of GTP or GMPPNP, RbgA can interact strongly with both the 50S and 45S subunits, although interaction with the mature 50S stimulates a 60-fold increase in GTPase activity, resulting in these complexes being remarkably short-lived (Matsuo *et al.*, 2007).

Suppressor screens were carried out in *B. subtilis* utilising a F6A variant of RbgA, which exhibits a 12-fold reduction in GTPase activation upon binding the mature 50S subunit (Gulati *et al.*, 2014). All identified suppressors mapped to a putative binding groove of the r-protein uL6, mutation of which appeared able to reverse the slow-growth phenotype of the F6A variant. Interestingly, these suppressor strains all accumulated 44S intermediates, which were distinct from the 45S intermediates observed in the F6A variant and RbgA knockdowns (Figure 1.3.2.3.1b), and exhibited an increase in 70S content relative to the F6A strain (Gulati *et al.*, 2014). The 44S subunits isolated were capable of stochastic maturation into mature 50S subunits *in vitro*, perhaps explaining the suppression of the F6A growth defect. Despite the lack of direct interaction between uL6 and RbgA, the suppressor mutations observed in the uL6 binding groove are postulated to destabilise the uL6-50S interaction, preventing the formation of premature intermediates. Likewise, RbgA association to the immature 23S rRNA is thought to properly position h38, h81 and h87 to facilitate the association of secondary r-proteins uL16, bL27 and bL36, which in turn facilitate tertiary r-protein association (such as uL6) at adjacent sites (Gulati *et al.*, 2014).

1.3.2.3.2 HflX

HflX is a universally conserved P-loop NTPase with previously reported GTPase and ATPase activity, implicated in a plethora of processes including rRNA unwinding, 70S and 100S ribosome splitting, manganese homeostasis, hypoxia tolerance and the heat shock response (Coatham *et al.*, 2016; Dey *et al.*, 2018; Jain *et al.*, 2009; Ngan *et al.*, 2021; Sengupta *et al.*, 2018), although despite genetic links, the mechanisms of many of these functions are unknown. Genomically, *hflX* is encoded on a heat shock operon directly downstream of the universal stress response protein *hfq* in *E. coli*, under the control of a heat sensitive promoter (Tsui *et al.*, 1996), although in *S. aureus*, this protein is encoded upstream of an unknown hypothetical protein in a bicistronic operon behind an uncharacterised promoter. This protein exhibits a three-domain architecture in *E. coli* and *S. aureus*, with a conserved HflX N-terminal domain (ND1), a central GTPase domain and a C-terminal domain of unknown function (Figures 1.3.2.1b and 1.3.2.3.2a) (Dutta *et al.*, 2009). ND1 and the GTPase domain are joined by an extended helical linker region, often referred to as the linker helical domain (Figure 1.3.2.3.2a). The conserved ND1 was previously shown to contain a unique nucleotide binding fold capable of binding and hydrolysing ATP in a P-loop independent manner, which was recently shown to be a functional ATP-dependent RNA helicase involved in unwinding heat damaged rRNA secondary structures to enable repair (Dey *et al.*, 2018). The helicase activity of HflX can be activated via generic salt washing using 1.5 M NaCl to induce aberrant secondary structure formation (Dey *et al.*, 2018), and as such it stands to reason that this protein could be involved in rescuing kinetically trapped ribosomal subunit

intermediates during the assembly process, both generally speaking and in the context of the heat shock response.
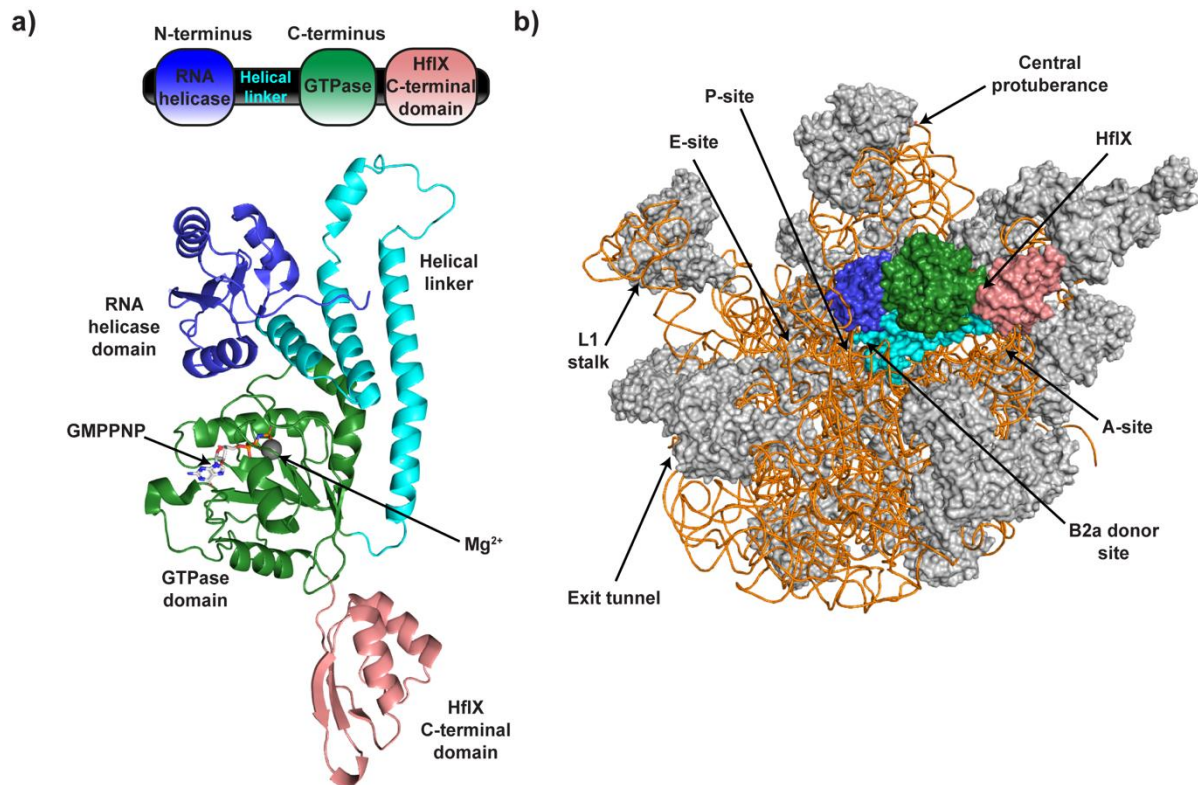
Figure 1.3.2.3.2: The structure and 50S association site of HflX. a) A cryo-EM structural model of *E. coli* HflX bound to GMPPNP (PDB: 5ADY) (Zhang *et al.*, 2015). The model is coloured by domains, with the ND1 RNA-helicase domain coloured blue, the helical linker domain coloured cyan, the GTPase domain coloured green and the C-terminal domain coloured pink. The Mg^{2+} cofactor is coloured grey, and the bound GMPPNP ligand is coloured by atom as follows: carbon, white; nitrogen, blue; oxygen, red; phosphorous, orange. b) Cryo-EM structure of *E. coli* HflX-GMPPNP associated with the *E. coli* 50S ribosomal subunit (PDB: 5ADY) (Zhang *et al.*, 2015). 50S r-proteins are coloured grey, and the rRNA is coloured orange. HflX is coloured as in (a). Note that the helical linker domain contacts deep into the ribosomal P-site, the presence of deacyl-tRNA in which regulates the RNA-helicase activity of HflX. Also note the position of the HflX N-terminal domain relative to the 50S donor site which contributes to formation of the critical intersubunit bridge, B2a, during 70S assembly. Nucleotide bases have been removed for clarity.

Historically, HflX has been reported to bind to the 30S, 50S (Figure 1.3.2.3.2b) and 70S ribosomal particles independently of guanine nucleotides (Blombach *et al.*, 2011; Jain *et al.*, 2009). This was clarified using isopycnic ultracentrifugation to example the interaction between HflX and the ribosomal particles in different nucleotide-bound states. An enrichment of HflX-50S and HflX-30S complexes were observed in the presence of GMPPNP, with dissociation of the RA-GTPase from the 50S requiring GTP hydrolysis (Basu and Yap, 2017; Zhang *et al.*, 2015). This pattern of nucleotide-dependence was recapitulated in the case of mature 70S ribosomes, with the addition that while bound to GTP, HflX is capable of rapid 70S splitting in a GTPase-independent fashion. The GTPase

activity of HflX was partially inhibited by the presence of aa-tRNA in the ribosomal P-site, but not by the presence of uncharged tRNA, suggesting that the preferred substrates of HflX-mediated splitting are translationally stalled ribosomes (Zhang *et al.*, 2015), potentially as a means of rescue and recycling of stalled complexes. The GTP-independent splitting activity of HflX can be explained due to the preferred binding site of this protein at the subunit interface, with the N-terminal domain protruding towards the 50S PTC and disrupting the intersubunit bridge B2a (Coatham *et al.*, 2016) in a manner similar to RRF during canonical post-termination subunit recycling. It is therefore apparent that HflX can act as an assembly factor, rescuing kinetically trapped assembly intermediates, as an anti-association factor through steric hindering of 70S formation, and as a 70S splitting factor, rescuing stalled ribosomes under stress conditions (Zhang *et al.*, 2015).

The dissociation of 100S ribosomal hibernation complexes has been attributed partially to IF3, EF-G and RRF *in vivo*, the predominant splitting factor has yet to be uncovered (Matzov *et al.*, 2017). HflX has demonstrated the capacity to split 100S complexes into first 70S, then 30S and 50S complexes in a GTPase dependent manner, as this dissociation was inhibited when HflX was bound to the non-hydrolysable GTP analogue, GMPPNP (Basu and Yap, 2017). The transcriptional regulation of *hflX* renders this protein unlikely to be the primary splitting factor, as expression is highest during heat shock and not during general growth (Tsui *et al.*, 1996), and as such the function of the 100S splitting activity of HflX is unknown. It remains a possibility that heat-damaged 70S ribosomes could be inactivated and stored in 100S complexes selectively, however this process has never been shown.

1.4 The stringent response

In situ, population dynamics of bacteria often follow repeat 'feast-famine' cycles, in which the stochastic environmental conditions, particularly relating to nutritional availability, define the opportunity for bacteria to undergo proliferative growth. Immediate utilisation and uptake of available micronutrients coupled with potentially toxic waste product efflux limit populations to stationary phase for the vast majority of the time, with changing conditions triggering outgrowth (Jaishankar and Srivastava, 2017). The control of this metabolic dichotomy relies on the highly conserved stress response network termed the stringent response, in which production of two guanine nucleotide alarmones (Figure 1.4), guanosine 3',5'-bis(diphosphate) and guanosine 3'-diphosphate 5'-triphosphate (ppGpp and pppGpp respectively), facilitate modulation of the cellular transcriptome and proteome in order to survive transient conditions of stress (Irving *et al.*, 2020; Steinchen *et al.*, 2020). Historically, (p)ppGpp was referred to as magic spot following the observation of a highly variable 'magic spot' on TLC plates when studying cellular nucleotide pools (Cashel, 1969;

Dalebroux and Swanson, 2012). A third alarmone, guanosine 3'-diphosphate 5'-monophosphate (pGpp) has been identified *in vitro* in *Enterococcus faecalis* (Gaca *et al.*, 2015) and *in vivo* in *B. subtilis* and *Bacillus anthracis* (Yang *et al.*, 2020), with functions distinct from the more well-studied (p)ppGpp molecules.
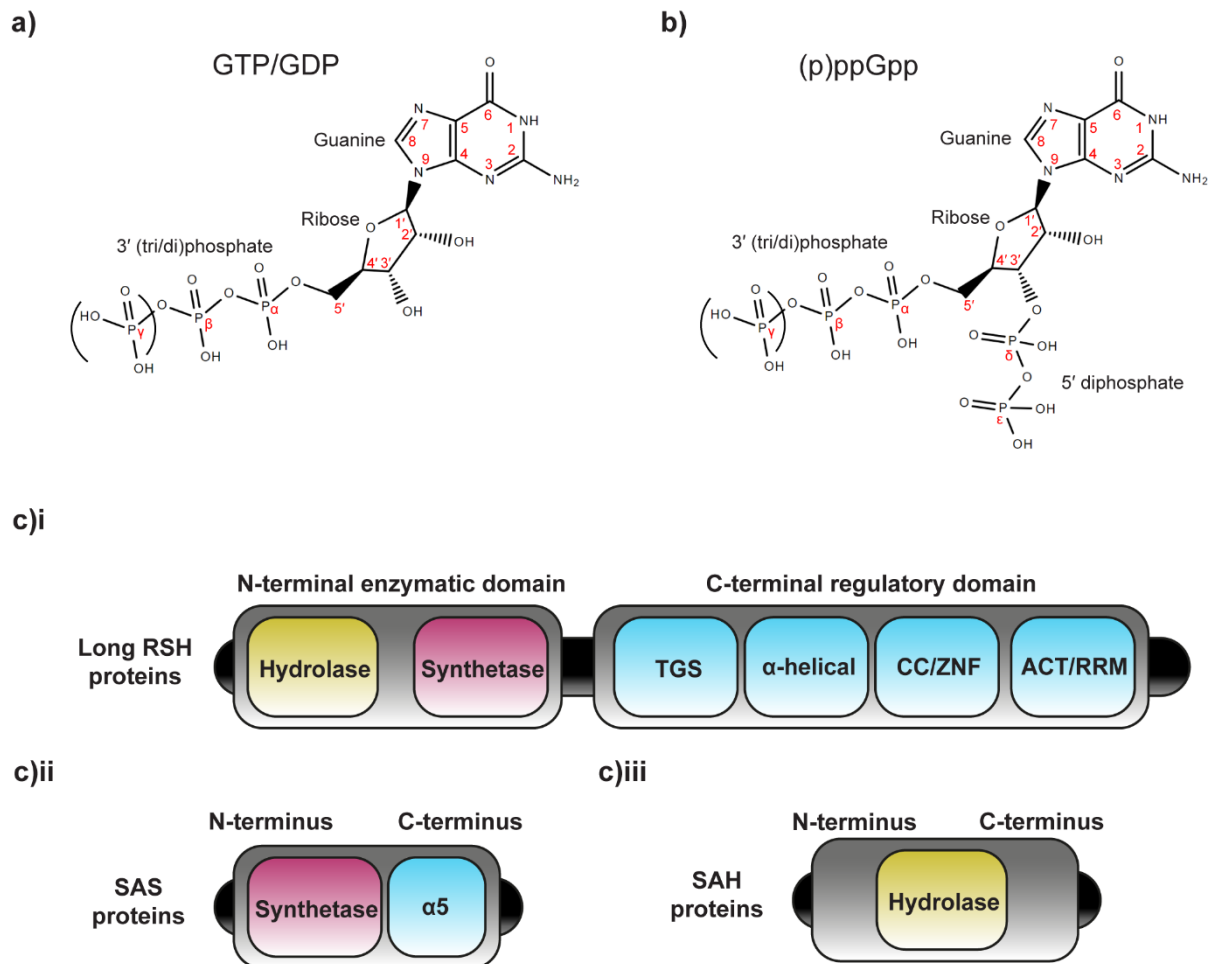
Figure 1.4: The structures of guanine nucleotides GTP, GDP, ppGpp and pppGpp. a) The displayed formula of GTP and GDP, differentiated by the respective presence and absence of the γ-phosphate group indicated with brackets. b) The displayed formula of (p)ppGpp, with pppGpp containing a GTP backbone and ppGpp containing a GDP backbone. The major guanine, ribose and di/triphosphate groups are named, and the standard nomenclature of specific groups and positions are indicated in red, as referenced throughout this thesis. For pGpp, both the β- and γ-phosphate are absent from the formula shown in (b). c) The domain structure of i) long RSH proteins, ii) SAS proteins and iii) SAH proteins. i) Long RSH proteins consist of a two-macrodomain structure, with an N-terminal enzymatic domain containing the hydrolase and synthetase subdomains, and a C-terminal regulatory domain containing the TGS, α-helical, CC/ZNF and ACT/RRM subdomains. ii) SAS proteins constitute a single synthetase domain with a C-terminal α-helix (α5), responsible for forming intermonomer contacts during tetramerization. iii) SAH proteins constitute a single hydrolase domain.

During the *E. coli* stringent response, intracellular concentrations of (p)ppGpp can rise to between 1 mM and 2 mM (Cashel, 1975), with a concurrent decrease in the intracellular pools of other guanine nucleotides such as GTP, GDP and GMP (Varik *et al.*, 2017). This leads to regulation of cellular

metabolism via both direct and indirect processes, including generally reducing transcription (Durfee *et al.*, 2008) and translation (Bennison *et al.*, 2019; Corrigan *et al.*, 2016; Kästle *et al.*, 2015). Ultimately, the major impact of the stringent response is greatly reduced growth and metabolism to impart enhanced tolerance to conditions of nutrient deprivation and environmental stress, which has been implicated in such events as virulence, stationary phase, sporulation, persister formation and biofilm formation (Li *et al.*, 2015; Steinchen *et al.*, 2020).

1.4.1 Regulation of the stringent response

Turnover of (p)ppGpp in bacteria is carried out by members of the RelA/SpoT homologue (RSH) superfamily, named as such after the initially characterised RelA and SpoT from *E. coli*. There are three main subclasses of RSH proteins, the long RSH enzymes containing both synthetase and hydrolase domains (Figure 1.4ci), the small alarmone synthetases (SAS) (Figure 1.4cii) and the small alarmone hydrolases (SAH) (Figure 1.4ciii), which together regulate the intracellular (p)ppGpp concentration (Irving and Corrigan, 2018). The activities of these proteins are regulated on both a transcriptional and post-translational level, with each responding to distinct environmental stimuli. The stringent response can be activated in response to a plethora of cellular stressors due to the range of signals detected by both RSH proteins and SAS proteins, such as acid stress, fatty acid starvation, and the highly characterised amino acid starvation (Cashel, 1969; Seyfzadeh *et al.*, 1993), although in the photosynthetic cyanobacteria *Synechococcus elongatus* the absence of UV light has been shown to induce (p)ppGpp synthesis in a unique manner reflective of this organism's lifestyle (Hood *et al.*, 2016).

1.4.1.1 Long RSH proteins

Long RSH proteins typically constitute distinct N and C terminal macrodomains (Figure 1.4ci). The N-terminal macrodomain constitutes the enzymatic Mg^{2+}-dependent synthetase subdomain, which can catalyse pyrophosphate transfer from an ATP donor to the 3' ribose hydroxyl group of the GDP/GTP acceptor, as well as the Mn^{2+}-dependent hydrolase subdomain which hydrolyses (p)ppGpp to either GTP or GDP via release of the 3' pyrophosphate (Figure 1.4.1.1a) (Lee *et al.*, 2018). The C-terminal macrodomain contains four signal receptive regulatory subdomains, namely the ThrRS, GTPase and SpoT (TGS), α-helical, conserved cysteine/ZNF (CC)/ZNF and aspartate kinase, chorismite and TyrA/RNA recognition motif (ACT/RRM) subdomains (Figure 1.4.1.1a), although the precise makeup of the long RSH C-terminal domain differs between homologues (Atkinson *et al.*, 2011; Loveland *et al.*, 2016). The C-terminal domain of long RSH proteins can facilitate homodimerization, enabling hydrolysis of (p)ppGpp but preventing synthesis (Yang and Ishiguro, 2001). These bifunctional proteins often constitute the sole means of (p)ppGpp hydrolysis within the cell, and as such are essential for

cellular viability as unchecked accumulation of (p)ppGpp is both bacteriostatic and toxic (Lee *et al.*, 2018). Due to this the default setting of long RSH protein during proliferative conditions is synthetase OFF hydrolase ON.
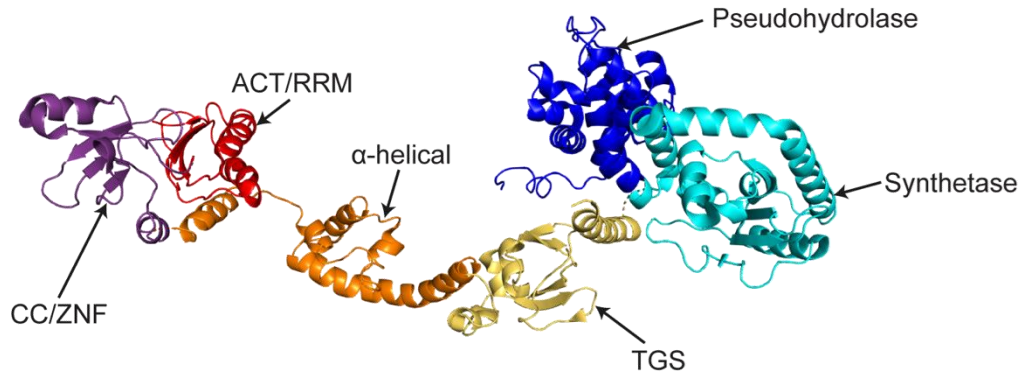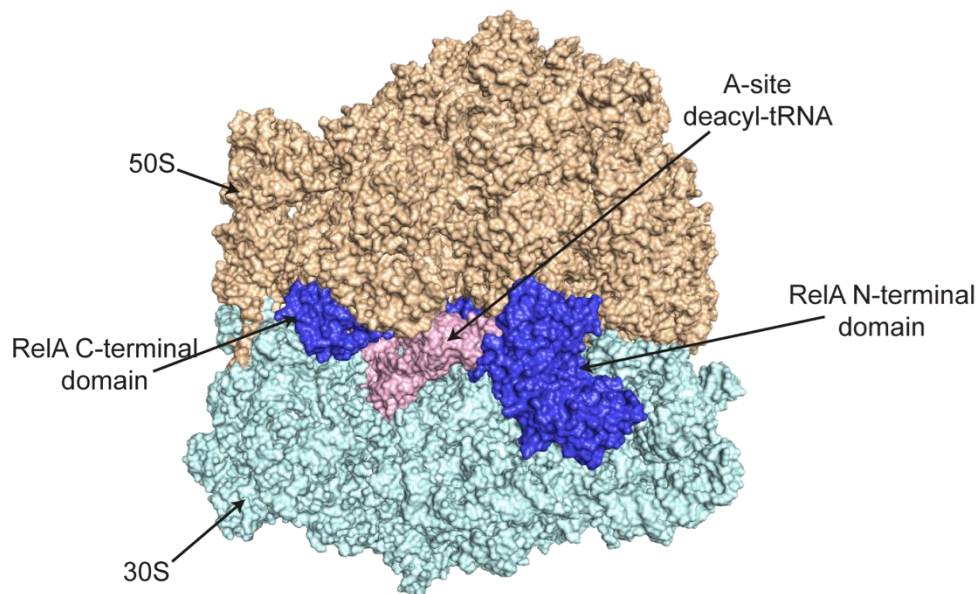
Figure 1.4.1.1: The interaction between RelA and the 70S ribosome. a) The domain structure of a long RSH protein, namely *E. coli* RelA (PDB: 5KPX, chain 33) (Loveland *et al.*, 2016). The enzymatic N-terminal macrodomain consists of the pseudohydrolase (blue) and the synthetase (cyan) subdomains, and the C-terminal regulatory domain consists of the TGS (beige), α-helical (orange), CC/ZNF (purple) and ACT/RRM (red) subdomains, which adopt an elongated conformation. b) The structure of *E. coli* RelA bound to the ribosome activation complex, including the 30S subunit (cyan, PDB: 5KPX, chains 6-26), the 50S subunit (tan, PDB: 5KPX, chains A-Z, 1-5, 27 and 28), the A-site deacylated-tRNA (pink, PDB: 5KPX, chain 30) and RelA (dark blue), PDB: 5KPX, chain 33). Note that the C-terminal regulatory domain of RelA wraps around the A-site tRNA, and the N-terminal enzymatic domain is exposed to the cytosol.

In Gram-negative organisms such as *E. coli*, the RSH gene is duplicated into the bifunctional SpoT and the homologous yet monofunctional synthetase RelA (Mittenhuber, 2001), which lacks hydrolase activity due to complete loss of the crucial HDxxED motif. Little is known regarding the activation of

SpoT, other than the fact that the hydrolase/synthetase switch depends on conformational antagonism between the N-terminal subdomains, governed by secondary factor association such as by the acyl carrier protein in response to fatty acid starvation (Battesti and Bouveret, 2006) and the HPr/Rsd sugar sensing network (Lee *et al.*, 2018). Upon fatty acid starvation, phosphate limitation or carbon limitation, pppGpp synthesis is activated by SpoT using the preferred GTP acceptor substrate (Germain *et al.*, 2019). The long RSH proteins in Gram-positive organisms, usually named Rel, bear similarity to the bifunctional *E. coli* SpoT due to a catalytic loop featuring the conserved RxKD motif, which imparts a strong electrostatic attraction to the γ-phosphate of GTP (Sajish *et al.*, 2007), although *S. aureus* Rel has been shown to synthesise (p)ppGpp in response to amino acid starvation (Geiger *et al.*, 2010). This preference in substrate indicates downstream differences between the potency and targets of ppGpp compared to pppGpp, which can be differentially synthesised in response to different stressors. Indeed, Gram-negative bacteria seem to prefer ppGpp synthesis, whereas Gram-positive bacteria seem to preferentially synthesise pppGpp, although the significance and rationale for this is unknown (Mechold *et al.*, 2013).

The evolutionary benefit of maintaining the pseudo-hydrolase domain in RelA was unknown until recently, when it was found that this domain while enzymatically inactive, is crucial for regulation of the synthetase activity via an extended loop between α6 and α7 (Sinha and Winther, 2021), possibly by sterically preventing (p)ppGpp binding to the pseudo-hydrolase domain active site, which would also prevent ATP binding to the synthetase subdomain (Tamman *et al.*, 2020). Activation of RelA synthetase activity relies on the association of uncharged tRNAs with the ribosomal A-site, which is followed by ribosome stalling (Sinha and Winther, 2021). The TGS can interact directly with uncharged tRNA (Figure 1.4.1.1b), while the CC/ZNF and ACT/RRM subdomains associate with the 23S h38 and the A-site finger respectively. The orientation of RelA on the ribosome displays the N-terminal synthetase and pseudo-hydrolase domains to the cytosol, where ppGpp synthesis occurs using the preferred GDP substrate (Brown *et al.*, 2016; Loveland *et al.*, 2016). It has also been proposed that an initial RelA-tRNA complex forms prior to ribosome association, suggesting that stringent response activation may occur in this manner upon amino acid starvation when charged tRNAs are scarce (Winther *et al.*, 2018).

1.4.1.2 SAS proteins

In addition to the bifunctional Rel protein, most Gram-positive bacteria in the Firmicutes phylum also encode two SAS proteins, namely RelQ and RelP in *S. aureus* and *B. subtilis* (Steinchen and Bange, 2016), although these are generally referred to as SAS1 and SAS2 respectively (Beljantseva *et al.*,

2017). These proteins consist of a single domain homologous to the synthetase domain of long RSH proteins (Figure 1.4cii), lacking both the hydrolase domain and C-terminal regulatory machinery. Despite their sequential homology, the activity of RelP and RelQ differs greatly, exhibiting different transcriptional profiles and responding to different stressors, although both are predominantly implicated in cell wall stress (Geiger *et al.*, 2014), including ethanol stress (Pando *et al.*, 2017) and antibiotic stress (Thackray and Moir, 2003). This regulation is primarily on the transcriptional level, with *relP* transcription induced early during the stringent response in response to cell wall stress, and *relQ* transcribed more heavily during exponential growth (Geiger *et al.*, 2014). The specialist cell wall stress alternative sigma factor σ^M in *B. subtilis* also upregulates transcription of *relP* proteins in response to teichoic acid depletion and cell envelope damage (Eiamphungporn and Helmann, 2008), and the two component system *vraRS* which is activated in response to cell wall damage has been shown to upregulate RelP production in *S. aureus* (Geiger *et al.*, 2014).

Structural data has revealed that RelQ and RelP from *B. subtilis* and *S. aureus* respectively form highly ordered homotetramers, displaying two-fold rotational symmetry with a central cleft and an extremely highly conserved helical interface (Manav *et al.*, 2018; Steinchen *et al.*, 2015; Steinchen *et al.*, 2018). This tetramerization is dependent on the presence of a stabilising C-terminal helix, α5. *In vitro*, the synthetase activity of *B. subtilis* RelP is significantly higher than RelQ, although RelQ can be stimulated in an allosteric fashion by the binding of pppGpp at the homotetramer interface which serves to stabilise the catalytic G-loop (Steinchen *et al.*, 2018), and it has been hypothesised that RelQ may function as a signal amplifier to augment the pppGpp production by RelP or Rel, supported by the semi-constitutive expression of this protein during exponential phase (Geiger *et al.*, 2014). *E. faecalis* RelQ can bind to small RNAs in the homotetramer cleft while in the absence of pppGpp, which inhibits the synthetase activity (Beljantseva *et al.*, 2017). Notably, the binding consensus GGAGG exhibits strong similarity to the SD sequence, however the specific single stranded RNA binding partners of RelQ are unknown. It remains a possibility that this protein could be involved in post-transcriptional regulation of stringent response associated genes, as the presence of pppGpp displaces RNA binding – potentially allowing transcription (Beljantseva *et al.*, 2017).

Recent bioinformatic analyses of the immediate genomic environment surrounding genomic SAS genes revealed that some subclasses can be encoded in overlapping two or three-gene operons in a similar manner to toxin-antitoxin (TA) systems in the genomes of Firmicutes, Proteobacteria and Actinobacteria, as well as 12 other classes on both Gram-negative and Gram-positive bacteria (Jimmy *et al.*, 2020). These have been coined toxic SAS (ToxSAS) systems, and have presumably evaded

detection to date due to their novel antitoxin-encoding genes avoiding the typical 'guilt by association' method of identifying TA systems, in addition to the fact that the long RSH SpoT is capable of detoxifying all tested ToxSAS proteins (Jimmy *et al.*, 2020). Within this subgroup of ToxSAS proteins, several were uncovered which synthesise adenosine 3',5'-bis(diphosphate) (ppApp). The SAS protein Tas1 from *Pseudomonas aeruginosa* is a toxin and a type VI secretion factor, leading to rapid synthesis of ppApp when within the target cell (Ahmad *et al.*, 2019), causing rapid growth inhibition and ultimately cell death. This protein is encoded adjacent to the cognate antitoxin. While the functions of these ToxSAS modules are as of yet unknown, it has been hypothesised that they may function, in addition to the regular TA system roles of genomic maintenance, during phage infection in order to prevent the lytic cycle and protect the population as a whole (Jimmy *et al.*, 2020) or potentially even as intercellular secreted toxins.

In Gram-negative bacteria, only one SAS protein has been identified to date, which forms a subclass referred to as RelV (Dasgupta *et al.*, 2014). Unique to bacteria of the *Vibrio* genus, RelV has been implicated in production of (p)ppGpp in response to fatty acid starvation (Dasgupta *et al.*, 2014) and anaerobic conditions, where in *Vibrio cholera* this protein plays a key role in the expression of cholera toxin (Oh *et al.*, 2014). This may be a key regulator of *V. cholerae* virulence while in the anaerobic gut environment.

1.4.1.3 SAH proteins

7 subgroups of SAH proteins have been predicted in bacteria through bioinformatic analyses (Atkinson *et al.*, 2011), although biochemical studies have only succeeded in identifying a single functional SAH protein to date. The $relH_{Cg}$ protein from the Gram-positive bacterium *Corynebacterium glutamicum* was shown to possess Mn^{2+}-dependent (p)ppGpp hydrolase activity *in vitro* and when recombinantly expressed in *E. coli* (Ruwe *et al.*, 2018). The independent loss of this gene in related species suggests a nonessential role in cellular homeostasis, and as such the precise function of this protein *in vivo* remains to be elucidated, but may be involved in efficient resumption of growth following re-entry into favourable conditions (Ruwe *et al.*, 2018).

In eukaryotic organisms such as humans (*Homo sapiens*) and fruit flies (*Drosophila melanogaster*), an RSH hydrolase domain homologue Mesh1 has been identified, although eukaryotic organisms lack long RSH or SAS proteins required to carry out a stringent response (Sun *et al.*, 2010). Mesh1 deletion in *D. melanogaster* retarded growth and impaired starvation resistance and severe reprogramming of the transcriptome (Sun *et al.*, 2010). Despite being a SAH and RSH hydrolase domain homologue, the

in vivo substrate for Mesh1 is nicotinamide adenine dinucleotide phosphate (NADPH). Upon transcription of *mesh1* under amino acid starvation conditions, Mesh1 dephosphorylates the dinucleotide NADPH, leading to depletion of NADPH and subsequent ferroptosis - iron-dependent cell death (Ding *et al.*, 2020). In humans, dysregulation of ferroptosis leads to a myriad of debilitating and fatal diseases, and research into the potential role of the SAH protein Mesh1 in this process is ongoing (Han *et al.*, 2020; Ying *et al.*, 2021).

1.4.1.4 Other proteins involved in (p)ppGpp turnover

Aside from long RSH, SAS and SAH proteins, (p)ppGpp turnover can be regulated by non-RSH factors. *E. coli* encodes the guanosine pentaphosphate phosphatase GppA, which is responsible for the conversion of pppGpp into ppGpp through hydrolysis of the γ,β-phosphodiester link (Mechold *et al.*, 2013). In *E. coli*, ppGpp is a much more potent effector relating to the regulation of cell growth, and as such pppGpp synthesised by SpoT can be rapidly converted to ppGpp. No homologues of GppA have been identified in Gram-positive organisms, suggesting a more nuanced role of the ppGpp/pppGpp ratio depending on the incident stressor.

Recently, the role of the third alarmone molecule pGpp has been highlighted in *B. subtilis* and *B. anthracis*, with distinct functions compared to (p)ppGpp (Yang *et al.*, 2020), with emphasis on purine metabolism as opposed to translation. While RSH homologues are capable of synthesising pGpp *in vitro*, the enzymatic activity in this context is much slower than for the synthesis of (p)ppGpp, and the affinity of these proteins for the substrate GMP is comparatively low (Yang *et al.*, 2019). Thus, this mechanism of pGpp production is thought to be irrelevant physiologically. The nucleoside diphosphate linked to any moiety 'X' (NuDiX) alarmone hydrolase A (NahA) from the *Bacillus* genus was found to be capable of the rapid conversion of both ppGpp and pppGpp to pGpp (Yang *et al.*, 2020), which facilitated rapid recovery from stationary phase. Furthermore, deletion of this gene reduced competitive fitness against wild-type cells, suggesting that the interconversion between (p)ppGpp and pGpp is a crucial aspect of nucleotide fine-tuning during the stringent response. Previously identified NuDiX hydrolases in *E. coli* and *Thermus thermophilus* are capable of hydrolysing (p)ppGpp, although they yield the stringent response-inactive guanosine 3',5'-bis(monophosphate) (pGp) (Ooga *et al.*, 2009; Zhang *et al.*, 2018), and as such are considered to be part of an alternative (p)ppGpp removal pathway during resumption of growth rather than part of the finely-tuned stringent response network, although the conditions under which these proteins function are unknown due to the continued essentiality of SpoT.

1.4.2 Downstream targets of the stringent response

1.4.2.1 Alteration of the transcriptome

In *E. coli*, induction of the stringent response leads to a change in the transcription of over 700 genes, including an increase in amino acid biosynthesis and transport related genes, other such nutrient scavenging effectors, and a decrease in the synthesis of rRNA (Sanchez-Vazquez *et al.*, 2019). In Gram-negative bacteria, this effect is mediated through direct association of (p)ppGpp to the RNAP at two distinct sites (Figure 1.4.2.1a): site 1, formed by the β'-ω subunit interface of RNAP, which is implicated in the response to DNA breakage and repair (Sivaramakrishnan *et al.*, 2017); and site 2, formed at the interface of RNAP β' subunit and the associated transcription factor DksA, which is implicated in full activation of the σ^S response in a synergistic manner via both direct binding and indirect downregulation of the housekeeping sigma factor, σ^{70} (Ross *et al.*, 2016). DksA-(p)ppGpp association with RNAP also destabilises intrinsically unstable open DNA-RNAP complexes, such as that formed during transcription of the rRNA-encoding *rrn* operon and during transcription of the housekeeping sigma factor σ^{70}, leading to a decrease in transcription of select genes. Likewise, positive allostery of the RNAP complex is thought to activate transcription of genes which form an innately stable open complex, including those involved in amino acid uptake and biosynthesis, in addition to alternative stress sigma factors such as σ^E and σ^S (Doniselli *et al.*, 2015).
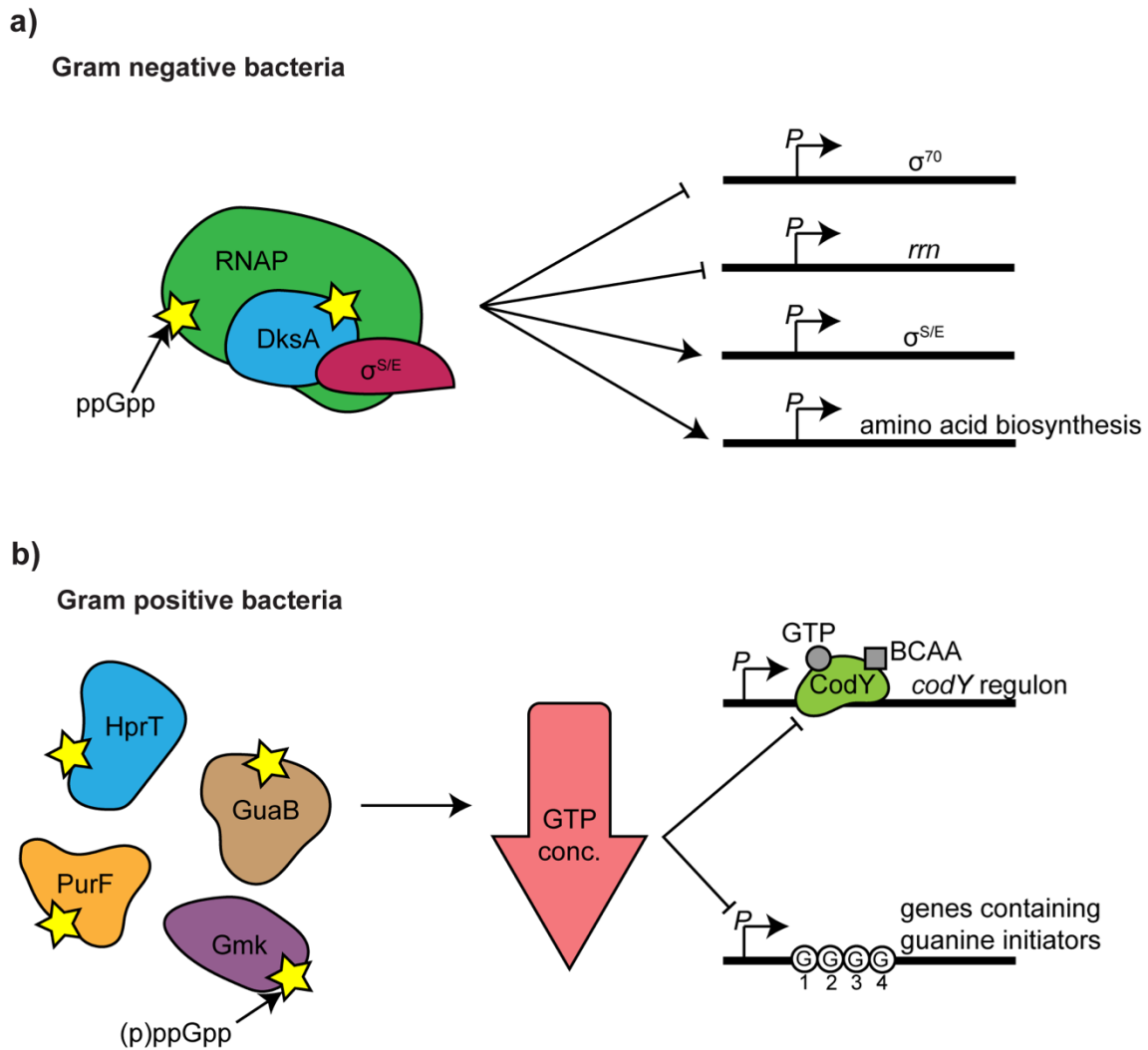
Figure 1.4.2.1: The effect of the stringent response on transcription in Gram-negative and Gram-positive bacteria. a) In Gram-negative organisms, an initial complex forms between RNAP, DksA and ppGpp, the latter of which binds at two distinct sites – both directly to the interface between RNAP and DksA and also at a distal site on RNAP. This leads to destabilisation of the open complex of a variety of promoters, including the *rrn* operon and *rpoD*, which encodes the housekeeping factor σ^{70}. Other genes are upregulated, depending on an intrinsically high open complex stability, such as genes encoding amino acid biosynthesis and uptake systems and the alternative stress response sigma factors σ^E and σ^S. **b)** In Gram-positive organisms, (p)ppGpp binds to and inhibits HprT, Gmk, GuaB and PurF, all of which are involved in the GTP synthesis pathway. This, coupled with the utilisation of GTP during (p)ppGpp synthesis, leads to a decrease in the cellular GTP pool and derepression of the *codY* regulon, increasing transcription of up to 150 genes involved in stationary phase and the stress response. Low GTP pools also leads to unfavourable transcription initiation from initiation sites containing guanine nucleotides in the +1, +2, +3 or +4 sites, which includes the *rrn* operon (Doniselli *et al.*, 2015; Geiger and Wolz, 2014).

In Gram-positive bacteria, a mutation of the MAR motif at the N-terminus of the RNAP ω-subunit renders (p)ppGpp incapable of association (Hauryliuk *et al.*, 2015). Instead, transcription is influenced by the rapid decrease in cellular GTP levels during induction of the stringent response (Geiger and Wolz, 2014), during which GTP is used as a pyrophosphate acceptor (Figure 1.4.2.1b). This decrease in GTP concentration is subject to positive feedback, as the newly synthesised (p)ppGpp can bind to and

inhibit the activity of four enzymes involved in purine synthesis: the inosine monophosphate (IMP) amidophosphoribosyl transferase PurF, the IMP dehydrogenase GuaB, the hypoxanthine phosphoribosyltransferase HprT and the guanylate kinase Gmk (Corrigan *et al.*, 2016; Irving *et al.*, 2020; Kriel *et al.*, 2012). This lowering of the GTP pool contributes to alteration of transcription in two major ways. Firstly, many genes contain guanine as an initiating nucleotide, which normally encompasses the +1 – +4 promoter sites. This selection of genes involves the *rrn* operon and genes encoding many ribosome maturation cofactors (Krasny and Gourse, 2004; Kästle *et al.*, 2015). While lowered GTP levels can reduce the transcription initiation rate of these promoters, low-level expression can still occur, which may facilitate low-level ribosome assembly and permissive translation during the stringent response (Vinogradova *et al.*, 2020). This method of transcriptional regulation seems restricted to Gram-positive bacteria, as in *E. coli* increasing (p)ppGpp concentration had no effect on initiation rate of guanine-containing promoters (Haugen *et al.*, 2008), despite being known to bind and inhibit GuaB and PurF (Wang *et al.*, 2018). The second mechanism of transcriptional regulation relies on the repressor protein of the *codY* regulon, CodY. Along with the branched chain amino acids leucine, isoleucine and valine, GTP is a cofactor which upon association with CodY, enables DNA binding and repression of transcription of many genes involved in late-stage growth, predominantly concerning amino acid biosynthesis, but also stationary phase entry, sporulation and biofilm formation (Geiger and Wolz, 2014; Pohl *et al.*, 2009). In *S. aureus*, over 150 genes are upregulated during the stringent response, seven of which are regulated independently of the *codY* regulon (Geiger and Wolz, 2014). Of the 161 downregulated genes in the *S. aureus* stringent response, none are dependent on CodY activity, and as such are considered to be regulated by the alternative stress response sigma factor σ^B (Miller *et al.*, 2012). Furthermore, a family of (p)ppGpp-specific riboswitches has recently been identified in the Firmicutes (Sherlock *et al.*, 2018), with associated genes including amino acid synthesis enzymes and ATP-binding cassette (ABC)-transporters such as NatA. This finding represents not only a novel link between (p)ppGpp and ABC-transporters, but also between NatA-mediated Na^+ homeostasis and highlights the fact that the plethora of genes under the control of (p)ppGpp is more varied than expected.

1.4.2.2 Inhibition of ribosome assembly and translation

It has long been known that the stringent response reduces *de novo* ribosome formation, however until recently this was attributed solely to the reduction in *rrn* transcription. Whole open reading frame (ORF)eome screening of initially *S. aureus* (Corrigan *et al.*, 2016) and subsequently *E. coli* (Zhang *et al.*, 2018) identified that five RA-GTPases are bound and inhibited by (p)ppGpp, namely RsgA, RbgA (Gram-positive bacteria only), Era, HflX and ObgE (Figure 1.4.2.2) (Feng *et al.*, 2014). The mechanism

of inhibition is currently uncertain, although multiple crystallographic studies and competition assays have revealed that (p)ppGpp is a competitive inhibitor of GTPase activity which associates with the active site (Corrigan *et al.*, 2016; Feng *et al.*, 2014; Pausch *et al.*, 2018), leading to a reduction in mature 70S biogenesis and a decrease in growth rate. Notably, the determinant features of these RA-GTPases which enables (p)ppGpp binding are unknown, although structural studies have revealed that the guanosine-5'-(tri/di)phosphate backbone of (p)ppGpp is recognised in an identical manner to GTP and GDP (Pausch *et al.*, 2018). The RsgA homologue from *B. subtilis*, YloQ, is incapable of this binding (Corrigan *et al.*, 2016), although further investigation into the mechanistics of this selectivity remain difficult due to the innate flexibility of the switch I loop rendering the precise (p)ppGpp interaction site unresolved during X-ray crystallography (Levdikov *et al.*, 2004).
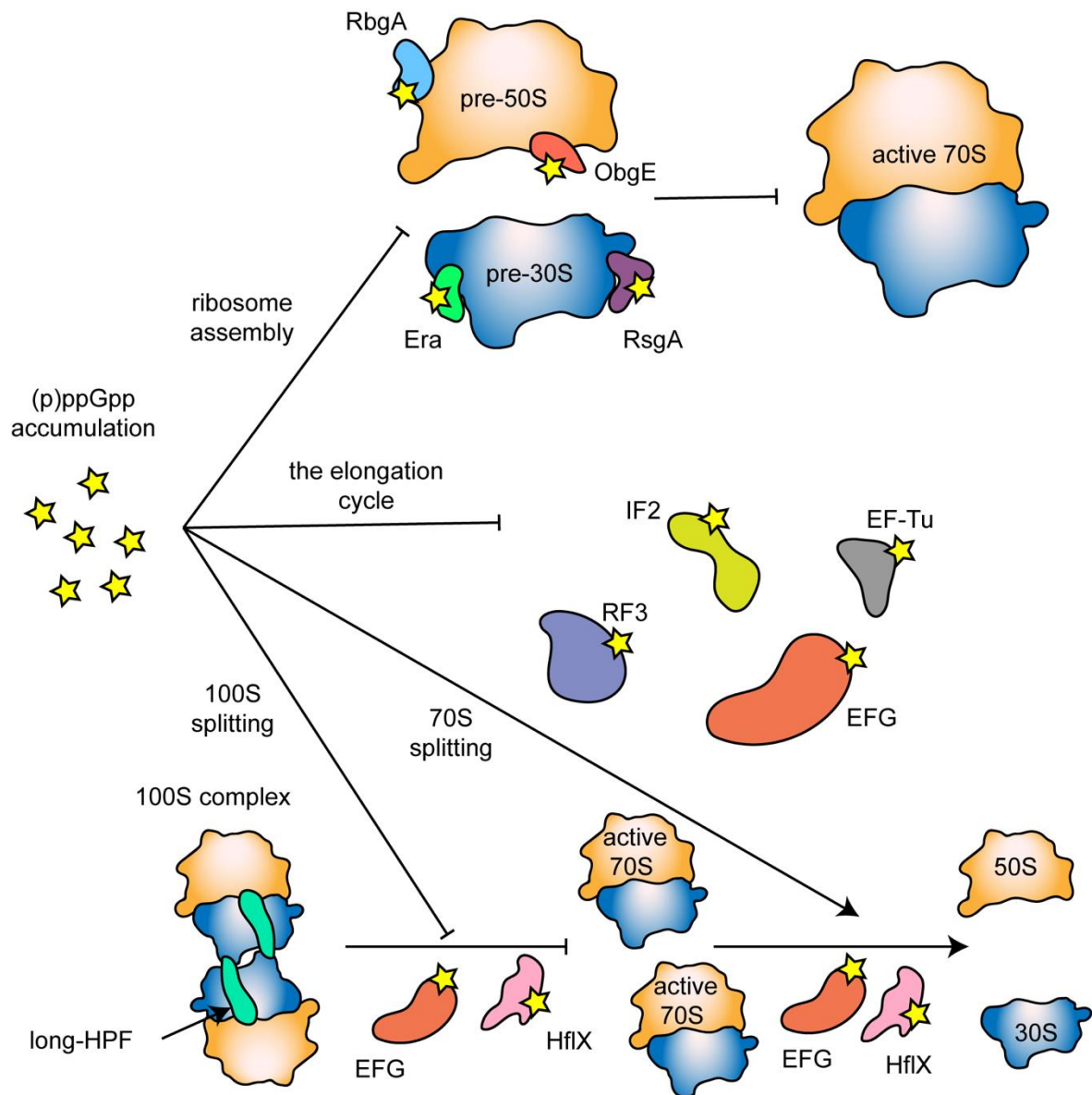
Figure 1.4.2.2: The effect of the stringent response on prokaryotic translation. (p)ppGpp synthesis by RSH superfamily enzymes can inhibit translation on a transcriptional and post-translational level. Through direct binding and inhibition of the GTPase activity of RsgA, RbgA, Era and ObgE, (p)ppGpp can inhibit the *de novo* biogenesis of mature ribosomes. (p)ppGpp can also bind to and inhibit translational GTPases IF2, EF-Tu, EF-G and RF3 to inhibit the initiation, elongation and termination steps of the translation cycle. The 100S ribosomal hibernation complex is usually split by a combination of EF-G and RRF, or HflX in a GTPase-dependent manner. Both EF-G and HflX are inhibited by (p)ppGpp, leading to the inhibition of 100S splitting into mature 70S subunits. Finally, while 100S splitting is GTPase dependent, both EF-G and HflX are involved in 70S splitting in a GTPase-independent manner, and as such the binding of (p)ppGpp may promote the dissociation of active 70S ribosomes into inactive 30S and 50S subunits (Basu and Yap, 2017; Corrigan *et al.*, 2016; Mitkevich *et al.*, 2010).

While not strictly considered assembly factors, extensive work has been carried out to define the interaction between (p)ppGpp and the RA-GTPase BipA and the TRAFAC GTPase DnaG (Fan *et al.*,

2015; Maciag *et al.*, 2010). BipA is a paralogue of EF-G, and has been shown to be capable of 70S ribosome association and regulation of many cellular processes including heat shock, cold shock, nutrient deprivation and virulence (Fan *et al.*, 2015). DnaG is a DNA primase responsible for synthesising 10-60 nucleotide long primers to facilitate DNA polymerase activity (Maciag *et al.*, 2010). Binding of (p)ppGpp to the BipA active site had no effect on the tertiary structure of the protein, suggesting that inhibition is caused simply through outcompetition of GTP association (Fan *et al.*, 2015). DnaG on the other hand has been studied in more detail. During elongation of the RNA primer, a crucial Mn^{2+} cofactor is coordinated towards the active site. The 3'-diphosphate of (p)ppGpp contacts this cofactor, leading to reorienting of the guanine base in a conformation distinct from that of the typical GTP substrate (Rymer *et al.*, 2012), preventing NTP substrates entering the active site using the specific nucleotidyl properties of (p)ppGpp. Since the binding site of RA-GTPases recognises guanine rings through stacking interactions via the conserved G4 lysine residue and via specific bifurcated hydrogen bonding between the G4 aspartate and guanine ring, it can be speculated that the presence of the 3'-diphosphate of (p)ppGpp could distort the RA-GTPase binding site in a similar manner to DnaG. Structural studies of *S. aureus* RbgA reveal a rearrangement in the switch I loop following (p)ppGpp binding, which differs from the position of this loop in the GMPPNP-bound homologue from *Saccharomyces cerevisiae*, preventing enzymatic activity in the former (Pausch *et al.*, 2018). This was attributed to steric inhibition due to the presence of the 3'-diphosphate of (p)ppGpp, preventing adoption of the active conformation and hydrolysis, prolonging inhibition.

It has previously been shown that pppGpp binding to *B. subtilis* RbgA (YlqF) enhances the affinity of this protein to the mature 50S subunit but not the immature 45S assembly intermediate (Achila *et al.*, 2012). This led to the proposition of a model of how RA-GTPases function during the stringent response. Upon competitive inhibition of these proteins by (p)ppGpp, they adopt a distinct conformation lacking GTPase activity yet retaining the capacity to associate with mature ribosomal subunits. The presence of these proteins on the mature ribosomal 30S and 50S subunits would sterically hinder 70S formation, preventing 70S formation and productive translation while under conditions of stress (Achila *et al.*, 2012).

In addition to inhibiting *de novo* formation of ribosomes via downregulation of *rrn* transcription and inhibition of RA-GTPase activity, the stringent response effector (p)ppGpp also directly targets the translation process through inhibition of the GTPase activity of IF2, EF-Tu, EF-G and RF3 (Figure 1.4.2.2) (Bergman, 2014; Milon *et al.*, 2006; Mitkevich *et al.*, 2010). Cumulatively, this leads to a profound decrease in each of the four stages of translation, namely initiation via IF2 inhibition, elongation via

EF-Tu and EF-G inhibition, termination via RF3 inhibition and recycling via EF-G inhibition. One of the mysteries surrounding the stringent response is that many upregulated genes are translated into functional proteins, requiring translation despite the known inhibition of ribosome assembly and translational GTPases. Recent kinetic insight into the regulation of 30S IC formation revealed that while bound to (p)ppGpp, IF2 was still capable of facilitating initiation – albeit in a permissive/restrictive manner (Vinogradova *et al.*, 2020) depending on the affinity of different mRNAs to the 30S pre-IC. This affinity is regulated depending on the nucleotide-bound state, potentially providing further translational regulation of the cellular proteome in response to rising (p)ppGpp concentrations. While the major targets of this regulation are unknown, it has been shown that *mtufA* mRNA encoding the GTPase EF-G is preferentially translated when compared to *minfA* mRNA encoding IF1 mRNA (Vinogradova *et al.*, 2020), suggesting that essential housekeeping mRNAs may be selected for permissive translation. Since (p)ppGpp has been shown to bind to and inhibit the GTPase activity of both HflX and EF-G, it is possible that this molecule inhibits the only two known mechanisms of dissociating the 100S ribosome complex, possibly maintaining a pool of inactive but mature ribosomes to utilise during growth resumption.

1.4.3 The stringent response and virulence

As mentioned previously, the stringent response is essential for the virulence of many bacterial pathogens including *S. aureus* and *P. aeruginosa* (Geiger *et al.*, 2010; Vogt *et al.*, 2011), with mutation in the long RSH protein synthetase domain *rel*$_{syn}$ exhibiting decreased fitness in murine infection models (Geiger *et al.*, 2010). Deletion of the CodY regulator in the CA-MRSA strain USA300 greatly increases virulence in a PVL-independent manner, suggesting that the transition between commensalism and virulence is at least in part dependent on the efficient transition between the repressive GTP-bound CodY and the permissive apo-CodY during the stringent response (Montgomery *et al.*, 2012) and the subsequent transcriptional alteration. The *codY* regulon in *S. aureus* encodes several important virulence factors, including haemolysin-α, the *agr* locus, and genes involved in PIA-independent biofilm formation (Majerczyk *et al.*, 2008). The stringent response has also been directly implicated in toxin expression in Gram-negative bacteria, including *V. cholerae* (Oh *et al.*, 2014) and *Salmonella enterica* (Pizarro-Cerdá and Tedin, 2004). Strains of *S. enterica* incapable of synthesising (p)ppGpp or carrying out a stringent response, namely *spoT/relA* double mutants (ppGpp^0), were avirulent in mice and exhibited decreased expression of positive regulators of pathogenicity islands, demonstrating the importance of (p)ppGpp in both direct and indirect expression of virulence factors (Pizarro-Cerdá and Tedin, 2004).

In the current post-golden era of antibiotics, the emergence of antibiotic resistance is a huge concern. While resistance is primarily governed by the acquisition of resistance markers, often via MBEs, phage or conjugation, the stringent response has also been implicated in regulation of these factors once incorporated into the genome (Aedo and Tomasz, 2016). The most well characterised determinant in *S. aureus* is the SCC*mec* cassette, in which the *mecA* gene is strongly expressed when (p)ppGpp concentrations are high despite a low cellular growth rate (Kim *et al.*, 2013). While the precise mechanism of this is unknown, the exogenous origin of the *mecA* gene has been hypothesised to render its regulation outside of stringent control, leading to maintenance of transcription during (p)ppGpp accumulation (Aedo and Tomasz, 2016). In *Helicobacter pylori*, SpoT-mediated (p)ppGpp accumulation has been shown to upregulate expression of the multidrug efflux pump GluP, which may have evolved as a mechanism to remove intracellular toxic metabolites when their accumulation becomes damaging during biofilm formation (Ge *et al.*, 2018). Efflux pumps of this class are ubiquitous amongst biofilm-forming bacteria, and it remains to be seen whether the stringent response is responsible for their regulation in other bacterial pathogens.

While resistance relies on genetic adaptation to resist a given antibiotic, there are other means of surviving transient antibiotic stresses, namely persistence. Persister cells are isogenic relative to the bacterial population, yet slow growing due to stochastic fluctuations in intracellular ATP concentrations (Fauvart *et al.*, 2011). The slow growth phenotype of persister cells leads to the ineffectiveness of antibiotics which target dynamic cellular processes, such as cell wall synthesis (β-lactams) and translation inhibitors (macrolides etc.), often leading to the failure of antibiotic therapy and recurrence of infection (Fauvart *et al.*, 2011). The similarity between the stringent response phenotype and persister cell phenotype is high, although it is important to consider that the stringent response is a direct reaction to stress whereas persister cells form stochastically, contributing to the bacterial bet-hedging strategy to ensure population survival. In Gram-negative bacteria, the link between the stringent response and persistence is apparent. (p)ppGpp-induced induction of TA modules results in a reversable decrease in intracellular ATP concentrations and a slowing of growth (Shan *et al.*, 2017), and the incidence of persister cell formation is decreased in *relA*/*spoT* double mutants – potentially implying that the direct effect of (p)ppGpp on cellular ATP levels via inhibition of PurA, PurF and HprT may induce persistence (Zhang *et al.*, 2018). In *S. aureus*, the link between persister cell formation and the stringent response is more disputed. Small colony variants (SCVs) are typically isogenic cells with a slow growth phenotype, although genetic alterations such as chromosome segment inversion can also mediate SCV formation in *S. aureus* (Cui *et al.*, 2012). In isogenic cells, this phenotype can be induced either stochastically through microfluctuations in gene

expression, or via prolonged stringent response as seen in a clinical isolate with a constitutively active Rel synthetase activity (Gao *et al.*, 2010) which is associated with an increased instance of antibiotic-insensitive chronic infection. Furthermore, the increased incidence of intraleukocytic *S. aureus* persister cells has been attributed to induction of the stringent response by the plethora of antimicrobial factors present in macrophage phagolysosomes, contributing to the success of infection and failure of antibiotic therapy (Peyrusson *et al.*, 2020).

1.4.4 The stringent response as a drug target

The importance of the stringent response in bacterial virulence has highlighted this signalling network as a target for novel antimicrobials, with the added benefit that if the stringent response network is mutated during the development of resistance, there is a chance of a concurrent decrease in virulence, such as during toxic overaccumulation of (p)ppGpp (Hall *et al.*, 2020). To date, several inhibitors of (p)ppGpp synthesis have been published and tested, although the efficacy of these molecules is disputed. Surprisingly, no inhibitors of the essential (p)ppGpp hydrolysis by long RSHs have been suggested to date.

Relacin is a synthetic, rationally designed inhibitor of (p)ppGpp synthesis designed using the crystal structure of Rel*seq* from *Streptococcus equisimilis* (Wexselblatt *et al.*, 2012). The first generation relacin was synthesised as a deoxyguanosine-based analogue of ppGpp (Figure 1.4.4a, b), with the 5' and 3' diphosphates substituted for glycyl-glycyl dipeptides linked to the ribose via carbamate bridges to maintain structure while reducing charge. This molecule can inhibit the synthetase activity of long RSH proteins in *B. subtilis*, *Mycobacterium tuberculosis* and *E. faecalis* at concentrations of around 2 mM *in vitro* and up to 12 mM when used to challenge enterococcal biofilms (Syal *et al.*, 2017; Wexselblatt *et al.*, 2012; Yanling *et al.*, 2018). The 12 mM concentration required to disrupt biofilm, while nontoxic to host epithelium, may prove clinically difficult to maintain depending on the bioavailability and half-life of relacin. *E. coli* survival was not affected by relacin, indicating that this molecule may be unable to transverse the Gram-negative cell wall. Relacin also has no inhibitory activity either *in vitro* or *in vivo* on SAS enzymes (Gaca *et al.*, 2015), yet could still be used in combination with conventional antimicrobials in an attempt to decrease levels of persistence. Furthermore, attempted optimisation of relacin yielded the second generation relacin-2d (Figure 1.4.4c), in which the glycyl-glycyl dipeptides were replaced with glutamyl-glutamic acid moieties (Wexselblatt *et al.*, 2013), increasing the potency against long RSH proteins but failing to inhibit the activity of SASs.
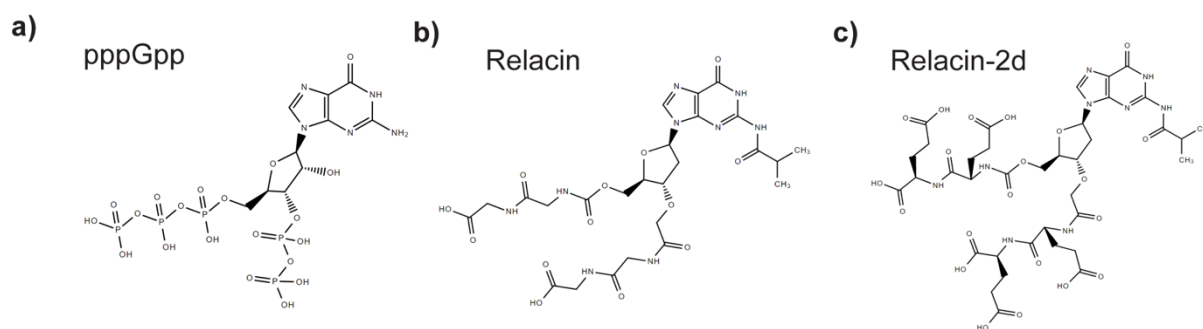
Figure 1.4.4: Displayed formulae of pppGpp and the analogous Relacin and Relacin-2d. a) The structure of pppGpp. b) The structure of Relacin, note that the 3'- diphosphate and 5'-triphosphate moieties of pppGpp have been substituted by glycyl-glycyl dipeptides. c) The structure of Relacin-2d, note the presence of glutamyl-glutamic acid moieties at the 3' and 5' positions (Wexselblatt *et al.*, 2013; Wexselblatt *et al.*, 2012).

The major hurdle in ppGpp-analogue development is the large, complex, and highly charged ribose-tetraphosphate moiety. Therefore, simpler nucleotide phosphonate compounds have been developed in an attempt to overcome this hurdle while maintaining efficacy in a similar manner to many clinically relevant and mass-produced antivirals (Groaz and De Jonghe, 2020). High-throughput screening of phosphonate compounds in an *E. coli* system revealed two potential candidates, termed DR-4250 and DR-M014 (Beljantseva *et al.*, 2017), which proved effective at inhibiting the synthetase activity of both *E. coli* RelA and *E. faecalis* RelQ at sub-millimolar concentrations, although when tested against live *B. subtilis* cells no effect was observed, and it was concluded that small phosphonate compounds may be incapable of entering bacterial cells (Beljantseva *et al.*, 2017).

The human immune system includes a multitude of antimicrobial peptides. One of which, IDR-1018, has been shown to exhibit activity against mature biofilms in a range of Gram-positive and Gram-negative bacteria, which was initially attributed to specific targeting of the stringent response via electrostatically sequestering (p)ppGpp (de la Fuente-Núñez *et al.*, 2014). This was disputed through use of minimal media either containing or lacking valine, in which the stringent response is nonessential and essential respectively, with the activity of IDR-1018 against *E. coli* consistent in both cases (Andreson *et al.*, 2016). Furthermore, *relA/spoT* double mutants were shown to be more sensitive to the activity of IDR-1018, directly contradicting the suggestion that this peptide targets (p)ppGpp specifically (Andreson *et al.*, 2016). A more potent derivative of IDR-1018, DJK5 was shown to downregulate transcription of *spoT* in *P. aeruginosa* during murine abscess infection models (Pletzer *et al.*, 2017), although the degree of specificity and molecular mechanism of this is unknown. Recently, another synthetic derivative of IDR-1018, 1018M, was developed to specifically target MRSA biofilms. While shown to be able to sequester ppGpp *in vitro* due to electrostatic interactions, there is no evidence that the anti-biofilm effect of this peptide is in any way stringent response related (Jiale *et al.*, 2021). Despite the disputed mechanism of action, these antimicrobial cationic peptides have

proven highly effective against broad-spectrum biofilms, which are frequently the cause of recurrent and antibiotic-tolerant infections.

1.5 Aims and objectives of this project

In this study, we aim to fully characterise the intersection between the stringent response and post-translational regulation of *de novo* ribosome biogenesis in *S. aureus*, using a variety of biochemical, microbiological and structural techniques. As detailed above, the stringent response is a vastly complex signalling network with far-reaching implications within the cell, and studying the stringent response in the absence of complex Omics studies is difficult.

Firstly, we aim to fully characterise the interaction between four (p)ppGpp-binding RA-GTPases, namely RsgA, RbgA, Era and HflX with the four predominant guanine nucleotides *in vitro* (Chapter 3). This is done in order to better understand the fundamental properties of these RA-GTPases, while simultaneously enabling contextualisation of downstream data due to a better understanding of the nucleotide binding affinities. We purified and characterised the wild-type proteins nucleotide binding capacity, GTPase activity and the competitive nature of inhibition by (p)ppGpp.

Having characterised the impact of (p)ppGpp on the enzymatic capacity of the four RA-GTPases, we next sought to determine the impact of this alarmone on the allostery and ribosome-binding function of these enzymes (Chapter 4). It had previously been proposed that *B. subtilis* RbgA sequesters mature ribosomal subunits during the stringent response. We initially hypothesised that this model is consistent among the four RA-GTPases, maintaining a pool of mature subunits which can facilitate rapid resumption of growth. However following use of a variety of techniques including pulldown assays and stopped-flow fast kinetics, we observed that that GDP and (p)ppGpp binding to RA-GTPases actually inhibited association to the ribosomal subunits, leading to the proposition of a new model in which the RA-GTPases are held in an isolated, inactive OFF-state during the stringent response.

X-ray crystallography was then employed in order to develop a molecular model of (p)ppGpp-mediated inhibition of RA-GTPases, as well as the general (p)ppGpp-active site binding interaction (Chapter 5). We hypothesised that the binidng of ppGpp has allosteric and conformational effects on the RA-GTPases, modulating the function to favour cell survival during the stringent response. Through comparison of our structural models of RsgA with models of RsgA homologues in other nucleotide-bound states, we propose a general model for the regulation of RA-GTPases activity during the stringent response.

Finally, in order to better understand the role of RA-GTPases in cell growth and the stringent response, we perform site-directed mutagenesis to yield conformationally trapped OFF-state Era variants (Chapter 6), under the hypothesis that the OFF-state variants would structurally mimic the (p)ppGpp-bound state *in vivo*. We hoped that by characterising the effect of these variants on nucleotide binding, enzymatic activity, cell growth, ribosome formation and rate of translation, our understanding of the intricacies of the ON/OFF switch in the case of RA-GTPases would increase to better understand the role of these proteins while bound to (p)ppGpp.

It is apparent that the stringent response is not only a crucial regulator of virulence in pathogenic bacteria, but also an emerging determinant concerning the repeated failure of antimicrobial therapy both through regulation of resistance cassettes and facilitation of the slow-growing persister cell phenotype. Ultimately, by investigating the mechanistics of (p)ppGpp-mediated inhibition of RA-GTPases in *S. aureus*, we aim to better gain insight into the complex and essential switch between the proliferative and virulent states by means of the stringent response, specifically regarding the modulation of translation to suit this purpose. It is our hope to contribute to the understanding of the complex regulatory network of the stringent response and the biochemical determinants which may in the future contribute to the design of true stringent response-targeting antimicrobials that may be essential in improving current therapies against a broad variety of bacteria, especially MRSA.

Chapter 2 – Materials and methods

2.1 Bacterial strains and growth conditions

E. coli strains were grown in lysogeny broth (LB) or on LB agar (Fisher) and *S. aureus* strains were growth in tryptic soy broth (TSB) or on tryptic soy agar (TSA) at 37°C or 30°C. Liquid cultures in LB or TSB were aerated by shaking at 200 rpm at the temperatures indicated. Strains used in this study are listed in Table 2.1. *E. coli* cultures were supplemented where appropriate with antibiotics at the following concentrations: kanamycin, 30 µg/ml; carbenicillin, 50 µg/ml in LB or 150 µg/ml in LB agar, chloramphenicol, 10 µg/ml. *S. aureus* cultures were supplemented where appropriate with antibiotics at the following concentrations: chloramphenicol, 7.5 µg/ml (or 100 µg/ml during production of mRNA-deficient runoff ribosomes); spectinomycin, 250 µg/ml; tetracycline, 2 µg/ml and erythromycin, 10 µg/ml. If required, anhydrotetracycline (Atet) was added at 100 ng/ml final concentration. Bacterial cultures were stored long-term by mixing 1:1 with freezer media consisting of 10% bovine serum albumen (BSA) and 10% monosodium glutamate, and freezing at -80°C.

Table 2.1: Bacterial strains used in this study

Strain	Relevant features	Reference
	***Escherichia coli* strains**	
XL1-Blue	Cloning strain: TetR	Stratagene
	endA1 gyrA96(nal^R) thi-1 recA1 relA1 lac glnV44	
	F'[*::Tn10 proAB$^+$ lacI^q lacZ hsdR17(r_K^- m_K^+)*	
BL21 (DE3)	Strain used for protein expression	Novagen
	F$^-$ *ompT gal dcm lon hsdS$_B$($r_B^-m_B^-$) λ(DE3 [lacI lacUV5-*	
	T7p07 ind1 sam7 nin5]) [malB$^+$]$_{K-12}$(λ^S)	
RMC0147	XL1-Blue pET28b XL1-Blue: KanR	Novagen
RMC0169	BL21 (DE3) pET28b-*gppA*: KanR	(Corrigan *et al.*, 2016)
RMC0178	BL21 (DE3) pET21a-*relseq*: CarbR	(Mechold *et al.*, 2013)
RMC0361	BL21 (DE3) pCN55iTETr862-*rsgA*-his T199A: CarbR	(Corrigan *et al.*, 2016)
RMC0395	XL1-Blue pET28b-*rsgA*: KanR	(Corrigan *et al.*, 2016)
RMC0396	XL1-Blue pET28b-*rbgA*: KanR	(Corrigan *et al.*, 2016)
RMC0397	XL1-Blue pET28b-*era*: KanR	(Corrigan *et al.*, 2016)
RMC0398	XL1-Blue pET28b-*hflX*: KanR	(Corrigan *et al.*, 2016)
RMC0399	BL21 (DE3) pET28b-*rsgA*: KanR	(Corrigan *et al.*, 2016)
RMC0401	BL21 (DE3) pET28b-*rbgA*: KanR	(Corrigan *et al.*, 2016)
RMC0402	BL21 (DE3) pET28b-*era*: KanR	(Corrigan *et al.*, 2016)
RMC0403	BL21 (DE3) pET28b-*hflX*: KanR	(Corrigan *et al.*, 2016)
RMC0531	XL1-Blue pCN55iTET: CarbR	(Wood *et al.*, 2019)
RMC0896	BL21 (DE3) pET28b: KanR	This study
RMC1035	XL1-Blue pET28b-*rsgA* T199A: KanR	This study

RMC1036	XL1-Blue pET28b-*rsgA* K113T: KanR	This study
RMC1037	XL1-Blue pET28b-*rbgA* T155A: KanR	This study
RMC1038	XL1-Blue pET28b-*rbgA* K59T: KanR	This study
RMC1040	XL1-Blue pET28b-*era* K123T: KanR	This study
RMC1041	XL1-Blue pET28b-*hflX* T239A: KanR	This study
RMC1042	XL1-Blue pET28b-*hflX* K326T: KanR	This study
RMC1043	BL21 (DE3) pET28b-*rsgA* T199A: KanR	This study
RMC1044	BL21 (DE3) pET28b-*rsgA* K113T: KanR	This study
RMC1045	BL21 (DE3) pET28b-*rbgA* T155A: KanR	This study
RMC1046	BL21 (DE3) pET28b-*rbgA* K59T: KanR	This study
RMC1048	BL21 (DE3) pET28b-*era* K123T: KanR	This study
RMC1049	BL21 (DE3) pET28b-*hflX* T239A: KanR	This study
RMC1050	BL21 (DE3) pET28b-*hflX* K326T: KanR	This study
RMC1052	XL1-Blue pCN55iTET-*rbgA* T155A: CarbR	This study
RMC1053	XL1-Blue pCN55iTET-*rbgA* K59T: CarbR	This study
RMC1055	XL1-Blue pCN55iTET-*era* K123T: CarbR	This study
RMC1067	XL1-Blue pET28b-*era* S268C: KanR	This study
RMC1068	BL21 (DE3) pET28b-*era* S268C: KanR	This study
RMC1070	XL1-Blue pCL55iTETr862-*rsgA*-His K113T: CarbR	This study
RMC1071	XL1-Blue pCL55iTETr862-*hflX*-His T239A: CarbR	This study
RMC1072	XL1-Blue pCL55iTETr862-*hflX*-His K326T: CarbR	This study
RMC1292	XL1-Blue pET28b-*mCherry-era*: KanR	This study
RMC1293	XL1-Blue pET28b-*mCherry-hflX*: KanR	This study
RMC1296	BL21 (DE3) pET28b-*mCherry-era*: KanR	This study
RMC1297	BL21 (DE3) pET28b-*mCherry-hflX*: KanR	This study
RMC1312	XL1-Blue pET28b-*era* T40A: KanR	This study
RMC1313	BL21 (DE3) pET28b-*era* T40A: KanR	This study
RMC1314	XL1-Blue pCN55iTET-*era* T40A: CarbR	This study
RMC1323	XL1-Blue pCN55iTET-*era*-His: CarbR	This study
RMC1531	XL1-Blue pET28b-*era* 1-180: KanR	This study
RMC1532	BL21 (DE3) pET28b-*era* 1-180: KanR	This study
RMC1684	XL1-Blue pET28b-*rbgA*-ΔG2: KanR	This study
RMC1685	BL21 (DE3) pET28b-*rbgA*-ΔG2: KanR	This study
RMC1686	XL1-Blue pET28b-*era*-ΔG2: KanR	This study
RMC1687	BL21 (DE3) pET28b-*era*-ΔG2: KanR	This study
RMC1747	BL21 (DE3) pET28b-*yjbM*: KanR	This study
	***Staphylococcus aureus* strains**	
SEJ1	RN4220 *spa;* protein A negative derivative of RN4220; ANG314	(Grundling and Schneewind, 2007)
LAC*	LAC*: Erm sensitive CA-MRSA LAC strain (AH1263) Accession number: CP000255	(Boles *et al.*, 2010)
RMC0355	LAC* pCL55iTETr862: CamR	(Corrigan *et al.*, 2016)

RMC0368	LAC* Δ*rsgA* pCL55iTETr862: CamR	(Corrigan *et al.*, 2016)
RMC0369	LAC* Δ*rsgA* pCL55iTETr862-*rsgA*-His: CamR	(Corrigan *et al.*, 2016)
RMC0371	LAC* Δ*rsgA* pCL55iTETr862-*rsgA*-His T199A: CamR	(Corrigan *et al.*, 2016)
RMC0372	LAC* Δ*hflX* pCL55iTETr862: CamR	This study
RMC0373	LAC* Δ*hflX* pCL55iTETr862-*hflX*-His: CamR	This study
RMC0562	LAC* pCN55iTET: SpecR	(Wood *et al.*, 2019)
RMC1081	RN4220 Δ*spa* pCL55iTETr862-*rsgA*-His K113T: CamR	This study
RMC1083	RN4220 Δ*spa* pCL55iTETr862-*hflX*-His T239A: CamR	This study
RMC1085	RN4220 Δ*spa* pCL55iTETr862-*hflX*-His K326T: CamR	This study
RMC1089	RN4220 Δ*spa* pCN55iTET-*era* K113T: SpecR	This study
RMC1106	LAC* Δ*rsgA* pCL55iTETr862-*rsgA*-His T199A: CamR	This study
RMC1107	LAC* Δ*rsgA* pCL55iTETr862-*rsgA*-His K113T: CamR	This study
RMC1114	LAC* Δ*hflX* pCL55iTETr862-*hflX*-His T239A: CamR	This study
RMC1115	LAC* Δ*hflX* pCL55iTETr862-*hflX*-His K326T: CamR	This study
RMC1262	LAC* Δ*era* pCN55iTET: TetR, SpecR	(Wood *et al.*, 2019)
RMC1263	LAC* Δ*era* pCN55iTET-*era*: TetR, SpecR	(Wood *et al.*, 2019)
RMC1315	RN4220 Δ*spa* pCN55iTET-*era* T40A: SpecR	This study
RMC1533	LAC* Δ*era* pCN55iTET-*era* T40A: TetR, SpecR	This study
RMC1534	LAC* Δ*era* pCN55iTET-*era* K123T: TetR, SpecR	This study
RMC1690	LAC* Δ*era* pCN55iTET-*era*-His: TetR, SpecR	This study

2.2.1 Analysis of bacterial growth

Strains were grown overnight in TSB supplemented with the appropriate antibiotics at 37°C and with shaking, before diluting into 5 ml of fresh TSB plus antibiotics and 100 ng/ml Atet if required. Cultures were grown at 37°C with shaking and absorbance at 600 nm (A_{600}) was measured at 2 hour (hr) intervals over a period of 8 hrs.

2.2 Manipulation of DNA

2.2.1 Isolation of plasmid DNA

The GeneJet Plasmid Miniprep Kit (ThermoScientific) was used to isolate plasmid DNA from *E. coli* as per the manufacturer's instructions, with the exception that column-bound DNA was eluted using MilliQ water (mqH$_2$O) instead of the provided elution buffer. For preparation of plasmids from *S. aureus* strains, 5 ml of stationary phase culture was resuspended in 100 µl of TSM (50 mM Tris-HCl pH 7.5, 0.5 M sucrose, 10 mM MgCl$_2$) and lysed via the addition of 0.5 µg/ml lysostaphin for 30 minutes (mins) at 37°C. Plasmid DNA was then isolated as for *E. coli*.

2.2.2 Isolation of genomic DNA

Genomic DNA (gDNA) was isolated from 5 ml overnight stationary phase cultures of *S. aureus* using the Wizard Genomic DNA Extraction Kit (Promega). Cells were harvested and resuspended in 100 µl of TSM (50 mM Tris-HCl pH 7.5, 0.5 M sucrose, 10 mM $MgCl_2$) and lysed using 0.5 µg/ml lysostaphin for 30 mins at 37°C. The extraction of gDNA was then carried out as per the manufacturer's instructions.

2.2.3 PCR

Primers were designed using SnapGene (GSL Biotech LLC) and synthesised by Eurofins, and those used in this study are listed in Table 2.2.3. Polymerase chain reaction (PCR) reactions which require high fidelity were typically carried out in a 50 µl volume using Phusion master mix with High-Fidelity buffer (ThermoScientific). For reactions which did not require high fidelity extension, such as colony PCR, typically Taq polymerase master mix (NEB) was used. Reaction mixtures contained approximately 10 ng of plasmid DNA or 100 ng of genomic DNA, 0.5 µM of each primer, and 1X final concentration of the respective Taq or Phusion master mix.

The T100 thermocycler (BioRad) was programmed to carry out a PCR reaction as follows: Initial denaturation for three mins at 95°C; five cycles of denaturation for 30 seconds at 95°C, primer annealing for 30 seconds at 45°C (may differ depending on specific melting temperature of certain primers), elongation at 72°C (15-30 seconds per kb when using Phusion, or 1 min per kb when using Taq); 25 cycles of the above with an annealing temperature of 53°C; a final 1 min extension at 72°C. PCR products were visualised using agarose gel electrophoresis and purified using the GeneJet Gel Extraction kit (ThermoScientific) as per the manufacturer's instructions with the exception that mqH_2O was used to elute column-bound DNA instead of the provided elution buffer. Mutagenic inverse PCRs were carried out using Phusion as above, with the exception that the second phase of reaction contained only 13 cycles at an annealing temperature of 53°C, and so templates were subject to 18 cycles of amplification instead of 30.

Colony PCRs were carried out using *E. coli* by directly adding a colony to the reaction mixture. The PCR reaction was then carried out using Taq polymerase as above. When carrying out colony PCR using *S. aureus*, the colonies were first resuspended in 50 µl TSM (50 mM Tris-HCl pH 7.5, 0.5 M sucrose, 10 mM $MgCl_2$) and lysed via the addition of 0.5 µg/ml of lysostaphin and incubation at 37°C for 1 hr. Cell debris was removed via centrifugation at 17,000 × gravity (*g*) for 5 mins, and 5 µl of the supernatant was added to the PCR reaction mixture.

Table 2.2.3: Primers used in this study

Number	Name	Sequence (5'-3')	Restriction site
RMC003	R-5'geh	CTTGCTTTCAATTGTGTTCC	
RMC004	F-5'geh	GTTGTTTTTGTACATGGATTTTTAG	
RMC005	R-pCL55	GCGCATAGGTGAGTTATTAGC	
RMC006	3-pCL55seq	CACGTTTCCATTTATCTGTATACGGATC	
RMC007	seq Ptet inserts	AATTCCTCCTTTTTGTTGACACTCTATC	
RMC014	F-RsgA-T199A	CATTAAATCGAGGAAAGCATACTGCAAGACATGTCGAACTATTCG	
RMC015	R-RsgA-T199A	CGAATAGTTCGACATGTCTTGCAGTATGCTTTCCTCGATTTAATG	
RMC062	T7 promoter	TAATACGACTCACTATAGGG	
RMC063	T7 Terminator	GCTAGTTATTGCTCAGCGG	
RMC065	R-BamHI-16B12-St	CCC<u>GGATCC</u>TTAATATCTAACCTTTCTATTTGA	BamHI
RMC066	F-NheI-16D7-St	CCC<u>GCTAGC</u>GTTATTCAATGGTATCCAGGAC	NheI
RMC067	R-BamHI-16D7-St	CCC<u>GGATCC</u>TTAATTGTTAGCGTCATTTGCTA	BamHI
RMC068	F-NdeI-16F3-St	CCC<u>CATATG</u>ACAGAACATAAATCAGCATTTGT	NdeI
RMC069	R-BamHI-16F3-St	CCC<u>GGATCC</u>TTAATCTTGGTCTTCAACATAACC	BamHI
RMC071	R-BamHI-21E7-St	CCC<u>GGATCC</u>TTATTTTTTAAATCCTTTTATACGA	BamHI
RMC157	F-KpnI-era	GGGG<u>GGTACC</u>TCAGGAAAGGATTTAGAATAAATG	KpnI
RMC169	F-iTET-pCN	GCAGCTCTAATGCGCTGTTAATCAC	
RMC171	R-pCN34	GTTATCCCCTGATTCTGTGGATAACCG	
RMC365	F-RsgA-K113T	GCGAGAATTTTGGTGACTACAAAAGATAAAACACCAATTG	
RMC366	R-RsgA-K113T	CAATTGGTGTTTTATCTTTTGTAGTCACCAAAATTCTCGC	
RMC367	F-RbgA-K59T	CACGTGTTGTTATATTAAATACAAAAGATATGTCTAATTTAAATG	
RMC368	R-RbgA-K59T	CATTTAAATTAGACATATCTTTTGTATTTAATATAACAACACGTG	
RMC369	F-RbgA-T155A	CTGGTAATAAACCAGGTGTGGCCAAACAACAACAATGGATTAAAG	
RMC370	R-RbgA-T155A	CTTTAATCCATTGTTGTTGTTTGGCCACACCTGGTTTATTACCAG	
RMC373	F-Era-K123T	CAGTATTTTTAGTATTAAATACAATAGATTTAGTGCATCCAG	
RMC374	R-Era-K123T	CTGGATGCACTAAATCTATTGTATTTAATACTAAAAATACTG	
RMC375	F-HflX-T239A	GAAAAAGATCAATTATTTGCAGCGTTAGATCCTAAAACACGACAAATTC	
RMC376	R-HflX-T239A	GAATTTGTCGTGTTTTAGGATCTAACGCTGCAAATAATTGATCTTTTTC	
RMC377	F-HflX-K326T	CTCAAATAGTTATTTTTAATACAAAGGACTTATGTGATCATG	
RMC378	R-HflX-K326T	CATGATCACATAAGTCCTTTGTATTAAAAATAACTATTTGAG	
RMC469	F-Era-S268C	GTGATATAGAAATGCTTCTAGGCTGTAAAGTTTACTTAGAATTATGG	
RMC470	R-Era-S268C	CCATAATTCTAAGTAAACTTTACAGCCTAGAAGCATTTCTATATCAC	
RMC510	R-NotI-Era 180	GGGG<u>GCGGCCGC</u>ATCATCTGGATAATATTTAGGTCC	NotI
RMC536	R-SacI-era-His	AAA<u>GAGCTC</u>TTAGTGATGGTGATGGTGATGACCATCTTGGTCTTCAACATAACC	SacI
RMC539	F-Era-T40A	AATCATGTCCGATAAAGCTCAAGCAACTAGAAATAAAATTCAAGGTGTT	
RMC540	R-Era-T40A	AACACCTTGAATTTTATTTCTAGTTGCTTGAGCTTTATCGGACATGATT	

RMC553	F-mCherry-BamHI	CCCGGATCCCGGCGTTAGTAAAGGCGAAGAAGATA	BamHI
RMC554	F-RsgA-mCherry	AGATCTCCGCGCGGCAGCAAGACAGGTCGAATAGTGAAATCA	
RMC555	R-mCherry-RsgA	TGTCTTGCTGCCGCGCGGAGATCTTTTATATAATTCATCCAT	
RMC556	F-RbgA-mCherry	AGATCTCCGCGCGGCAGCGTTATTCAATGGTATCCAGGACAT	
RMC557	R-mCherry-RbgA	AATAACGCTGCCGCGCGGAGATCTTTTATATAATTCATCCAT	
RMC558	F-Era-mCherry	AGATCTCCGCGCGGCAGCACAGAACATAAATCAGGATTTGTT	
RMC559	R-mCherry-Era	TTCTGTGCTGCCGCGCGGAGATCTTTTATATAATTCATCCAT	
RMC560	F-HflX-mCherry	AGATCTCCGCGCGGCAGCGCTCAGCAACAAATTCATGATACT	
RMC561	R-mCherry-HflX	CTGAGCGCTGCCGCGCGGAGATCTTTTATATAATTCATCCAT	
RMC735	F-Era-dG2	CATGTCCGATAAAGTTATGACAAGAGATGACGCGCAA	
RMC736	R-Era-dG2	TCTTGTCATAACTTTATCGGACATGATTGCTATTTTATGGC	
RMC737	F-RbgA-dG2	GGTAATAAACCAAAAGTTGGTAATGCATTACAACTA	
RMC738	R-RbgA-dG2	CATTACCAACTTTTGGTTTATTACCAGTCTGCGCAAT	

2.2.4 Agarose gel electrophoresis

Agarose gels were made up of TAE buffer (40 mM Tris-acetate pH 8.0, 1 mM ethylenediaminetetraacetic acid (EDTA)) with 1% (w/v) agarose, which was dissolved via heating of the TAE and cast into a gel mould of the desired size, and a 1:10,000 dilution of SybrSafe (Invitrogen). Prior to loading, DNA samples were mixed with 6X DNA loading dye (ThermoScientific), with the exception of PCR reactions using Taq, which already contain 1X DNA loading dye in the Taq master mix and so can be loaded into the agarose gel directly. Band sizes were estimated by reference to a DNA 1 kb ladder (ThermoScientific). Electrophoresis was carried out submerged in TAE buffer with a field strength of 7.5 V cm^{-1} for at least 20 mins, and the resulting gels were imaged using a ChemiDoc MP imager (BioRad).

2.2.5 Restriction digestion of DNA

Digestion of 10 ng of plasmid DNA, gDNA or PCR product was carried out in a 25 µl reaction with a final concentration of 1X CutSmart buffer (NEB) or an alternative suitable reaction buffer (NEB), and 10 U of the suitable restriction enzyme (NEB). Reaction mixtures were incubated at 37°C for at least 3 hrs, and then either heat inactivated, or the digested DNA was purified using the GeneJet Plasmid Miniprep Kit (ThermoScientific) as per the manufacturer's instructions, and visualised via agarose gel electrophoresis. When carrying out site-directed mutagenesis via inverse PCR, 10 µl of product was digested with 10 U of DpnI (NEB) directly in the 1X Phusion polymerase master mix (ThermoScientific) at 37° for at least 3 hrs, heat inactivated then used directly for transformation.

2.2.6 Ligation of DNA fragments

If required due to digestion with a single restriction enzyme, digested plasmid vector was treated with Antarctic Phosphatase (AnP) (NEB) to dephosphorylate the 5' and 3' ends of DNA and prevent self-ligation. This was carried out using the entire inactivated digested mixture or purified, digested vector. 0.25 U/µl reaction volume was added along with 1X AnP buffer (NEB) and the DNA sample, and the reaction mixture was incubated at 37°C for at least 1 hr. AnP was heat inactivated at 80°C for 5 mins prior to purification of the dephosphorylated plasmid DNA using the GeneJet Gel Extration Kit (ThermoScientific).

Ligations between digested DNA insert fragments and digested plasmid vectors were carried out using at least a 5:1 ratio of insert:vector, using 125 ng digested insert and 25 ng digested plasmid. Ligations were carried out in a reaction volume of 15 µl, using 1X T4 ligase buffer (NEB) and 400 U T4 DNA ligase (NEB). Reaction mixtures were incubated for at least 4 hrs at 16°C, then were heat inactivated for 20 mins at 65°C and either immediately used for transformation or stored at -20°C.

2.2.7 Preparation and transformation of chemically competent *E. coli* cells

E. coli cultures were grown in 20 ml of LB at 37°C overnight with shaking at 200 rpm, then diluted 1:100 (v/v) into 1 litre PSI broth (0.5% (w/v) yeast extract, 2% (w/v) tryptone, 20 mM $MgSO_4$, pH adjusted to 7.4 using 0.1 M KOH) and grown until an A_{600} of 0.5-0.7 was reached. Cells were cooled to 4°C, harvested via centrifugation at 6,000 × g for 10 mins, and kept on ice for the remainder of this protocol. Cell pellets were washed with 200 ml ice cold filter-sterilised Transformation Buffer (Tfb) I (30 mM CH_3COOK, 100 mM RbCl,10 mM $CaCl_2$, 50 mM $MnCl_2$, 15% glycerol, adjusted to pH 5.8 using acetic acid). Cell suspension was kept on ice for 15 mins, before cells were re-harvested and resuspended in 25 ml ice cold, filter-sterilised Tfb II (10 mM MOPS adjusted to pH 6.5 using KOH, 75 mM $CaCl_2$, 10 mM RbCl, 15% glycerol). Cells were incubated on ice for 15 mins, then aliquoted into 500 µl aliquots and flash frozen in a dry ice/ethanol bath and stored at -80°C.

To transform chemically competent *E. coli* cells with plasmid DNA, 100 µl of cells were incubated on ice with 1 ng plasmid DNA for 30 mins. To transform with ligation product, 100 µl of cells were incubated on ice with 8 µl ligation product for 30 mins. Cells were then heat shocked at 42°C for 50 seconds before immediate incubation on ice for 2 mins. 900 µl of SOC medium (0.5% yeast extract, 2% tryptone, 0.025% NaCl, 20 mM glucose and 2.5 mM KCl, adjusted to pH 7.5 using 0.1 M HCl) was then added and cells were incubated at 37°C for 1 hr with shaking to enable outgrowth. Cells were then plated onto LB agar with the appropriate antibiotic to select for positive transformants. Plates

were incubated at 37°C overnight to enable growth of colonies. If lawn cultures were obtained, these were re-streaked on LB agar plus the appropriate antibiotic for single colonies, and were subsequently screened using colony PCR.

2.2.8 Preparation and transformation of electrocompetent *S. aureus* cells

5 ml overnight cultures of *S. aureus* RN4220 Δ*spa* were grown at 37°C with shaking and diluted 1:100 (v/v) into 200 ml TSB and grown at 37°C for 3 hrs until mid-exponential phase was reached (A_{600} between 0.6 and 0.8). Cells were then cooled on ice, harvested via centrifugation at 6,000 × *g* for 10 mins, and kept on ice for the remainder of this protocol. Cell pellets were washed thrice with 200 ml ice cold sterile 0.5 M sucrose solution and resuspended in 2 ml ice cold sterile 0.5 M sucrose. Cells were aliquoted into 110 μl aliquots and flash frozen in a dry ice/ethanol bath before storage at -80°C.

Before electroporation, all plasmids were dialysed against mqH$_2$O for at least 1 hr using a 0.025 μm filter (Millipore) to remove dissolved salts. 10 μl of dialysed plasmid DNA was added to 110 μl electrocompetent *S. aureus* RN4220 Δ*spa* cells in a GeneFlow 1 mm electroporation cuvette (Cell Projects). The cells were then subject to an electrical pulse of 2.5 kV, with a resistance of 100 Ω and a capacitance of 25 μF, and recovered using 900 μl of Brain-Heart Infusion (BHI) broth with the addition of 0.5 M sucrose and incubated at 37°C with shaking for 1 hr. Cells were then plated on TSA plates supplemented with the appropriate antibiotic to select for positive transformants, and the plates were incubated at 37°C overnight.

2.2.9 Phage transduction in *S. aureus*

In order to produce a phage lysate from the donor strain of *S. aureus*, a 5 ml overnight culture was grown at 37°C in 2:1 LB:TSB supplemented with the appropriate antibiotics and 5 mM CaCl$_2$ with shaking. This culture was diluted 1:50 (v/v) into 5 ml of fresh 2:1 LB:TSB with antibiotic and 5 mM CaCl$_2$, and grown at 37°C for 3 hrs in order to reach mid-exponential phase. 100 μl of phage lysate from wild-type *S. aureus*, diluted to a concentration which would provide confluent but not complete lysis, was added to 500 μl of mid-exponential phase culture, and incubated statically at room temperature (RT) for 30 mins to enable one round of replication. The phage used for *S. aureus* were typically φ85, φ80α or φ11. 5 ml of liquid top agar (0.8% bacto-agar, 0.8% NaCl, 5 mM CaCl$_2$) was added to the lysate/culture mixture and overlaid onto prewarmed TSA plates supplemented with the appropriate antibiotics. Overlays were left to solidify and incubated lid-side-up overnight at 37°C. 3 ml of TMG (10 mM Tris-HCl pH 7.5, 10 mM MgSO$_4$, 0.1% (w/v) gelatine) was added to overlay plates containing confluent plaques, and the top agar was removed and clarified via centrifugation at 13,000

× g for 10 mins. Supernatants were filtered through a 0.22 μm membrane (Millipore), and stored at 4°C.

Overnight cultures of the recipient *S. aureus* strain were grown overnight in 5 ml 2:1 LB:TSB supplemented with the appropriate antibiotics and 5 mM $CaCl_2$, before harvesting via centrifugation and resuspension in 1 ml fresh 2:1 LB:TSB with antibiotic and 5 mM $CaCl_2$. Add 500 μl of phage lysate to 250 μl concentrated recipient culture and incubate at 37°C for 20 mins with shaking to enable infection. Cells were cooled to 4°C on ice and kept on ice for the remainder of this procedure. 1 M ice cold, sterile trisodium citrate was added to a final concentration of 40 mM, and cells were harvested via centrifugation at 17,000 × g for 1 min in a pre-cooled microcentrifuge. Supernatant was discarded, and pellet was washed twice in 1 ml ice cold, sterile 40 mM trisodium citrate, and then resuspended in 300 μl of ice cold trisodium citrate before plating onto TSA plates supplemented with the appropriate antibiotic and 40 mM trisodium citrate. Plates were incubated at 37°C overnight or longer until single colonies formed, and colonies were restreaked at least 3 times to cure of phage.

2.3 Protein purification and analysis

2.3.1 Expression of recombinant proteins in *E. coli* BL21 (DE3)

For exponential phase expression, overnight cultures of *E. coli* BL21 (DE3) harbouring the appropriate pET28b or pET21a expression vector were diluted to an A_{600} of 0.05 into fresh LB supplemented with antibiotics and grown for 3 hrs at 37°C until an A_{600} of 0.5-0.7 was reached. Cultures were induced with 1 mM isopropyl β- d-1-thiogalactopyranoside (IPTG) and incubated for 3 hrs at 30°C to enable protein expression.

For stationary phase expression of *E. coli* BL21 (DE3) containing pET28b-*rsgA*, overnight cultures were diluted to an $A_{600\,nm}$ of 0.05 into 1 litre of fresh LB supplemented with the appropriate antibiotics and incubated overnight at 30°C with shaking. Saturated cultures were induced with 0.75 mM IPTG for 6 hrs at 30°C with shaking to enable protein expression.

Cells were harvested via centrifugation at 6,000 × g at 4°C for 10 mins, washed with 50 ml Protein Storage Buffer (50 mM Tris-HCl pH 7.5, 200 mM NaCl, 5% (v/v) glycerol), before the pellets were flash frozen in a dry ice/ethanol bath and stored at -80°C.

2.3.2 Purification of hexahistidine-tagged proteins using IMAC

Prior to preparation of hexahistidine (6xHis)-tagged proteins via Immobilised Metal Affinity Chromatography (IMAC), cell pellets were defrosted on ice, and resuspended in 30 ml Purification Buffer A (50 mM Tris-HCl pH 7.5, 200 mM NaCl, 5% (v/v) glycerol, 10 mM imidazole) supplemented with one cOmplete, Mini, EDTA-free Protease Cocktail tablet (Sigma), and lysed using 20 µg/ml lysozyme and 30 µg/ml RNase A before sonication for 10 mins (30 seconds ON, 30 seconds OFF) using an 20 kHz Ultrasonic Liquid Processor (Fisher) at 40% amplitude. Cell debris was removed via centrifugation at 18,000 × g for 40 mins at 4°C, and the resulting supernatant was then filtered using a 0.45 µm membrane (Millipore). The filtered lysate was applied using a peristatic pump to a 1 ml HisTrap HP Ni^{2+} column, using a flow rate of 1 column volume (c.v.) per minute (GE Healthcare) before elution using a 30 c.v. gradient of Purification Buffer B (50 mM Tris-HCl pH 7.5, 200 mM NaCl, 5% (v/v) glycerol, 500 mM imidazole) from 0% to 100%. Protein containing fractions were subject to 3 successive rounds of dialysis into Protein Storage Buffer, concentrated to the desired volume and concentration using a 10 kDa centrifugal filter (ThermoScientific), flash frozen using a dry ice/ethanol bath and stored at -80°C after ensuring low levels of DNA/RNA contamination shown by an $A_{260/280}$ ratio of below 0.8 (<5% contamination) (Layne, 1957). The extinction coefficients at 280 nm for each protein and their mutant variants were calculated from their primary amino acid sequence and are as follows assuming no cysteine residues were oxidised to cystine: RsgA, 23505 M^{-1} cm^{-1}; RbgA, 40910 M^{-1} cm^{-1}; Era, 25900 M^{-1} cm^{-1}; HflX, 24870 M^{-1} cm^{-1}; Era 1-180, 10430 M^{-1} cm^{-1}. Unless specifically stated, the extinction coefficient of mutant variants was identical to the wild-type. Typically, protein purity was above 95% as assayed by sodium dodecyl sulphate polyacrylamide gel electrophoresis (SDS-PAGE) and Coomassie Brilliant Blue staining.

Proteins for use in crystallography were purified as above but dialysed into Crystallisation Buffer (25 mM Tris-HCl pH 7.5, 200 mM NaCl), concentrated as much as possible and used immediately. Proteins to be covalently labelled with Atto488-maleimide were purified as above but dialysed into Labelling Buffer (50 mM HEPES pH 7.1, 200 mM KCl, 5% (v/v) glycerol and 120 µM Tris(2 carboxyethyl)phosphine (TCEP)), then stored at -80°C prior to labelling.

2.3.3 SDS-PAGE

SDS-PAGE gels contain two distinct phases, the stacking gel in which samples were loaded and the resolving gel. The stacking gel was made up of 5.6% acrylamide, 25% (v/v) Stacking Buffer (0.5 M Tris-HCl pH 6.8, 120 mM NaCl, 8 mM EDTA (stock solution pH 8.0), 0.4% (w/v) SDS), 0.1% (w/v) ammonium persulphate (APS) and 0.1% (v/v) tetramethylethylenediamine (TEMED). Resolving gels were made up

of between 7.5% and 15% acrylamide depending on protein size and the resolution required, 25% Resolving Buffer (1.5 M Tris-HCl pH 8.8, 120 mM NaCl, 8 mM EDTA (stock solution pH 8.0), 0.4% (w/v) SDS), 0.1% (w/v) APS and 0.1% TEMED. During analysis of protein expression in *E. coli*, cell pellets were resuspended in 1X SDS-PAGE Loading Buffer (31.25 mM Tris-HCl pH 6.8, 1% (w/v) SDS, 2.5% (v/v) β-mercaptoethanol, 5% (v/v) glycerol, 0.005% (w/v) bromophenol blue) to an A_{600} of 1.0 and incubated at 95°C for at least 10 mins. During analysis of proteins in solution, samples were mixed 1:1 with 2X SDS-PAGE Loading Buffer and incubated at 95°C for at least 10 mins before loading onto the SDS-PAGE gel. Electrophoresis was performed with the gel submerged in SDS-PAGE Running Buffer (25 mM Tris-HCl pH 8.6, 192 mM glycine, 0.1% (v/v) SDS) at a field strength of 25 V cm^{-1} for at least 1 hr or until the dye front had run the full length of the gel. Gels were stained using Coomassie Brilliant Blue R-250. Gels were incubated in hot Stain (45% (v/v) methanol, 10% (v/v) acetic acid, 0.25% (w/v) Coomassie Brilliant Blue R-250) for at least 1 hr, then in Destain (45% (v/v) methanol, 10% (v/v) acetic acid) until bands become clear.

2.3.4 Western Blotting

Sample proteins were separated using SDS-PAGE, and then transferred to a polyvinylidene fluoride (PVDF) membrane via wet transfer. The PVDF membrane was hydrated in methanol for 1 min to remove hydrophobicity, and then rinsed in mqH$_2$O before equilibrating in Transfer Buffer (25 mM Tris, 192 mM glycine, 10% (w/v) glycine) for 1 min. The polyacrylamide gel was also rinsed in mqH$_2$O and equilibrated in Transfer Buffer. The PVDF membrane and polyacrylamide gel were stacked firmly against each other, with the gel on the negative side, and pressure was maintained using 3 sheets of Whatmann paper soaked in transfer buffer either side of the gel and membrane. The wet transfer was carried out at 400 mA for 60 mins, with ice cold transfer buffer to preventing overheating.

Following transfer, the membrane was rinsed with TBST (20 mM Tris-HCl pH 7.6, 0.14 mM NaCl, 0.1% Tween 20) and nonspecific binding sites were blocked using TBST with 5% (w/v) skimmed milk powder at RT for 1 hr or at 4°C overnight, with gentle shaking. If using crude *S. aureus* lysates, 10 μg/ml IgG was added to saturate protein A. The membrane was then incubated with 1:1000 dilution of primary antibody, predominantly murine α-His-horseradish peroxidase (HRP)-conjugated (Sigma) in TBST with 5% milk and 10 μg/ml IgG for 1 hr at room temperate or for 16 hrs at 4°C with shaking. Membranes were rinsed 3 times in TBST, then developed using enhanced chemiluminescence (ECL) (2.5 mM luminol, 0.4 mM P-coumaric acid, 100 mM Tris-HCl pH 8.5, 0.01% H$_2$O$_2$) and imaged using a ChemiDoc MP imager (BioRad). Bands were quantified using pixel densitometry within the ImageJ software. Following western blotting image analysis, general protein content of the samples was assessed by

staining with Ponceau S in 5% acetic acid. Membranes were incubated with the Ponceau solution for up to 5 mins until bands developed, and washed with distilled water until the background was clear. Membranes were imaged using a ChemiDoc MP imager (BioRad).

2.4 Isolation of highly pure 30S, 50S and 70S ribosomes from *S. aureus*

70S ribosomes were purified essentially as described previously (Daigle and Brown, 2004), with some exceptions. Briefly, saturated overnight cultures of *S. aureus* strain LAC* were diluted 1:100 into 4 litres of fresh TSB, and incubated with shaking at 37°C until an A_{600} of 0.8 was reached. 100 µg/ml chloramphenicol was added, and cultures were slowly cooled to 4°C following a 3 min incubation with the antibiotic in order to produce runoff ribosomes free of mRNA. Cells were harvested via centrifugation at 6,000 × g for 10 mins, and washed with ice cold Buffer A (20 mM Tris-HCl pH 7.5, 10.5 mM Mg(CH$_3$COO)$_2$, 100 mM NH$_4$Cl, 0.5 mM EDTA, 3 mM β-mercaptoethanol) before resuspension in Buffer A and lysis using 0.5 µg/ml lysostaphin and 75 ng/ml deoxyribonuclease (DNase) I. Crude lysates were centrifuged at 30,000 × g for 1 hr to produce an S30 fraction, and clarified lysates were applied to an equal volume of 1.1 M sucrose made up in Buffer B (20 mM Tris-HCl pH 7.5, 10.5 mM Mg(CH$_3$COO)$_2$, 500 mM NH$_4$Cl, 0.5 mM EDTA, 3 mM β-mercaptoethanol). The clear ribosome pellet was separated from the flocculent material above it, and washed and resuspended in Buffer A. This sucrose and salt-washing step was repeated. The pellet was then washed via two resuspensions in Buffer C (10 mM Tris-HCl pH 7.5, 10.5 mM Mg(CH$_3$COO)$_2$, 100 mM NH$_4$Cl, 0.5 mM EDTA, 7 mM β-mercaptoethanol). Ribosomes were re-pelleted following washing via ultracentrifugation at 100,000 × g for 16 hrs. Pure 70S ribosomes were obtained by resuspending the washed pellet in Buffer D (10 mM Tris-HCl pH 7.5, 5.25 mM Mg(CH$_3$COO)$_2$, 60 mM NH$_4$Cl, 0.25 mM EDTA, 3 mM β-mercaptoethanol) and applied to a continuous sucrose gradient made up of 10-30% sucrose in Buffer D. These gradients were then ultracentrifuged for 16 hrs at 48,000 × g, and fractionated via upwards displacement into 250 µl fractions which were analysed for RNA content at A_{260}. Fractions deemed to contain 70S ribosomes were pooled, and washed in Buffer E (10 mM Tris-HCl pH 7.5, 10 mM Mg(CH$_3$COO)$_2$, 60 mM NH$_4$Cl, 3 mM β-mercaptoethanol), and pelleted at 56,000 × g for 24 hrs before being flash frozen in a dry ice/ethanol bath and stored at -80°C.

To obtain 30S and 50S subunits, 70S ribosomes were resuspended in Ribosome Dissociation Buffer (20 mM Tris pH 7.5, 120 mM NH4Cl, 1.5 mM MgCl2 and 2 mM β-mercaptoethanol) following washing in Buffer E. 50S A_{260} units of 70S ribosomes were applied to a continuous 10-40% sucrose gradient made up in Ribosome Dissociation Buffer, and separated at 111,000 × g for 16 hrs. Gradients were again fractionated using upwards displacement and analysed for RNA content. Fractions containing 30S and

50S subunits were pooled separately, and pelleted via ultracentrifugation at 200,000 × g for 16 hrs, before being resuspended in Buffer E and stored at -80°C as above. 70S, 50S and 30S subunits were quantified using the A_{260} as follows: 1 A_{260} unit of 70S, 50S and 30S subunits equates to 23 pmol, 34.5 pmol and 69 pmol respectively (Daigle and Brown, 2004). Therefore, for 70S ribosomes, 1000 A_{260} units would equate to a concentration of 23 µM (Francisco-Velilla *et al.*, 2016), with the same logic applied to the 50S and 30S subunits.

2.5 Synthesis of [α-^{32}P]-labelled nucleotides

[α-^{32}P]-labelled GTP (Perkin Elmer) was diluted to the appropriate working concentration (typically 1:180 from the 3.3 µM stock solution to give a working stock of 18.3 nM) in GTP Binding Buffer (40 mM Tris-HCl pH 7.5, 100 mM NaCl, 10 mM $MgCl_2$). In order to produce [α-^{32}P]-labelled GDP, 18.3 nM [α-^{32}P]-labelled GTP was incubated with 0.1 µM purified recombinant RsgA and 0.1 µM purified *S. aureus* 70S ribosomes in GTP Binding Buffer and incubated for at least 1 hr at 37°C. Samples were then passed through a 3 kDa microcentrifugal filter (VWR) to remove RsgA and the ribosomes, leaving pure pppGpp. [α-^{32}P]-labelled pppGpp was produced by incubating a final concentration of 18.3 nM [α-^{32}P]-labelled GTP with 2 µM Rel$_{Seq}$, 8 mM ATP in Rel$_{Seq}$ binding buffer (25 mM Bis-Tris propane pH 9, 100 mM NaCl, 15 mM $MgCl_2$). The reaction was incubated at 37°C for 16 hrs, and halted using a microcentrifugal filter as above. In order to convert [α-^{32}P]-labelled pppGpp to [α-^{32}P]-labelled ppGpp, 1 µM final concentration of purified recombinant GppA was added, and the reaction mixture was incubated at 37°C for 15 mins, before halting as above. Final yields of the desired nucleotides were determined using thin layer chromatography (TLC), where 1 µl of each reaction mixture was spotted on a polyethylenimine-cellulose TLC plate (SupelCo), and samples were separated using a running buffer of 1.5 M KH_2PO_4 at pH 3.6. TLC plates were allowed to dry and were then exposed to a photostimulable phosphor imaging plate (IP) (Fujifilm) for 5 mins, and visualised using a Typhoon FLA7000 Phosphorimager (GE Healthcare). Spot intensity was calculated via pixel densitometry using the ImageQuant software (GE Healthcare), and stock purity of above 85% was deemed sufficient for use. Nucleotides were then stored at -20°C.

2.6 Synthesis of cold (p)ppGpp

Stocks of cold ppGpp or pppGpp were prepared to a concentration of 10 mM as follows. *B. subtilis* YjbM at a final concentration of 5 µM was incubated with 10 mM ATP and 10 mM GDP or GTP for 16 hrs at 37°C in YjbM Reaction Buffer (100 mM Na-HEPES pH 7.5, 200 mM NaCl, 20 mM $MgCl_2$, 20 mM KCl) in 100 µl. A simultaneous reaction was set up as above in 10 µl, spiked with 1.83 nM [α-^{32}P]-GTP/GDP to monitor reaction progress. Reactions were halted via passage through a 3 kDa cutoff

microcentrifugal filter at 17,000 × *g* for 10 mins, and reaction products were separated using TLC with a 1.5 M KH_2PO_4 running buffer at pH 3.6. TLC plates were allowed to dry, before exposure to the IP for at least 5 mins and subsequent visualisation using a Typhoon FLA7000 Phosphorimager (GE Healthcare). Percentage conversion from reactants to products was calculated via pixel densitometry within the ImageQuant software (GE Healthcare). Following confirmation of above 85% product purity, the large-scale cold reaction was taken as complete and halted as above before aliquoting and storage at -20°C.

2.7 Differential Radial Capillary Action of Ligand Assays

Differential Radial Capillary Action of Ligand Assays (DRaCALA) (Roelofs *et al.*, 2011) were carried out by incubating purified recombinant protein with 1.83 nM [α-^{32}P]-labelled nucleotide in GTP Binding Buffer (40 mM Tris-HCl pH 7.5, 100 mM NaCl, 10 mM $MgCl_2$). For K_D analyses, doubling dilutions of protein from an initial concentration of 100 μM was used. For fixed point binding assays, 10 μM protein was used. During RNA-binding assays, 10 μM recombinant protein was incubated with 0.4 μM [^{32}P]-RNA and 100 μM cold GTP, GMPPNP, GDP, ppGpp or pppGpp in GTP binding buffer. For competition assays, the reaction mixture was supplemented with 100 μM cold, unlabelled competitor nucleotide. Following mixing, samples were incubated at RT for 5 mins before the spotting of 2.5 μl in duplicate on nitrocellulose membrane. Spots were allowed to dry before exposure to the IP for at least 5 mins. Membranes were visualised using a Typhoon FLA7000 Phosphorimager (GE Healthcare), and the inner and outer spot intensity was calculated via pixel densitometry using the ImageQuant software (GE Healthcare). Quantification of the fraction bound was calculated using Equation 1, with the fraction of nucleotide bound (F_B), the area of the spot (*A*) and the intensity of the spot (*I*) (Roelofs *et al.*, 2011). The dissociation constant (K_D) and the maximum ligand occupancy (B_{max}) values were calculated using the GraphPad Prism 8.0 software.

Equation 1:
$$F_B = \frac{I_{inner} - (A_{inner} \times \frac{(I_{total} - I_{inner})}{(A_{total} - A_{inner})})}{I_{total}}$$

2.8 NTPase assays

Either 2.5 μM recombinant protein and 2.5 μM *S. aureus* 70S ribosomes, or 100 nM recombinant protein and 100 nM *S. aureus* 70S ribosomes (as specified in the figure legends) were incubated with 1 μM cold GTP or ATP and spiked 1.83 nM [α-^{32}P]-GTP or [α-^{32}P]-ATP in GTP Binding Buffer (40 mM Tris-HCl pH 7.5, 100 mM NaCl (replaced with 100 mM KCl when using RbgA), 10 mM $MgCl_2$) at 37°C for up to 1 hr as indicated in the figure legends. Where specified, cold (p)ppGpp was added to a final

concentration of 100 µM was added. All reactions were also carried out in the absence of enzymes to monitor spontaneous hydrolysis due to the heat lability of (p)ppGpp. Reactions were heat inactivated for 5 mins at 95°C to denature proteins and release bound nucleotides, and precipitated proteins were pelleted via centrifugation at 17,000 × g for 10 mins. Reaction products were separated using TLC and a running buffer of 0.75 M KH_2PO_4 at pH 3.6 for GTPase assays, or 0.5 M LiCl and 1 M formic acid for ATPase assays, and exposed to the IP for at least 5 mins. TLC plates were visualised using a Typhoon FLA7000 Phosphorimager (GE Healthcare), and the percentage hydrolysis was calculated via pixel densitometry using the ImageQuant software (GE Healthcare).

2.9 *In vitro* ribosome association assays

2.9.1 Association of mCherry fusion proteins to the ribosomal subunits

In a final volume of 150 µl, 3 µM mCherry-Era or mCherry-HflX was mixed with 2 µM purified *S. aureus* ribosomes and 30 µM GTP or ppGpp in Ribosome Dissociation Buffer (20 mM Tris pH 7.5, 120 mM NH4Cl, 1.5 mM MgCl2 and 2 mM β-mercaptoethanol) and incubated at RT for 5 mins. The sample was applied to an ice cold continuous 10-40% sucrose gradient made up in Ribosome Dissociation Buffer, and the 30S and 50S subunits were separated at 111,000 × g for 16 hrs at 4°C. Gradients were split into 250 µl fractions via upwards displacement, and each fraction was assayed for RNA content using A_{260}, and for the presence of mCherry fusion proteins using fluorescence detection following excitation at 590 nm and detection at 620 nm, gated at 610 nm using a long-pass filter using a SpectraMax M2 96-well plate reader (Molecular Devices).

2.9.2 Detection of ribosome association using western blotting

2.9.2.1 In vitro *ribosome association assays*

Recombinant His-tagged RA-GTPase at a final concentration of 0.5 µM was incubated with 0.2 µM 70S ribosomes from *S. aureus* in Ribosome Dissociation Buffer (20 mM Tris pH 7.5, 120 mM NH4Cl, 1.5 mM MgCl2 and 2 mM β-mercaptoethanol) for 5 mins at RT either in the apo form or in the presence of 40 µM guanine nucleotide, namely GTP, GMPPNP, GDP, ppGpp or pppGpp. The resulting 150 µl reaction mixture was layered onto an ice cold continuous 10-40% sucrose gradient made up in Ribosome Dissociation Buffer, and subject to ultracentrifugation at 111,000 × g for 16 hrs at 4°C in order to achieve complete isopycnic separation of the 30S and 50S subunits. Gradients were fractionated by upwards displacement into 250 µl aliquots, and the A_{260} was taken to calculate total RNA content of each fraction. Fractions containing 30S and 50S subunits were pooled separately, and then the proteins were precipitated through the addition of 10% (v/v) trichloroacetic acid (TCA)

followed by an incubation on ice for 3 hrs. Samples were then centrifuged for 10 mins at 17,000 × g, and washed twice with an equal volume of ice cold acetone, and protein pellets were dried at 37°C. Pellets were resuspended in 50 µl 2X SDS-PAGE Loading Buffer (62.5 mM Tris-HCl pH 6.8, 2% (w/v) SDS, 5% (v/v) β-mercaptoethanol, 10% (v/v) glycerol, 0.01% (w/v) bromophenol blue) and separated using SDS-PAGE, followed by western blotting as described in Section 2.3.4.

2.9.2.2 In vivo *ribosome association assays*

Saturated overnight cultures of *S. aureus* were diluted 1:100 into fresh TSB containing the appropriate antibiotics and 100 ng/ml Atet, and were grown at 37°C with shaking until an A_{600} of 0.6 was reached. Cultures were then split into 3 identical cultures, and were either left uninduced or were induced with 0.05 µg/ml or 60 µg/ml mupirocin at 37°C for 30 mins. After growth and induction, cultures were treated with 100 µg/ml chloramphenicol and incubated at 37°C for 3 mins before slowly cooling to 4°C to produce runoff ribosomes free of mRNA. Cells were harvested at 6,000 × g for 10 mins, and washed and resuspended to an A_{600} of 35 in Ribosome Dissociation Buffer (20 mM Tris pH 7.5, 120 mM NH4Cl, 1.5 mM MgCl2 and 2 mM β-mercaptoethanol). Lysis was carried out via the addition of 0.5 µg/ml lysostaphin and 75 ng/ml DNase I, and a 60 min incubation at 37°C, followed by clarification at 17,000 × g for 10 mins and separation of the 30S and 50S subunits as per the *in vitro* method. 30S- and 50S-containing were pooled and normalised to an A_{260} of 0.65 and 0.85 respectively to ensure equal loading in terms of ribosome content, and were precipitated and concentrated using TCA as per the *in vitro* method. Protein content was resolved using SDS-PAGE and quantified via western blotting as per Section 2.3.4.

2.10 Analysis of fast-kinetics using stopped-flow fluorometry

2.10.1 Fluorescent labelling of proteins using Atto488-maleimide

200 µM recombinant protein in Storage Buffer was mixed with 5 mM dithiothreitol (DTT) and incubated for 1 hr at RT in order to reduce target cysteine residues, before removal of DTT via passage through a PD-10 Sephadex G-25 M Buffer Exchange Column (GE Healthcare) as per the manufacturer's instructions. These columns were used to transfer the protein into Maleimide Labelling Buffer (50 mM HEPES pH 7.1, 200 mM KCl, 120 µM Tris(2 carboxyethyl)phosphine (TCEP), 5% glycerol). The flow-through was analysed via A_{280} using the extinction coefficients defined in Section 2.3.2 for protein content, and 50 µM of reduced protein was incubated with 100 µM Atto488-maleimide (ATTO-TEC) overnight at 4°C, protected from light and with consistent rotation. The reaction was terminated through addition of 6 mM β-mercaptoethanol and the mixture was applied to a 1 ml HisTrap HP Ni^{2+} column (GE Healthcare) before washing with Purification Buffer A (50 mM Tris pH 7.5, 200 mM NaCl,

5% glycerol, 10 mM imidazole) and elution using a gradient of Purification Buffer B (50 mM Tris pH 7.5, 200 mM NaCl, 5% glycerol, 500 mM imidazole), followed by extensive dialysis to remove imidazole. The degree of labelling was calculated as per the manufacturer's instructions, using an A_{500}:A_{280} correction factor of 0.05.

2.10.2 Stopped-flow monitoring of ribosome association

Initially, 200 nM Atto488-labelled RbgA or HflX were mixed rapidly with 200 nM 50S ribosomal subunits from *E. coli* in TAKM7 buffer (25 mM Tris-HCl pH 7.4, 70 mM ammonium acetate, 30 mM KCl and 7 mM MgCl₂) using an SX20 stopped-flow apparatus (Applied Photophysics). This was carried out both in the presence and absence of GTP, GDP, ppGpp and pppGpp. 60 μl samples each containing a 2X concentration of one of the two major interacting partners were rapidly mixed at 25°C. Atto488 was excited using a light emitting diode (LED) at 470 nm and fluorescence was monitored through a 515 nm long-pass filter for 10 seconds using logarithmic sampling over 1000 datapoints. Each condition was subject to at least 5 technical repeats, which were averaged to yield the final trace.

When titrating, 0.075 μM RbgA-Atto488 or 0.05 μM HflX-Atto488 were mixed with 15 μM and 10 μM GTP, ppGpp or pppGpp in TAKM7 just prior to usage. *E. coli* 50S subunits were used in excess relative to the fluorescently labelled proteins, with concentrations between 0.075 μM and 0.6 μM used as specified in the figure legends. Similar to the protein reactants, the 50S subunits were preincubated with nucleotides to prevent any rapid changes in nucleotide concentration following mixing. Samples at 2X concentration were loaded separately into the SX20 apparatus, and equal volumes (60 μl) of each reactant was rapidly mixed at 25°C. Atto488 was excited using a 470 nm LED and fluorescence was monitored through a 515 nm long-pass filter using logarithmic sampling for 10 seconds, over 1000 datapoints per reaction. The resulting traces were fitted using a double exponential function (Equation 2), with amplitude of fluorescence at time t (F), initial amplitude of fluorescence (F_0), the change in fluorescence of the first exponential phase (A_1), the apparent rate of the first exponential (k_{app1}), thee change in fluorescence of the second exponential phase (A_2), the apparent rate of the second exponential (k_{app2}) and time (t). Each trace was fitted individually, and averages were taken of at least five technical replicates. If necessary, a linear term was included (k_{app3}). The fluorescence amplitude was normalised to the mean average of the initial 10 fluorescence measurements. The microscopic rate constants k_1, k_{-1}, k_2 and k_{-2} (Equation 3) were calculated by plotting the sum and the product of the apparent rates k_{app1} and k_{app2} for each titration and analysing their relationship through linear regression. Taking a as the curve resulting from linear regression of the sum of k_{app1} and k_{app2} and b as the curve resulting from linear regression of the product of k_{app1} and k_{app2}, Equation 4, Equation 5,

Equation 6 and Equation 7 apply to enable calculation of the microscopic constants. The K_D of each interaction can then be estimated using Equation 8.

Equation 2: $$y = A_0 + A_1 exp(-k_{app1}x) + A_2 exp(-k_{app2}x) + k_{app3}x$$

Equation 3: $$P + S \underset{k_{-1}}{\overset{k_1}{\rightleftharpoons}} PS' \underset{k_{-2}}{\overset{k_2}{\rightleftharpoons}} PS$$

Equation 4: $$k_1 = gradient_a$$

Equation 5: $$k_{-1} = intercept_a - \left(\frac{gradient_b}{gradient_a}\right)$$

Equation 6: $$k_2 = intercept_a - k_{-1} - k_{-2}$$

Equation 7: $$k_{-2} = \frac{intercept_b}{k_{-1}}$$

Equation 8: $$K_d = \frac{k_{-1}k_{-2}}{k_1(k_2+k_{-2})} \equiv \frac{intercept_b}{gradient_b}$$

2.10.3 FRET using IF3$_{DL}$

Briefly, 0.2 µM IF3 dual-labelled (IF3$_{DL}$) with the Förster Resonance Energy Transfer (FRET) pair Atto488 and Atto540Q was either preincubated or rapidly mixed with 0.1 µM *E. coli* 30S ribosomal subunits and 0.2 µM recombinant, unlabelled Era, along with 20 µM GTP using the SX20 apparatus as described above. Equal volumes (60 µl) of each reactant was rapidly mixed, and the change in fluorescence was monitored using an excitation LED at 470 nm and a long-pass emission filter at 515 nm. Logarithmic sampling was carried out over 10 seconds, with 1000 total datapoints.

2.11 Ribosome profiles from *S. aureus* cell extracts

Crude isolations of *S. aureus* ribosomes were obtained as described previously (Uicker *et al.*, 2006), with some modifications as defined here. Briefly, 100 ml cultures of *S. aureus* were grown to mid-exponential phase, with an A$_{600}$ of 0.4 in TSB supplemented with the appropriate antibiotic and 100 ng/ml Atet. 100 µg/ml chloramphenicol was added, and following a 3 min incubation cultures were

slowly cooled to 4°C in order to produce runoff ribosomes free of mRNA. Cells were harvested via centrifugation at 6,000 × g for 10 mins, and pelleted cells were washed and resuspended in Ribosome Association Buffer (20 mM Tris-HCl pH 7.5, 8 mM MgCl$_2$, 30 mM NH$_4$Cl, 2 mM β-mercaptoethanol), normalised to an A$_{600}$ of 15, and lysed using 0.5 μg/ml lysostaphin and 75 ng/ml DNase I at 37°C for 60 mins. Cell debris was removed via centrifugation at 17,000 × g for 10 mins, and 250 μl of the supernatant was applied to an ice 10-50% discontinuous sucrose gradient made up in Ribosome Association Buffer. Following 7 hrs of ultracentrifugation at 192,100 × g, gradients were fractionated into 250 μl aliquots by upwards displacement and analysed for RNA content using A$_{260}$.

2.12 Synthesis of [^{32}P]-labelled RNA

Prior to any work concerning RNA, all surfaces and equipment was thoroughly treated with RNaseZAP (Sigma) to remove residual RNase. Filter pipette tips were also used, along with RNase-free water where possible. 4 μM of the 12-ribonucleotide RNA oligo AUCACCUCCUUU (IDT) was incubated with 10 units of T4 polynucleotide kinase (PNK) (NEB) in 1X PNK buffer (NEB), 10 mM DTT, and 1.4 MBq [γ-^{32}P]-ATP for 30 mins at 37°C. Any excess [γ-^{32}P]-ATP was removed using NucAway columns (Invitrogen) as per the manufacturer's instructions. Final quality of the preparation was analysed using TLC, with a 0.5M LiCl, 1 M formic acid running buffer such that the radiolabelled RNA would remain in the well and the free [γ-^{32}P]-ATP would migrate up the gel for quantification. High quality [^{32}P]-RNA was snap frozen in a dry ice/ethanol bath and stored at -20°C, ideally for use either immediately or within a few days to avoid degradation.

2.13 Crystallisation of RsgA

Purified, recombinant RsgA consisted of 311 amino acid residues, of which 291 were attributed to RsgA and 20 (MGSSHHHHHHSSGLVPRGSH) were attributed to the N-terminal hexahistidine tag. Purification was carried out as described in Section 2.3.2, with dialysis being carried out post-purification into Crystallisation Buffer (25 mM Tris-HCl pH 7.5, 200 mM NaCl), and concentration to 30 mg/ml. Crystallisation screening was carried out using the sitting drop vapour diffusion method, with each droplet consisting of 200 nl protein solution and 200 nl screening buffer from the adjacent well of 50 μl volume. The commercial screens employed were the PACT *premier* anion/cation screen (Newman *et al.*, 2005), the ProPlex targeted sparse matrix screen (Radaev *et al.*, 2006) and the JCSG+ optimised polyethylene glycol (PEG) sparse matrix screen (McPherson, 2001; Page *et al.*, 2003). Figures were prepared in Coot (Emsley and Cowtan, 2004; Emsley *et al.*, 2010) or PyMOL (The PyMOL Molecular Graphics System, Version 2.0 Schrödinger, LLC).

2.13.1 Crystallisation of RsgA-ppGpp

The concentrated 30 mg/ml RsgA solution was supplemented with 2 mM $MgCl_2$ and 2 mM ppGpp, giving a final RsgA molar concentration of 973 μM. Successful rod-shaped crystal formation was observed when this sample was mixed 1:1 with screening solution containing 0.2 M sodium citrate tribasic dihydrate, 0.1 M Bis-Tris propane pH 6.5 and 20% (w/v) PEG 3350 (PACT *premier* condition F11) and incubated at 17°C for approximately 2 weeks. The crystals were transferred using a loop to a cryoprotectant solution consisting of the mother liquor supplemented with 15% ethylene glycol (EG), before flash cooling in liquid N_2. Crystals were shipped under liquid N_2 to the Diamond Light Source national synchrotron facility beamline i04, and X-ray diffraction data was collected from a single crystal using a wavelength of 0.97949 Å. The ppGpp-bound crystals diffracted to 1.94 Å, and the diffraction patterns were processed initially using the Xia2 pipeline (Winter, 2010). The crystals belonged to the space group $P2_12_12_1$, and contained one RsgA monomer per asymmetric unit. For crystallographic data and statistics see Chapter 5. The structure of RsgA-ppGpp was solved via molecular replacement, using the previously solved YloQ homologue from *B. subtilis* (PDB: 1T9H) (Levdikov *et al.*, 2004) as a template model. Density due to residues 181-200 was lacking, and as such were not included in the model. Molecular replacement was carried out using Phaser from within the CCP4+ suite (McCoy *et al.*, 2007; Winn *et al.*, 2011), and iterative rounds of manual modelling and refinement was carried out using COOT and RefMac (Murshudov *et al.*, 1997). The final model was validated using MolProbity (Williams *et al.*, 2018) and submitted to the Protein Data Bank in Europe (PDBe) under the accession code 6ZHL.

2.13.2 Crystallisation of apo RsgA

Apo RsgA was successfully crystallised upon mixing of the RsgA stock solution diluted to 973 μM in Crystallisation Buffer 1:1 with screening buffer solution containing 0.15 M $(NH_4)_2SO_4$, 0.1 M MES pH 6 and 15% (w/v) PEG 4000, corresponding to ProPlex condition B10, and subsequent incubation at 17°C. A single rod shaped crystal formed after a few weeks, and was treated as described above. This crystal diffracted to a resolution of 2.01 Å, and was initially processed using the Xia2 pipeline, revealing a space group of $P12_11$ with two RsgA monomers in the asymmetric unit, displaying no rotational symmetry. The crystal structure was solved by molecular replacement using the RsgA-ppGpp model as a template, following removal of all ligands to leave only the main chain residues. Chain A was missing density relating to residues 180-200, and Chain B was missing density relating to residues 179-200, and so these residues were omitted from the final model. Iterative rounds of modelling and refinement were carried out as above, and post validation this model was uploaded to the PDBe servers under the accession code 6ZJO.

2.13.3 Crystallisation of RsgA-GDP

The rod-shaped RsgA-GDP crystals were successfully obtained when mixing apo-RsgA (as per solving the apo RsgA structure) 1:1 with screening buffer containing 0.2 M sodium citrate tribasic dihydrate, 0.1 M Bis-Tris propane pH 6.5 and 20% (w/v) PEG 3350 (PACT *premier* condition F11) and incubated at 17°C for approximately 2 weeks. Note that this is the same condition under which the RsgA-ppGpp was obtained following supplementation of the RsgA stock solution with 2 mM ppGpp. Crystal processing was carried out as above, and it was found that the crystals diffracted to 2.15 Å, belonged to the $P2_12_12_1$ space group and contained one monomer in the asymmetric unit. The structure was solved using the RsgA-ppGpp model as a template following removal of all ligands, and iterative rounds of modelling and refinement were carried out as above. Residues 180-200 were omitted due to lack of electron density. Post validation, this model was uploaded to the PDBe servers under the accession code 6ZHM.

2.14 CD spectroscopy

Recombinant protein was purified as per Section 2.3.2 and dialysed into circular dichroism (CD) Buffer (50 mM sodium phosphate pH 7.4, 100 mM NaCl) and was diluted to 10 μM as calculated by the A_{280}. A UV-clear quartz cuvette was used throughout, with a 1 mm path length. The CD spectra were measured using a J810 Spectropolarimeter (Jasco) flushed with inert, gaseous nitrogen for 20 mins prior to use. Spectra were taken between 190 nm and 250 nm with a sampling interval of 0.5 nm and a scanning speed of 20 nm/min. Each sample was subjected to 5 technically independent measurements, from which the mean values were taken and used for comparison.

2.15 ELISA

Doubling dilutions of purified *S. aureus* 30S or 50S ribosomes were carried out vertically in 96-well microplate (ThermoFisher) format, with final volume being 100 μl in TAKM7 (5 mM Tris-HCl pH 7.4, 70 mM ammonium acetate, 30 mM KCl and 7 mM $MgCl_2$). In the case of Era, 30S subunits were used from an initial concentration of 200 μM. These dilutions were left static at 4°C for 16 hrs in order to coat the wells. The plates were then washed three times using PBST (10 mM phosphate buffer pH 7.4, 137 mM NaCl, 2.7 mM KCl, 0.1% Tween20) and blocked using 5% (w/v) BSA made up in PBST for 2 hrs at RT to prevent nonspecific interactions. Following blocking, 100 μl of 500 nM His-tagged protein made up in TAKM7 plus 5% (w/v) BSA were added to each well and incubated statically at RT for 1 hr. Wells were washed three times as above and 100 μl of anti-His HRP conjugated antibodies (Sigma), diluted 1:10,000 in TAKM7 plus 5% (w/v) BSA was added, and incubated at RT for 1 hr. Wells were

washed three times as above and developed using 100 µl 3, 3′, 5, 5′-tetramethylbenzidine for up to 10 mins until colour develops, protected from light. Development was stopped and fixed through the addition of 0.67 M final concentration H_2SO_4, and association of the incident protein to ribosomal subunits was quantified through measuring the A_{450} in a Sense 425-301 microplate reader (Hidex). Control lanes were set up for each protein tested, either lacking ribosomal subunits or incident protein to check for any cross-reactivity.

2.16 Methionine uptake assays

Overnight cultures of *S. aureus* were grown overnight in TSB supplemented with the appropriate antibiotics, then diluted to an A_{600} of 0.1 in 10 ml fresh TSB with antibiotics and 100 ng/ml Atet. Samples of 1 ml were taken from each culture 5 mins post dilution (A_{600} ~ 0.1), and when the A_{600} of the culture reached 0.5. Mupirocin and Chloramphenicol controls were also included, using wild-type *S. aureus* cultures exposed to either 60 µg/ml mupirocin or 30 µg/ml chloramphenicol, and aliquots were taken simultaneously with the wild-type samples as these antibiotics prevented growth. Samples were normalised to A_{600} of 0.5, and incubated with 2 µCi ^{35}S-methionine at RT for 10 mins, then chased with 0.5 mg/ml cold methionine at room temperature for 10 mins. Cells were then washed three times with 70% ethanol, with pellet in between washes carried out at 17,000 × *g* for 1 min. Following washing, cells were resuspended in 20 µl 70% ethanol and spotted onto Whatmann paper. Spots were allowed to air dry, then were exposed to the IP for 16 hrs before visualisation using a LA 7000 Typhoon Phosphorimager (GE Healthcare), and the resulting signal strength was quantified using ImageQuant (GE Healthcare). Samples were corrected for immediate (and variable) background signal through adaptation of the DRaCALA equation (Equation 9) to calculate the signal intensity due to background by extrapolating the immediate background around each spot (Roelofs *et al.*, 2011), with signal intensity (I) and area of sampling (A).

Equation 9: $$I_{corrected} = I_{inner} - A_{inner}\left(\frac{I_{total} - I_{inner}}{A_{total} - A_{inner}}\right)$$

2.17 Statistical analyses

All statistical analyses were performed using Graphpad Prism 8.0 software. Statistical differences between samples were assessed using either Student's t-tests or one-way mixed-effect analysis of variance (ANOVA), followed by Tukey's multiple comparisons test. *P* values are represented as follows, or as described in the figure legends: *, $p < 0.05$; **, $p < 0.01$; ***, $p < 0.001$; ****, $p < 0.0001$.

2.18 Drawing and rendering of molecular graphics

All molecular graphics were drawn by the author using PyMOL (The PyMOL Molecular Graphics System, Version 2.0 Schrödinger, LLC) with available PDB entries as defined in the figure legends being used. All schematics were produced using Adobe Illustrator.

Chapter 3 – Biochemical characterisation of staphylococcal RA-GTPases

3.1 Introduction

It is widely accepted that during periods of exponential growth, with high nutrient and energy availability, that the rate of protein synthesis is the chief determinant of growth rate for bacteria (Bosdriesz *et al.*, 2015; Dai *et al.*, 2016), with the number of ribosomes per amount of total protein being directly proportional to growth rate (Dennis *et al.*, 2004). During rapid growth, actively translating ribosomes can account for between 28% and 49% of the dry mass of an *E. coli* cell (Bremer and Dennis, 2008; Hu *et al.*, 2020; Piir *et al.*, 2011), *de novo* synthesis and maintenance of which represents a substantial energetic cost to the cell. In order to maximise efficiency of ribosome synthesis, key stages are presided over by checkpoint proteins to ensure the correct maturation state has been reached prior to continuation of assembly (Britton, 2009; Karbstein, 2007; Verstraeten *et al.*, 2011). The majority of these proteins are GTPases within the TRAFAC family (Bennison *et al.*, 2019), and can have several key roles within the cell, though to include acting as scaffold proteins to enable association of processing factors to the ribosomal subunits (Vercruysse *et al.*, 2016; Wood *et al.*, 2019), direct remodelling of rRNA into a mature conformation (Dey *et al.*, 2018), or sterically hindering premature r-protein association or 30S and 50S joining (Feng *et al.*, 2014).

Due to the requirement of high levels of both ATP and GTP during active protein translation (Hu *et al.*, 2020), it is crucial for the cell to correctly regulate this process in response to changing growth conditions. *In situ*, bacterial cells are rarely exposed to consistent high nutrient levels, and instead progress through repeat feast-famine cycles which enable proliferation when possible, and survival when nutrients are low (Sebastián *et al.*, 2019). The primary bacterial response to low nutrient availability is known as the stringent response (Irving *et al.*, 2020), and is characterised by production of two alarmone nucleotides collectively referred to as (p)ppGpp (Hauryliuk *et al.*, 2015; Hobbs and Boraston, 2019; Potrykus, 2008; Steinchen and Bange, 2016). There are several routes by which the stringent response can regulate translation, of which inhibition of translation factors such as IF2, EF-Tu and EF-G (Cheng-Guang and Gualerzi, 2020; Mitkevich *et al.*, 2010) and downregulation of rRNA and r-protein synthesis are the most well-understood (Krasny and Gourse, 2004; Kriel *et al.*, 2012). Recently, however, (p)ppGpp has been found to bind to and inhibit the GTPase activity of four RA-GTPases in *S. aureus*, namely RsgA, RbgA, Era and HflX (Corrigan *et al.*, 2016), each of which are known as ribosome assembly factors. Inhibition of these proteins negatively impacts the assembly of 70S

ribosomes, thus reducing the translational capacity of the cell, although the precise mechanism by which this occurs is unknown.

In order to commence investigation into the role of these proteins as ribosome assembly factors and stringent response effectors, we first needed to perform a full biochemical characterisation of each. In this chapter, we purify recombinant *S. aureus* RsgA, RbgA, Era and HflX and perform biochemical evaluation of the nucleotide binding affinity and enzymatic activity of each, establishing that the mechanism of inhibition by (p)ppGpp is competitive and specific. Altogether, this work was carried out with the intention of providing a general understanding of the activity and mechanism of action of these proteins, knowledge that can be applied to more nuanced study downstream.

3.2 Purification of 6xHis-tagged RA-GTPases

In order to carry out *in vitro* experiments to determine the binding affinity and enzymatic activity of RsgA, RbgA, Era and HflX, we first had to obtain highly pure, functional protein. Previously in our lab, these RA-GTPases had been purified using an N-terminal His-maltose binding protein (MBP) tag (Corrigan *et al.*, 2016) to enable purification via IMAC, as well as to enhance solubility via by the MBP (Kapust and Waugh, 1999). However, one of the major aims of this project was to carry out crystallographic studies to examine the structural consequences of (p)ppGpp binding (Chapter 5), and as such the protein used should be modified as little as possible, as large tags can hinder crystal packing or introduce conformational artifacts. Already present in the laboratory strain collection were *E. coli* protein expression strains containing pET28b:*RA-GTPase* plasmids, which encodes the protein of interest fused to an N-terminal hexahistidine (6xHis) tag, under the control of a T7 promoter. The expression strain used was the commercially available BL21 (DE3), an *E. coli* strain which houses the DE3 phage, which in turn encodes the phage-borne T7 polymerase behind a tightly-regulated IPTG inducible promoter. The presence of the N-terminal 6xHis tag enables IMAC to be used to selectively purify the protein of interest using a column containing Nickel-NTA-agarose resin.

3.2.1 Small-scale overexpression trials of the four RA-GTPases

The first step to carrying out a purification was to optimise expression of the protein of interest. Standard procedure when using BL21 (DE3) cells is to induce with 1 mM IPTG, and as such an initial small-scale induction was performed using these conditions (Figure 3.2.1a). Overnight cultures of the expression strains were back diluted into two fresh 5 ml cultures containing kanamycin to maintain the pET28b plasmid, and grown at 30°C until an A_{600} of 0.5 was reached. At this point, cultures were either induced with 1 mM IPTG or left uninduced as controls, and then incubated for a further 3 hrs

at 30°C. The A_{600} was measured post-induction, and cultures normalised to be loaded onto an SDS-PAGE gel to analyse protein content. The expected molecular weights of RsgA, RbgA, Era and HflX including the N-terminal 20 residue tag were 36053.77 Da, 35702.19 Da, 36505.03 Da and 49499.07 Da respectively. Overexpression of RbgA, Era and HflX was observed following the 3 hr exponential phase induction using 1 mM IPTG (Figure 3.2.1a), however RsgA was lacking any clear band present in the induced lysate compared to the uninduced. This could be due to several factors, including potential product toxicity. To reduce the burden of inducing potentially toxic RsgA during exponential phase growth, we opted to trial a stationary phase induction (Figure 3.2.1b), during which saturated overnight cultures of BL21 (DE3) pET28b:*rsgA* were directly induced with between 0.4 mM and 1.0 mM IPTG and incubated for 6 hrs or 24 hrs at 30°C before normalisation and analysis via SDS-PAGE. Contrary to the exponential phase induction, overexpression bands of the expected size were observed in all conditions tested (Figure 3.2.1b). More intense overexpression occurred at 0.4 mM IPTG, which decreased as the concentration of inducer increased, lending weight to the product toxicity hypothesis. However, the reason for this potential toxicity is currently unknown. Overall, we have established overexpression conditions for each of the four RA-GTPases, namely a 6 hr stationary phase induction using 0.4 mM IPTG for RsgA, and 3 hr exponential phase inductions using 1 mM IPTG for RbgA, Era and HflX, and can now proceed to large scale purification.
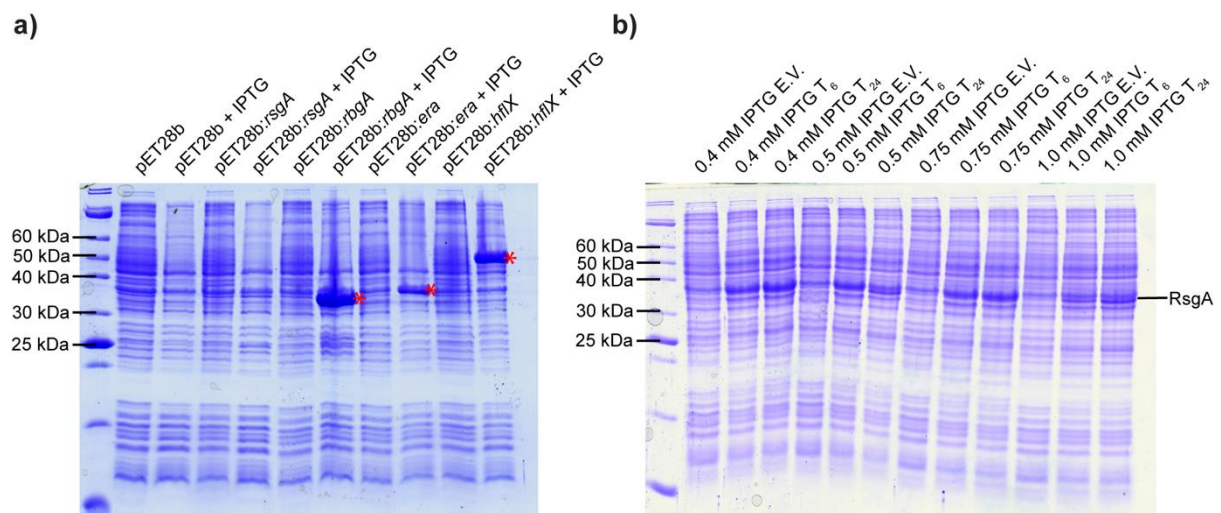
Figure 3.2.1: Small-scale protein overexpression trials for RsgA, RbgA, Era and HflX. a) Exponential phase overexpression trials of RsgA (lanes 4 and 5), RbgA (lanes 6 and 7), Era (lanes 8 and 9) and HflX (lanes 10 and 11). Overnight cultures were backdiluted to an A_{600} of 0.05, and grown to mid-exponential phase before induction using 1 mM IPTG and incubation for 3 hrs at 30°C. Cells were harvested and normalised to an A_{600} of 1.0 in 100 μl of SDS-PAGE loading buffer, and run on a 12% SDS-PAGE gel. Empty vector controls were included for comparison (lanes 2 and 3). Bands concerning the proteins of interest are highlighted with a red asterix. b) Stationary phase overexpression trials of RsgA. Saturated cultures were split and induced with either 0.4 mM (lanes 2-4), 0.5 mM (lanes 5-7), 0.75 mM (lanes 8-10) or 1 mM (lanes 11-13) IPTG for either 6 hr 24 hrs as indicated. In each case, an empty vector control induced with the same concentration of IPTG for 6 hrs is

included for comparison (labelled E.V.). SDS-PAGE gels were stained using Coomassie Brilliant Blue as described in the methods section. The band size concerning RsgA is highlighted.

3.2.2 Large scale protein purifications using IMAC

To achieve a good yield of protein following IMAC, purification trials were carried out using culture volumes of one litre, mimicking the conditions decided upon following small scale expression trials. The His-tagged proteins of interest were isolated from crude cell lysates using an ÃKTA prime liquid chromatography system programmed to carry out a gradient elution protocol. Fractions containing protein (Figure 3.2.2a, b) were collected and pooled, before thoroughly dialysed to remove excess imidazole, as prolonged incubation of protein with high concentrations of imidazole can act to destabilise and reduce both the solubility and activity of the protein (Hamilton *et al.*, 2003). Concentration of the protein of interest was then carried out using membrane ultrafiltration, final concentration was measured using the A_{280} as specified in the methods section, and serial dilutions of the protein were run on SDS-PAGE and subject to band densitometry as a measure of purity (Figure 3.2.2c). Typically, a purity of a least 95% is required for *in vitro* protein experimentation, however our preps were frequently above 99% pure. Furthermore, the A_{260}:A_{280} ratio of the protein was measured, as each of the four RA-GTPases being purified are well-documented RNA-binding proteins (Verstraeten *et al.*, 2011), so it was crucial to ensure a low level of RNA contamination due to co-purification. An A_{260}:A_{280} ratio of 0.8 or below typically indicates <5% RNA contamination, and this was used as the upper limit of an acceptable preparation (Wood *et al.*, 2019). To reduce this contamination, lysates were treated with RNase prior to the purification step as specified in the methods section. Figures referred to during this section are taken from the same purification of RbgA, and are representative of the process employed for each protein purified.
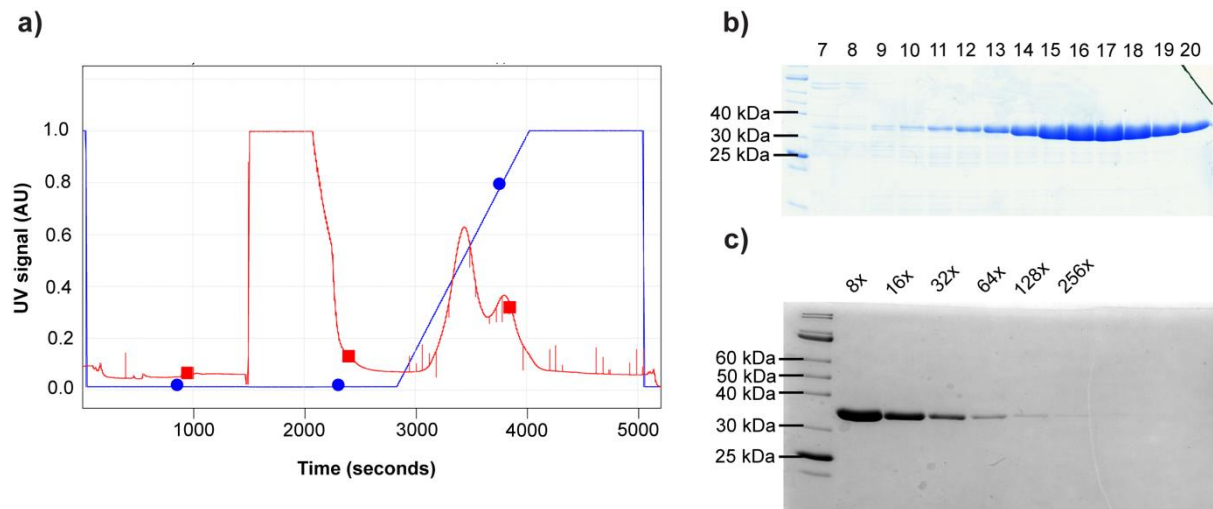
Figure 3.2.2: Stepwise example of a typical IMAC purification. a) Chromatogram of an RbgA purification protocol, indicating the proportional representation of imidazole-containing buffer B (blue trace) and the UV signal of the elution volume (red trace). Note two major peaks in UV signal, a singlet from around 1500-2400 seconds, indicating the cell lysate passing through the column, and a doublet following 3000 seconds, indicating elution of bound proteins due to the increasing imidazole concentration. b) SDS-PAGE showing the fractions obtained from the purification shown in (a). Fractions containing a high proportion of RbgA to contaminating proteins were pooled together for dialysis and purification. c) SDS-PAGE of serial dilutions (indicated) of the neat protein prep following dialysis and concentration as a measure of purity. SDS-PAGEs in (b) and (c) were stained with Coomassie Brilliant Blue as detailed in the methods section.

3.3 The ability of RsgA, RbgA, Era and HflX to bind guanine nucleotides

3.3.1 Binding curves of the RA-GTPases

During rapid cellular growth, GTP is the predominant guanine nucleotide within the cell, with concentrations rising to between 200 µM and 500 µM (Traut, 1994). Despite this, many eukaryotic GTPases have evolved to have relatively high affinities for GTP in the mid-nanomolar range (Verstraeten *et al.*, 2011), requiring the use of GTPase activating factors (GAPs) and guanine nucleotide exchange factors (GEFs) to progress through the GTPase cycle from the GTP-bound ON state to the GDP-bound OFF state, and back again. Conversely, these GAPs and GEFs are rare in prokaryotes, where GTPases have evolved relatively low nucleotide affinities with K_D values around the physiological GTP concentrations during exponential growth (Verstraeten *et al.*, 2011). This allows GTPases to fine-tune their nucleotide binding preferences reliant on the cellular energy level, and as such adapt the processes they control, for example translation, to suit the current energetic environment. It has been previously reported, however, that ribosome assembly factors have relatively high nucleotide affinities (Corrigan *et al.*, 2016; Fischer *et al.*, 2012; Shimamoto and Inouye, 1996), although these data are lacking in regard to the affinity of the RA-GTPases for GDP – despite the essentiality of GDP exchange for GTP during the GTPase cycle. Therefore, we set out to fully characterise the binding affinities of the four RA-GTPases to the four major guanine nucleotides within

bacterial cells which may play a role in the GTPase cycle of ribosome assembly factors: GTP, GDP, ppGpp and pppGpp. To this end, we utilised the DRaCALAs (Roelofs *et al.*, 2011) to generate binding curves (Figure 3.3.1a-d). Doubling dilutions of each recombinant protein, starting at a concentration of 100 μM, were incubated with a constant concentration of radiolabelled nucleotide for 5 mins before spotting onto a nitrocellulose membrane. Quantification of binding can be achieved by calculating the ratio of labelled ligand bound to protein, which remains sequestered at the point of contact, compared to the unbound ligand which flow outwards due to capillary action (see methods section). Resulting binding curves can be fitted with a single exponential function, accounting for an undetermined level of background signal, which enables derivation of binding parameters (Table 3.3.1), namely the K_D and B_{max}.

Overall, the calculated binding affinities were all within the low micromolar range in agreement with what has been previously observed (Corrigan *et al.*, 2016; Shimamoto and Inouye, 1996), with the exception of HflX binding to GTP and pppGpp, neither of which generated derivable K_D values under the conditions used (Table 3.3.1). Each of the four proteins tested exhibited a greater affinity for the 5'-diphosphate containing nucleotides GDP and ppGpp, with both RbgA and Era binding 5'-triphosphate containing nucleotides GTP and pppGpp around 3-fold less tightly than the GDP or ppGpp. The fitting of a single exponential function for the nucleotide binding curves here is indicative of a single binding site, and in all cases the Hill coefficient was between 0.91 and 1.15, together suggesting the presence of a single nucleotide binding site.
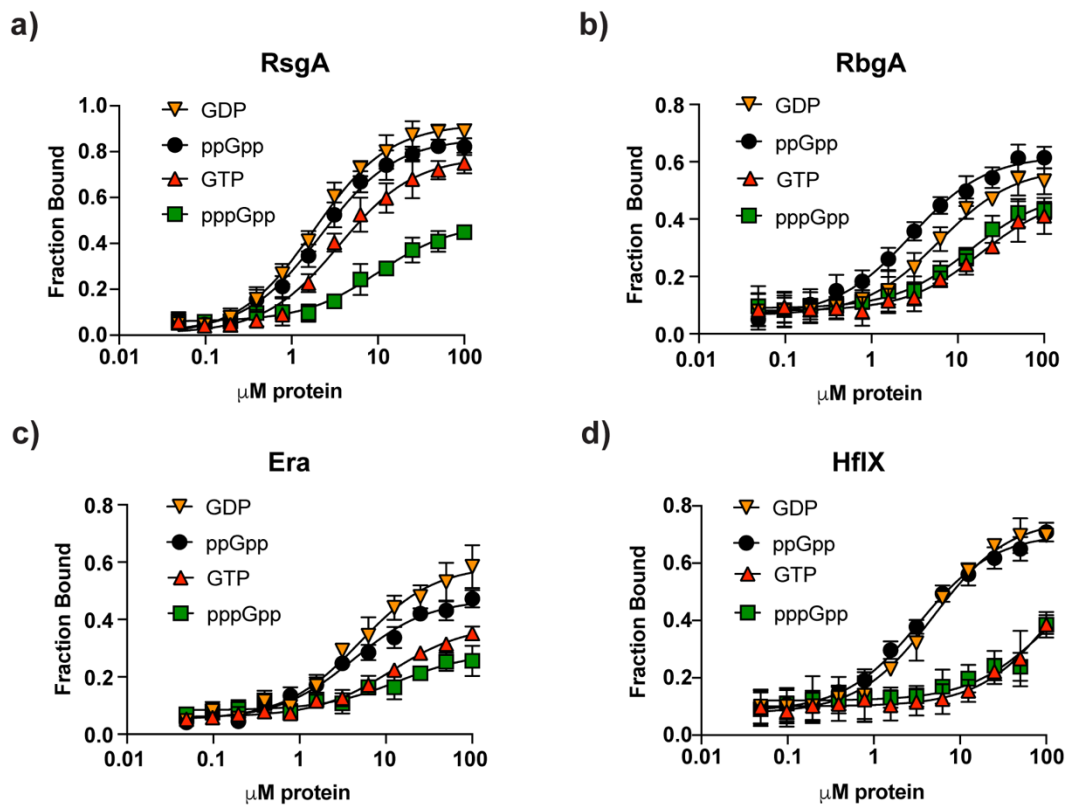
Figure 3.3.1: Nucleotide binding curves of RsgA, RbgA, Era and HflX. Doubling dilutions of recombinant a) RsgA, b) RbgA, c) Era and d) HflX from an initial concentration of 100 µM were incubated with with 1.83 nM [α-^{32}P] labelled GTP, GDP, ppGpp or pppGpp. Following incubation at room temperature for 5 mins, samples were spotted onto a nitrocellulose membrane and exposed to a photostimulable phosphor screen and visualised using a phosphorimager. Pixel densitometry was carried out as specified in the methods section. Resulting curves were fitted using the One Site Specific Binding model on the Graphpad Prism 8.0 software, amended to include a background signal. Experiments were performed in triplicate, with error bars representing the standard deviation between replicates.

Table 3.3.1: Binding parameters of guanine nucleotides to recombinant RsgA, RbgA, Era and HflX

		K_d (µM)	B_{max} (% bound)
RsgA	GTP	3.56 ± 0.41	0.77 ± 0.02
	GDP	1.83 ± 0.16	0.92 ± 0.02
	ppGpp	2.17 ± 0.20	0.85 ± 0.02
	pppGpp	10.06 ± 2.16	0.43 ± 0.03
RbgA	GTP	18.48 ± 5.35	0.40 ± 0.04
	GDP	6.07 ± 1.05	0.52 ± 0.02
	ppGpp	2.86 ± 0.40	0.56 ± 0.02
	pppGpp	13.76 ± 4.04	0.41 ± 0.03
Era	GTP	11.50 ± 1.61	0.34 ± 0.02
	GDP	4.94 ± 0.72	0.54 ± 0.02
	ppGpp	4.21 ± 0.55	0.42 ± 0.01
	pppGpp	13.87 ± 4.71	0.20 ± 0.02
HflX	GTP	ND	0.65 ± 0.03
	GDP	4.92 ± 0.70	0.68 ± 0.02
	ppGpp	3.37 ± 0.44	0.62 ± 0.02
	pppGpp	ND	0.48 ± 0.02

ND = Not Determined

3.3.2 Competition binding assays

There are two accepted modes of ligand-mediated protein inhibition, competitive and non-competitive (Ramsay and Tipton, 2017). Competitive inhibitors directly compete with the intended substrate by binding to the same site, often with a higher affinity than the substrate, preventing intended enzyme function. Noncompetitive inhibitors bind at a distal site on the enzyme, allosterically preventing function in a substrate-independent manner. The stringent response alarmones (p)ppGpp are known to interact with target proteins in both a competitive and allosteric fashion. Structural studies into (p)ppGpp binding to the *E. coli* DNA primase and *S. aureus* RbgA have shown competitive modes of inhibition (Pausch *et al.*, 2018; Rymer *et al.*, 2012), in which (p)ppGpp binds to the active site in an identical manner to GTP due to the backbone guanosine tri/diphosphate moiety. The Gram-positive small alarmone synthetase RelQ, however, binds pppGpp allosterically at two tetramerisation interfaces in order to stimulate synthetase activity (Steinchen *et al.*, 2018). Similarly, the Gram-negative RNAP-DksA complex is allosterically influenced by ppGpp to adapt the cellular transcriptome in response to stress conditions (Molodtsov *et al.*, 2018). Although the former is allosteric activation, and the latter allosteric remodelling, these systems demonstrate the potential of (p)ppGpp to influence the activity of proteins through allosteric means, and as such we could not rule out that this is the case with RsgA, RbgA, Era and HflX.

To investigate whether the inhibition of these RA-GTPases by (p)ppGpp is competitive or noncompetitive, we carried out competition binding assays (Figure 3.3.2). The capacity of the protein to bind [α-^{32}P] labelled GTP, ppGpp and pppGpp was tested through the addition of a roughly 55,000-fold molar excess of a range of cold competitor nucleotides (100 µM competitor vs 1.83 nM radiolabelled nucleotide), to see if the competitor could displace the radiolabelled ligand in the RA-GTPase ligand binding site. For competitive inhibition, presence of the cold competitor nucleotide would decrease radiolabelled ligand binding. In the case of noncompetitive inhibition, the binding of radiolabelled ligand would likely be unaffected by distal binding of the inhibitor molecule. Based on the structural studies of Pausch *et al.* concerning *S. aureus* RbgA (Pausch *et al.*, 2018), we anticipated that the mechanism of inhibition would be competitive. Indeed, in the case of all four proteins, the binding of radiolabelled GTP was reduced compared to binding in the absence of competitor by addition of cold GTP, GDP, ppGpp and pppGpp in an affinity-dependent manner, i.e. GDP and ppGpp were comparably competent inhibitors, and the four RA-GTPases also exhibit the greatest affinity for these two nucleotides (Figure 3.3.1). In the case of radiolabelled ppGpp, cold GDP and ppGpp effectively reduce binding, whereas the effect of GTP and pppGpp is lessened. The affinity of the bound radiolabelled ppGpp is much greater than that of GTP or pppGpp, and as such the 5'-triphosphate containing nucleotides are less effective at inhibiting binding. Finally, binding of radiolabelled pppGpp was effectively inhibited in the case of RsgA, RbgA and Era, although it is worthy of note that the initial binding of HflX to radiolabelled pppGpp (around 10%) was so low that identifying inhibition was difficult. The ability of cold ATP to inhibit binding of the guanine nucleotides was also assessed in order to determine whether the binding preference of these proteins was guanine-specific. In each tested case, ATP was unable to compete with binding of radiolabelled GTP, ppGpp or pppGpp, with the fraction bound being highly similar to in the absence of cold competitor. This indicates that despite the structural similarity between ATP and GTP, the four RA-GTPases in question were highly specific for guanines. Overall, these experiments highlight the specific, competitive nature of (p)ppGpp-mediated inhibition of GTPase activity and support the binding hierarchy determined in section 3.3.1, in which RsgA, RbgA, Era and HflX have increased binding affinity for 3'-diphosphate containing nucleotides compared to their 5'-triphosphate containing counterparts.
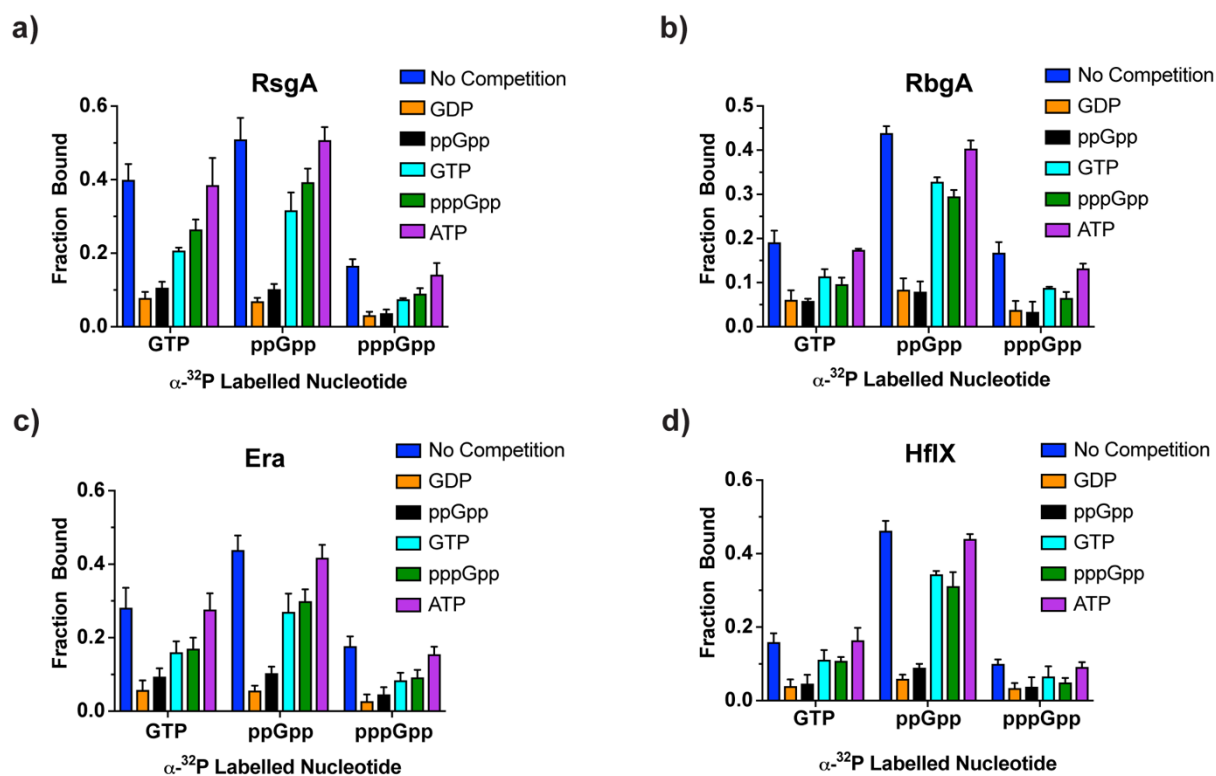
Figure 3.3.2: Competition binding assays of radiolabelled GTP, ppGpp and pppGpp in the presence and absence of cold competitor nucleotides. 10 µM of recombinant a) RsgA, b) RbgA, c) Era and d) HflX were incubated with 1.83 nM [α-^{32}P]- containing GTP, ppGpp or pppGpp as well as 100 µM GDP, ppGpp, GTP, pppGpp or ATP for 5 mins. Samples were spotted onto nitrocellulose, visualised with a photostimulable phosphor screen and pixel densitometry was carried out as described in the methods section. Each experiment was carried out in triplicate, and error bars represent standard deviation between replicates.

3.4 Investigating the NTPase activity of RsgA, RbgA, Era and HflX

3.4.1 The NTPase activity of RsgA, RbgA, Era and HflX can be inhibited by ppGpp

While it is currently well known that (p)ppGpp can inhibit the GTPase activity of the four RA-GTPases (Corrigan *et al.*, 2016), in what we have established is a competitive manner (section 3.3.2), the first step in beginning to formulate a potential mechanism of inhibition was confirming our proteins were both functional (that is to say GTPase active) and could be inhibited by ppGpp. While unlikely, the presence of a different purification tag compared to that used for previous studies could have adverse effects on protein stability or activity. While the capacity of these recombinant proteins to bind to guanine nucleotides has already been shown (section 3.3.1), suggesting that the proteins are structurally correct, the GTPase activity of these proteins remains to be tested. In order to investigate the GTPase activity of RsgA, RbgA, Era and HflX, we incubated 2.5 µM recombinant protein in the presence and absence of an excess of cold ppGpp with [α-^{32}P]-labelled GTP in the presence of purified *S. aureus* ribosomes. Ribosomes have previously been shown to increase the rate of GTP hydrolysis by up to 120-fold (Guo *et al.*, 2011) through *in trans* provision of a GTPase activating element, similarly to eukaryotic GAPs. Reactions were incubated for 60 mins at 37°C, with the exception of the reaction

involving RsgA which was incubated for 10 mins. Samples were then incubated at 95°C to release any bound nucleotide, and the percentage GTP hydrolysis was determined using TLC and pixel densitometry (Figure. 3.4.1a). Each of the four RA-GTPases were capable of hydrolysing GTP to differing extents during the aforementioned reaction times, with RsgA achieving 100% hydrolysis after 10 mins, reducing to 30% in the presence of an excess of ppGpp. RbgA, Era and HflX achieved 49.7%, 47.8% and 58.8% hydrolysis respectively, which reduced to 4.8%, 4.3% and 3.9% in the presence of ppGpp, indicating significant inhibition (Figure 3.4.1a). The 100% hydrolysis of GTP by RsgA suggests that these reaction conditions require further optimisation (see section 3.4.2). Overall, we have shown that our recombinant RsgA, RbgA, Era and HflX are GTPase active, and can be inhibited by ppGpp consistent with previous reports (Corrigan *et al.*, 2016).

HflX has been suggested to exhibit ATPase activity (Dutta *et al.*, 2009; Shields *et al.*, 2009) attributed to the presence of a unique ATP-binding domain (Jain *et al.*, 2013) which has since been discovered to convey ATP-dependent RNA helicase activity (Dey *et al.*, 2018). We sought to investigate whether RsgA, RbgA and Era also exhibited ATPase activity, and if so whether it could be inhibited by ppGpp (Figure 3.4.1b). Reaction conditions were set up in an identical fashion to the GTPase assays mentioned above, with the exception that [α-^{32}P]-labelled ATP was included instead of GTP. RsgA (Figure 3.4.1bi), Era (Figure 3.4.1bii) and HflX (Figure 3.4.1biv) were capable of hydrolysing ATP, with 95.0%, 56.0% and 22.9% hydrolysis respectively. Furthermore, each could be inhibited by the addition of an excess of ppGpp. RbgA, on the other hand, showed the relatively low ATPase activity of 11.9% following the 60 min incubation, albeit with a large variation between repeats (Figure 3.4.1bii). In addition, the inclusion of ppGpp failed to significantly reduce ATP hydrolysis in this case. While high levels of substrate specificity were observed during the competition assays in section 3.3.2, ATP was still capable of binding in the absence of guanine nucleotides. This suggests that while the G4 motif of these RA-GTPases is sufficient to skew binding affinity strongly in favour of guanine nucleotides, it remains insufficient to completely occlude adenine nucleotide binding in the absence of guanines.
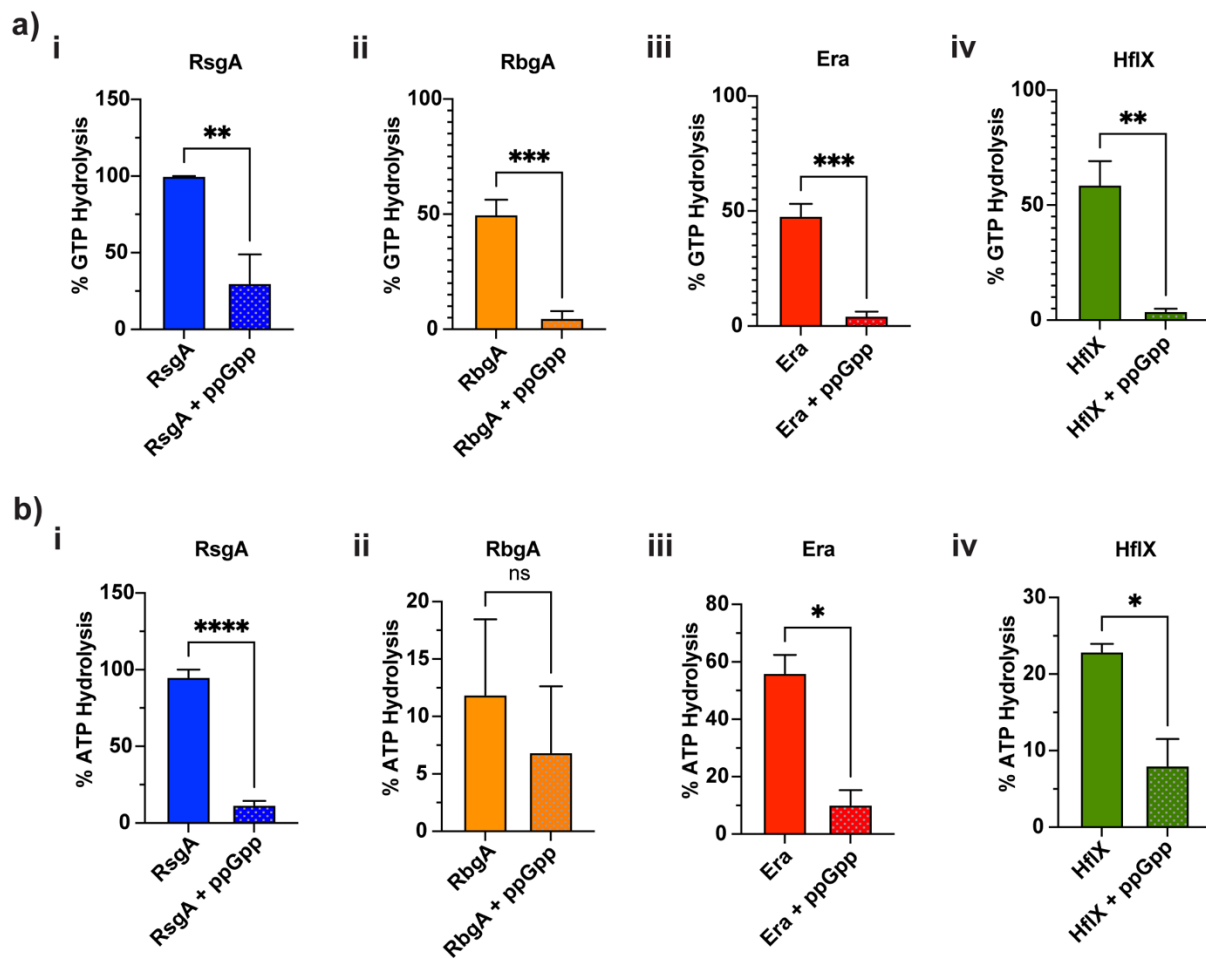
Figure 3.4.1: The NTPase activity of RsgA, RbgA, Era and HflX can be inhibited by ppGpp. The a) GTPase and b) ATPase activity of i) RsgA, ii) RbgA, iii) Era and iv) HflX in the presence and absence of ppGpp. 2.5 µM recombinant protein was incubated with 1.83 nM [α-^{32}P]-labelled a) GTP or b) ATP, purified 70S ribosomes from *S. aureus* and either in the presence or absence of 100 µM cold ppGpp. Reaction mixtures were incubated for 10 mins in the case of RsgA, or 60 mins in the case of RbgA, Era and HflX at 37°C, then for 5 mins at 95°C to release bound nucleotide. Samples were resolved using TLC, and imaged using a photostimulable phosphor as described in the methods section. Experiments were carried out in triplicate, and error bars represent the standard deviation between replicates. Statistical significance was determined using unpaired *t* testing, with *p* values represented as follows: *, $p < 0.05$; **, $p < 0.01$; and ***, $p < 0.001$.

3.4.2 Optimisation of GTPase activity assays of RsgA and RbgA

During the previous GTPase assays, 2.5 µM RsgA hydrolysed 100% of the GTP in the reaction mixture within a 10 min incubation, whereas RbgA, Era and HflX could not fully hydrolyse the substrate within 60 mins. This suggests that RsgA has a much greater activity than the other three RA-GTPases, and despite showing that ppGpp does in fact inhibit the GTPase activity of RsgA, the reaction conditions require optimisation prior to downstream experiments to allow identification of any alteration in activity between samples, as two samples with different activities could both fully hydrolyse the GTP following a given incubation time, rendering these differences impossible to evaluate. To this end, serial dilutions of RsgA were incubated with 1 µM GTP, spiked with radiolabelled GTP, and an

equimolar concentration of 70S ribosomes purified from *S. aureus*. The excess of cold GTP was added so as to not introduce initial substrate limitation of GTPase activity. Reaction mixtures were incubated for 10 mins at 37°C, before resolution using TLC (Figure 3.4.2a). At 1 μM concentrations, RsgA was capable of fully hydrolysing the GTP within the mixture. At 0.1 μM, a conversion of 41% was observed, which diminished to control levels of GTP hydrolysis with further dilution of RsgA to 0.01 μM and 0.001 μM (Figure 3.4.2a). In order to analyse changes in activity during subsequent GTPase assays, a wild type hydrolysis of around 50% is desired. Therefore, downstream experiments used a concentration of 0.1 μM RsgA with a 10-fold excess of GTP and a 10 min incubation.

Previous reports have identified RbgA as a K-loop containing protein in *B. subtilis* (Achila *et al.*, 2012), which requires a coordinated K^+ ion as a GTPase activating element. There are currently two other TRAFAC GTPases which are known to require K^+ ions, namely MnmB and FeoB (Ash *et al.*, 2011; Scrima and Wittinghofer, 2006). To test whether the presence of K^+ ions would increase the GTPase activity of *S. aureus* RbgA, we substituted 100 mM NaCl in our typical GTPase assay buffer (see methods section) for 100 mM KCl, and analysed the GTPase activity of 0.1 μM RbgA in the presence of an equimolar concentration of *S. aureus* 70S ribosomes and a 10-fold molar excess of GTP, spiked with radiolabelled GTP. Samples were incubated for 60 mins at 37°C, then resolved using TLC (Figure 3.4.2b). Worthy of note was that since increasing the concentration of GTP within the reaction mixture from 1.83 nM to 1 μM, no hydrolysis of GTP by RbgA was visible compared to the assays in Figure 3.4.1. Despite the presence of the same concentration of radiolabelled GTP, an excess of cold GTP could mask the low GTPase activity of RbgA. However, upon inclusion of KCl in the GTPase buffer, RbgA activity increased significantly, and 57.2% of the GTP was successfully hydrolysed (Figure 3.4.2b). Due to this result, future assays regarding the GTPase activity of RbgA were carried out using the amended reaction buffer including KCl.
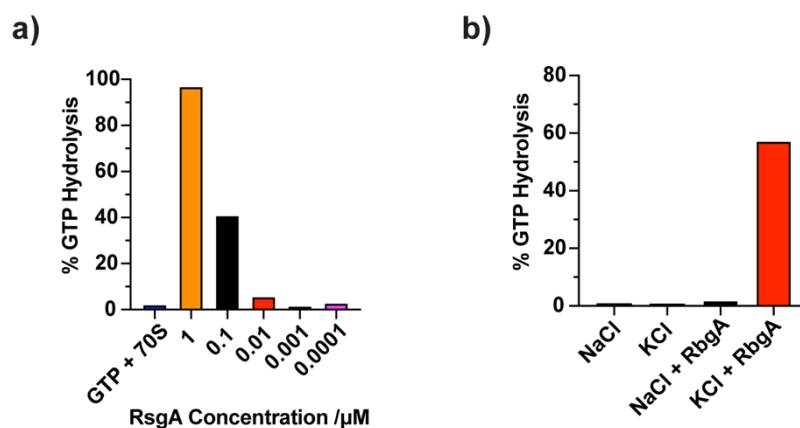
Figure 3.4.2: Optimisation of RsgA and RbgA GTP hydrolysis assays. a) Differing concentrations of RsgA were incubated with 1 μM cold GTP, 1.83 nM [α-^{32}P] labelled, an equimolar concentration of purified *S. aureus* 70S ribosomes and GTP hydrolysis buffer as per the methods section. A reaction containing GTP and 1 μM 70S ribosomes was included as a control. Reaction mixtures were incubated for 60 mins at 37°C, before heat inactivation for 5 mins at 95°C, resolution using TLC and imaging using a photostimulable phosphor. Percentage hydrolysis was calculated using pixel densitometry. b) The GTPase activity of RbgA in the presence of Na$^+$ and K$^+$ ions. 0.1 μM RbgA was incubated with 1 μM cold GTP, 1.83 nM [α-^{32}P]-labelled GTP, 0.1 μM *S. aureus* 70S ribosomes and GTPase assay buffers containing either 100 mM NaCl or 100 mM KCl. The two assay buffers including GTP and ribosomes were included as controls. The reaction were carried out and analysed as for part (a). All experiments were carried out once.

3.6 Discussion

In this chapter, we aimed to purify and characterise the nucleotide binding capacity and GTPase activity of four RA-GTPases from *S. aureus*, namely RsgA, RbgA, Era and HflX. This characterisation was to provide a basal understanding of the wild-type protein activity in order to provide a point of comparison and to be able to better interpret more in depth structural, biochemical and mutagenic analyses carried out downstream.

We first carried out IMAC purifications of 6xHis-tagged proteins, the expression vectors for which were readily available in our strain collection. Ni^{2+}-NTA charged columns are highly effective at separating proteins of interest from the majority of protein present in the cell lysate, however this technique comes with several caveats. Primarily, divalent metal cation chelating proteins would also bind to the column due to a lack of a unique binding partner, which may decrease sample purity. Ideally IMAC would be used as a primary purification step followed by a more stringent gel filtration approach to separate any potential contaminants. The quality of the protein preparations following IMAC purification was deemed to be >95% in all cases, with the majority of preparations being >99%, which for our purposes was sufficient. Another potential drawback arose when purifying RsgA, which contains a C-terminal zinc-finger domain (Levdikov *et al.*, 2004). The tertiary structure of this domain is highly dependent on the precise chelation of a Zn^{2+} ion by three highly conserved cysteine residues

and one highly conserved histidine. While unlikely due to the extremely high affinity of these domains for Zn^{2+} ions, between 10^{-9} and 10^{-11} M (Kluska *et al.*, 2018), exposing this protein to a Ni^{2+}-charged IMAC column may lead to substitution of the bound ion for Ni^{2+}, compromising the domain structure and functionality (Voráčková *et al.*, 2011). Instead, IMAC columns should be pre-emptively charged with Zn^{2+} ions, which are still able to be chelated by polyhistidine tags. Due to the activity of the purified RsgA however, it is highly unlikely that any such substitution occurred.

We have shown that purified recombinant RsgA, RbgA and Era have a high affinity in the low micromolar range for the four predominant cellular guanine nucleotides, namely GTP, GDP, ppGpp and pppGpp (Figure 3.3.1a – c and Table 3.3.1), in agreement with previous studies investigating these proteins (Corrigan *et al.*, 2016; Shimamoto and Inouye, 1996), although the affinity to GDP has never been investigated. HflX also demonstrated high affinity for 5'-diphosphate containing nucleotides GDP and ppGpp, although the K_D for GTP and pppGpp binding was not calculable under the conditions tested (Figure 3.3.1d and Table 3.3.1), indicating a much lower affinity. The binding of all four guanine nucleotides was shown to occur at the same site due to the ability of each to specifically compete with each other (Figure 3.3.2), during which the extent of competitive fitness of each nucleotide follows the hierarchy of binding affinity established in Figure 3.3.1. In the absence of GEFs, one would expect GDP to freely dissociate following GTP hydrolysis to facilitate re-entry into the ON state. The increased affinity of RsgA, RbgA, Era and HflX to GDP compared to GTP suggests that this cycling event is highly likely to rely on the physiological concentrations of GTP compared to GDP, which during proliferation are around 5-fold greater in *E. coli*, with GTP levels peaking at 1.1 mM compared to GDP at 220 µM during exponential growth (Varik *et al.*, 2017). Upon entry into conditions of nutrient limitation and induction of the stringent response, intracellular concentrations of ppGpp can rise to around 1 mM in *E. coli* (Kuroda *et al.*, 1997), swiftly becoming the dominant guanine nucleotide in the cell. The higher affinity of 5'-diphosphate containing nucleotides compared to 5'-triphosphate containing nucleotides may enable rapid inactivation of these proteins upon stringent response activation, with the OFF state being favoured even during early stringent conditions as (p)ppGpp concentrations rise.

DRaCALA is a technique which enables rapid, precise and high-throughput analysis of protein-small ligand binding affinity, although it is not without caveats. The capacity to measure total ligand present as well as the fraction bound dramatically decreases experimental errors, for example due to pipetting, as the bound fraction is always calculated against the exact total amount of labelled ligand present rather than some theoretical value. All single step biochemical binding interactions, such as the small ligand binding being investigated here, involve at least two major events which contribute

to the overall equilibrium, i.e. the association stage and the dissociation stage (k_1 and k_{-1}) (Bernasconi, 1976). During the 5 min incubation step during DRaCALA, the ratio of bound:unbound protein-ligand complexes is equilibrating, and it is this equilibrium that is being measured when spotting during DRaCALA. While this has little effect on the calculated K_D values *in vitro*, in biological systems, protein-ligand complexes with a similar K_D often have greatly different nucleotide exchange rates which depend more on the individual microscopic constants k_1 and k_{-1}. As such, the role of a certain protein-ligand pair in biological systems, particularly in the context of the rate of ligand exchange, cannot be extrapolated from the DRaCALA data obtained in this chapter. While this technique does enable for the k_{-1} (and therefore k_1) to be calculated through use of chase-exchange assays (Roelofs *et al.*, 2011), this was not carried out here.

Future GTPase assays should not be limited to a single timepoint, and an excess of substrate should be included (Figure 3.4.2a). Instead, hydrolysis timecourses should be carried out using an excess of GTP in each case to prevent saturation of the reaction. The monitoring of a reaction over time will give us a better understanding of the reaction progression, and enable nonlinear curve fittings to calculate apparent rates, as well as the application of Michaelis-Menten kinetics to derive both the maximum reaction rate (V_{max}) and the Michaelis constant (K_m). Under current conditions, the 2.5 μM concentration of protein used is vastly in excess of the 1.83 nM radiolabelled nucleotide, and as such the hydrolysis observed can be attributed to a single hydrolysis event from a very small portion of present protein monomers. Despite this, the results in this section can be considered valid due to the empirical difference between GTPase activity in the presence and absence of ppGpp in a qualitative rather than quantitative manner.

The G4 motif is a conserved sequence motif present in all known P-loop GTPases, of consensus (N/T)(K/Q)xD (Verstraeten *et al.*, 2011). This motif is essential for the binding of the guanine ring of GTP, and as such confers binding specificity to guanine nucleotides such as GTP compared to adenine nucleotides through specific hydrogen bonding between the carboxyl group of the conserved aspartate (D) residue of the G4 motif, and the protons of the N2 and N3 amino groups on the guanine ring (Rogne *et al.*, 2020; Rogne *et al.*, 2018). RsgA, Era and HflX were found to be able to hydrolyse ATP in the physiologically irrelevant absence of guanine nucleotides (Figure 3.4.1), although data from Section 3.3.2 suggests that the presence of even low concentrations of guanine nucleotides would completely outcompete ATP binding as signified by the ability of ppGpp to inhibit ATPase activity. Previously, the IC_{50} values of both ppGpp and pppGpp have been calculated in the context of GTP hydrolysis by RsgA (Corrigan *et al.*, 2016). In order to fully assess the ability of (p)ppGpp to inhibit the

ATPase activity of these proteins, a similar quantitative measure of inhibitory power should be calculated. Interestingly, the ATPase activity of HflX could be inhibited by ppGpp, despite HflX containing a distinct N-terminal ATP-binding domain (ND1) (Dey *et al.*, 2018; Jain *et al.*, 2013). The structure of this domain is as of yet considered unique in terms of sequence identity, with some structural similarity between ND1 and the well-understood dinucleotide binding Rossmann fold in the cases of both *Sulfolobus solfataricus* (Jain *et al.*, 2013) and *E. coli* (Dey *et al.*, 2018). However, ATP recognition is achieved in a Walker A and Walker B-independent manner. Whether or not ppGpp would be capable of associating with this domain is unknown, due to the inherent differences in nucleotide recognition between the HflX ND1 and canonical P-loop NTPases. Furthermore, the ATPase domain is known to be an RNA-helicase, stimulated by the lack of structure representative of heat-damaged RNA (Dey *et al.*, 2018), in fitting with the role of HflX as a heat shock protein. Seeing as, to the best of our knowledge, the ribosomes included in the NTPase reactions were not heat damaged, it is likely that the ATPase activity of the HflX ND1 is negligible compared to the activity of the GTPase domain stimulated by correctly structured RNA. As such, the results shown in Figure 3.4.1d can be considered primarily due to the GTPase domain of HflX.

In conclusion, here we have purified and characterised the nucleotide binding capacity and GTPase activity of the four RA-GTPases RsgA, RbgA, Era and HflX from *S. aureus*, finding that our recombinant proteins had activity in agreement with that observed in previous studies. We have also investigated the relationship between RNA binding and GTP hydrolysis in the case of Era, identifying that RNA binding alone is insufficient to stimulate hydrolytic activity. These data will prove invaluable downstream to provide insight into more in depth investigation, particularly in the case of the impact of point mutations on protein function. The increased affinity of each RA-GTPase for GDP and ppGpp over GTP and pppGpp enables conclusions to be drawn regarding the functional cycle of these proteins, particularly in the context of GDP/GTP exchange and during the shift in nucleotide concentrations during the stringent response.

Chapter 4 – The effect of (p)ppGpp on RA-GTPase-interactions

4.1 Introduction

In eukaryotic cells, and in the notable case of prokaryotic EF-Tu (Schümmer *et al.*, 2007), GEFs are required to stimulate nucleotide exchange following GTP hydrolysis to enable re-entry into the GTP-bound ON state. Primarily in prokaryotes, however, the intracellular excess of GTP (Varik *et al.*, 2017) drives nucleotide exchange under favourable, high energy conditions. Therefore, the activity of many GTPases involved in ribosome assembly, the translation elongation cycle and intracellular signalling can be coupled to the cytosolic GTP concentration. While it is known that when bound to GTP, these proteins are capable of target association, and that hydrolysis of the bound GTP to GDP is the trigger for dissociation, little is known about the effect of (p)ppGpp binding to GTPases during stringent conditions when these alarmones become the dominant guanine nucleotide in the cell. Previous work has suggested that while associated with pppGpp, the affinity of *B. subtilis* RbgA and *E. coli* ObgE for the 50S subunit increases (Achila *et al.*, 2012; Feng *et al.*, 2014). This led to the proposal that during the stringent response, (p)ppGpp-bound RA-GTPases sequester the mature ribosomal subunits to prevent 70S formation (Achila *et al.*, 2012; Pausch *et al.*, 2018).

The ribosomal binding site recognised by RA-GTPases is largely determined by their accessory RNA-binding domains (López-Alonso *et al.*, 2017b; Razi *et al.*, 2017; Tu *et al.*, 2009; Verstraeten *et al.*, 2011), which usually target specific rRNA sequences on either the 30S or 50S subunit. Our observations in Chapter 3 corroborate previous findings that the GTPase activity of these proteins is activated in the presence of ribosomes, however this hydrolysis activity is inhibited by (p)ppGpp binding. Two major ideas were considered: that (p)ppGpp is simply a non-hydrolysable competitive inhibitor of these proteins, and that binding of RA-GTPases to (p)ppGpp may interfere with RA-GTPase-ribosome association.

In this chapter, we sought to investigate the effect of (p)ppGpp binding to RsgA, RbgA, Era and HflX in order to better understand the role of these proteins when associated with these alarmones during the heights of the stringent response. To this end, α-His immunoblotting was used to investigate the effect of different nucleotide-bound states on ribosome association. We then utilised stopped-flow fluorometry in order to elucidate the kinetics of RA-GTPase association to the ribosome, and to identify the microscopic rate constants which were affected when in the (p)ppGpp-bound state. Finally, we utilised a truncated Era mutant to further investigate he specific role of rRNA binding in the activation of GTPase activity. Altogether, the results presented here enable us to propose a two-

step binding model regarding the association and activation of RA-GTPase to their cognate ribosome subunit.

4.2 Assessing interactions between ribosomal subunits and RA-GTPases using mCherry fusions

4.2.1 Generating mCherry fusion proteins

In order to investigate the association between the RA-GTPases and ribosomal subunits, we first had to define a strategy for detection of the desired proteins in a given sample. There are typically several ways of doing this, namely translational modification or covalent modification to introduce a detectable fluorophore or tag (i.e. HIS or SNAP) onto the protein, or by using antibodies which specifically recognise the protein of interest to carry out western blots. The major difference between these methods is sensitivity, with western blotting being able to detect as little as 0.1 ng of protein, whereas fluorescent techniques require a concentration in the high nanomolar to low micromolar range in a larger volume. We opted to initially fuse our RA-GTPases translationally to the fluorescent protein mCherry (Shaner *et al.*, 2004), as in addition to the association experiments mentioned here, these constructs would be a useful tool in the case of future investigation involving fluorescence, microscopy or Förster resonance energy transfer (FRET). mCherry is an engineered derivative of the tetrameric GFP, constructed using random mutagenesis in order to tweak the fluorescence spectrum of the imidazolinone chromophore (Shu *et al.*, 2006), introducing excitation and emission peaks at 587 nm and 610 nm respectively.

The first step in generating mCherry-RA-GTPase translational fusions was planning the cloning strategy. Two major methods were considered, namely blunt end ligation and splicing by overlap extension (SOE), and the latter was deemed more suitable as the rate and efficiency of ligation is known to be in the region of 100-fold higher when ligating sticky compared to blunt ends. Primers were designed to generate complimentary 24 bp overhangs between the C-terminus of mCherry and the N-terminus of the GTPase, introducing a four residue PRGS linker derived from the extant thrombin site of the pET28b GTPase template plasmid (Figure 4.2.1a). The N-terminal and C-terminal fragments (Figure 4.2.1b, c) were joined using SOE PCR, and the resulting construct was digested using BamHI, treated with phosphatase to prevent re-ligation of the backbone vector and ligated into the pET28b vector as described in the methods section, before transformation into *E. coli* XL1 Blue. Plasmids were reisolated and confirmed using Sanger sequencing (Figure 4.2.1d) before transformation into *E. coli* BL21 (DE3) for recombinant expression and purification as per Chapter 3.2.2. Figures shown here refer to the cloning of the pET28b:HflX-mCherry construct, and are

representative of the process used for RsgA, RbgA and Era. Despite obtaining correctly sized N-terminal and C-terminal fragments for the RsgA and RbgA fusions (Figure 4.2.1c), we were unable to successfully splice the two fragments together. Various PCR conditions were tested, including attempts at optimisation of the concentration of the template DNA, annealing temperature and extension time, however no conditions tested yielded substantial product. Experimentation concerning Era-mCherry and HflX-mCherry were ongoing during this attempted optimisation. Interestingly, the solubility of both fusions were increased dramatically compared to recombinant 6xHis-tagged Era and HflX, with both constructs reaching concentrations above 1 mM when tested. This highlights the potential for using fluorescent proteins as purification aids in proteins with low intrinsic solubility, a concept that has been suggested and trialled previously (Mestrom *et al.*, 2019; Su, 2005).
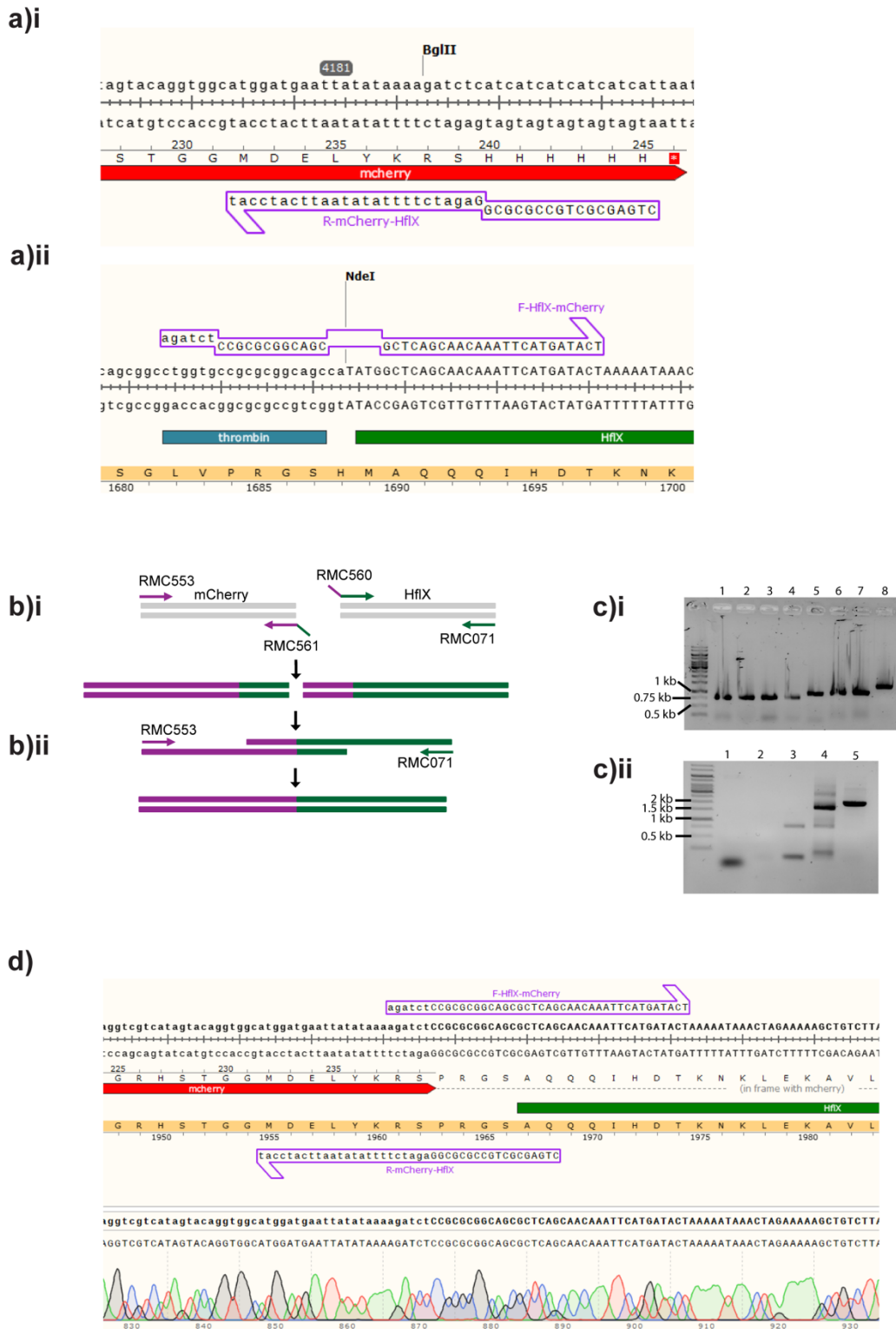
Figure 4.2.1: Construction of RA-GTPase-mCherry fusions using SOE PCR. a) Primer design for the fusion of HflX and mCherry. Note the complimentary overhangs generated for (ai) the mCherry fragment and (aii) the HflX fragment, leading to a 24 nucleotide complimentary region. The PRGS four residue linker was incorporated into the complimentary region, and the native START codon of *hflX* was removed. Primer sequence alignments were carried out using SnapGene. b) Schematic overview of the SOE PCR strategy. bi) fragments were amplified encoding the genes of interest, with the *mcherry* fragment including a 3' overhang, amplified using RMC553 and RMC561,and the *hflX* fragment including a 5' overhang amplified by RMC560 and RMC071. bii) Complimentary sticky ends anneal to form a complete fused template. Forward and reverse primers RMC553 and RMC071 were used to span the entire region, which can then be digested and transformed as required. c) 1% agarose gel

electrophoresis of steps i and ii as described in panel (b). ci) amplification of the forward (*mcherry)* and reverse (*gtpase*) fragments. Lane 1: *mcherry* with *rsg*A compatible overhang (742 bp). Lane 2: *mcherry* with *rbg*A compatible overhang (742 bp). Lane 3: *mcherry* with *era* compatible overhang (742 bp). Lane 4: *mcherry* with *hfl*X compatible overhang (742 bp). Lane 5: *rsg*A with *mcherry* compatible overhang (900 bp). Lane 6: *rbg*A with *mcherry* compatible overhang (909 bp). Lane 7: *era* with *mcherry* compatible overhang (924 bp). Lane 8: *hfl*X with *mcherry* compatible overhang (1263 bp). cii) Lane 4: the 1642 bp product of splicing the *mcherry* and *era* fragments from lanes 3 and 7 of part (ci). Lane 5: the 1981 bp product of splicing the *mcherry* and *hfl*X fragments from lanes 4 and 8 of part (ci). Lanes 1-3 were failed attempts at generating the *mcherry-rsg*A and *mcherry-rbg*A fusions. d) Sanger sequencing analysis of *mcherry-hfl*X. Internal splicing primers are indicated, and sequencing was carried out from the 5' using primer RMC553. Sequencing alignments were carried out using SnapGene.

4.2.2 Investigating RA-GTPase-mCherry association to the ribosomal subunits

The 70S prokaryotic ribosome is a large macromolecular machine, with an estimated molecular weight of around 2.5 MDa in *E. coli* (Stark *et al.*, 1995). The two constituent subunits, namely the 30S and 50S in prokaryotes, have sedimentation rates at 30 Svedberg units and 50 Svedberg units respectively, a property which enables separation from other cellular constituents such as proteins. One application of this is the isolation of ribosomes or ribosomal subunits and analysis of the bound protein which cosediments, whereas any unbound protein would sediment at a much lower rate due to a comparatively lower size and mass. Here, we apply this principle using isopycnic ultracentrifugation in order to investigate association of our RA-GTPase-mCherry fusion proteins to the 30S and 50S ribosomal subunits. Applying a mixture of 70S ribosomes purified from *S. aureus*, our mCherry fusion proteins and either GTP or ppGpp to a sucrose density gradient enabled a comparison between binding in the GTP-bound and ppGpp-bound states. A low content of $MgCl_2$ in the buffer encouraged 70S dissociation into the 30S and 50S, both of which could be assessed for the presence of mCherry through fluorescence detection using an excitation wavelength of 580 nm and an emission detection wavelength of 620 nm, gated with a long-pass filter at 610 nm.

Firstly, the activity of the Era and HflX mCherry fusions was compared to the wild-type (Figure 4.2.2a). Following incubation of both variants with radiolabelled GTP and purified 70S ribosomes, it was found that the activity of the wild-type and mCherry fusions were similar, and was therefore concluded that these fusions are fully functional. It was crucial during these experiments to separate the 30S and 50S subunits as much as possible to prevent subunit overlap during fractionation, and after optimisation it was found that for *S. aureus* ribosomes, ultracentrifugation through a 10%-40% sucrose gradient at 111,000 × *g* for 16 hrs was sufficient. *E. coli* ribosomes however split optimally at 90,000 × *g* for 16 hrs, indicating a slight increase in buoyant density compared to the *S. aureus* samples (data not shown). Following splitting of the 30S and 50S subunits in the absence of mCherry fusions, we fractionated and measured the fluorescence of the subunits to define a level of background autofluorescence (Figure 4.2.2b). The 30S peak between fractions 16 and 20 showed an increased

fluorescence, rising to a 2.1 V maxima, whereas the 50S peak between fractions 29 and 35 showed background levels of fluorescence.

Given that the sucrose gradient used here was continuous and started at 10%, we expected a high concentration of RA-GTPase-mCherry fusion proteins to remain within the first several fractions and not migrate too far through the column unless associated with the more dense ribosome. This was observed when Era-mCherry (Figure 4.2.2c) and HflX-mCherry (Figure 4.2.2d) were mixed with 70S ribosomes and applied to the column, with background fluorescence starting at around 60 V and exponentially decreasing with migration distance to a stable background of between 2 V and 4 V. Era is a known 30S binding protein that has to date had no implication in 50S assembly. In the presence of GTP, peaks in fluorescence were observed in both the 30S- and 50S-containing fractions (Figure 4.2.2ci). In the presence of ppGpp, however, the fluorescence peak relative to 50S association was absent while the 30S association peak remained, indicating a decreased 50S association in the presence of ppGpp. HflX has been previously shown to bind to both the 30S and 50S subunits (Coatham *et al.*, 2016). Consistent with this, peaks in fluorescence were observed in both the 30S and 50S fractions in the presence of GTP (Figure 4.2.2di), whereas in the presence of ppGpp the 50S peak was severely reduced (Figure 4.2.2dii). This suggests that both Era and HflX may associate with the 50S subunit in the presence of GTP, which is abrogated in the presence of ppGpp. While it appears that the nucleotide-bound state has no effect on 30S association, the background fluorescence of the 30S subunit may be concealing any change. Therefore further investigation is required using more precise, quantitative techniques in order to determine the accuracy of these observations.
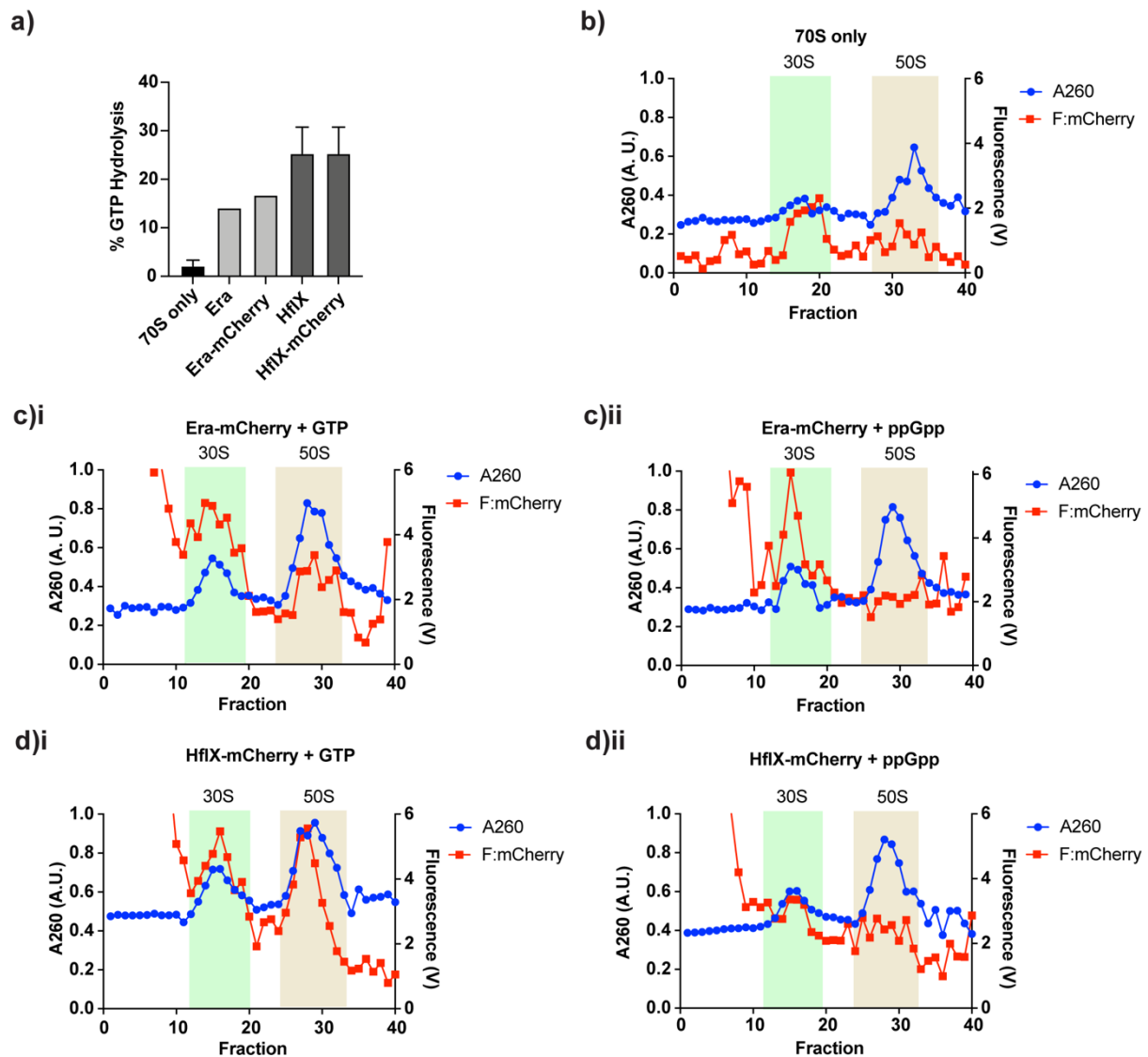
Figure 4.2.2: The cosedimentation of RA-GTPase-mCherry fusions with ribosomal subunits. a) 2.5 µM of Era, HflX or their mCherry fusion derivatives were mixed with *S. aureus* 70S ribosomes and 1.83 nM [α-^{32}P]-GTP, and incubated at 37°C for 60 mins. Percentage GTP hydrolysis was visualised using TLC and quantified using pixel densitometry. Experiments involving HflX were carried out in triplicate, with error bars representing standard deviation between replicates. The experiment involving Era was carried out once, and as such should be considered preliminary. b) 70S ribosomes only, c) 70S ribosomes and Era-mCherry and d) 70S ribosomes and HflX-mCherry in the presence of either i) GTP or ii) ppGpp were separated along a sucrose gradient using ultracentifugation. 3 µM purified recombinant protein was mixed with 2 µM 70S *S. aureus* ribosomes and 30 µM nucleotide and applied to a 10%-40% continuous sucrose gradient made up in ribosome dissociation buffer containing 1.5 mM MgCl$_2$ as per the methods section. Subunits were separated at 111,000 × *g* for 16 hrs, and 250 µl fractions were analysed for both RNA content by A$_{260}$ and fluorescence within the mCherry spectrum using a 590 nm excitation and 620 nm emission wavelength gated by a long-pass filter at 610 nm. The 30S and 50S peaks are highlighted using green and beige boxes respectively. Controls containing the 70S subunits only were carried out in duplicate, and all remaining experiments in triplicate, with one representative example shown.

4.3 Assessing the nucleotide dependence of interactions between RA-GTPases and ribosomal subunits using western blotting

The observations made in the previous section indicate that ppGpp may have an effect on RA-GTPase interactions, however the methodology employed using mCherry fusion proteins was not quantifiable, and background autofluorescence made the results, at best, difficult to interpret. In order to further investigate the effect of ppGpp and other nucleotides on interactions between the ribosomal subunits and RA-GTPases in a more quantifiable and statistically amenable fashion, we carried out western blotting to detect the presence of 6xHis-tagged recombinant protein in sedimentation fractions containing the 30S and 50S subunits following splitting (Figure 4.3). GTPases were incubated with GTP, GMPPNP, GDP, ppGpp or pppGpp, as well as purified 70S *S. aureus* ribosomes, and subunits were separated using a 10%-40% sucrose gradient as in Section 4.2.2. The amount of associated RA-GTPase was detected via western immunoblotting using antibodies raised against the polyhistidine tag, and quantified using densitometry.

In the case of all four RA-GTPases, we observed a significant decrease in association when bound to GDP, ppGpp or pppGpp compared to when bound to the non-hydrolysable GTP analogue GMPPNP (Figure 4.3), which was included to trap the GTPases in the ON conformation for the duration of the centrifugation step. Both RsgA (Figure 4.3a) and RbgA (Figure 4.3b) exhibited a similar level of association while in the apo, GDP, GTP, ppGpp and pppGpp-bound states, with a 3-fold increase in association when bound to GMPPNP. This is in contrast to previously published data suggesting that the affinity of *B. subtilis* RbgA for 50S subunits it increased in the presence of pppGpp (Achila *et al.*, 2012). The low level of association while in the GTP-bound state is thought to be due to spontaneous hydrolysis during the 16 hr ultracentrifugation step, causing the protein to enter the GDP-bound state and dissociation to occur. Era (Figure 4.3c) and HflX (Figure 4.3d) exhibited a slightly different pattern, in which they were equally capable of associating whether in the apo, GTP or GMPPNP-bound state, suggesting that these two RA-GTPases can associate with the ribosomes in the absence of nucleotides. When bound to GDP, ppGpp or pppGpp, the ability of Era and HflX to associate with the ribosomal subunits decreases 2-fold and 3-fold respectively. In the figures presented here, we show binding of RsgA, RbgA and Era to their preferred ribosomal subunit – namely the 30S, 50S and 30S respectively. No association was observed for the unfavoured subunit in any of these cases, in disagreement with the apparent observation from Chapter 4.2.2 that Era associates with the 50S. HflX association was detected for both the 30S and 50S subunits, shown below (Figure 4.3di, dii) corroborating the role of HflX in both 30S and 50S subunit processing (Coatham *et al.*, 2016). Furthermore, there appears to be no difference in the inhibitory effect of GDP, ppGpp or pppGpp despite a lower binding affinity for

pppGpp compared to the 5'-diphosphate containing nucleotides (Chapter 3.3.1, Table 3.3.1). Under the conditions tested here the excess of each nucleotide over the GTPases would shift the binding equilibrium towards the GTPase-nucleotide complex, despite the slight differences in affinity. Overall, we show here that RsgA, RbgA, Era and HflX association to the ribosomal subunits is favoured in the GTP-bound ON conformation, and that binding to GDP, ppGpp or pppGpp inhibits this interaction *in vitro*.
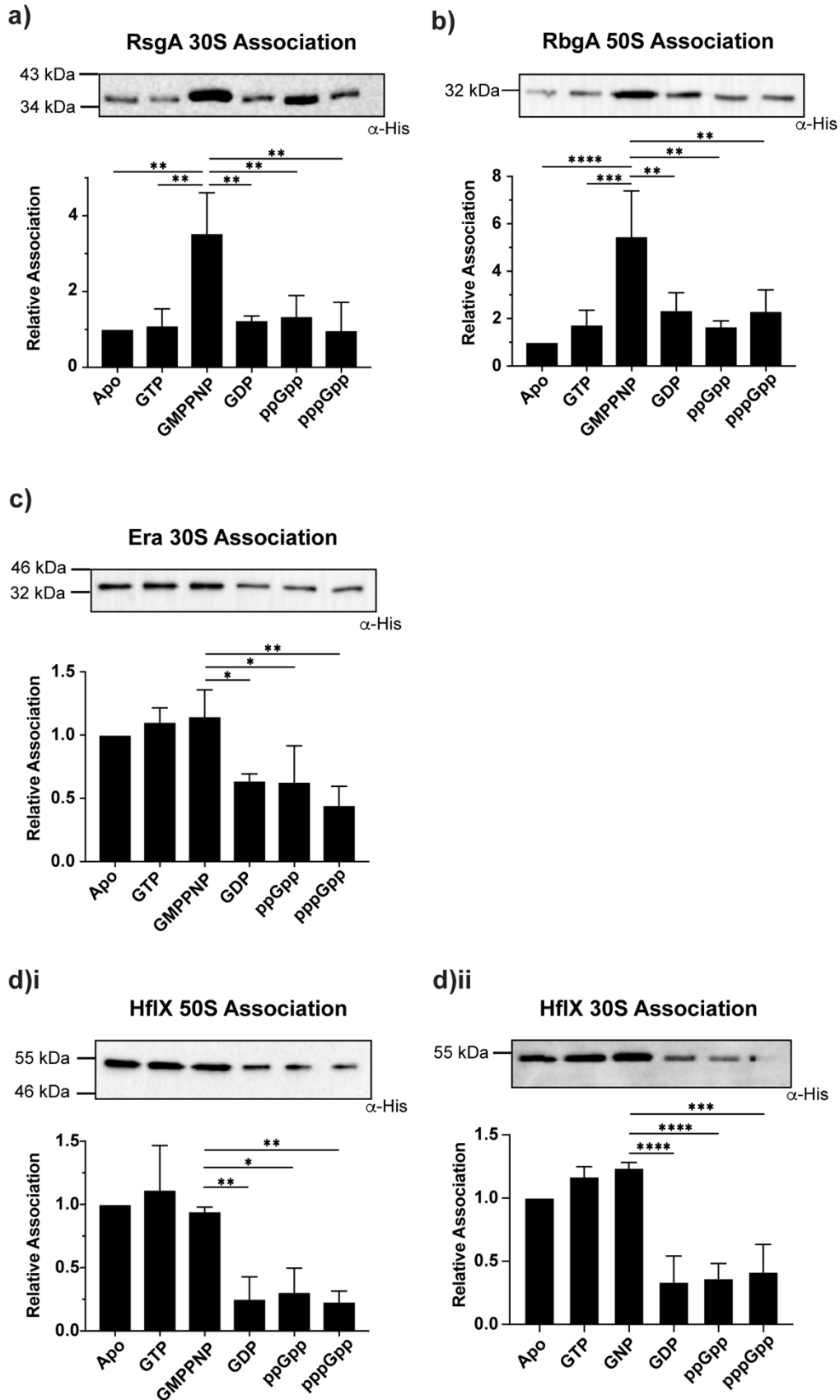
Figure 4.3: RA-GTPases interactions are inhibited while in the GDP- and (p)ppGpp-bound state. a-d) Top panels: Purified 70S ribosomes were incubated with recombinant 6xHis-tagged a) RsgA, b) RbgA, c) Era or d) HflX in the presence and absence of GTP, GMPPNP, GDP, ppGpp or pppGpp, and applied to a 10%-40% sucrose

gradient made up in low MgCl$_2$ subunit splitting buffer as per the methods section. Following subunit separation at 111,000 × g for 16 hrs, fractions containing 30S and 50S subunits were precipitated and concentrated, and associated proteins were detected using HRP-conjugated α-His antibodies. Experiments were carried out in triplicate or quadruplicate, with one representative image shown. Bottom: The signal intensities relative to the apo state were calculated using pixel densitometry, and mean values between replicates were plotted with error bars indicating standard deviation. Statistical analyses were carried out using one-way ANOVA, followed by Tukey's multiple comparison test, with p values represented as follows: *, $p < 0.05$; **, $p < 0.01$; ***, $p < 0.001$; and ****, $p < 0.0001$.

4.4 Defining kinetic parameters of RA-GTPase interactions with ribosomal subunits using stopped-flow fluorescence spectroscopy

4.4.1 Fluorescently labelling recombinant RbgA, Era and HflX

Having determined that binding of the RA-GTPases to (p)ppGpp inhibits association with the ribosomal subunits, we next sought to understand the kinetic mechanism of this inhibition, in order to define the point at which inhibition occurs. To this end, we opted to use fluorescent approaches in order to directly observe the fast kinetics of association by utilising stopped-flow apparatus. Stopped-flow is a ubiquitous term for a device capable of rapidly mixing two or more fluids (Figure 4.4.1a), usually achieving complete mixing in under 1 ms. The alternative method employed to study steady-state dynamics is termed continuous-flow, and was not trialled here. Such devices are often coupled with a variety of spectrometers, such as fluorometers or spectrophotometers in order to observe fast-phase changes in the reaction constituents following mixing. Here, we utilised this stopped-flow technique in order to investigate the mechanism of RA-GTPase binding to the ribosomal subunits using two general approaches: chemical fluorescence changes upon association of the RA-GTPase with the ribosome (Figure 4.4.1b), and FRET using a double labelled IF3 molecule as a sensor of RA-GTPase binding (Figure 4.4.1c). IF3 is a well-characterised 30S binding protein, with two domains separated by a flexible linker (Kycia et $al.$, 1995), and conformational changes between these domains upon accessory protein binding to the 30S has been used previously as a sensitive intramolecular FRET sensor of their binding (Chulluncuy et $al.$, 2016). The latter method, while theoretically more sensitive due to FRET intensity decaying with the 6th power of range, relies on RA-GTPase binding in close proximity of the IF3 sensor, and so cannot be used for the 50S binders RbgA and HflX.
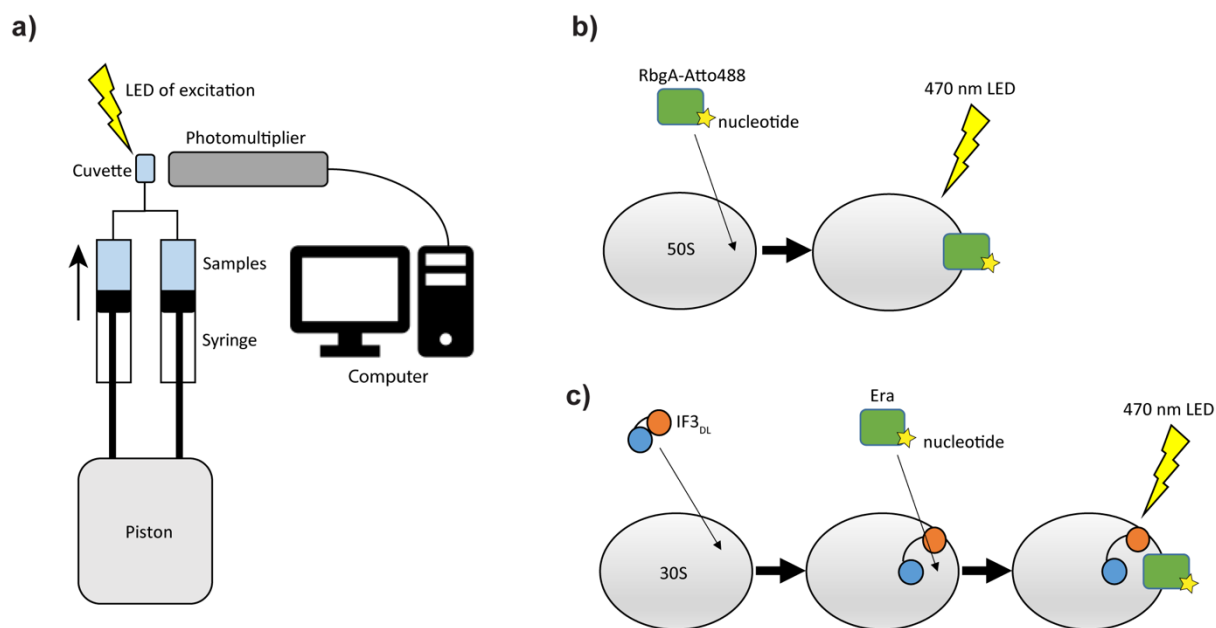
Figure 4.4.1: Schematic overview of stopped-flow experimental design. a) A representation of the stopped flow apparatus. Briefly, rapid pressure-driven piston movement simultaneously injects equal volumes of two reaction mixtures into the cuvette, and excited using a 470 nm excitation LED to enable changes in fluorescence to be detected via a photomultiplier. b) Changes in chemical fluorescence can be observed following mixing of ribosomal subunits with the Atto488-labelled protein of interest in the presence of different nucleotides. Upon entry into the cuvette, the fluorophore will be excited by a 470 nm LED and fluorescence changes following alteration of fluorophore environment upon subunit association can be measured. c) 30S ribosomal subunits preincubated with IF3 dual-labelled with the Atto488 and Atto540Q FRET pair will be rapidly mixed with unlabelled Era. Upon entry into the cuvette, Atto488 will be excited by a 470 nm LED. Era association may affect the relative domain position of IF3, leading to altered quenching by Atto540Q and a change in fluorescence, which can be taken as an indirect measure of Era binding.

4.4.1.1 Analysis of target residues for labelling

We began by generating fluorescently labelled variants of purified recombinant protein. The change in chemical environment of the fluorophore upon binding of the RA-GTPases to the ribosomal subunits would be the responsible for the change in fluorescence observed (Galbán *et al.*, 2009), and as such the mCherry fusion proteins purified in Chapter 4.2.1, while remaining suitable for FRET, were unsuitable for investigating chemical fluorescent change due to a rigid chemical environment around the central imidazolinone chromophore (Shu *et al.*, 2006). For optimal signal strength, the fluorophore used should be located as close as possible to either the interface between the RA-GTPase and ribosomal subunit, or a point of conformational change within the RA-GTPase itself which is affected by subunit binding, while remaining small enough so as not to interfere with protein activity in any way. In practice, there is no reliable way to predict whether any given position will yield productive signal when labelled without access to the full functional cycle and high resolution structures of the modified protein. The polycyclic fluorophore Atto488 was used, conjugated to a highly thiol-reactive

maleimide group to enable selective covalent labelling of cysteine residues with a highly stable thioether bond.

In order to determine kinetic parameters in this manner, each protein molecule in a sample should be homogenously labelled at a single known site, so that all fluorescent changes observed can be attributed as net due to constructive interference between similar signals, rather than in a heterogenous mixture of labelled proteins where some fluorophore molecules may be reducing in signal intensity while others are increasing. To do this, the proteins of interest may require engineering to limit available cysteines. Structures of the four RA-GTPases were predicted via homology modelling using the Phyre2 server (Kelley *et al.*, 2015) and *S. aureus* sequence data (Figure. 4.4.1.1). RsgA contains three highly conserved cysteine residues in the ZNF domain, which are responsible for coordinating the Zn^{2+} ion which stabilises the domain fold (Levdikov *et al.*, 2004). Inadvertent covalent modification of these residues would compromise the structure of the C-terminal RNA binding domain, and as such RsgA was unfit for labelling in this way (Figure 4.4.1.1a). RbgA was found to contain a single cysteine residue at position 277, which appears to be relatively highly conserved and may be buried within the interface between the GTPase and ANTAR domains (Figure 4.4.1.1b). Due to the presence of this single cysteine, native labelling of RbgA was attempted. Wild-type Era lacks any cysteine residues, and as such cannot be labelled natively. Instead, a serine residue can be conservatively mutated to a cysteine to introduce a single site for modification. Analysis of the structure and interaction site of Era with the 16S rRNA (Tu *et al.*, 2011; Tu *et al.*, 2009) led to the selection of two candidate serines at positions 222 and 268 (Figure 4.4.1.1c), which are situated close to the rRNA binding site within the KH domain. S268 was selected for initial testing, as S222 is directly involved in rRNA recognition and hence modification of this residue may interfere with protein function. HflX contains two cysteine residues at positions 45 and 330, however the residue 45 appears to be buried in the predicted structure (Figure 4.4.1.1d). Thus, incubation of this protein with a maleimide-conjugate would likely selectively label the exposed C330 residue and produce a single-labelled protein. As such, we opted to attempt to label native HflX.
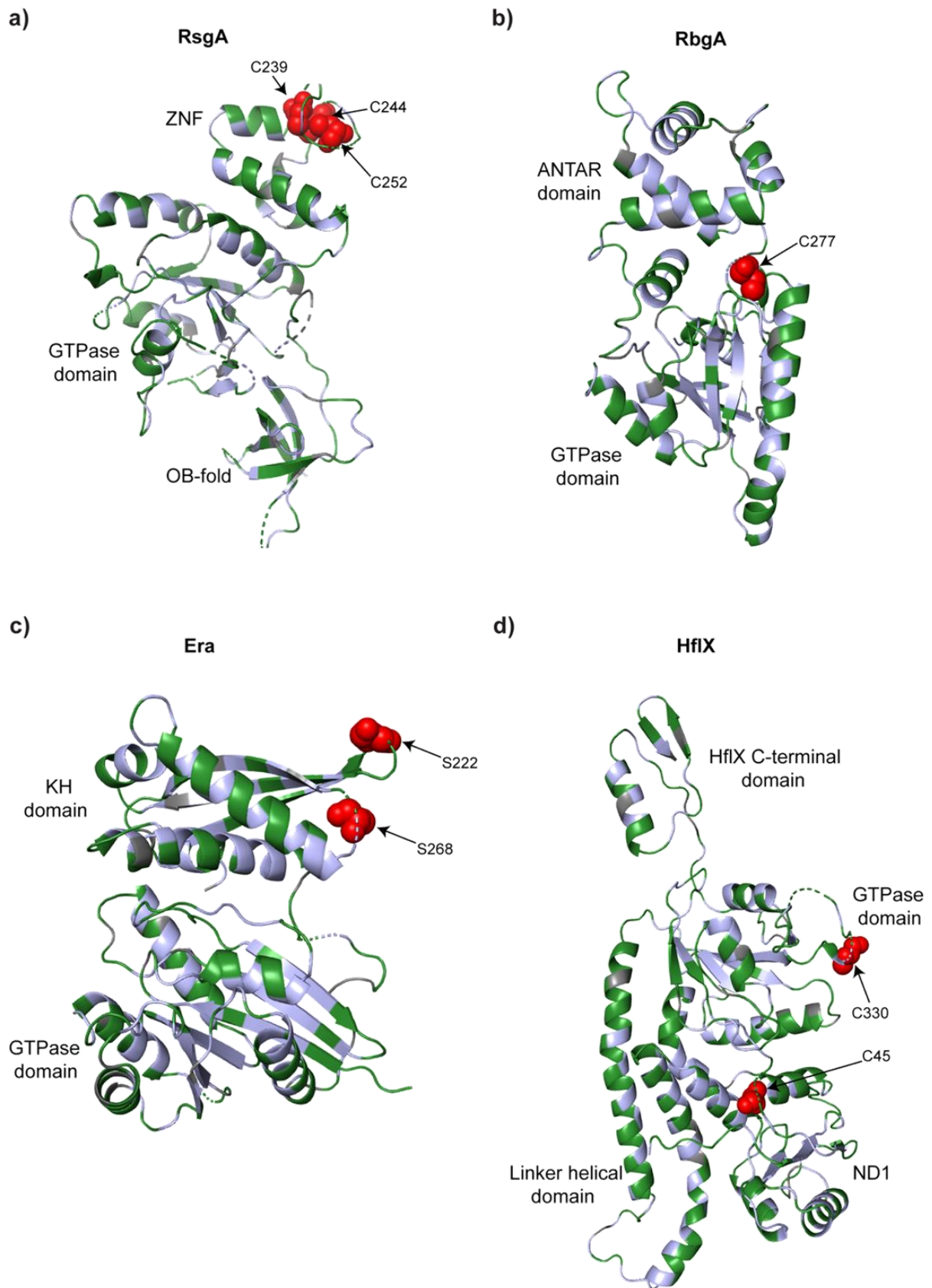
Figure 4.4.1.1: Phyre2 modelling of candidate residues for Atto488-maleimide labelling. Predicted full-length structures of a) RsgA, b) RbgA, c) Era and d) HflX. Candidate cysteine and serine residues amenable to labelling with Atto488-maleimide are represented by red spheres, and domains are indicated. Hydrophilic residues are

shown in green, and hydrophobic residues in blue. Models were predicted using the Phyre2 server (Kelley *et al.*, 2015), using *S. aureus* gene sequences and the following templates: RsgA, PDB 1T9H chain A; RbgA, PDB 1PUJ chain A; Era, PDB 3R9W chain A; and HflX, PDB 5ADY chain A.

4.4.1.2 Covalent labelling of RbgA, Era and HflX using Atto488 maleimide

Prior to labelling, site-directed mutagenesis was carried out to generate the Era S268C mutant variant using complimentary overlapping mutagenic primers, designed to convert the serine-encoding TCT codon to cysteine-encoding TGT (Figure 4.4.1.2a). The maleimide conjugation reaction requires cysteines in the reduced state, and as such the reducing agent TCEP was included during the post-purification dialysis step (see methods section). Following modification, the protein was separated from the unreacted fluorophore molecules via Ni^{2+}-affinity chromatography, and the degree of labelling was calculated by analysing the absorbance spectrum of each purified, labelled protein (Figure 4.4.1.2b). The Atto488-maleimide dye absorbs weakly at 280 nm and very strongly at 500 nm, and the manufacturer provides a correction factor in order to convert the A_{500} into a predicted A_{280} value, which enables the concentration of protein and the concentration of dye to be calculated. Then, assuming a maximum of one dye molecule per protein molecule, the degree of labelling can be calculated based on the concentration of each in the sample analysed. For a more detailed description of this calculation, see the methods section. The degree of labelling for RbgA, Era S268C and HflX was calculated to be 12%, 30% and 46% respectively. The activity of Atto488-labelled proteins was also assessed by measuring GTP hydrolysis in the presence and absence of ppGpp (Figure 4.4.1.2c), and it was found that the modified and mutant variants had similar activity to the wild-type unlabelled GTPases, and as such were concluded to be functional.
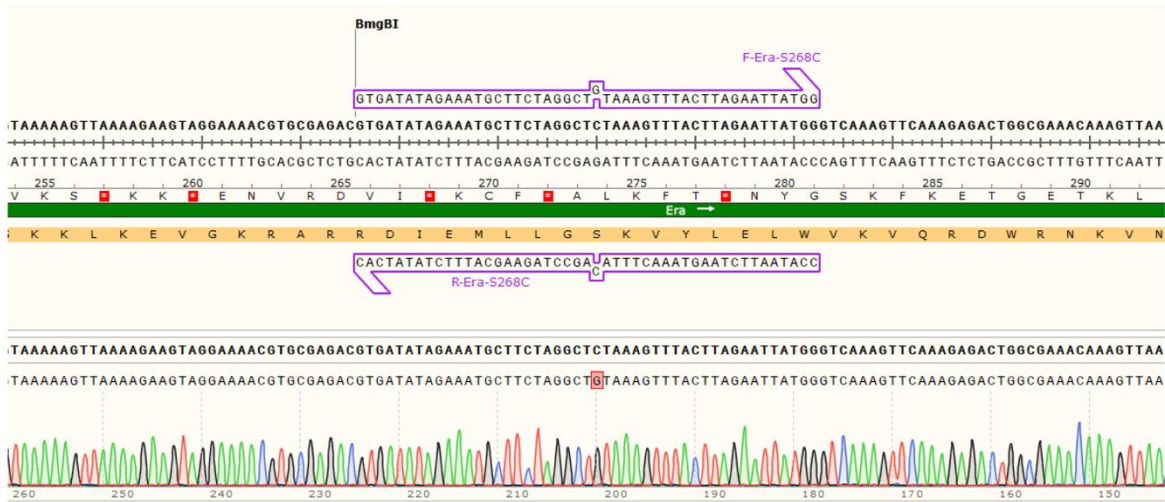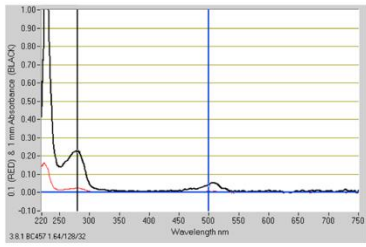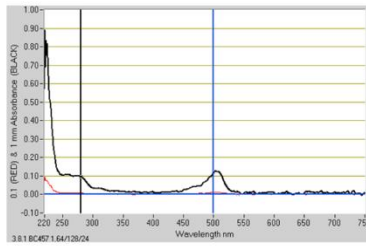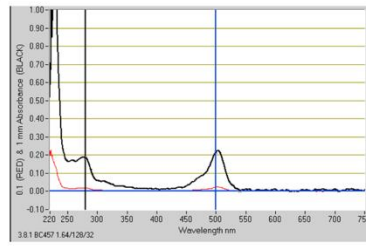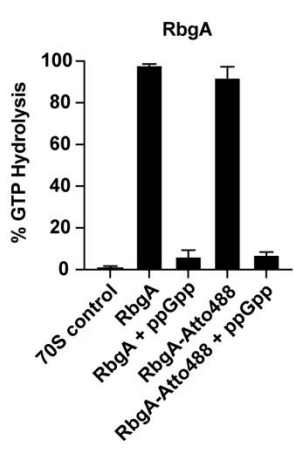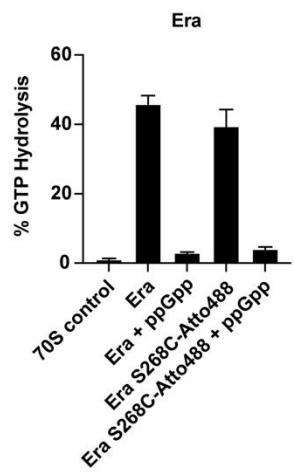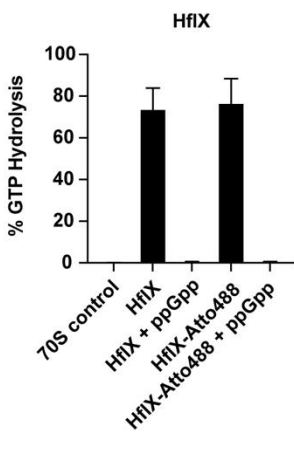
Figure 4.4.1.2: Analysis of labelling efficiency of Atto488-labelled RbgA, HflX and Era S268C. a) Primer design for the site-directed mutagenesis of Era S268C. Note the complimentary primers which differ from the template by a single nucleotide, so as to introduce the desired mutation. Primer sequence and sanger sequencing alignments were carried out using SnapGene. b) Absorbance spectra of bi) RbgA-Atto488, bii) Era S268C-Atto488 and biii) HflX-Atto488. Absorbance intensity for a pathlength of 1 mm (red trace) and 10 mm (black trace) were obtained, with the 280 nm and 500 nm points represented by blue and black vertical lines respectively. c) GTPase assays of ci) RbgA-Atto488, cii) Era S268C-Atto488 and ciii) HflX-Atto488. 0.1 µM protein was incubated with 0.1 µM 70S *S. aureus* ribosomes and 1 µM cold GTP spiked with 1.83 nm [α-^{32}P]-GTP in the presence and absence of 100 µM ppGpp. Reaction mixtures were incubated at 37°C for 60 mins, resolved via TLC and the GTP hydrolysis was quantified via pixel densitometry.

4.4.2 Probing for detectable interactions between Atto488-labelled RA-GTPases and the ribosomal subunits

Before any detailed kinetic experiments could be undertaken using the Atto488-labelled proteins, conditions which enable observable changes in fluorescence intensity must be determined. Commonly, ribosomal subunits involved in activity assays such as *in vitro* translation are activated by incubation at 37°C in the presence of $MgCl_2$ and KCl (Vinogradova *et al.*, 2020). A mature 70S ribosome from *E. coli* contains over 170 Mg^{2+} ions, which neutralise the negative charge present on the polyribonucleotide backbone of rRNA to enable productive folding and therefore correct association of assembly factors and r-proteins (Nierhaus, 2014). Mg^{2+} ions also form a critical component of the interface between the 30S pre-initiation complex (pre-IC) and 50S subunits during active 70S formation. Equally important are the K^+ ions, which serve a similar function but are liable to compete with Mg^{2+} binding sites at high concentrations between 0.5 M and 1 M, leading to subunit dissociation (Nierhaus, 2014). Therefore, preincubation of these purified subunits with both monovalent and divalent cations serves to prime the subunit, in this case, for binding to the assembly cofactors RbgA, Era and HflX.

Due to the unpredictable change in fluorescence upon association with the subunits, it was unknown whether this change would be positive or negative. Furthermore, samples would be subject to photobleaching or photoactivation after a certain period of time. As with any concentration driven equilibrium, the initial rate of change will be initially high and then exponentially decrease to an equilibrium, at which point there should be zero net change in fluorescence. Photobleaching or photoactivation would result in a linear decrease or increase in fluorescence intensity following the exponential change, and should not be considered during analysis of fast-kinetics. Due to this effect, observation times should be kept as short as possible to observe the intended effect – in this case the initial association of labelled protein to the ribosome. To probe for fluorescence changes, Atto488-labelled RbgA (Figure 4.4.2a), Era S268C (Figure 4.4.2b) or HflX (Figure 4.4.2c) were rapidly mixed with an excess of either 30S or 50S subunits in the presence of GTP, GDP, ppGpp or pppGpp as indicated. The nucleotide concentrations were equal in both the RA-GTPase-containing syringe and the ribosomal subunit containing syringe to prevent any rapid changes in the nucleotide concentration following mixing from impacting the nucleotide-bound state. Upon mixing, fluorescence was observed and changes were normalised to enable comparison.

No change was observed for RbgA while in the apo state, indicating that in the absence of guanine nucleotides this protein was unable to associate with the ribosome. When bound to guanine nucleotides, a large decrease in fluorescence intensity was observed which spanned the entire 10 second sampling period, consistent with some association to the 50S occurring In the nucleotide-bound state (Figure 4.4.2a). Era S268C exhibited no change in fluorescence when mixed with activated 30S subunits in the presence of GTP, and was observed for a longer period of time until the linear stage of fluorescence change was reached. This lack of signal may be due to one of two factors: either Era S268C is incapable of interacting with the ribosome, or the interaction does not sufficiently influence the Atto488 fluorophore to produce a change in fluorescence. Previous activity assays of Era S268C-Atto488 (Figure 4.4.1.2) showed that the GTPase activity of this protein can be stimulated by the presence of the 70S ribosome comparably to the wild-type, and therefore suggests that the interaction interface between Era and the 30S subunit is still functional. As such it was determined that the fluorophore environment was not sufficiently affected by 30S binding to confer a detectable signal (Figure 4.4.2b). HflX on the other hand exhibited a decrease in fluorescence intensity whether in the apo or nucleotide-bound state when mixed with the 50S subunit, suggesting that nucleotide binding is not a prerequisite of ribosome association in this instance, albeit the amplitude of change is lesser in the apo state so this interaction may be weaker or less favoured (Figure 4.4.2c). This relative dependence and independence on bound nucleotide for even low level ribosome association in the case of RbgA and HflX is consistent with the observations made during Section 4.3.

A further observation is that the change in fluorescence is uniform across nucleotides for RbgA, suggesting a common mechanism of interaction. These patterns in fluorescence differ between the GTP-, GDP-, ppGpp- and pppGpp-bound states of HflX, indicating that slight differences in the mechanism of interaction may be present dependent on the bound nucleotide. Further kinetic experimentation should be undertaken to further clarify this. Overall, changes in fluorescence intensity can be observed and taken as measures of ribosome interaction for RbgA-Atto488 and HflX-Atto488, whereas Era S268C-Atto488 interaction does not yield a useful signal.
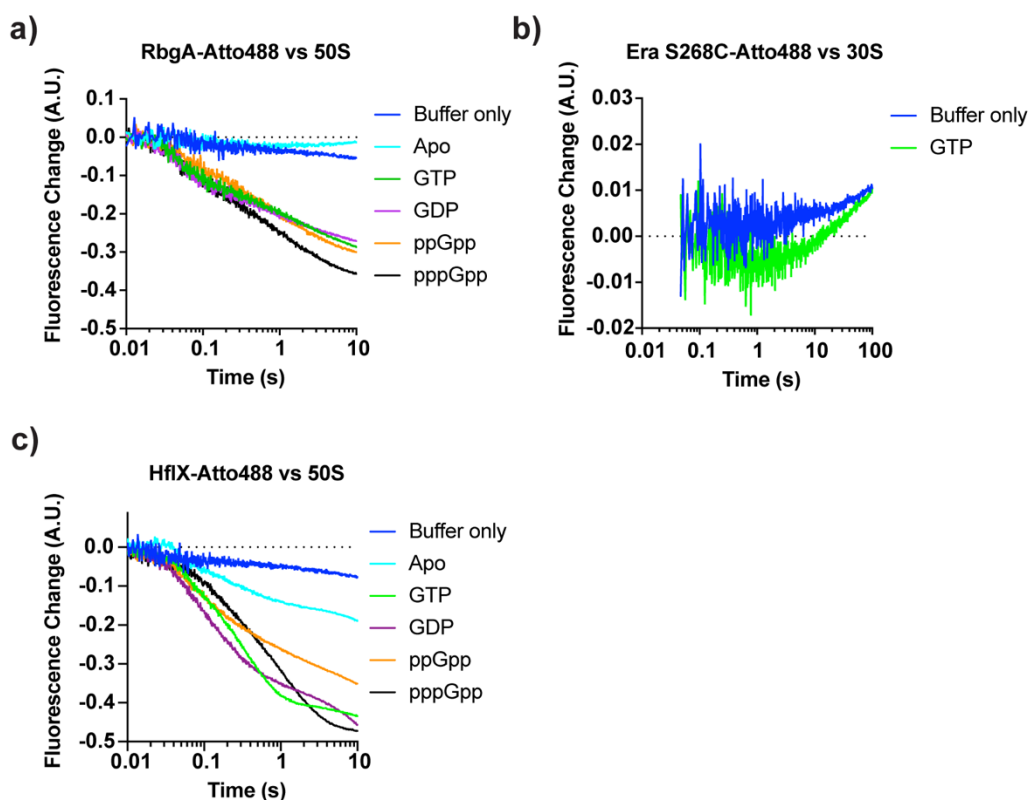
Figure 4.4.2: Initial probing for fluorescence change upon Atto488-labelled RA-GTPase variants binding to the ribosomal subunits. 0.05 µM Atto488-labelled a) RbgA, b) Era S268C or c) HflX was rapidly mixed with 0.15 µM *E. coli* 30S or 50S subunits in the presence of a constant concentration of 100 µM GTP, GDP, ppGpp or pppGpp using stopped-flow apparatus (Applied Photophysics). Atto488 was excited using a 470 nm LED, and emission was detected following passage through a 515 nm long-pass filter. Measurements were taken using logarithmic sampling of 1000 datapoints over either a 10 second or 100 second time period, and each curve is the mean average of at least 5 technical replicates.

4.4.3 Determination of kinetic parameters of RbgA and HflX association to the 50S subunit

Having established conditions which allow for a detectable change in fluorescence upon RbgA-Atto488 and HflX-Atto488 binding to the 50S subunit, the next step was to begin to define the kinetic parameters of this interaction. Calculation of these parameters becomes increasingly complicated as the interaction mechanism becomes more complicated, however the majority of conditions require adaptation of the quintessential Michaelis-Menten dynamic, in which the reaction being observed is in fact the formation of a complex rather than the processing of a ligand, and involves separating distinct phases in the reaction progression.

4.4.3.1 Titrating RbgA and HflX against increasing excesses of 50S subunits

The rate constants of a kinetic system, by definition, describe the relationship between the reaction progression and concentration of constituent components (Bernasconi, 1976). The first step in determining such constants is to investigate the effect of substrate concentration on the rate of

reaction, or in this case, the effect of ribosomal subunit concentration on the rate of RA-GTPase association. While it is possible to maintain a constant concentration of subunits and titrate different concentrations of Atto488-labelling proteins, this would result in changes in expected fluorescence amplitude due to increasing fluorophore concentration. Maintaining a constant concentration of fluorophore while titrating the ribosomal subunit avoids this logistical issue of recalibrating the photomultiplier following every titration. Four concentrations of the 50S subunit were used, namely a 1.5-fold, 3-fold, 5-fold and 6-fold molar excess relative to the concentration of Atto488-labelled protein, and the fluorescence intensities were measured over a 10 second period. These titrations were somewhat resource limited by ribosome availability, and as such were only carried out using GTP, ppGpp and pppGpp to investigate any difference in association kinetics depending on these three nucleotides.

Time traces for both RbgA (Figure 4.4.3.1a) and HflX (Figure 4.4.3.1b) appeared to be concentration dependent in terms of apparent rate, as expected for interactions investigated under sub-diffusion-limited conditions. The concentration dependent difference in amplitude, however, was unexpected due to the assumption that the reaction would saturate, achieving a similar final amplitude at difference rates depending on concentration. The increase in concentration of ribosomal subunits may have skewed the equilibrium more in favour of the GTPase-subunit complex, accounting for this variation. After several rounds of iterative regression analysis and curve fitting, we concluded that the resulting curves (in each nucleotide-bound state) are best described by a biphasic equation (Equation 2) including two exponential terms, accounting for two steps in the overall reaction mechanism. It is important to stress that the *k* values described in Equation 2 are not considered constants, instead they are the apparent rates observed under the specific condition used in each experiment and will henceforth be referred to as k_{app1} and k_{app2} (Table 4.4.3.1). This biphasic, double exponential relationship is indicative of a binding mechanism composed of two consecutive steps between the protein (P) and ribosomal subunit (S), namely an initial unstable complex formation (PS'), followed by a stabilisation step often accompanied by a conformational change (PS) (Equation 3).

Equation 2: $$y = A_0 + A_1 exp(-k_{app1}x) + A_2 exp(-k_{app2}x) + k_{app3}x$$

Equation 3: $$P + S \underset{k_{-1}}{\overset{k_1}{\rightleftharpoons}} PS' \underset{k_{-2}}{\overset{k_2}{\rightleftharpoons}} PS$$
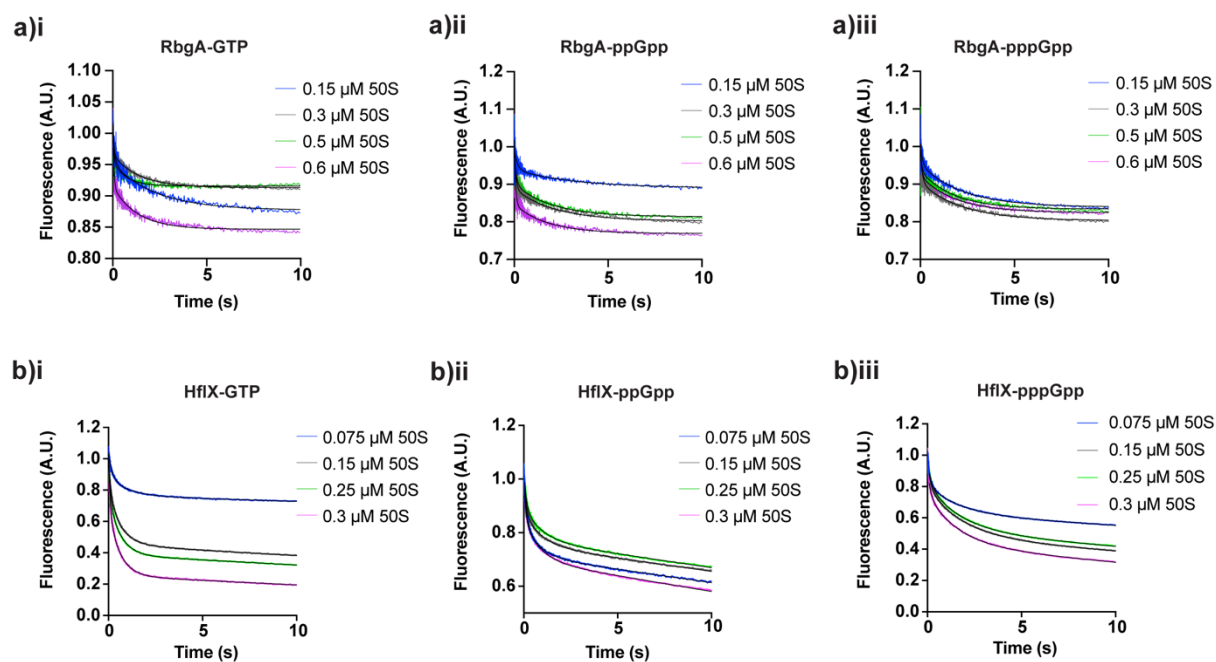
Figure 4.4.3.1: Stopped-flow association experiments of Atto488-labelled RbgA and HflX and the 50S ribosome. a) 0.1 µM RbgA-Atto488 or b) 0.05 µM HflX-Atto488 were rapidly mixed with increasing molar excesses of purified *E. coli* 50S ribosomal subunits in the presence of 100 µM i) GTP, ii) ppGpp or iii) pppGpp. Logarithmic sampling was carried out over a 10 second period, and resulting traces were analysed through nonlinear regression using two exponential terms (Equation 2) in order to derive apparent reaction rates, with fitting shown as a solid black line. Traces are the mean average of at least 5 replicates.

Table 4.4.3.1: Observed microscopic rate constants k_{app1} and k_{app2} of RbgA and HflX association with the 50S ribosomal subunit in the GTP-, ppGpp-, and pppGpp-bound states

	50S (µM)	GTP		ppGpp		pppGpp	
		k_{app1} (s^{-1})	k_{app2} (s^{-1})	k_{app1} (s^{-1})	k_{app2} (s^{-1})	k_{app1} (s^{-1})	k_{app2} (s^{-1})
RbgA	**0.150**	4.81 ± 0.70	0.40 ± 0.04	5.99 ± 0.82	0.30 ± 0.08	9.18 ± 1.00	0.44 ± 0.03
	0.300	5.98 ± 2.37	0.65 ± 0.10	11.65 ± 0.78	0.46 ± 0.05	9.56 ± 0.82	0.45 ± 0.04
	0.500	8.75 ± 3.35	0.77 ± 0.10	10.29 ± 0.76	0.50 ± 0.05	13.58 ± 1.57	0.56 ± 0.04
	0.600	10.49 ± 4.94	0.63 ± 0.08	14.97 ± 0.76	0.56 ± 0.07	14.08 ± 1.33	0.53 ± 0.04
HflX	**0.075**	7.58 ± 1.84	1.10 ± 0.11	7.45 ± 0.98	1.14 ± 0.10	6.76 ± 0.30	0.62 ± 0.01
	0.015	9.22 ± 1.97	1.41 ± 0.11	8.81 ± 0.83	1.10 ± 0.08	7.26 ± 0.64	0.57 ± 0.00
	0.025	10.62 ± 1.34	1.53 ± 0.04	9.77 ± 1.05	1.08 ± 0.05	5.91 ± 0.17	0.59 ± 0.01
	0.030	11.92 ± 0.81	1.65 ± 0.02	9.35 ± 0.85	1.05 ± 0.08	7.16 ± 0.82	0.60 ± 0.03

Errors shown represent standard error in nonlinear regression analysis.

4.4.3.2 Analysis of RA-GTPase-subunit titrations

From the nonlinear regression analyses from the previous section, the apparent *on* rates (i.e. k_{app1} and k_{app2}) for each condition tested can be derived (Table 4.4.3.1). For standard two step reactions, the relationship between k_{app1} and the ligand concentration is expected to be linear and concentration-dependent, while the relationship between k_{app2} and ligand concentration is expected to be hyperbolic (Bernasconi, 1976). Plotting the apparent rates of RbgA and HflX association against the concentration of 50S subunits used (Figure 4.4.3.2a, b) enabled fitting of this relationship. In the case of RbgA, each of the nucleotide-bound conditions appeared to adhere to a two-step binding model, with k_{app1} (Figure 4.4.3.2ai) and k_{app2} (Figure 4.4.3.2aii) exhibiting respective linear and hyperbolic relationships, with comparable apparent rates. HflX differed in apparent mechanism. When bound to GTP, the reaction adhered to the two-step mechanic, and as such we can conclude that productive ON-state binding of HflX to the 50S subunit occurs via a two-step mechanism. When bound to ppGpp, however, the k_{app1} (Figure 4.4.3.2bi) increased linearly while k_{app2} (Figure 4.4.3.2bii) was constant, independent of ribosome concentration. This indicates that the second step of HflX association to the ribosome is inhibited while in the ppGpp-bound state. When in the pppGpp-bound state, both k_{app1} and k_{app2} were constant, indicating that the binding mechanism is drastically altered from the two-phase norm and

unproductive in response to this nucleotide. This consistent inhibition of the second reaction phase while bound to (p)ppGpp indicates that one or more of the microscopic rate constants which contribute to this step tend towards zero, providing a potential mechanistic cause of inhibition. The convergence in *y*-intercept of k_{app1} (Figure 4.4.3.2bi) indicates a minimum rate threshold for the first reaction phase, and as such it is possible that the interaction is rate limited to around 6 s^{-1} by an isomerisation step upon nucleotide-binding preceding the initial GTPase-subunit interaction. Furthermore, the gradient representing the increase in rate of the initial reaction phase (Figure 4.4.3.2bi) was 2-fold greater in the presence of GTP, indicating that the ON-conformation of the RA-GTPase favours not only the second, but also the first reaction phase.

While intuitive analysis of the relationship between subunit concentration and k_{app1} and k_{app2} can give a good indication of reaction progression, estimation of the microscopic *on* and *off* rate constants (i.e. k_1, k_{-1}, k_2 and k_{-2}) (Equation 3) is required for precise identification of the inhibitory step. This estimation requires calculation of the sum and product of the k_{app1} and k_{app2} for each substrate concentration (Figure 4.4.3.2c, d) (Bernasconi, 1976). Linear regression of these relationships enables estimation of the microscopic constants (Table 4.4.3.2) through application of Equation 4, Equation 5, Equation 6 and Equation 7, taking the plot of the sum and product of k_{app1} and k_{app2} as *a* and *b* respectively.

Equation 4:
$$k_1 = gradient_a$$

Equation 5:
$$k_{-1} = intercept_a - \left(\frac{gradient_b}{gradient_a}\right)$$

Equation 6:
$$k_2 = intercept_a - k_{-1} - k_{-2}$$

Equation 7:
$$k_{-2} = \frac{intercept_b}{k_{-1}}$$

In the case of RbgA binding the 50S subunit, (p)ppGpp increased the dissociation rate of the first reaction phase (k_{-1}) by 3-5-fold when compared to GTP, while the initial association velocity (k_1) remained unaffected (Table 4.4.3.2). Furthermore, ppGpp appeared to completely inhibit the progression of the second phase of the reaction (k_2), whereas pppGpp did not. The dissociation rate of the second reaction phase was largely unaffected (k_{-2}), indicating that this inhibition disfavours the progression of the forward reaction steps. In the case of HflX association to the 50S subunit, we estimated the microscopic constants when in the GTP- and ppGpp-bound state, as there was no

ligand-dependence of either reaction phase in the pppGpp-bound state, and as such these conditions do not follow a two-phase mechanism. The rate of the initial forward reaction (k_1) was reduced by 2.5-fold when bound to ppGpp, while the second reaction phase (k_2) was tending towards zero, indicating that this reaction phase is drastically affected and almost completely unproductive while HflX was in the ppGpp-bound state. The ability of ppGpp to inhibit the forward reaction in the case of both RA-GTPases tested indicates that the protein adopts a conformation incompatible with ribosome association, with the secondary accommodation step the most negatively affected. The reverse reaction rates (k_{-1}, k_{-2}) were largely unaffected, reiterating that (p)ppGpp-mediated inhibition of ribosome association is likely to reduce the association rate, rather than increase the dissociation rate.

Estimation of the K_d (Equation 8) of both RA-GTPases interacting with the 50S subunit reveals an overall decrease in binding affinity while in the (p)ppGpp-bound state (Table 4.4.3.2), confirming that the stringent response alarmones prevent stable association of RbgA and HflX to the ribosome. The slight increase in k_{-1}, taken together with the almost complete inhibition of k_2, may indicate a shift in the binding equilibrium to favour the dissociated state, as the kinetically stable RA-GTPase-50S complex is removed from the system. Taken together, these kinetic analyses of the binding system of RbgA and HflX to the 50S ribosome are in accordance with previous observations that the stringent response alarmones reduce the capacity of the RA-GTPases to associate with ribosomal subunits, as compared to the productive GTP-bound state. Specifically, (p)ppGpp appears to adversely affect the forward reactions (k_1 and k_2), suggesting that a nonproductive conformation is adopted by the GTPases when bound to these alarmones, through inhibition of a conformational change which usually imparts complex stability. This in turn would lead to disfavouring of the associated state under physiological nucleotide and ribosomal subunit concentrations, and subsequent reduction of ribosome maturation under stress.

Equation 8:
$$K_d = \frac{k_{-1}k_{-2}}{k_1(k_2+k_{-2})} \equiv \frac{intercept_b}{gradient_b}$$
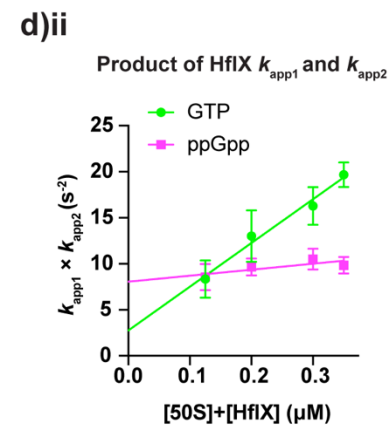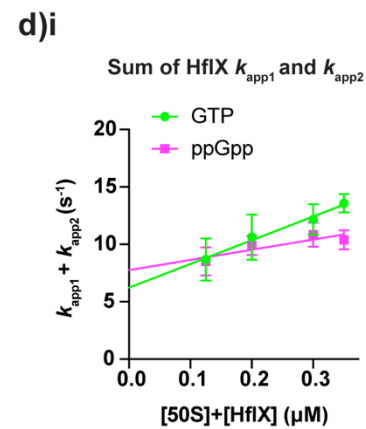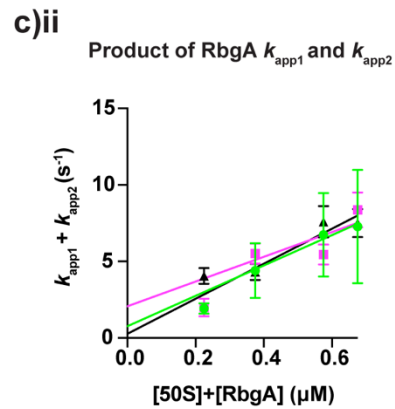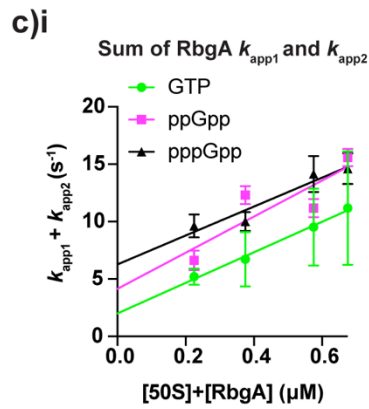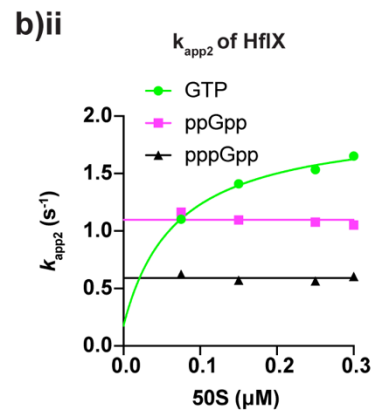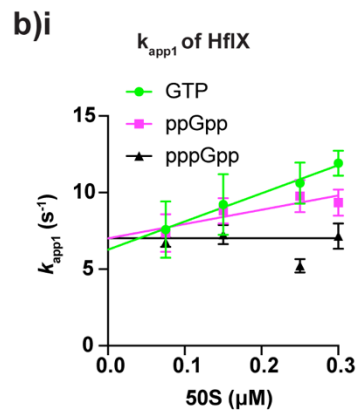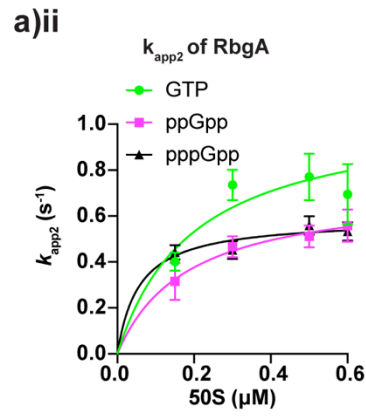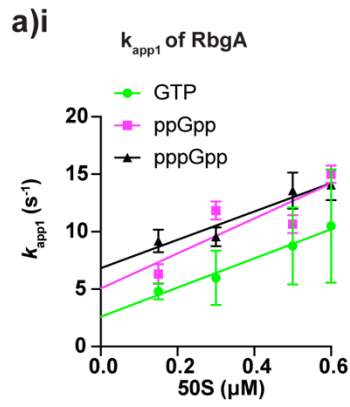
Figure 4.4.3.2: Kinetic analyses and rate constant determination of RbgA and HflX association with the 50S subunit. a) and b) the i) k_{app1} and ii) k_{app2} dependence on 50S subunit concentration of a) RbgA and b) HflX while in complex with GTP (green), ppGpp (pink) and pppGpp (black). c) and d) The i) sum and ii) product of the k_{app1} and k_{app2} of c) RbgA and d) HflX association with the 50S subunit in complex with GTP (green), ppGpp (pink) and pppGpp (black). The association traces from Section 4.4.3.1 were analysed using Equation 2 to derive apparent rates. The sum and product of these apparent rates were plotted as a function of net reaction constituent concentration (protein + 50S) to estimate the microscopic constants k_1, k_2, k_{-1} and k_{-2} and the K_D (Table 4.4.3.2). Error bars represent the standard deviation of the apparent rates (a and b) or the compound standard error of the two-phase analysis (c and d).

Table 4.4.3.2: Estimated microscopic association (k_1, k_2) and dissociation (k_{-1}, k_{-2}) rate constants, and estimated K_d of the association of RbgA and HflX to the 50S ribosomal subunit in the presence of GTP, ppGpp and pppGpp.

		k_1 (s^{-1})	k_{-1} (s^{-1})	k_2 (s^{-1})	k_{-2} (s^{-1})	K_d (μM)
HflX	**GTP**	20.65 ± 1.71	3.93 ± 0.53	1.60 ± 0.43	0.70 ± 0.32	0.06 ± 0.03
	ppGpp	8.87 ± 3.29	7.02 ± 0.97	~0 ± 0.51	1.15 ± 0.20	1.24 ± 0.92
RbgA	**GTP**	13.24 ± 0.92	2.15 ± 0.42	0.63 ± 0.40	0.22 ± 0.38	0.04 ± 0.07
	ppGpp	16.08 ± 7.1	4.79 ± 3.02	~0 ± 0.38	0.12 ± 0.37	0.23 ± 0.71
	pppGpp	12.59 ± 2.60	6.50 ± 1.13	0.36 ± 0.28	0.36 ± 0.16	0.26 ± 0.15

Negative rate values for k_2 approximated to ~0 s^{-1}. HflX did not obey a two-step binding mechanism while complexed with pppGpp, and as such was omitted from this analysis. Error values shown represent the compound standard error of the two-phase analysis.

4.4.4 Using IF3$_{DL}$ as a FRET sensor of Era association to the 30S

IF3 is an essential protein in most bacteria, and is involved in the formation of the bacterial 30S pre-IC (Chulluncuy *et al.*, 2016) and ribosome maturation (Sharma and Woodson, 2020), and as such is crucial during the translation elongation cycle. IF3 contains two domains separated by a flexible linker region, and in the absence of 30S ribosomal subunits these two domains interact in a compact conformation (Elvekrog and Gonzalez, 2013). Upon association of the C-terminal domain with the 30S ribosomal subunit, IF3 adopts an elongated conformation characterised by increased separation between domains, which enables the N-terminal domain to effectively enhance the fidelity of translation initiation by avoiding non-AUG codons and selecting against initiator tRNAs lacking three conserved GC pairs in the anticodon stem (Ayyub *et al.*, 2017).

Previously, this conformational change of IF3 has been exploited as a FRET sensor, in which a fluorophore and quenching chromophore have been conjugated to the N- and C-domains of IF3 respectively (Chulluncuy *et al.*, 2016). FRET is a form of nonradiative energy transfer between two

chromophores with overlapping spectra, enabling signal quenching when the interaction radius is low. Since the FRET efficiency between the donor and quencher decays with the 6th power of the interaction range, small conformational changes in the protein can be visualised by monitoring relatively large changes in fluorescence (Figure 4.4.4a). Between the FRET pair Atto488 and Atto540Q, the Förster radius at which 50% of emitted energy from the donor is absorbed by the quencher is 64 Å, making this system useful when measuring mid-range micromolecular interactions. This model has been used to monitor assembly of the 30S pre-IC (Chulluncuy *et al.*, 2016), during which association of proteins affects the relative domain conformation of IF3. Here, we attempted to adapt and use this model as a means of monitoring the association of Era to the 30S in the presence of difference nucleotides (Figure 4.4.1c). Note that unlike the previous experiments focusing on chemical fluorescence of the fluorophore, in this instance Era is unlabelled as the intra-IF3 FRET pair is responsible for the signal.

Firstly, we set out to confirm that the FRET system was fully functional. Mixing activated 30S subunits with dual-labelled IF3 (IF3$_{DL}$) using stopped-flow apparatus was accompanied by a large increase in fluorescence, as expected due to IF3 entering the extended conformation (Figure 4.4.4b) and therefore indicating that the FRET sensor is functional. In order to probe for a change in signal upon Era binding, we first preincubated Era-GTP with the 30S in order to establish whether Era and IF3 binding is mutually exclusive, as both Era and IF3 are considered to associate close to the 3' of the 16S rRNA, with Era binding to the terminus (Tu *et al.*, 2009) and IF3 having been show to crosslink with h45 (Dallas and Noller, 2001). If so, we expect a signal similar to the aforementioned buffer control, with IF3 only capable of self-interaction, and thus high FRET and low signal. However, we instead saw the rapid increase in fluorescence indicative of IF3 association with the 30S subunit and the subsequent domain extension, suggesting that IF3 and Era are simultaneously able to associate with the 30S subunit, or that the binding affinity of IF3 is significantly greater than that of Era to the 30S, resulting in extremely rapid outcompetition. We next sought to establish whether IF3 can be used to detect Era association when preincubated with the ribosome. Rapid mixing of Era with IF3-30S complexes yielded no change in fluorescence, with signal remaining constant throughout the 10 second sampling period, suggesting that the domain structure of IF3 remains unperturbed in the extended conformation throughout sampling. Altogether, this suggests that this system is unsuitable for monitoring Era association, as this association fails to alter IF3 domain conformation in a detectable manner.
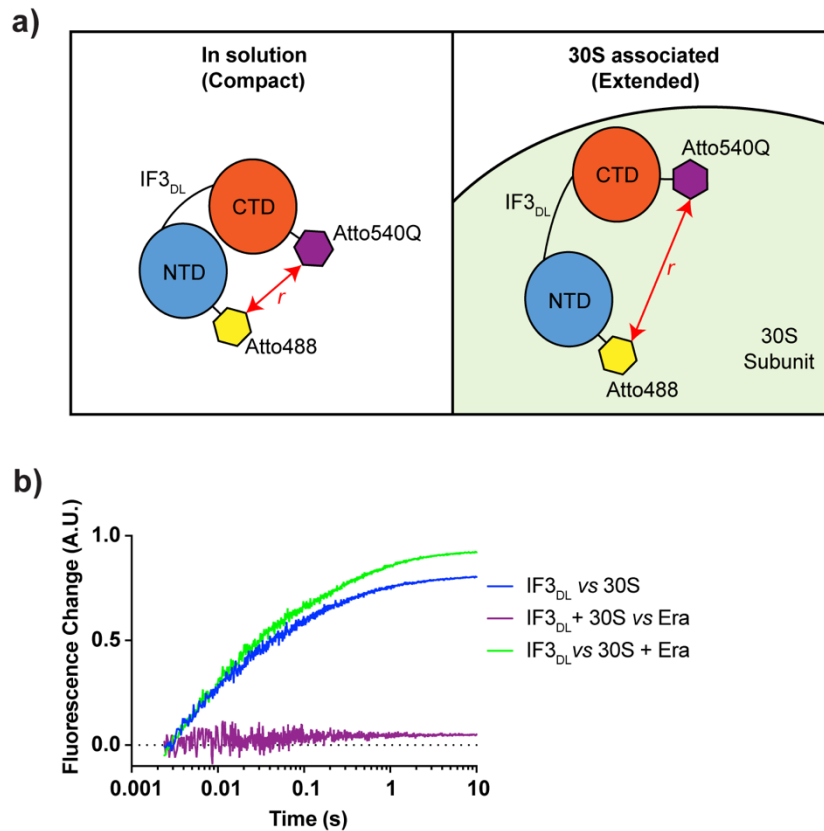
Figure 4.4.4: Era association with the 30S subunit is not detectable through use of IF3 as an intramolecular FRET sensor. a) Schematic representation of the IF3$_{DL}$ FRET sensor. In solution (left panel), the NTD and CTD of IF3 interact in a compact conformation, leading to a low radius (r) and high FRET between the Atto488 fluorophore and Atto540Q quenching chromophore, and therefore low detectable fluorescence. When 30S-associated (right panel), the CTD and NTD adopt an elongated conformation leading to a large r and low FRET, leading to high detectable fluorescence. b) 0.2 µM of IF3$_{DL}$, 0.1 µM 30S subunits and 0.2 µM Era were mixed along with 20 µM GTP in the manner described using stopped-flow apparatus. Atto488 was excited using a 470 nm LED, and detected through a 515 nm long-pass filter. Logarithmic sampling was carried out over a 10 second period, and each trace is the average of at least 5 replicates.

4.5 Induction of the stringent response inhibits Era-30S interactions *in vivo*

During the stringent response, an increase in cellular (p)ppGpp concentration leads to a decrease in GTP levels (Kriel *et al.*, 2012; Varik *et al.*, 2017), both by usage of GTP as a precursor for pppGpp production and also through inhibition of two guanylate kinases named Gmk and HprT in many bacteria, including *S. aureus* and *B. subtilis* (Corrigan *et al.*, 2016), but only HprT is inhibited in β- and γ-proteobacteria such as *E. coli* (Liu *et al.*, 2015b). Having established that binding to (p)ppGpp reduces the affinity of RA-GTPases to the ribosome *in vitro* (Sections 4.3, 4.4), we next sought to investigate this interaction under more physiologically relevant conditions, specifically within the bacterial cell. To achieve this, we used an *era* deletion mutant in the CA-MRSA USA300 LAC* background, which was available in our laboratory strain collection (Wood *et al.*, 2019). Previously considered essential in *S. aureus*, deletion of *era*, while viable, is followed by a profound growth defect (Figure 4.5a) and

abnormal ribosome profile (Figure 4.5b) indicative of a reduction in mature 30S subunits (Wood *et al.*, 2019).

To enable detection of 30S-associated Era in bacterial cells via α-His immunoblotting, we utilised the available complementation strain LAC* Δ*era* pCN55iTET:*era*-His containing a 6xHis-tagged Era variant under the control of an anhydrotetracycline (Atet)-inducible promoter. Induction of this strain with 100 ng/ml Atet restored growth to wild-type levels (Figure 4.5a), indicating that this variant of *era* is both expressed and functional. In order to carry out cosedimentation assays of Era-His and the ribosomal subunits, cells were grown to mid-exponential phase, and the stringent response induced with either 0.05 μg/ml or 60.0 μg/ml of mupirocin, an antibiotic known to induce the stringent response in *S. aureus* through inhibition of isoleucyl tRNA synthetase, leading to an accumulation of uncharged tRNA$_{Ile}$ (Reiss *et al.*, 2012). Cells were lysed using lysostaphin and DNase, and the lysates were applied to a 10%-40% sucrose gradient and ribosomal subunits separated as in Section 4.2.2. Associated Era-His was identified using α-His immunoblotting (Figure 4.5c, upper panels). It is well known that the stringent response negatively impacts cellular translation rate, and as such the crude lysates were included in the western blotting to ensure equal expression of Era-His between samples containing different mupirocin concentrations. Furthermore, nonspecific protein staining was carried out using Ponceau S to ensure equal loading (Figure 4.5c, lower panels). Together, these ensure that any differences observed in the level of Era-His association observed were not due to differential expression or loading error.

In agreement with our previous observations (Figure 4.3), a 4-fold decrease in association of Era-His to the 30S subunit was observed upon stringent response induction, with a comparable level of association whether induced with 0.05 μg/ml or 60.0 μg/ml mupirocin (Figure 4.5d). As expected, no Era-His was detected in the 50S-containing fractions, which suggests that the crude subunit separation protocol employed here was sufficient to prevent overlap between 30S- and 50S-containing fractions. In all three lysates, intense bands were observed on the western blot at around 42 kDa. These can be attributed to protein A, a protein capable of binding the F$_c$ region of immunoglobulins in order to evade the immune system (Falugi *et al.,* 2013; Kobayashi and DeLeo, 2013). All in all, the *in vivo* data presented here supports the previous observation that while in the (p)ppGpp-bound state, RA-GTPases are less capable of interacting with the ribosomal subunits, suggesting that the stringent response may impair 70S assembly and therefore translation by limiting the activity of assembly factors.
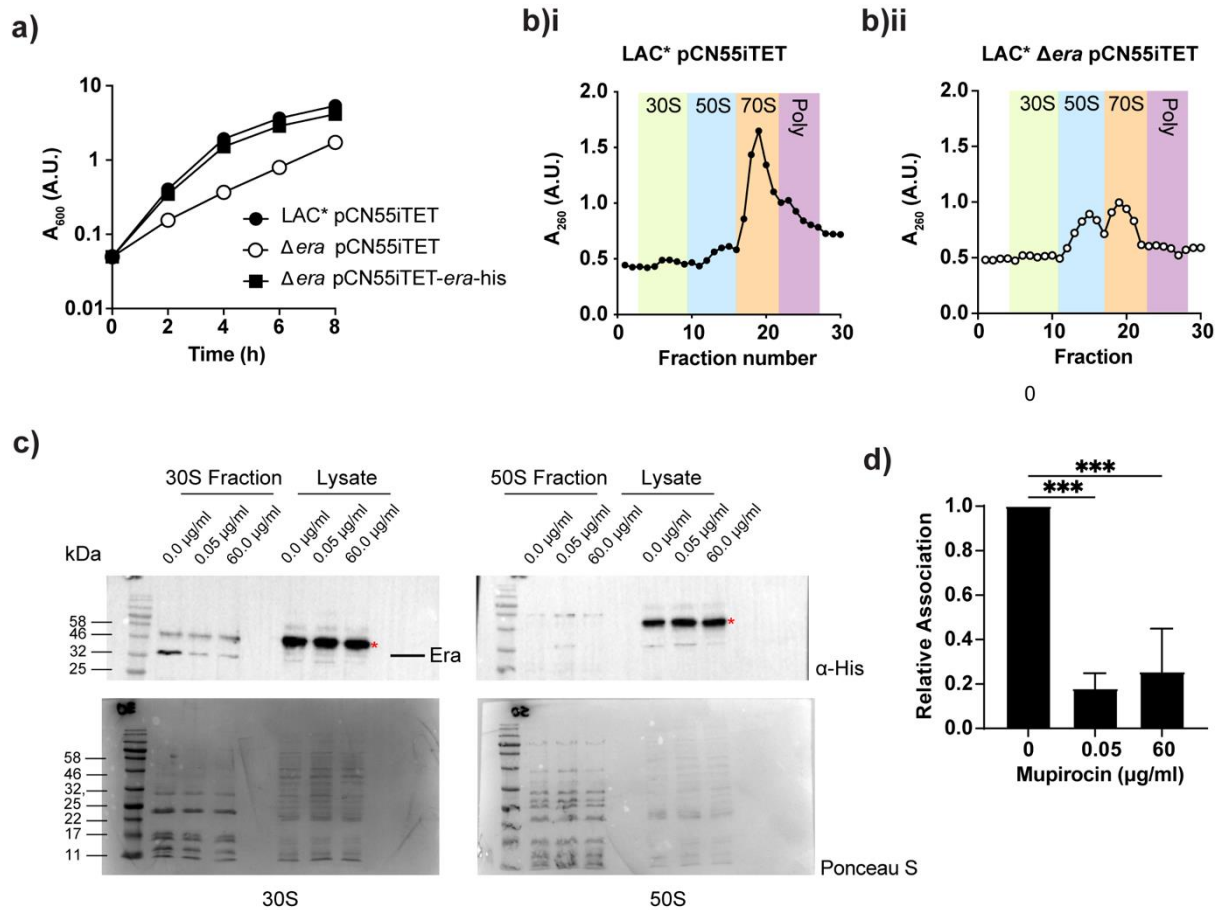
Figure 4.5: Activation of the stringent response inhibits Era-30S interactions *in vivo*. a) Growth curve of *S. aureus* strains LAC* pCN55iTET, LAC* Δ*era* pCN55iTET and LAC* Δ*era* pCN55iTET:*era*-His. Saturated *S. aureus* cultures were backdiluted to A_{600} of 0.05 before the addition of 250 µg/ml spectinomycin and 100 ng/ml Atet. Cultures were grown at 37°C for 8 hours with shaking, with sampling at 2 hr intervals. Experiments were carried out in triplicate, with error bars representing the standard deviation between replicates. b) Ribosome profiles from *S. aureus* strains i) LAC* pCN55iTET and ii) LAC* Δ*era* pCN55iTET. Crude cell lysates were applied to a 10%-50% sucrose gradient and ribosomal subunits were separated at 192,100 × *g* for 7 hrs. 250 µl fractions were analysed using A_{260} to determine RNA content. Expected peaks representing the 30S subunits (green), 50S subunits (blue), 70S subunits (orange) and polysomes (red) are indicated. c) Western immunoblotting using α-His antibodies to detect the presence of Era-His in 30S- and 50S-containing fractions (left and right panels respectively). LAC* Δ*era* pCN55iTET:*era*-His was grown to an A_{600} of 0.5 in the presence of 100 ng/ml Atet. Cells were either left untreated or induced with either of 0.05 or 60 µg/ml mupirocin for 30 mins to activate the stringent response. Ribosomal subunits were separated by isopycnic ultracentrifugation along a 10%-40% sucrose gradient at 111,000 × *g* for 16 hrs, and the 30S- and 50S- containing fractions were pooled and concentrated. Associated Era-His was detected using HRP-conjugated α-His antibodies. Lysates were also analysed to ensure equal Era expression (top panels). Total protein content was analysed using Ponceau S staining to ensure consistent loading (bottom panels). Experiments were carried out in triplicate, with one representative example shown. Bands marked with a red star correspond to *S. aureus* Protein A (Spa) d) Relative association levels of Era-His from the immunoblots shown in (c) were derived using band densitometry and plotted, with error bars representing standard deviation between replicates. Statical analyses were performed using one-way ANOVA and Tukey's multiple comparisons test, with *p* values represented as follows: ***, $p < 0.001$.

4.6 Characterisation of the relationship between rRNA binding and the GTPase activity of Era

For many RA-GTPases, the interaction interface with the ribosome is extremely complex, often comprising multiple rRNA helices interacting at multiple sites throughout the protein, often including both the accessory and GTPase domains (López-Alonso *et al.*, 2017b). Structural studies of Era have in contrast identified a single 16S rRNA motif which is subject to recognition by the C-terminal RNA-binding KH domain (Tu *et al.*, 2011; Tu *et al.*, 2009). This 10 ribonucleotide motif, situated towards the 3' end of the 16S rRNA, has the following sequence in *E. coli*: $_{1530}$GAUCACCUCC$_{1539}$. The two adenine nucleotides are essential for stimulation of the GTPase activity of Era, although A1531 is somewhat tolerant of semi-conservative mutation (Tu *et al.*, 2011). The seven remaining nucleotides were individually redundant in terms of GTPase stimulation, although removal of the $_{1535}$CCUCC$_{1539}$ region removed any stimulatory effect (Tu *et al.*, 2011). This well-understood single RNA binding site of Era paves the way for investigation into the role of RNA recognition in nucleotide binding and GTPase activity, and the potential signal transduction between the KH domain and GTPase domain.

4.6.1 The nucleotide bound state has no effect on RNA-binding by Era

The first step in investigating the role of RNA recognition by the KH domain of Era was identifying the cognate recognition sequence in *S. aureus*. Since this motif is situated at the extreme 3' of the 16S rRNA and contains an identical consensus sequence to the *E. coli* sequence, identification in *S. aureus* was straightforward. Following synthesis of the 12 ribonucleotide AUCACCUCCUUU fragment, the first step in order to visualise rRNA binding interactions was radiolabelling. This was achieved using polynucleotide kinase (PNK) as per the methods section, with [γ-^{32}P]-ATP as a radiolabelled phosphate donor. Using this protocol, RNA polynucleotides were 5' labelled with ^{32}P and excess [γ-^{32}P]-ATP was removed from the reaction mixture using NucAway desalting columns (Invitrogen). Pre-reaction, post-reaction and post-purification samples were analysed using TLC to follow reaction progress and assess purity, which was deemed to be >95% using pixel densitometry following sample purification (Figure 4.6.1a). As mentioned previously, cell lysates were treated with RNase prior to IMAC purification of proteins to remove potential contaminants. RNA contamination is usually assessed using the A$_{260}$:A$_{280}$ ratio of purified protein preparations, however in this case since the presence of even small amounts of RNA could interfere with binding assays, we opted to also carry out chloroform RNA extractions from purified Era as a more sensitive approach to ensure the absence of RNA in the preparation (Figure 4.6.1b). We were unable to detect the presence of any RNA in the Era sample. Next, we assessed the ability of Era to bind to the 12 bp RNA fragment while in different nucleotide-bound states, in order to investigate whether the affinity of Era to the 70S may be increased when in the GTP-bound ON

state due to enhanced rRNA binding (Figure 4.6.1c). Recombinant MBP was included as a negative control. No difference was observed in the RNA binding capacity when bound to GTP, GDP, ppGpp, pppGpp or in the apo state, with 85%-90% of the radiolabelled RNA bound in each case. This indicates that binding of short RNA (in the absence of the ribosome as a whole) by the KH domain of Era occurs with high affinity independently of whether the protein is in the ON or OFF state.
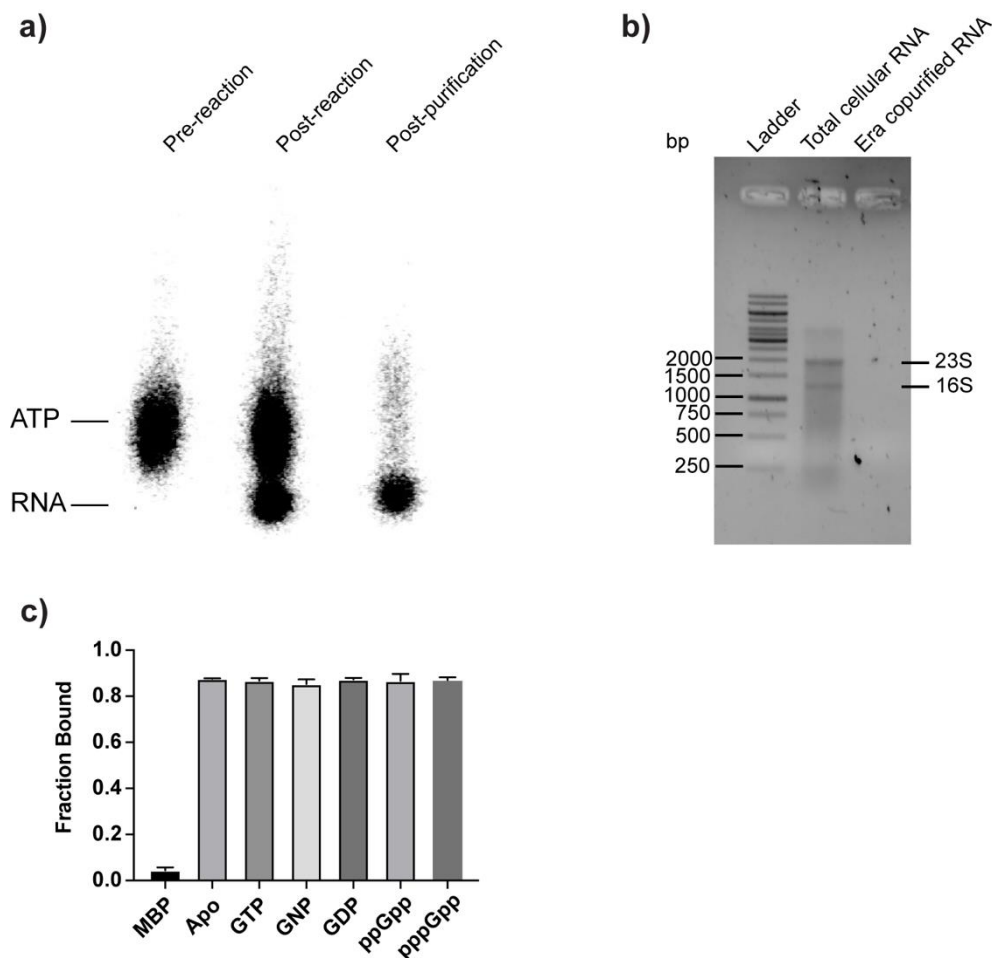
Figure 4.6.1: The nucleotide bound state of Era has no effect on RNA binding capacity. a) 5' labelled RNA fragments were generated via a polynucleotide kinase (PNK) reaction using [γ-^{32}P]-labelled ATP as a donor. 10 pmol of the 12 nucleotide AUCACCUCCUUU oligo was incubated with 1.4 MBq [γ-^{32}P]-labelled ATP and 10 units of PNK at 37°C for 15 mins. Pre-incubation, post-incubated and post-purification samples were analysed using TLC, and visualised using a photostimulable phosphor. The purity of the final RNA sample was assessed using pixel densitometry and was determined to be >95%. b) 1% agarose gel electrophoresis of Lane 2: total *S. aureus* cell RNA content and Lane 3: RNA chloroform extraction from purified recombinant Era. c) DRaCALAs were carried out as specified in the methods section using 10 µM recombinant Era or MBP. The protein was incubated with 0.4 µM 5'-labelled AUCACCUCCUUU RNA for 5 mins before spotting onto nitrocellulose membrane and visualisation using a phosphorimage and subsequent analysis using pixel densitometry. Experiments were carried out in triplicate, with error bars representing the standard deviation between replicates.

4.6.2 The effect of the KH domain of Era on nucleotide binding and GTPase activity

Next, we sought to determine whether the affinity of Era for different nucleotides was influenced by RNA binding. To do this, we cloned an Era variant lacking the KH rRNA-binding domain, termed Era 1-180 (Figure 4.6.2a), This variant should still maintain a structured GTPase domain, but should be totally incapable of binding to the 16S rRNA recognition site, enabling comparison between wild-type Era and Era 1-180 in the presence of ribosomes as the RNA-bound and unbound states respectively. Era 1-180 was expressed and purified using the expression protocol developed for wild-type Era in Chapter 3.2.2, and interestingly proved to have a much greater solubility than the wild-type.

Firstly, end-point binding assays were carried out in the presence of the unlabelled AUCACCUCCUUU fragment in order to determine whether the ability of Era 1-180 to bind nucleotides differed than the wild-type (Figure 4.6.2b). To this end, DRaCALAs were carried out using 2.5 μM recombinant Era or Era 1-180, an equimolar concentration of the 12 bp rRNA fragment and [α-^{32}P]-labelled GTP, GDP, ppGpp or pppGpp. No difference was found between the ability of Era and Era 1-180 to bind to GTP, GDP, ppGpp or pppGpp following t testing (Figure 4.6.2b), indicating that whether or not the KH domain of Era is bound to the rRNA recognition motif has no effect on the capacity of Era to bind to guanine nucleotides.

Since nucleotide binding can occur in the absence of RNA binding, we next investigated the effect of KH domain deletion on the GTPase activity of Era. Hydrolysis timecourses were carried out (Figure 4.6.2c), in which recombinant protein was incubated with 70S ribosomes and an excess of cold GTP spiked with [α-^{32}P]-labelled GTP and samples taken every 10 mins to monitor reaction progression. Despite retaining the ability to bind to GTP and other guanine nucleotides, the Era 1-180 mutant was found to be completely GTPase inactive, corroborating previous observations that the GTPase activity of these checkpoint proteins is activated upon recognition of mature rRNA (Verstraeten *et al.*, 2011). The GTP hydrolysis over time for both Era 1-180 and the GTP-only control show a slight positive gradient, resulting in a hydrolysis of around 5%. This could be due to spontaneous hydrolysis of GTP over time, especially considering that samples taken at each timepoint were subject to incubation at 95°C in order to release bound nucleotides from the proteins.
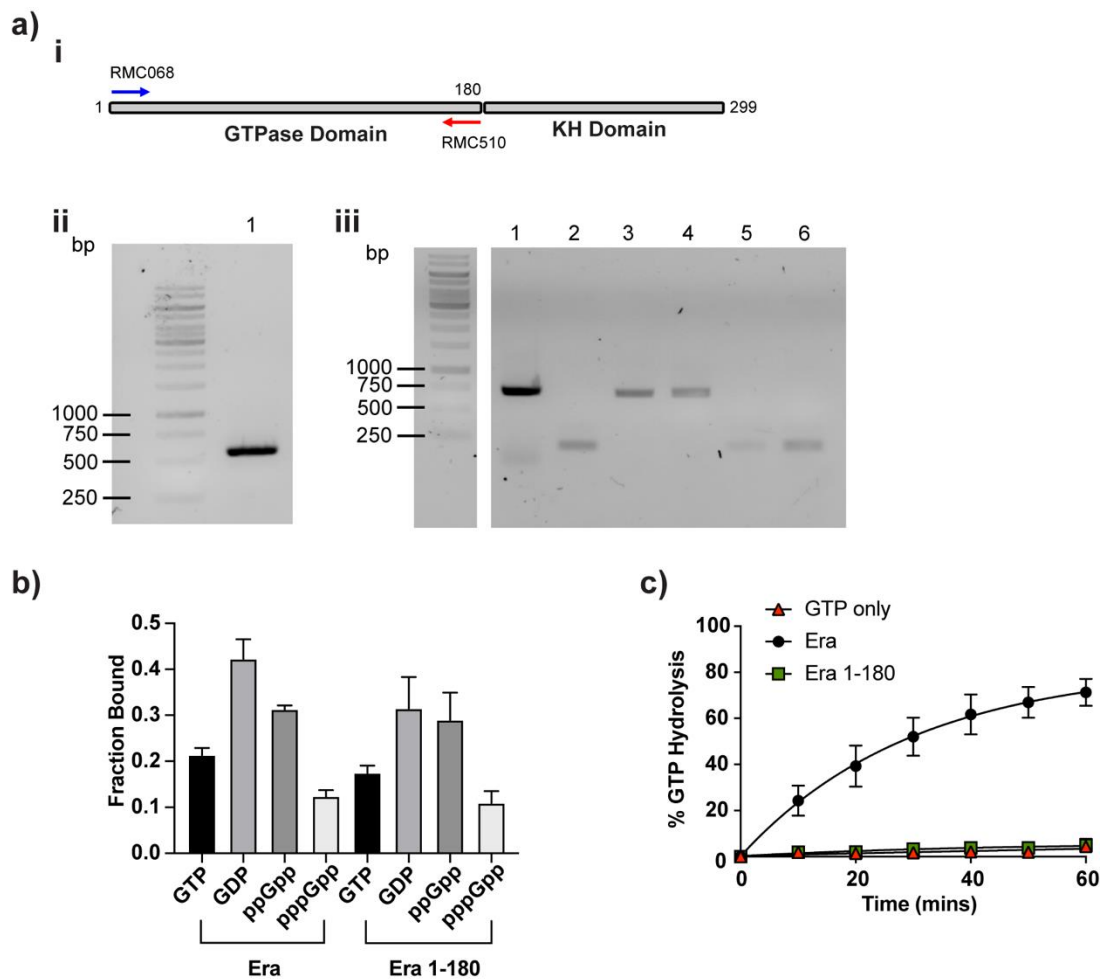
Figure 4.6.2: Deletion of the KH domain of Era affects GTPase activity but not nucleotide binding. ai) Schematic view of the design of the Era 1-180 mutant, indicating domain structure and primer positioning. aii, aiii) 1% agarose gel electrophoresis of the PCR products of aii) Era 1-180 fragment amplification using primers RMC068 and RMC510, with an expected fragment size of 612 bp, and aiii) colony PCR following product digestion and ligation into a pET28b vector using screening primers RMC062 and RMC063. Positive colonies with an insert of 720 bp are present in lanes 1, 3 and 4. b) 10 μM Era or Era 1-180 was incubated with 1.83 nM [α-^{32}P]-labelled GTP, GDP, ppGpp or pppGpp in the presence of 10 μM AUCACCUCCUUU RNA fragment for 5 mins at room temperature. Samples were then spotted onto nitrocellulose membrane and visualised using a photostimulable phosphor before analysis using pixel densitometry. Experiments were carried in triplicate and error bars represent the standard deviation between replicates. c) 0.1 μM recombinant Era or Era 1-180 was incubated with 0.1 μM 70S ribosomes and 1 μM cold GTP spiked with 1.83 nM [α-^{32}P]-labelled GTP, and incubated at 37°C for 60 mins. Samples were taken every 10 mins and percentage hydrolysis was determined using TLC and pixel densitometry as described in the methods section. Experiments were carried out in triplicate, with error bars representing standard deviation between replicates.

4.6.3 KH domain-rRNA interactions alone are not sufficient to stimulate GTPase activity

Mutagenic analysis of the nucleotides within the Era binding site of *E. coli* 16S rRNA identified A1531 and A1534 as the critical determinants of GTPase activity stimulation (Tu *et al.*, 2011), in addition to the $_{1535}$CCUCC$_{1539}$ moiety. While it is known that RsgA contains an unconventional catalytic histidine residue within switch I as opposed to the conventional residue in switch II, which may be correctly positioned by rRNA association (López-Alonso *et al.*, 2017b), Era has been suggested to hydrolyse GTP in a substrate assisted stochastic mechanism (Pasqualato and Cherfils, 2005; Tu *et al.*, 2009), with the

γ-phosphate of GTP acting as a general base and an adjacent water molecule as the activating acid to avoid the requirement of a GAP. This would imply that the GTPase activity of Era is stimulated in the presence of RNA due to enhanced stability of the Era-GTP complex to increase the efficiency of hydrolysis (Tu *et al.*, 2009).

In order to investigate this further, we carried out GTP hydrolysis assays of wild-type Era in the presence of different rRNA samples, namely the 70S *S. aureus* ribosome, total *S. aureus* RNA content and the 12 nucleotide recognition sequence (Figure 4.6.3). Era was only capable of hydrolysing GTP in the presence of the complete 70S ribosome, with negligible GTP hydrolysis observed in the absence of RNA and the presence of total cellular RNA or the 12 nucleotide fragment. This observation provides evidence that the GTPase Era is not stimulated in a substrate-assisted manner as has been previously suggested (Tu *et al.*, 2009), and that RNA binding alone is insufficient to enhance activity. Taken together with the results from Sections 4.6.1, and 4.6.2, this suggests that RNA binding by the KH domain and nucleotide binding by Era are independent of each other and that this RNA binding alone is not sufficient to stimulate GTP hydrolysis. Instead, stimulation of GTPase activity is facilitated by the presence of a transactivating element provided by the body of the ribosome following correct positioning of Era through KH domain-rRNA interactions, despite a lack of specific interactions between the GTPase domain of Era and the ribosome.
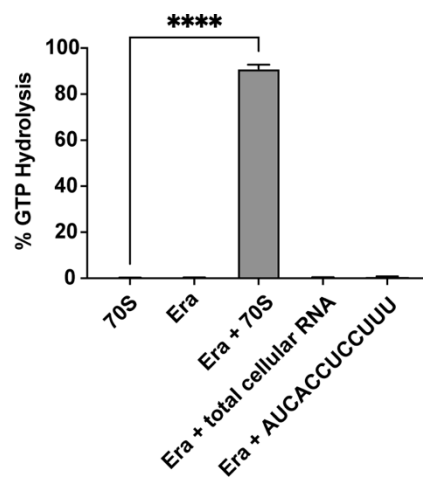
Figure 4.6.3: RNA binding by the KH domain of Era cannot stimulate GTPase activity in the absence of the mature ribosome. 0.1 μM recombinant Era was incubated with 0.1 μM 70S ribosomes, total cellular RNA extract or 0.1 μM of the 12 nucleotide AUCACCUCCUUU motif and 1 μM cold GTP spiked with 1.83 nM [α-^{32}P]-labelled GTP. Samples were incubated for 60 mins at 37°C, and percentage hydrolysis was determined using TLC and pixel densitometry as described in the methods section. Experiments were carried out in triplicate, with error bars representing standard deviation between replicates. Statistical differences were determined using unpaired *t* testing, with *p* values represented as follows: ****, *p*<0.0001.

4.7 Discussion

In this chapter, we sought to biochemically characterise the interactions between the four RA-GTPases RsgA, RbgA, Era and HflX with the 30S and 50S ribosomal subunit. To achieve this, we employed several different techniques, namely isopycnic subunit separation, α-His immunoblotting and stopped-flow fluorescence spectroscopy. These were used to thoroughly investigate the nucleotide-dependence of RA-GTPase-subunit interactions, as well as how the efficacy of this interaction changes when in the GMPPNP-bound ON state compared to the GDP-bound OFF state, and indeed whether the binding of (p)ppGpp reflects either ON or OFF state activity more closely.

We first aimed to develop a technique which allows accurate detection of RA-GTPases associated with the ribosomal subunits. Firstly, we used SOE-PCR to generate translational fusions of Era and HflX to the monomeric fluorescent protein mCherry (Figure 4.2.1), in an attempt to make use of this fluorescence as a detectable marker of the presence of these proteins. At first it appeared that a signal was visible for both Era and HflX in both the 30S and 50S containing fractions (Figure 4.2.2). However, upon investigating the background fluorescence exhibited by the ribosomal subunits following splitting, it became apparent that the 30S subunit fluoresced similarly to mCherry upon excitation at 580 nm, with a signal strength of around 0.3 V above background, rendering the two signals from the 30S subunit and any associated mCherry fusion protein inseparable. Interestingly, the 50S background fluorescence was very low in the mCherry range, and signal was observed for both RA-GTPases included, despite Era having never been considered capable of 50S binding. This signal decreased in the presence of ppGpp, suggesting a decrease in protein association with the subunit. An alternative strategy was to generate GFP fusion proteins instead of mCherry, and to verify the potential of this we investigated the background fluorescence of the ribosomal subunits using an excitation wavelength of 480 nm, gated using a long-pass filter at 500 nm (data not shown). The background fluorescence under these conditions was much greater, with both the 30S and 50S subunits exhibiting fluorescence of around 0.8 V above background. As such, the use of GFP as a detection marker was decided against. mCherry and mAzami (Day and Davidson, 2009) have both previously been used as fluorescent labels of both the 30S and 50S in *E. coli* (Nikolay *et al.*, 2015) when fused to S15 and L1 respectively. mAzami is a green fluorescent protein with an absorbance/emission spectrum very similar to that of GFP. This suggests that the fluorescence when in a 1:1 ratio with the ribosome is detectable, and perhaps in our system the ratio of fusion protein to ribosome was too small. To circumvent this issue, a greater excess of mCherry fusion could be used to encourage binding, however this comes with the caveat of increasing the initial background fluorescence due to unbound protein, which would increase the overall background while in exponential decline. All in all, it seems that this

system of monitoring protein association with the ribosome is flawed, and unlikely to yield any reliable results.

In an effort to improve on the mCherry-fusion technique mentioned previously, we also used α-His immunoblotting following ribosomal subunit separation to decrease the level of background signal (Figure 4.3). We have shown using this technique that for RsgA, RbgA, Era and HflX that optimum association to the cognate subunit occurs while the RA-GTPase is in the GMPPNP-bound ON state, which is decreased in the GDP-bound state. This is in agreement with the generally accepted mechanism of the prokaryotic GTPase cycle, in which GTP hydrolysis and entry into the GDP-bound OFF state is the trigger for GTPase dissociation from the interaction target (Verstraeten *et al.*, 2011). For each of the four proteins tested, the presence of ppGpp or pppGpp reduced ribosome association to comparable levels to when in the GDP-bound OFF state. This data is in disagreement with previously published results suggesting that the interaction between *B. subtilis* RbgA and the 50S subunit is enhanced in the presence of pppGpp (Achila *et al.*, 2012), which was determined following ultrafiltration of samples and subsequent recovery from the 100 kDa cutoff membrane. This could potentially have led to inaccuracies in recovering the 50S-RbgA complexes, as there was no way of ensuring the 100% recovery necessary for accurate quantification of interaction strength. Nevertheless, this observation has led to the development of the current dogma, in which inhibited assembly cofactors sequester immature ribosomal subunits to prevent complete maturation under conditions of stress. Furthermore, it has been observed that another TRAFAC GTPase in *E. coli*, ObgE, has enhanced affinity to the 50S subunit while bound to ppGpp (Feng *et al.*, 2014), although this could reflect the activity of ObgE as an anti-association factor rather than an assembly cofactor, which would therefore benefit from the enhanced affinity to prevent 70S formation during the stringent response. Era and HflX also showed a high level of association to the 30S and 50S subunits respectively when in the apo state. This is unheard of in HflX, for which guanine nucleotide binding has always been considered a requirement for ribosome association and the subsequent passive 70S splitting activity (Basu and Yap, 2017; Coatham *et al.*, 2016). Despite this, when trialling HflX-Atto488 binding to the 50S subunit in the presence of different nucleotides (Figure 4.4.2c), a change in fluorescence was observed while in the apo state, indicating some level of association, although this change was much lower in amplitude than while in the GTP- or even GDP-bound states. Era, on the other, has previously been suggested to associate with the 30S subunit while in the apo state (Sharma *et al.*, 2005) in a conformation which differs from that adopted when bound to GMPPNP or GDP (Tu *et al.*, 2011; Tu *et al.*, 2009).

Using stopped-flow fluorometry to monitor the association of RbgA and HflX to the 50S subunit enabled us to propose a simple two-step mechanism of association, in which the protein first forms an unstable complex with the ribosomal subunit, and then undergoes a conformational change to stabilise this interaction. We could also isolate the second step as the most likely step inhibited by (p)ppGpp binding, suggesting that these alarmones disrupt stable complex formation between the RA-GTPase and the subunit seemingly through inhibition of a conformational change. In both previous cases of (p)ppGpp being reported to increase RA-GTPase-ribosome assocaition, no kinetic parameters or K_d values were estimated, making comparison of binding mechanics impossible (Achila *et al.*, 2012; Feng *et al.*, 2014). The signal strength in the case of RbgA-Atto488 was very weak, as demonstrated by the high level of noise and low overall amplitude of the observed change in Figure 4.4.3.1. This is likely due to the very low degree of labelling of this protein (Figure 4.4.1.2) of 11.97%, which leads to the requirement of very high intensity incident light to enable detection of fluorescence and a subsequently low signal:noise ratio. Analysis of the predicted structure of RbgA (Figure 4.2.1.1) revealed that the native cysteine 277 residue is buried within the domain interface, which may account for the low labelling efficiency, and indeed this residue was confirmed to be buried upon the release of crystallographic structures of RbgA from *S. aureus* (Pausch *et al.*, 2018). Attempts were made to undertake the labelling reaction anaerobically (Winther and Thorpe, 2014) to increase the efficiency of the maleimide conjugation and also following protein unfolding to expose the residue, although following conjugation the RbgA protein was unable to re-fold correctly, suggesting that the Atto488 fluorophore was disrupting a crucial interface. Introducing a novel, exposed cysteine residue may be the best way to improve signal intensity through preferential labelling. Furthermore, the low degree of labelling for RbgA may affect the quality of post-labelling activity assays through dilution of the potentially inactive labelled variant with active, unlabelled protein, masking any change in activity that would be apparent in homogenous protein preparations. However due to the changes in fluorescence observed between binding conditions, we can conclude that the labelled variant is indeed functional and therefore results obtained in this section can be considered valid.

The use of the stopped-flow spectroscopy technique, while incredibly powerful, also comes with several caveats. First and foremost is that several assumptions have to be made in order to estimate kinetic parameters in any given reaction. In the case of the RbgA- and HflX-50S association, the interaction is likely to follow a two-step mechanism due to the double-exponential fitting of the observable signal. However in reality, we have no way of being able to tell whether the two observable phases are the only phases involved (i.e. other reaction phases may not alter the observed signal), and by extension whether our proposed mechanism is accurate. Secondly, the compounding

of errors in curve fitting may skew the estimated microscopic constants, which are derived by extrapolating from the linear regression analysis of the relationships between the sum and the product of k_{app1} and k_{app2} with the concentration of the 50S subunit (Bernasconi, 1976). Simply put, any slight inaccuracy in the fitting of a primary experimental curve (Figure 4.4.3.1) would impact the observed apparent rate, which would in turn affect the linear regression (Figure 4.4.3.2) and subsequent analyses. This is an important source of error, and as such one can never consider the output values as definite and instead these must be used to identify trends between samples. In this case, the observation that k_2 seems to be most dramatically affected suggests that (p)ppGpp inhibition mainly affects the second phase of association, although a numerical quantifier of this level of inhibition cannot be derived.

Furthermore, we showed using α-His immunoblotting that induction of the stringent response *in vivo* using mupirocin reduced the association of Era with the 30S ribosomal subunit. Two concentrations of mupirocin were used, 0.05 µg/ml and 60 µg/ml. The former is representative of physiological conditions mid-stringent response (Reiss *et al.*, 2012), whereas the latter was included in an attempt to amplify any signal should nothing be visible in the more relevant sample. For both concentrations of mupirocin, we observed a decrease in Era association to the 30S compared to the uninduced sample, and as such conclude that the physiological nucleotide concentrations during the stringent response (Varik *et al.*, 2017) are sufficient to inhibit ribosome association. This supports our previous observations and our hypothesis that during stringent conditions, the RA-GTPases associate less readily to immature ribosomal subunits and therefore reduce the biogenesis of 70S ribosomes.

Finally, we have shown here that the KH domain of Era is required for, but not directly responsible for stimulation of the GTPase activity of Era, in contrast to the substrate-activation model suggested by Tu *et al.* (Tu *et al.*, 2009). Instead, the presence of the 70S ribosome body is required for stimulation of GTP hydrolysis (Figure 4.6.3), and as such we hypothesise that the KH domain is responsible for binding to the target rRNA sequence and correctly positioning Era in such a way to enable nonspecific interactions with the ribosome in a similar manner to how interactions with h44 of the 30S subunit position the switch I region of RsgA into a catalytically active conformation (López-Alonso *et al.*, 2017b). We further hypothesise that the reduction in Era-30S association observed in the presence of ppGpp may be due to innate flexibility of the GTPase domain altering the nonspecific binding interface. The lack of specific GTPase domain-30S interactions would suggest that the overall domain structure of Era is rigid despite the presence of multiple domains in order to accommodate for the single point of interaction, supported by the extensive array of interdomain interactions observed in

the crystallographic structures of GMPPNP- and GDP- bound Era, which differ between nucleotide bound states (Figure 4.7) (Tu *et al.*, 2011). Currently available cryo-EM data regarding the association of Era to the 30S ribosomal subunit is low resolution (Razi *et al.*, 2019; Sharma *et al.*, 2005), with generic husks of electron density assigned to Era without much structural detail, rendering identification of specific interactions impossible. High resolution crystal structures are available (Tu *et al.*, 2011; Tu *et al.*, 2009), albeit these focus primarily on the interaction between the KH domain and the cognate binding RNA fragment in the absence of the remainder of the ribosome. Considering that the mature 30S ribosomal subunit is essential for GTPase stimulation, more detailed high resolution cryo-EM studies of the Era-30S complex would be required to identify the precise effect of ribosome association on Era which leads to this increase in activity.
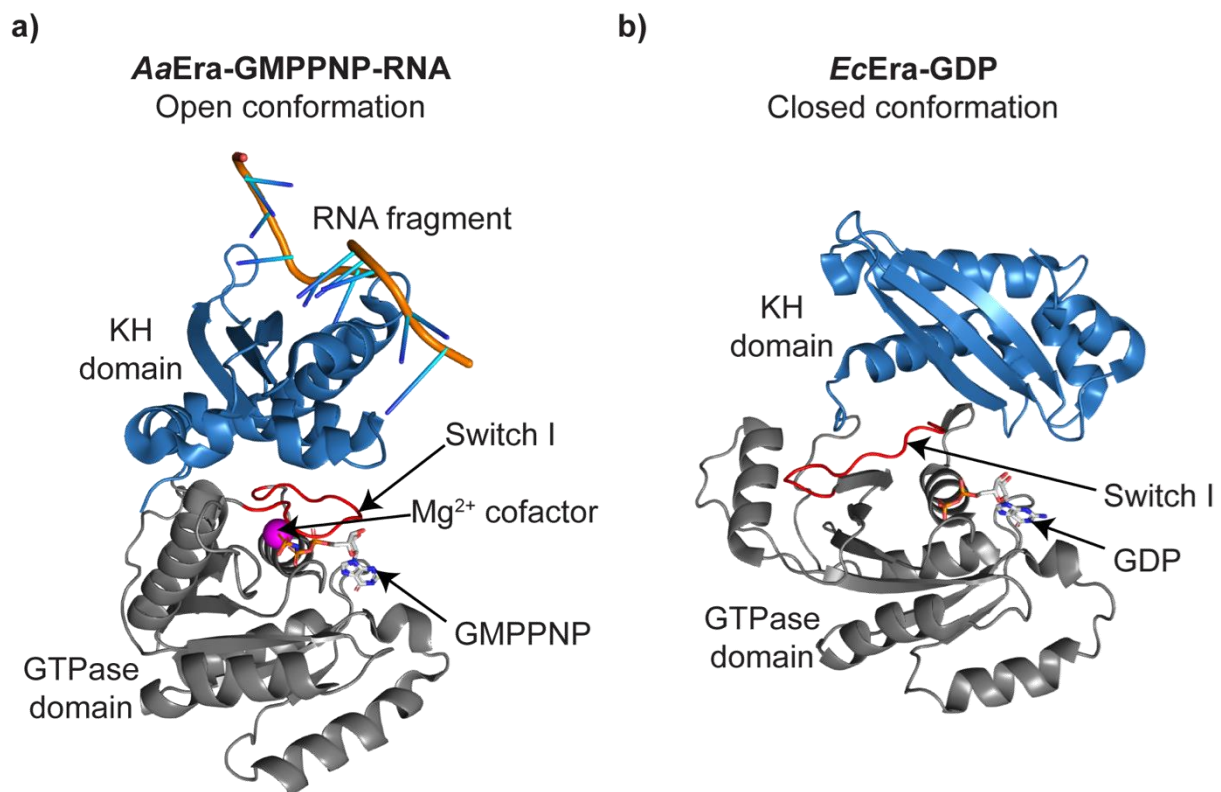
Figure 4.7: Conformational rearrangement of Era during the OFF/ON transition. Structural model of a) *A. aeolicus* Era-GMPPNP associated with the rRNA binding fragment AUCACCUCCUAA (PDB: 3IEV). The Mg^{2+} cofactor is represented by a magenta sphere, and b) *E. coli* Era-GDP (PDB: 3IEU). The GTPase domain is shown as a grey cartoon, and the rRNA-binding KH domain is shown as a blue cartoon. The associated GMPPNP/GDP ligands are shown as stick models coloured by atom as follows: carbon, white; nitrogen, blue; oxygen, red; phosphorous, orange. The Switch I loop is indicated and coloured red, note the dramatic difference between the switch I loop, the domain interface and overall domain structure of the GMPPNP-bound ON state and the GDP-bound OFF state. *Aa*Era and *Ec*Era adapted from PDB entries and 3IEV and 3IEU respectively (Tu *et al.*, 2009).

Given that the accessory domain interaction with rRNA alone is independent of nucleotide binding (Section 4.6.2), it stands to reason that the conformational change which is inhibited while bound to (p)ppGpp (Equation 3, Table 4.4.3.2) could occur within the GTPase domain. When determining this experimentally (Section 4.6.1), in hindsight we should have included a nonspecific oligoribonucleotide as a control for the specificity of KH domain binding to the target sequence. The switch I and switch II regions are well documented to be extremely flexible in canonical Ras-like GTPases, and both are known to alter conformation dependent on bound nucleotide (Hauryliuk *et al.*, 2008; Moore, 2005; Toma-Fukai and Shimizu, 2019). Furthermore, switch I forms a crucial point of interface between the GTPase domain and the ribosome (López-Alonso *et al.*, 2017b; Razi *et al.*, 2017), highlighting this region as a potential determinant of (p)ppGpp-mediated inhibition of ribosome association in RA-GTPases. In *S. aureus* RbgA, binding to pppGpp prevents proper switch I association with the main body of the protein (Pausch *et al.*, 2018), which has been proposed to inhibit hydrolysis of this alarmone by preventing coordination of the Mg^{2+} cofactor. To clarify the effect of this on ribosome association, further structural and biochemical investigations should be undertaken.

A recurring point of consideration during this chapter is the use of mature ribosomal subunits, as opposed to the immature assembly intermediates to which RA-GTPases would often bind *in situ*. In the case of all known ribosome assembly GTPases, including RsgA, RbgA, Era and HflX, binding is observed to the immature subunit, and GTPase activity is triggered when the correct maturation state is reached, enabling entry into the GDP-bound OFF state and dissociation. Here, we use exclusively mature subunits. This highlights the importance of using GMPPNP in all lengthy association experiments to prevent GTP hydrolysis, as was observed during the 16 hr ultracentrifugation steps in this chapter (Figure 4.3). The *in trans* provision of a GTPase-catalytic factor from the ribosomal subunits (López-Alonso *et al.*, 2017b; Pausch *et al.*, 2018; Verstraeten *et al.*, 2011) suggests that the major method of interaction remains identical to both the immature and mature subunits, with the difference being the nonspecific interface between the GTPase domain and the ribosome, and indeed association experiments have been done previously with mature subunits (Achila *et al.*, 2012; Razi *et al.*, 2019; Sharma and Woodson, 2020). This suggests that the association analyses carried out above are relevant. During the stopped-flow experiments in this chapter, the ribosomal subunits used were purified from *E. coli*, whereas the Atto488-labelled proteins were from *S. aureus*. While this may alter the rates of binding slightly, the overall mechanism should be consistent, and furthermore the binding sites for Era, RbgA and HflX are all in highly conserved regions of 16S or 25S rRNA which form the intersubunit interface or the peptidyltransferase centre (Dey *et al.*, 2018; Doris *et al.*, 2015; Tu *et al.*, 2009). In order to account for this, all experiments should be repeated using ribosomal subunits

purified from *S. aureus*, and also from Δ*RA-gtpase* strains of *S. aureus* to provide physiologically relevant immature ribosomal subunits (Achila *et al.*, 2012; Gulati *et al.*, 2014; Razi *et al.*, 2019). Until these have been carried out, values derived from the kinetics of RA-GTPase association with *E. coli* subunits should not be quoted as fact and should instead be interpreted as a general reflection of the mechanism of association.

In conclusion, here we have biochemically characterised the interactions between RA-GTPases and the ribosomal subunits, specifically in different nucleotide-bound states, using α-His immunoblotting and stopped-flow fluorometry. We propose that while in the GTP-bound ON state, RA-GTPases are capable of association with the ribosomal subunits via a two-step binding mechanism in order to monitor the maturation and enable 70S biogenesis. However, in the (p)ppGpp-bound state, stable RA-GTPase-subunit complex formation is inhibited, promoting RA-GTPase dissociation and therefore a reduction in 70S biogenesis under conditions of stress. In both the ON and OFF state, we propose that the rRNA binding domains remain fully functional independent of the bound nucleotide, and that governance of the ribosome binding potential is achieved solely by steric inhibition provided by the varied positioning of the switch I loop.

Chapter 5 – Structural insights into the mechanism of (p)ppGpp-mediated inhibition of RsgA association to the ribosome.

5.1 Introduction

GTPases play a crucial role in regulation of myriad cellular processes in all domains of life (Wuichet and Søgaard-Andersen, 2014), and members of the GTPase superfamily can be traced back to the last universal common ancestor (LUCA) of all forms of life (Leipe *et al.*, 2002). The majority of ancestral GTPases were involved in translation and elongation, and these have since diversified to occupy roles in signalling pathways, transport and protein trafficking (Leipe *et al.*, 2002). There exist many different folds known to bind and hydrolyse nucleotides, including but not limited to the protein kinase fold (McClendon *et al.*, 2014), histidine kinase folds (Dago *et al.*, 2012), the Rossmann fold (Laurino *et al.*, 2016) and the P-loop NTPase fold (Romero Romero *et al.*, 2018), however proteins that bind to and hydrolyse GTP are exclusively members of the P-loop NTPase superfamily (Freymann *et al.*, 1997; Leipe *et al.*, 2002; Wuichet and Søgaard-Andersen, 2014), containing the same highly conserved sequence motifs which facilitate recognition and hydrolysis of GTP (Bennison *et al.*, 2019; Verstraeten *et al.*, 2011). Throughout the course of evolution, these GTPases have diverged to become more specialised, with altered ligand affinity, reaction rates and target specificity, while retaining the same general fold. The structure-function relationship between GTPases is the topic of ongoing research (Najmanovich, 2017).

The stringent response alarmones (p)ppGpp are known to bind to and inhibit a variety of GTPases in bacteria, including those involved in translation elongation (Mitkevich *et al.*, 2010; Rojas *et al.*, 1984), DNA replication (Maciag *et al.*, 2010; Rymer *et al.*, 2012) and ribosome assembly (Corrigan *et al.*, 2016). However, not all proteins involved in these processes are capable of binding (p)ppGpp, and the precise determinant of this binding capability is unknown. Previously solved structures of GTP binding proteins in the (p)ppGpp-bound state have revealed two major modes of binding (Fig 5.1). The structures of the *S. aureus* DNA primase DnaG and the RA-GTPase RbgA demonstrate (p)ppGpp binding in an 'open' conformation (Pausch *et al.*, 2018; Rymer *et al.*, 2012), in which the 3' and 5' phosphate moieties are distally oriented, whereas the structure of the *E. coli* GTPases BipA and ObgE bound to (p)ppGpp demonstrate a 'closed' conformation in which the 3' and 5' phosphates form a ring (Buglino *et al.*, 2002; Fan *et al.*, 2015; Kumar *et al.*, 2015). The purpose of this difference in binding conformation is currently unknown, save potentially for enabling a greater variety of proteins to accommodate (p)ppGpp in their nucleotide binding sites. The difference in binding mechanic between

different proteins such as BipA and DnaG, as well as ObgE and RbgA, suggests convergent evolution of (p)ppGpp binding downstream of the evolutionary separation and specialisation individual GTPases.

Comparisons between the crystallographic structures of the GTP-bound ON state of RbgA and the GDP-bound OFF state suggests no interdomain conformational change in the case of RbgA, although there is slight rearrangement in the flexible switch I and switch II regions within the GTPase domain (Pausch *et al.*, 2018). The RA-GTPase Era exhibits large-scale conformational changes in domain configuration depending on the nucleotide bound (Tu *et al.*, 2009). Both proteins exhibit structural rearrangements of the switch I region into active conformations while in the ON state, and in the case of RbgA it has been proposed that correct arrangement of this loop is prevented by the 3'-diphosphate moiety of pppGpp (Pausch *et al.*, 2018), providing rationale for the inability of RA-GTPases to hydrolyse (p)ppGpp. It is possible that the switch I loop of Era, which is located at the domain interface, also facilitates this interaction. Upon entry into the ON state, this loop rearranges to completely remodel the domain interface (Tu *et al.*, 2009), altering protein conformation. While this could be a contributing factor to the reduced ribosome association in the OFF and (p)ppGpp-bound states in Era, the lack of overall domain reorganisation in RbgA argues against this as a general model. In order to further understand the contributing factors to (p)ppGpp-mediated inhibition of ribosome association, structural studies encompassing the different nucleotide-bound states of other RA-GTPases, such as RsgA and HflX, should be carried out for a more overall perspective.

In this chapter, we carry out structural investigations via X-ray crystallography in order to better understand the mechanism of ppGpp binding by the four RA-GTPases RsgA, RbgA, Era and HflX, and any concurrent effect on protein conformation. We were unable to solve the crystal structure of RbgA, Era or HflX however, and as such the majority of what is discussed in this chapter will concern RsgA. We also carried out comparisons between the tertiary conformation of this protein and available homologues in different nucleotide-bound states, which in addition to the kinetic studies from Chapter 4 allow us to propose a mechanism by which (p)ppGpp binding inhibits the association of RA-GTPases to the ribosomal subunits.
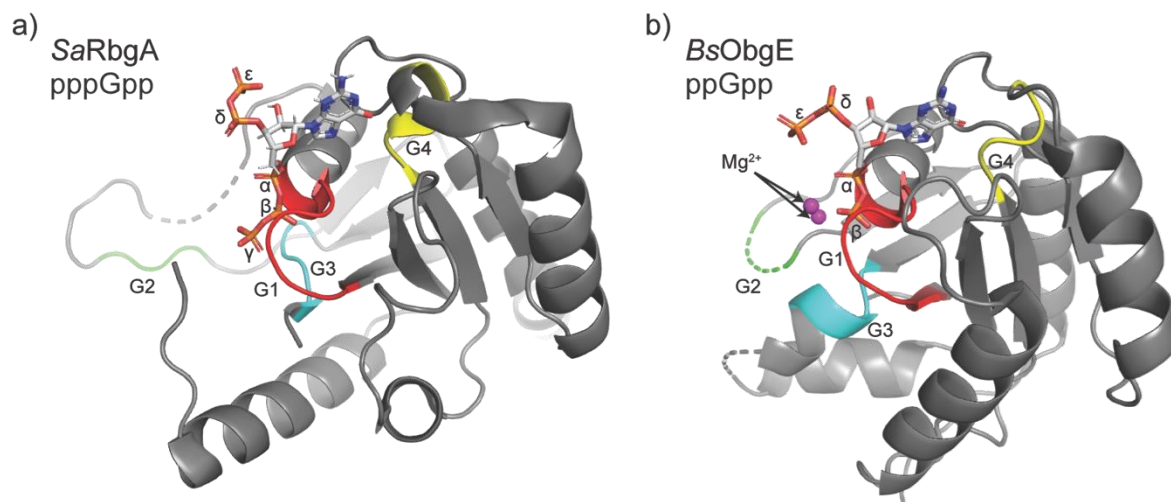
Figure 5.1: (p)ppGpp can associate with GTPases in either the 'open' or 'closed' conformation. Comparison of the GTPase domains of a) *S. aureus* RbgA bound to pppGpp (PDB: 6G15) (Pausch *et al.*, 2018) and b) *B. subtilis* ObgE bound to ppGpp (PDB: 1LNZ) (Buglino *et al.*, 2002). RbgA and ObgE shown as grey cartoon representations, with the conserved nucleotide-binding motifs coloured as follows: G1, red; G2, green; G3, cyan; G4, yellow. The associated nucleotide is represented by a stick model and coloured by atom as follows: carbon, white; nitrogen, blue; oxygen, red; phosphorous, orange. Where present, bound Mg^{2+} cofactors are indicated in magenta. Note the position and orientation of the 3'-diphosphate (constituting the δ- and ε-phosphate).

5.2 High-throughput screening for RsgA crystallisation conditions

Macromolecular crystallography is a remarkably complex physical phenomenon, and one that we understand very little about. The major tangible barrier when carrying out X-ray crystallography is the initial attainment of useful crystals, however the lack of understanding regarding the specifics of what drives crystallography renders this a largely empirical process. Numerous physiochemical conditions are thought to affect crystallisation, including pH, ionic strength, protein concentration and many more. At the upper limits of protein solubility, there is a fine line between the disordered precipitation of the solute and stable solution, and it is this intercept between the two that is exploited to encourage crystal growth (McPherson and Gavira, 2014). By generating a supersaturated solution, we can begin to exploit slow, diffusion driven increase in the concentrations of solvent constituents in order to gradually decrease protein solubility, encouraging slow precipitation which may result in the highly ordered nucleation of proteins to form crystals.

There are three major techniques employed when attempting to grow crystals, each using the same principle of salting-out soluble proteins, and each with different advantages. The most common approach is vapour diffusion, in which the protein solution is kept separate from a buffer reservoir containing a higher concentration of precipitants and salts in a closed environment, enabling gradual equilibration of the two liquid phases. This gentle equilibration allows for the formation of larger, more well-ordered crystals. (Benvenuti and Mangani, 2007). There are two comparable methods of

vapour diffusion commonly used, namely hanging drop and sitting drop, which differ only in their arrangement. The second major method of crystallisation is microbatching, in which protein droplets are suspended in mineral oil so as to prevent evaporation. Over time, stochastic nucleation within these droplets can result in crystal formation. This method is useful when working with extremely limited volumes of protein solution, as volumes in the low microlitre range have been used successfully (Brumshtein *et al.*, 2008). Finally, microdialysis can also be used to enable the slightly more rapid alteration of buffer constituents between a reservoir and protein droplet separated by a semi-permeable membrane, enabling crystallisation in a similar manner to the vapour diffusion methods (Russo Krauss *et al.*, 2013). Nowadays, advancements in microfluidics handling robots have rendered microbatching near obsolete, and the full automation of vapour diffusion methods have led to these being the favoured approach, often using protein droplets with volumes as low as 100 nl. In this chapter, we employ sitting-drop vapour diffusion (Figure 5.2a) in an attempt to obtain high-quality crystals of RsgA, RbgA, Era and HflX in different nucleotide bound states, although only RsgA was successfully crystallised. Therefore, from this point onwards, this chapter will relate to RsgA.

In order to achieve this state of supersaturation, the initial protein solution should be of a very high concentration, tending towards the solubility limit under the buffer conditions used. Therefore, purification of hexhistidine-tagged RA-GTPases was carried out using IMAC as described in Chapter 3.2, with the exception that a minimal purification buffer was used containing 25 mM Tris pH 7.5 and 150 mM NaCl. The concentration of salts was kept as low as possible during this step (while still enabling high solubility) for two reasons, firstly that salts have a tendency to crystallise and give false positives, and secondly that the salt would augment precipitant conditions within the crystallisation buffer. Post purification, proteins were concentrated by centrifugal filtration until a near maximum concentration was acquired (Figure 5.2b), which in the case of RsgA in the aforementioned buffer was calculated to be 1179 µM using A_{280}. Crystallisation was attempted in the GMPPNP- and ppGpp-bound states, with the nucleotide and $MgCl_2$ binding cofactor included in excess in the protein solution.

Although not much is understood regarding specific physiochemical factors which drive crystallisation, systematic screens have been developed which include a variety of pH ranges, precipitants and ionic concentrations to give as broad a spectrum of trial as possible. In the case of RsgA crystallisation, we used three common systematic screens: the PACT premier anion/cation crystallisation trial (Newman *et al.*, 2005), the ProPlex targeted sparse matrix screen (Radaev *et al.*, 2006) and the JCSG+ optimised PEG sparse matrix screen (McPherson, 2001; Page *et al.*, 2003). With each coming in a 96-well format for a combined 288 conditions, this represents a powerful shotgun approach to crystallisation. Screens

were set up using RsgA at 973 µM, with 2 mM nucleotide and 2 mM MgCl$_2$ using a Mosquito liquid handling robot (SPT Labtech). 200 nl droplets containing 100 nl protein solution and 100 nl screening buffer were set up adjacent to a 50 µl reservoir of screening buffer (Figure 5.2a), and the 96 well plates were sealed and incubated at 19°C, with crystals forming after approximately 2 weeks for both the GMPPNP and ppGpp-containing screens, a selection of which are shown in Figure 5.2c. Rod shaped crystals formed in both conditions (Figure 5.2c, left, centre panel), with additional needle clusters forming in the ppGpp-bound state (Figure 5.2c, right panel). In total, crystals were recovered from the following wells: For RsgA + GMPPNP, PACT premier F11, PACT premier E11 and ProPlex B10; For RsgA + ppGpp, PACT premier E11 and PACT premier F11. Note that following diffraction analysis and the acquirement of electron density maps, none of the crystals were found to contain RsgA in the GMPPNP-bound state. Specific details of the screening composition of the aforementioned wells are given in Table 5.2. Crystals were flash frozen in screening buffer containing 15% ethylene glycol as a cryoprotectant, and stored under liquid nitrogen in preparation for diffraction analysis.
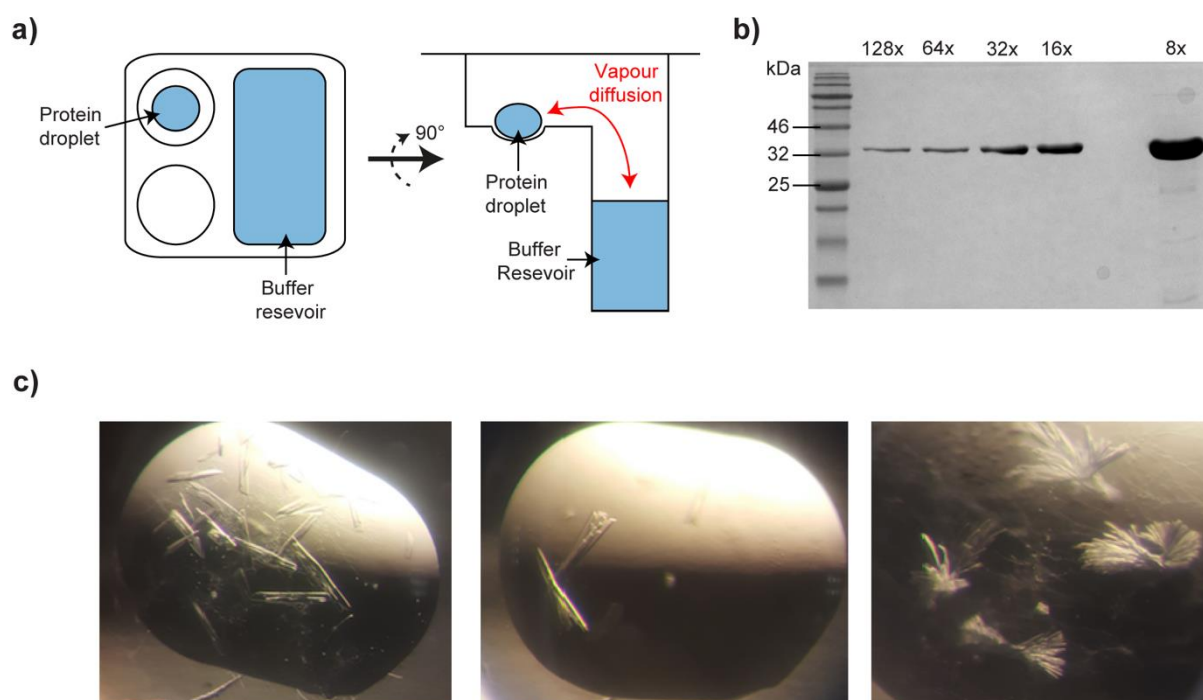
Figure 5.2: Crystallisation of RsgA using systematic PACT, ProPlex and JCSG+ screens. a) Schematic representation of the sitting-drop method of vapour diffusion, showing one of the 96 sealed wells present on a standard plate. The 200 nl protein droplet containing 50% protein solution and 50% screening buffer sits in a small well, adjacent to a 50 µl screening buffer reservoir. Vapour diffusion between the two liquid droplets (represented by a red arrow) will increase the concentration of protein and precipitants in the protein droplet, encouraging nucleation. b) SDS-PAGE analysis of the RsgA sample to be used in crystallisation trials post-IMAC and dialysis. Serial dilutions starting at an 8-fold dilution (indicated) from neat 1179 µM solutions were loaded on a 12% polyacrylamide gel for SDS-PAGE to assess the purity of the preparation. SDS-PAGE gels were stained using Coomassie Brilliant Blue as detailed in the methods section. c) Photographs of RsgA crystal morphology within the 200 nl protein droplet of the following screening conditions: left: irregular rod-shaped crystals from RsgA + ppGpp in PACT premier F11; centre: clustered rods from RsgA + GMPPNP in PACT premier F11; right:

clustered needles from RsgA + ppGpp in PACT premier E11. Photographs were taken through a light microscope with 60x magnification. For specific conditions within the screening conditions mentioned see Table 5.2.

Table 5.2: Crystallisation conditions of RsgA in the apo, GDP-bound and ppGpp-bound state

RsgA state	Screening Condition	Buffer Conditions	Comments	Actual Bound Nucleotide
RsgA + GMPPNP	ProPlex B10	0.15 M $(NH_4)_2SO_4$, 0.1 M MES pH 6.0, 15% PEG 4000	Single rod-shaped crystal	Apo
	PACT premier E11	0.20 M sodium citrate tribasic dihydrate, 20% PEG 3350	Clusters of fine needle-shaped crystals	GDP
	PACT premier F11	0.20 M sodium citrate tribasic dihydrate, 0.10 M bis-tris propane pH 6.5 20% PEG 3350	Clusters of rod-shaped crystals	GDP
RsgA + ppGpp	PACT premier E11	0.20 M sodium citrate tribasic dihydrate, 20% PEG 3350	Clusters of fine needle-shaped crystals	ppGpp
	PACT premier F11	0.20 M sodium citrate tribasic dihydrate, 0.10 M bis-tris propane pH 6.5 20% PEG 3350	Clusters of rod-shaped crystals	ppGpp

RsgA state refers to the ligand included in the initial crystallographic screening solution. Actual Bound Nucleotide refers to the bound state of RsgA in the crystal matrix. Given well corresponds to the intended well location as described by the commercial crystal screen. PEG percentages given in w/v.

5.3 Diffraction analysis and structural modelling of ppGpp-bound, apo and GDP-bound RsgA

When cooled to liquid nitrogen temperatures or below, protein crystals become much more resistant to damage imparted by prolonged exposure to high-intensity X-ray radiation (Henderson, 1990), and therefore the quality of diffraction data obtained is massively improved. This has led to the use of particle accelerators known as synchrotrons, which use magnets to accelerate electrons close to the speed of light. Electrostatic manipulation of these electrons as they circulate a pentacontagonal storage ring leads to the emission of electromagnetic radiation, including X-rays of extremely high brilliance. Three rod-shaped crystals were analysed using X-ray radiation of wavelength 0.97949 Å, two from GMPPNP-containing conditions (PACT F11 and ProPlex B10), and one from ppGpp-containing conditions (PACT F11). Regarding diffraction, multiple crystals in the sample can lead to overlapping of diffraction patterns and difficulty during initial phasing and molecular replacement. Therefore the rods were separated and the most high-quality individual crystal from each well was used during analysis. The clustered needles from PACT E11 (Figure 5.2c, right panel) were extremely fragile and shattered when trying to separate them, and as such could not be analysed.

Electron density maps were generated by analysis of the X-ray diffraction patterns using the Xia2 pipeline integrated into the systems of the UK national synchrotron facility (Winter, 2010), using

molecular replacement (McCoy *et al.*, 2007), as described in the methods section. The first crystal to be solved, namely the ppGpp PACT F11 condition, diffracted to 1.94 Å and was solved using an existing structure of the RsgA homologue YloQ from *B. subtilis* (PDB: 1T9H) (Levdikov *et al.*, 2004), which exhibits a 43.6% sequence similarity to the *S. aureus* homologue . The crystal was found to belong to the space group $P2_12_12_1$, containing one RsgA monomer per asymmetric unit (Table 5.3). Following molecular replacement and iterative maximum-likelihood refinement (Emsley *et al.*, 2010; Murshudov *et al.*, 1997) to generate a well-fitted RsgA model, it became apparent that there was a region of electron density unaccounted for within the ligand binding site of RsgA. Different guanine nucleotides were considered, and the region was assigned to ppGpp due to the unambiguous presence of electron density in the expected position of the 3'-diphosphate (Figure 5.3a). Similarly to the previously solved DnaG and RbgA (Pausch *et al.*, 2018; Rymer *et al.*, 2012), RsgA appears to bind ppGpp in the 'open' conformation, in which the 3'- and 5'-diphosphate moieties extend outwards in a distal manner.

The crystal from ProPlex B10 that formed under GMPPNP-containing conditions was the next to be processed, in a similar manner with the exception that the RsgA-ppGpp structure with ligands removed was used as a template for molecular replacement. This crystal diffracted to 2.01 Å, and was found to belong to the $P12_11$ space group, with two monomers per asymmetric unit (Table 5.3). Following construction of the RsgA backbone, there was found to be no electron density corresponding to a bound nucleotide in the ligand binding site of either monomer (Figure 5.3b). Therefore, this structure was allocated as apo. Finally, the crystal from the GMPPNP-containing solution PACT F11 condition was processed in an identical manner to the ProPlex B10 crystal, and was found to diffract to 2.15 Å and belong to the $P2_12_12_1$ space group, with a single monomer in the asymmetric unit (Table 5.3). Following modelling of the backbone, there was found to be electron density corresponding to GDP in the ligand binding site, lacking density for the 3'-diphosphate and 5'-γ-phosphate (Figure 5.3c), and as such could not be allocated to GMPPNP. The fact that no exogenous GDP was added to the crystallisation solution raises concerns regarding the nucleotide-bound state of purified proteins, as GDP must have already been present in the RsgA nucleotide binding site in this instance.

In each of the three structures, consistent with previously solved structures of RsgA in the absence of the 30S subunit (PDB: 1T9H, PDB: 2YV5) (Levdikov *et al.*, 2004), density for the switch I region remains unresolved between residues 179-201 in the apo structure 181-201 in the GDP-bound structure and 180 and 201 in the ppGpp-bound structure, and is therefore omitted from the model. Altogether, we

have solved the structures of *S. aureus* RsgA in the ppGpp-bound (PDB: 6ZHL), apo (PDB: 6ZJO) and GDP-bound (PDB: 6ZHM) (Figure 5.3d-f) to 1.94 Å, 2.01 Å and 2.15 Å resolution respectively.
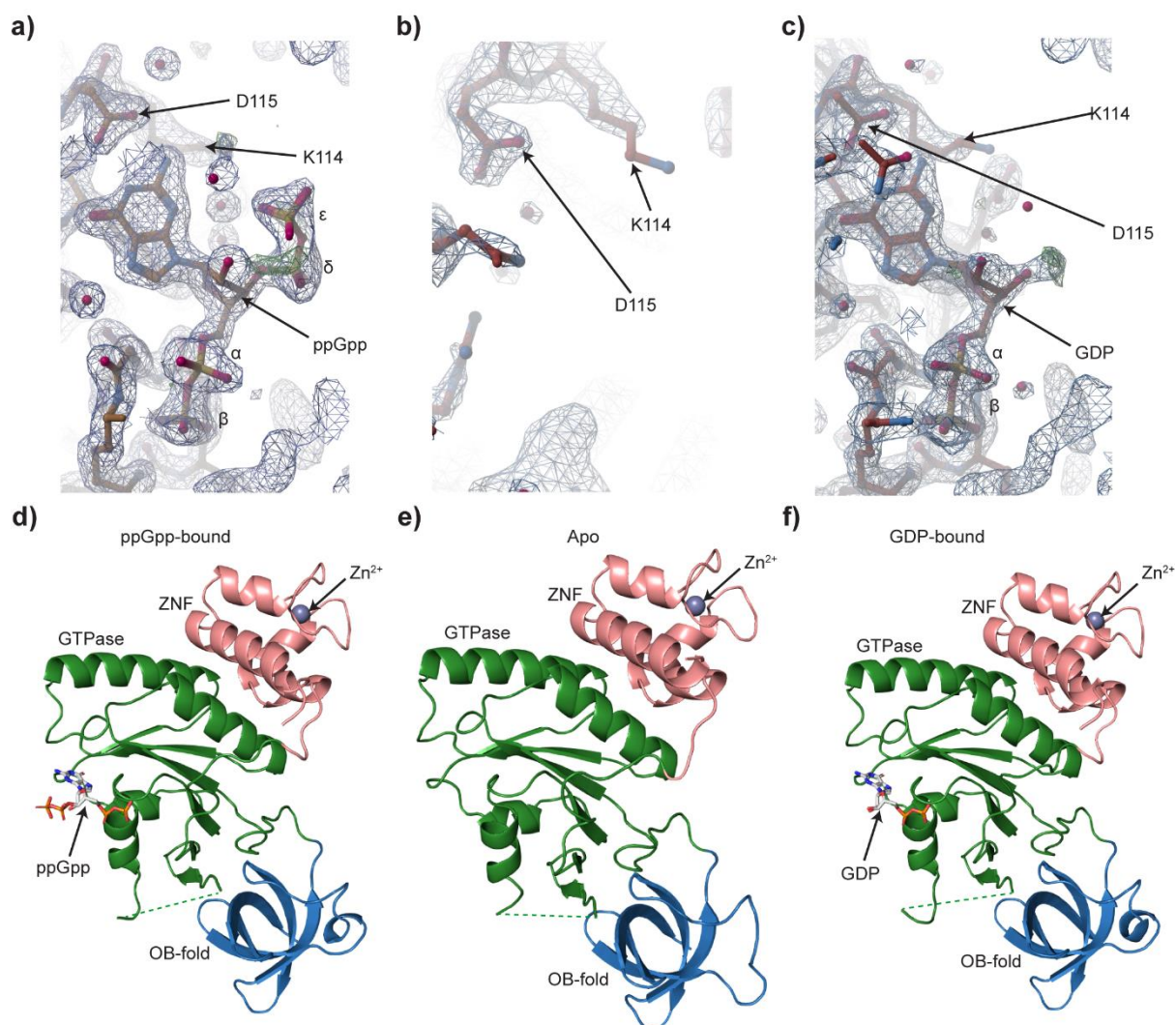
Figure 5.3: The structure of *S. aureus* RsgA in the ppGpp-bound, apo and GDP-bound states. a-c) Localised Fo-Fc/2Fo-Fc omit map (blue/red/green mesh) of the nucleotide binding site of a) ppGpp-bound, b) apo and c) GDP-bound RsgA overlaid with stick models of the bound nucleotide if present and the protein structure. Atoms coloured as follows: carbon, yellow; nitrogen, blue; oxygen, red; phosphorous, yellow. Note the clear electron density due to the presence of a 3'-diphosphate in the ppGpp-bound model (a), which is lacking in the GDP-bound model (c). Notable residues and the nucleotide phosphates are indicated. The Fo-Fc maps for (a), (b) and (c) are contoured to 3.1 σ, 3.1 σ and 4.1 σ respectively, and the 2Fo-Fc maps are contoured to 1.6 σ, 1.6 σ and 1.9 σ respectively. Unmodelled regions of electron density around the periphery relate to adjacent monomers and have not been included for clarity. (d-f) The ray-trace models of a) ppGpp-bound, b) apo and c) GDP-bound RsgA to 1.94 Å, 2.01 Å and 2.15 Å respectively. Domains are coloured as follows: OB-fold, blue; GTPase domain, green; ZNF, red. The Zn^{2+} cofactor is represented by a grey sphere, and the bound nucleotide is represented by a stick model coloured by atom as follows: carbon, white; nitrogen, blue; oxygen, red; phosphorous, orange. Note the absence of the switch I region, indicated by a green dashed line.

Table 5.3: Crystallographic data and refinement statistics.

	RsgA Apo (PDB: 6ZJO)	RsgA-GDP (PDB: 6ZHM)	RsgA-ppGpp (PDB: 6ZHL)
Crystal data			
Space Group	P 1 2$_1$ 1	P 2$_1$ 2$_1$ 2$_1$	P 2$_1$ 2$_1$ 2$_1$
Unit Cell Dimensions (a, b, c (Å))	54.67 93.53 68.18	50.24 66.97 113.36	50.47 66.93 114.12
Unit Cell Dimensions (α, β, γ (°))	90.00 90.72 90.00	90.00 90.00 90.00	90.00 90.00 90.00
Data Collection			
Wavelength (Å)	0.97949	0.97949	0.97949
Resolution (Å)	47.20-2.01	101.94-2.15	57.73-1.94
	(2.06-2.01)	(2.26-2.15)	(1.99-1.94)
Reflections (measured/unique)	306,023	239,084	375,925
R_{meas} (%)	0.149 (0.895)	0.282 (2.320)	0.165 (0.990)
$R_{p.i.m.}$ (%)	0.057 (0.336)	0.109 (0.909)	0.063 (0.381)
$<I/\sigma I>$	8.4 (1.8)	5.5 (1.0)	11.0 (2.5)
Multiplicity	6.8 (7.0)	6.4 (6.1)	12.8 (12.7)
Completeness (%)	98.2 (97.0)	99.9 (99.6)	99.9 (99.5)
Refinement Statistics			
R_{work}/R_{free} (%)	22.41/27.83	24.00/27.27	21.63/26.22
Average B factor (Å^2) protein	38.423	40.11	29.398
Average B factor (Å^2) solvent	42.832	43.03	34.955
Rmsd bond lengths (Å)	0.0083	0.0115	0.0096
Rmsd bond angle (°)	1.5890	1.890	1.8108
Protein residues	533	269	268
Water molecules	212	111	81
Ions	5	1	1
Ramachandran (Favoured/Generous/Disallowed)	494/27/4	253/8/4	255/7/1

Outer shell data in parenthesis. $R_{work} = \frac{\Sigma||F_{obs}|-|F_{calc}||}{\Sigma|F_{obs}|}$, where F_{obs} and F_{calc} are the observed and calculated factorial amplitudes of the structure respectively. R_{free} is calculated as above, except for a random subsection of data that was withheld from refinement. Ramachandran plot calculated within *Coot*. B factors calculated using $B_{average}$ within the CCP4 suite. Refinement statistics were read from the output log following crystallographic refinement via RefMac5 within the CCP4 suite (Emsley *et al.*, 2010; Murshudov *et al.*, 1997).

5.3 Analysis of the apo, GDP-bound and ppGpp-bound structure of RsgA

RsgA is a highly conserved protein, which functions as a ribosome assembly checkpoint in order to ensure correct processing of the 30S decoding centre, in particular leading to RbfA dissociation and subsequent docking of h44 onto the main body of the 30S (López-Alonso *et al.*, 2017b). Binding of this protein to the target site (Figure 5.4a) on the 30S subunit is facilitated by two accessory domains, which provide strong, specific electrostatic interactions with the target rRNA. The N-terminal oligonucleotide/oligosaccharide binding (OB)-fold domain is situated between h18 and h44 of the 16S rRNA, the C-terminal Zn^{2+}-finger domain (ZNF) contacts the 30S head between h29 and h30, and the GTPase domain exhibits weak electrostatic interactions with between h24, h44 and h45 (Figure 5.4b) (López-Alonso *et al.*, 2017b).
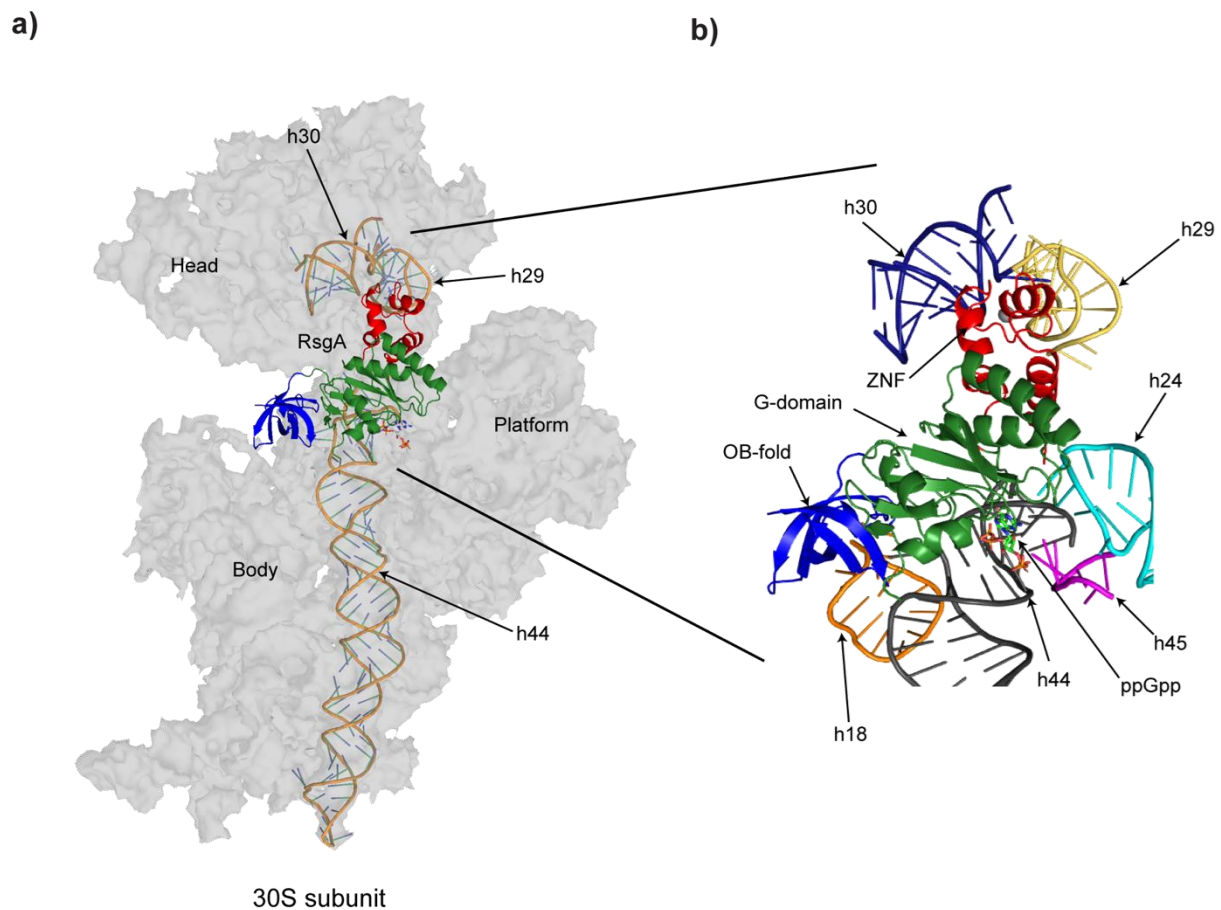
Figure 5.4: The RsgA binding site on the 30S. a) *S. aureus* ppGpp-bound RsgA (PDB: 6ZHL, this study) computationally docked onto the *E. coli* 30S subunit (PBD: 5ZU4, chain A) (Razi *et al.*, 2017) using Cα alignment with the bound YjeQ-GMPPNP (PDB: 5ZU4, chain Z). The RsgA monomer is represented by a cartoon, with the OB-fold, GTPase domain and ZNF coloured blue, green and red respectively. Bound ppGpp is represented by a stick model and coloured as follows: carbon, white; nitrogen, blue; oxygen, red; phosphorous, orange. Major interacting rRNA helices are labelled, and the 30S head, platform and body are indicated. b) Zoomed perspective of the 16S rRNA helices which constitute the RsgA binding site. Target rRNA helices are coloured as follows: h24, cyan; h18, orange; h29, yellow; h30, navy blue; h44, grey; h45, magenta.

5.4.1 The domain structure of RsgA

5.4.1.1 The N-terminal OB-fold domain

RsgA and homologues are well known to consist of three domains, the N-terminal OB-fold, the central GTPase domain and the C-terminal ZNF (Guo *et al.*, 2011; Levdikov *et al.*, 2004). Our structures agree with this model. The 63 residue N-terminal domain (Figure 5.4.1.1a) consists of five antiparallel β-strands, arranged into a β-barrel and capped with a small α-helix in accordance with the archetypal OB-fold domains (Flynn and Zou, 2010). The interstrand linker loops in the case of RsgA appear to be relatively short, as most OB-fold domains consist of between 70 and 150 residues with the majority of variation attributed to loop heterogeneity (Murzin, 1993). Ligand binding interactions are thought to occur via the loop connecting β_3 and β_4 as well as residues towards the N-terminus of β_5, with this interface containing many hydrophilic and basic residues (Figure 5.4.1.1b), the latter of which, namely $_{32}$RKKK$_{35}$, may electrostatically interact with the negatively charged backbone of rRNA. Note that structural order of the side chain corresponding to K34 was lacking, and as such it is omitted from Figure 5.4.1.1b below due to low electron density, although this residue represents another basic residue in the proposed interaction region. Interestingly, the β_3-β_4 loop had the largest B-factor of all three models, indicating a high degree of flexibility. The barrel structure appears to be stabilised between β_4 and β_5 by electrostatic bridging between the carboxyl group of D42 and guanidinium group of R62, which appears conserved between the *S. aureus* RsgA structure here and previously determined *E. coli* YjeQ and *B. subtilis* YloQ (Levdikov *et al.*, 2004; López-Alonso *et al.*, 2017b; Razi *et al.*, 2017) (Figure 5.4.1.1a). A further stabilising element is the well-defined kink in β_1 facilitated by the innate Ramachandran flexibility of the glycine residue at position 4, which enables packing against both β_2 and β_4 in a manner common amongst OB-fold domains.
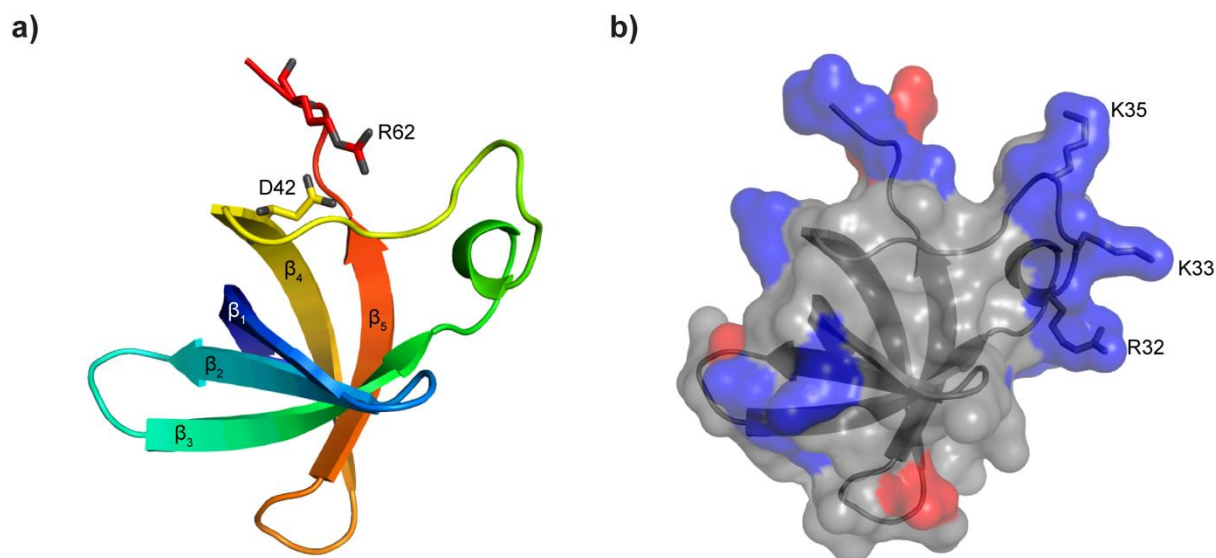
Figure 5.4.1.1: Structure of the N-terminal OB-fold domain of *S. aureus* RsgA. a) Cartoon representation of the OB-fold domain. Domain is coloured as a spectrum from the N-terminus (blue) to the C-terminus (red), with secondary structures β_{1-5} labelled. The two residues responsible for the stabilising electrostatic interaction, D42 and R62 are also indicated using stick modelling. b) Surface view of the OB-fold domain, with basic areas coloured blue and acidic areas coloured red. The general structure of the domain is represented by a grey cartoon in an identical configuration to part (a). The side chains of the basic residues at the proposed interaction surface $_{32}$RKKK$_{35}$ are represented by stick models. Structure taken from *S. aureus* RsgA in the ppGpp-bound state (PDB: 6ZHL) residues 1-63.

5.4.1.2 The GTPase domain

The central domain in RsgA is the GTPase domain, spanning residues 64-225 and responsible for guanine nucleotide binding and GTP hydrolysis (Figure 5.4.1.2a). The N-terminal OB-fold domain is connected to the GTPase domain via a β-hairpin spanning the domain interface, leading directly into the N-terminus of β_6. The core of the domain consists of a curved β-sheet made up of six individual β-strands arranged in a β_{10}-β_{11}-β_9-β_6-β_7-β_8 conformation, with β_{10} running antiparallel to the remaining five parallel strands. The curvature of the β-sheet presents two faces, the convex and concave, against which four α-helices pack in a globular fashion. α_1 and α_2 pack against the convex face, whereas α_3 and α_4 are enveloped by the concave surface, with elements from the connecting loops on the concave face forming the canonical GTP binding pocket.

The GTPase domain is highly conserved throughout all domains of life, featuring at least four conserved motifs which enable recognition, binding and hydrolysis of GTP (Verstraeten *et al.*, 2011), including the G1 ($_{164}$GQSGVGKS$_{171}$), or α/β-phosphate binding P-loop, the G2 (T199) and G3 ($_{213}$DTPG$_{217}$) which coordinate the catalytic Mg^{2+} ion required for γ-phosphate stabilisation and for generation of the pentavalent water intermediate during hydrolysis, and the G4 ($_{112}$TKKD$_{115}$) which specifically recognises guanine nucleobases via stacking between the guanine ring and

lysine/glutamine residues. The conserved aspartate is capable of differentiating between adenine and guanine bases via preferential H-bonding to the latter. The G5 motif is not conserved, with no apparent consensus. In canonical Ras-like GTPase domains, the motifs are arranged as G1-G2-G3-G4-G5. In RsgA and a small family of circularly-permuted GTPases (cpGTPases), the motif arrangement is shifted to G4-G5-G1-G2-G3, which is the only stable permutation known to date (Anand *et al.*, 2006). This permutation does not affect the spatial positioning of the GTP binding elements, which still form a surface binding pocket (Figure 5.4.1.2b), and as such these proteins bind GTP in an identical manner to canonical variants. In our models, the mechanism of binding appeared identical for both GDP and ppGpp (Figure 5.4.1.2 c, d), with the G1-G4 motifs electrostatically recognising the ligand. Noticeably, the guanidinium group of R148 interacts with the carbonyl at position 6 of the guanine ring, suggesting that R148 may constitute one residue of the previously undetermined G5 motif. The location of this residue C-terminal of the G4 motif is fitting with this proposition, given the circular permutation of the RsgA GTPase domain. In our structure there are no short-range contacts observable between the protein and the 3'-diphosphate, although in this instance there appears to be a long-range, 5.5 Å electrostatic contact between the basic K116 and the lone electron pair of the ε-phosphate of ppGpp, which extends away from the core of the protein in an open conformation (Figure 5.4.1.2ci). The position of this residue (and indeed other nucleotide-recognition motifs) remains constant whether bound to ppGpp or in the apo state (Figure 5.4.1.2cii), and as such does not seem to be involved in sensing of the 3'-diphosphate or as a facilitating or transducing nucleotide involved in (p)ppGpp-mediated inhibition of ribosome association or GTPase activity. Interestingly, this interaction would not be possible in the instance of ppGpp adopting the 'closed' conformation as in the case of BipA and ObgE (Fan *et al.*, 2015; Feng *et al.*, 2014), and as such long range interactions such as that from K116 could be a mediator of the conformation adopted by ppGpp upon binding.

Switch I and II are located within the separating loop between β_9 and β_{10}, and to the C-terminus of β_{12} respectively. In cpGTPases, the length of switch I is extended compared to the equivalent in canonical GTPase domains (Levdikov *et al.*, 2004; Pausch *et al.*, 2018), which tends to reduce the order of this region, and therefore the visibility in structural studies. In our case, the density corresponding to switch I is completely absent from residues 181-201, likely due to the innate flexibility when not contacting the γ-phosphate. Furthermore, no density which could be attributed to the Mg^{2+} ion is found in the active site. This permutation also positions the innately flexible switch II at the extreme disconnected C-terminus of the GTPase domain, which imparts the necessity of a stabilising C-terminal domain found within all cpGTPases (Anand *et al.*, 2006). In the case of RsgA, this role is fulfilled by a C-terminal rRNA-binding ZNF domain.
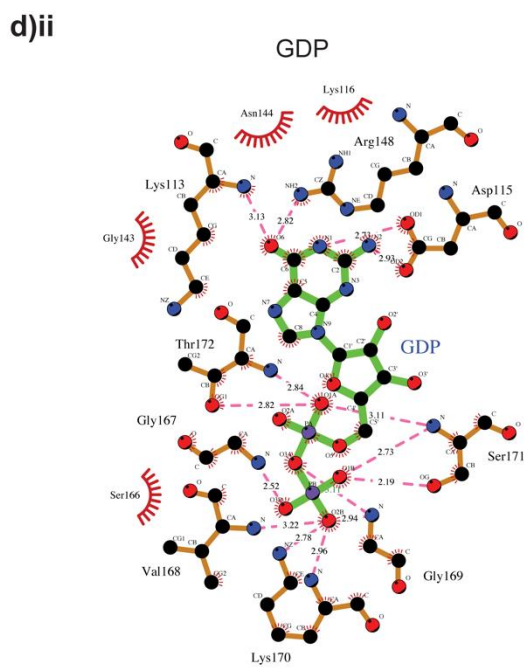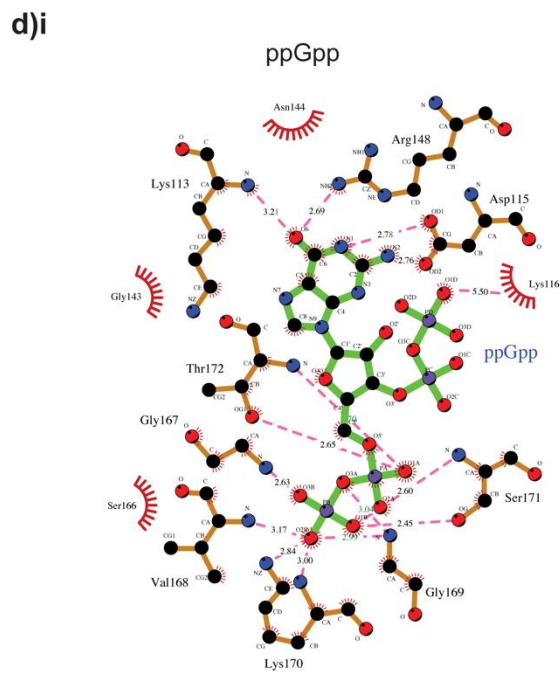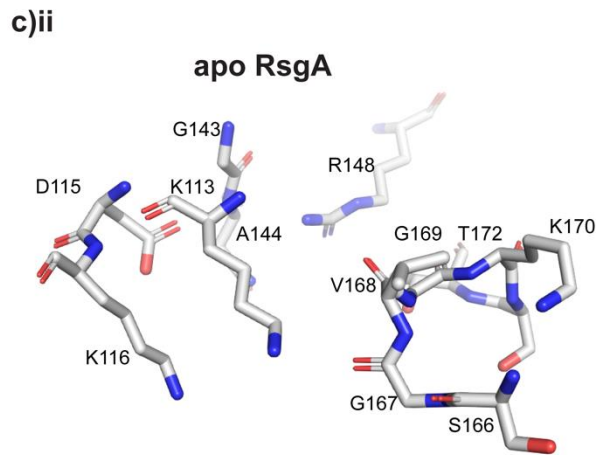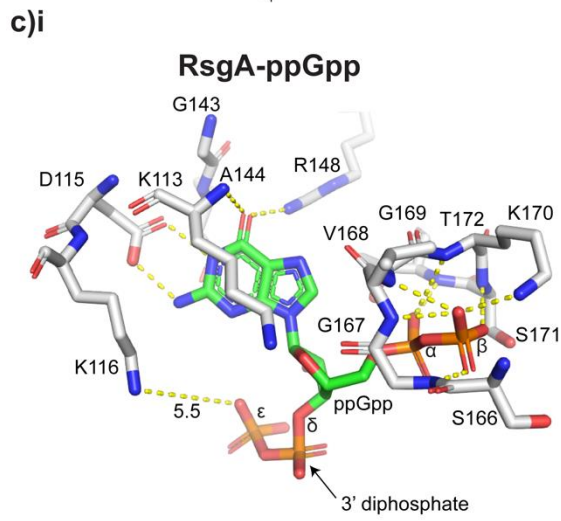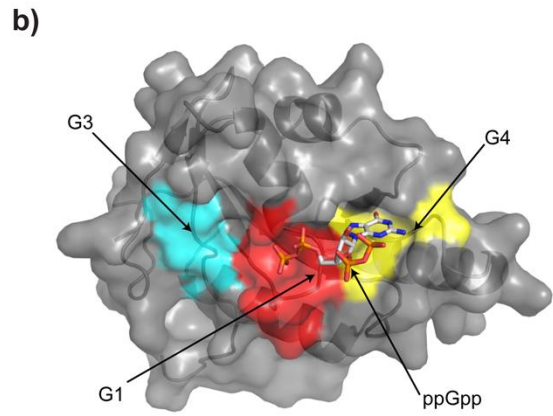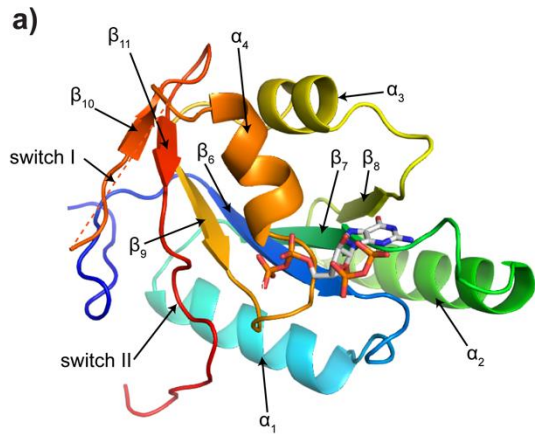
Figure 5.4.1.2: Structure of the central GTPase domain of *S. aureus* RsgA. a) Cartoon representation of the ppGpp-bound GTPase domain of *S. aureus* RsgA. This model is coloured as a spectrum from the N-terminus (blue) to the C-terminus (red), with switch I, switch II and the secondary structures α_{1-4} and β_{6-11} indicated. Switch I is represented by a dashed line. The bound ppGpp molecule is represented by a stick model coloured by atom as follows: carbon, white; nitrogen, blue; oxygen, red; phosphorous, orange. b) Surface view of the ppGpp-bound GTPase domain, with the bidning pocket formed by the G1, G3 and G4 motifs indicated in red, cyan and yellow respectively. The G2 motif is omitted due to lack of resolution in the model. The general structure of the GTPase domain is represented by a grey cartoon in the same orientation as part (a). The bound ppGpp molecule is represented as in part (a). The ppGpp-bound structure was chosen as representative of the overall domain structure and included here due to the high resolution. c) detailed view of the nucleotide binding site of RsgA in the (i) ppGpp-bound and (ii) apo state. RsgA residues are represented as sticks, with atoms coloured as follows: carbon, white; nitrogen, blue; oxygen, red. The bound ppGpp ligand is represented as a stick model with atoms coloured as above, with the exception of carbon being represented as green. Residue-nucleotide interactions are shown as yellow dashed lines, with the bond length of the long-range electrostatic interaction between K116 and the ε-phosphate of ppGpp is labelled (Å). d) LigPlot (Wallace *et al.*, 1995) maps of RsgA interactions with the bound i) ppGpp and ii) GDP substrate. Bonds within the nucleotide are represented in green, while those within the protein are represented in orange. Hydrogen bonds and electrostatic interactions are shown as pink dashed lines with their respective bond lengths indicated (Å). Protein residues are labelled and Van der Waal's contacts are represented as red curves.

5.4.1.3 The C-terminal ZNF

As mentioned above, the C-terminus of switch II is stabilised by the presence of a C-terminal ZNF, a small helical domain from residue 226-291. ZNFs are known the be extremely abundant yet structurally and functionally diverse, capable of binding to protein, nucleotides and even small ligands (Kluska *et al.*, 2017). The C-terminal domain of RsgA comprises four α-helices, with the loop connecting α_6 and α_7 coordinating a central Zn^{2+} ion to confer domain fold stability (Figure 5.4.1.3a). The tetravalent nature of Zn^{2+} requires four coordinate sites for stable binding, the nature of which forms the grouping of subclasses of ZNFs, of which the most common are the C_4 or C_2H_2 subclass indicating that coordination is achieved via four cysteine residues, or two cysteine and two histidine residues respectively (Pace and Weerapana, 2014). RsgA and related homologues constitute the sole members of the CCHC class of ZNF domains, with the central Zn^{2+} coordinated by C245, C250, H252 and C258. The Zn^{2+}-thiol bond lengths of 2.3 Å and the Zn^{2+}-amine bond length of 2.2 Å represent near ideal values, which are likely partly maintained by the structural rigidity conferred by an adjacent proline at position 256.

A grouping of solvent-exposed basic residues on the same face of RsgA as those in the OB-fold domain may be involved in binding to the rRNA phosphate backbone (Figure 5.4.1.3b), namely H225, R240, K246 and R248. Furthermore, aromatic phenylalanine residues F223, F247 and F272 project towards the solvent on this face, which are known to bind the major and minor grooves of nucleotides via insertion stacking (Baker and Grant, 2007). The disparate positioning of these residues suggests that the ZNF may bind at the interface between two or more ribosomal helices, and indeed this domain has been mapped to bind to h29 and h30 towards the head of the 30S subunit (Figure 5.4), close to

the tRNA interaction site (López-Alonso *et al.*, 2017b). Altogether, analysis of exposed aromatic and basic residues on the surface of our RsgA model enables predictions as to the binding orientation, in line with cryo-EM structures of the RsgA-30S complex (López-Alonso *et al.*, 2017b; Razi *et al.*, 2017).
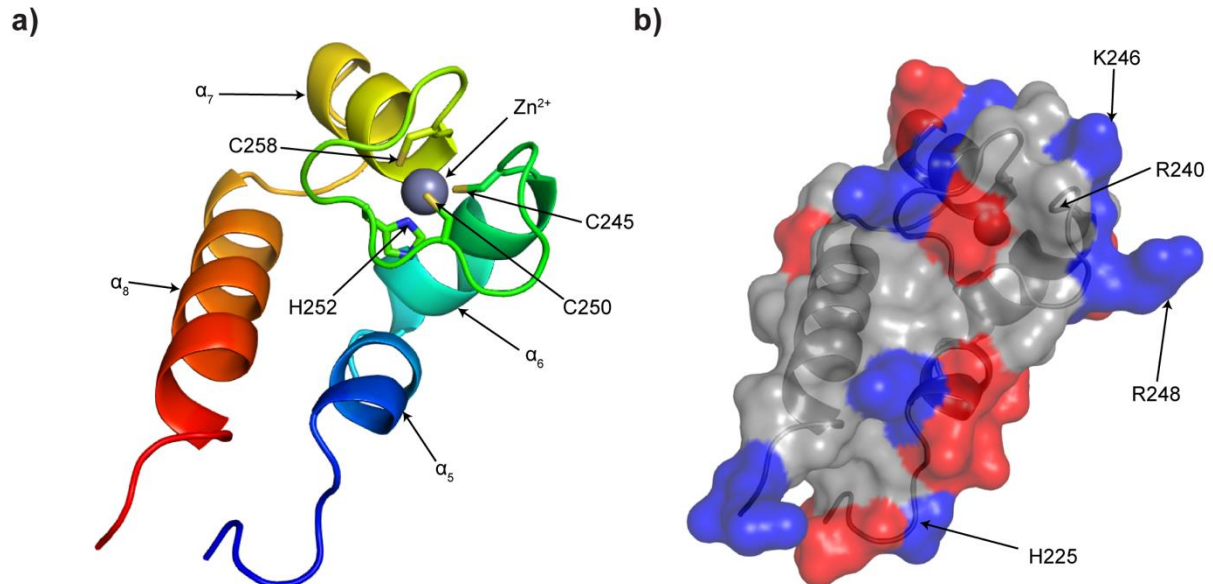
Figure 5.4.1.3: Structure of the C-terminal ZNF of *S. aureus* RsgA. a) Cartoon representation of the ZNF of *S. aureus* RsgA, coloured as a spectrum from the N-terminus (blue) to the C-terminus (red). Associated Zn^{2+} ion is shown as a grey sphere, and the side chains of the coordinate CCHC residues are represented as stick models and indicated. Secondary structures α_{5-8} are indicated. b) Surface representation of the ZNF, with basic regions coloured blue and acidic regions red. The overall structure of the ZNF is represented by a grey cartoon in the same orientation as in part (a). Key basic residues H225, R240, K246 and R248 on the interaction surface are labelled.

5.4.2 Comparison of the tertiary structure of the apo, GDP-bound and ppGpp-bound states

The ON/OFF cycling of RA-GTPases is well understood to be reliant on the nucleotide-bound state, with conformationally and functionally distinct conformations observed between the GTP-bound and GDP-bound state. In the case of Era, relative repositioning of the N-terminal and C-terminal domain alters the position of switch I into an active conformation (Tu *et al.*, 2009), remodelling not only the relative domain positioning but also the entire interdomain interface. In the case of RsgA, it has been suggested following comparison of the *E. coli* GMPPNP-bound structure with the *Salmonella typhimurium* homologue bound to GDP, that rearrangements in GTPase domain β-hairpins and the OB-fold domain close the GTP-binding pocket into an active conformation (López-Alonso *et al.*, 2017b). In order to identify the effect of ppGpp binding on the overall state of RsgA, we carried out

structural alignments between the GTPase domains of our Apo, GDP- and ppGpp-bound structures (Figure 5.4.2a, b).

To avoid skewing the alignment process due to differences between bound ligands and other monomers within the crystal matrix, such as PEGs or uncoordinated water molecules, the GTPase domain alignments were performed using backbone models with all ligands removed. Both the apo and GDP-bound GTPase domains showed an extraordinarily high similarity with the ppGpp-bound following alignment, with root-mean-square deviation (RMSD) values of 0.340 Å and 0.131 Å respectively. RMSD is the average measure of C_α displacement between superimposed proteins, and as such gives an indication of tertiary similarity. For reference, the average backbone length of an amino acid residue is reported to be between 4 Å and 10 Å (Ching *et al.*, 1989). The OB-fold domain of RsgA in the apo structure seems slightly disordered in comparison to the ppGpp-bound and GDP-bound models (Figure 5.4.2a), and upon closer inspection the electron density of this region is inconsistent in the apo electron density map. This reduction in order occurs at the binding interface of the OB-fold domain and rRNA (Figure 5.4.1.1a), which may affect ribosome association while in the apo form. An alternate hypothesis is that this difference in apparent conformation could be due to an artifact of crystallography, with the apo structure being solved from different buffer conditions to either the ppGpp-bound or GDP-bound. Despite the presence of a second RsgA monomer in the asymmetric unit, disordered loop of the OB-domain is solvent facing and as such unlikely to be influenced by monomer contacts. Alignment of the entire structure to get a better idea of overall conformation similarity yielded RMSD values of 0.722 Å and 0.154 Å respectively. From these values we can conclude that the backbone conformation of RsgA while in the ppGpp-bound state does not differ majorly from either the apo or GDP-bound state, suggesting that ppGpp may in fact restrict this RA-GTPase in the OFF conformation.

Due to our inability to crystallise RsgA in the GMPPNP-bound ON state, we next carried out structural alignment between the GTPase domains of our *S. aureus* RsgA-ppGpp model and an available *E. coli* YjeQ-GMPPNP model (Figure 5.4.2c) (PDB: 5UZ4) (Razi *et al.*, 2017), which was solved in complex with the 30S and has a resolved switch I loop. During the alignment, the cognate loop segment in the GMPPNP-bound model was occluded. The RMSD for this GTPase domain alignment was 2.073 Å, and 3.164 Å for the entire protein, although this value may be biased towards a large difference due to the presence of an N-terminal helix and extended β-hairpin between the OB-fold domain and GTPase domain in the *E. coli* homologue. Overall, the structure of these two models are remarkably similar, with the exception of a rearrangement in the switch II region (Figure 5.4.2c), which appears to 'flip'

and extend towards the expected binding site of the Mg^{2+} cofactor in the GMPPNP structure, although this could not be verified as the relatively low resolution of the cryo-EM map failed to resolve the bound Mg^{2+} ion (Razi *et al.*, 2017). Additionally, the *E. coli* GMPPNP-bound structure exhibits a 7 Å translocation and 20° rotation in the OB-fold domain as compared to the *S. aureus* ppGpp-bound structure. This translocation is also present in the *S. typhimurium* RsgA-GDP structure (PDB: 2RCN) (Nichols *et al.*, 2007), but not the *A. aeolicus* RsgA-GDP complex (PDB: 2YV5, unpublished), so may be consistent among γ-proteobacteria and should not be considered a direct effect of ON/OFF state transition. This lack of macromolecular rearrangements between the GMPPNP-bound state and ppGpp-bound state indicates that in the case of RsgA, no overall conformational rearrangement takes place when transitioning between the ON and OFF states, and that instead repositioning of the switch I and switch II loops may be the defining structural consequence of binding to GTP, as proposed by Pausch *et al.* in the context of another circularly permuted *S. aureus* RA-GTPase, RbgA (Pausch *et al.*, 2018).
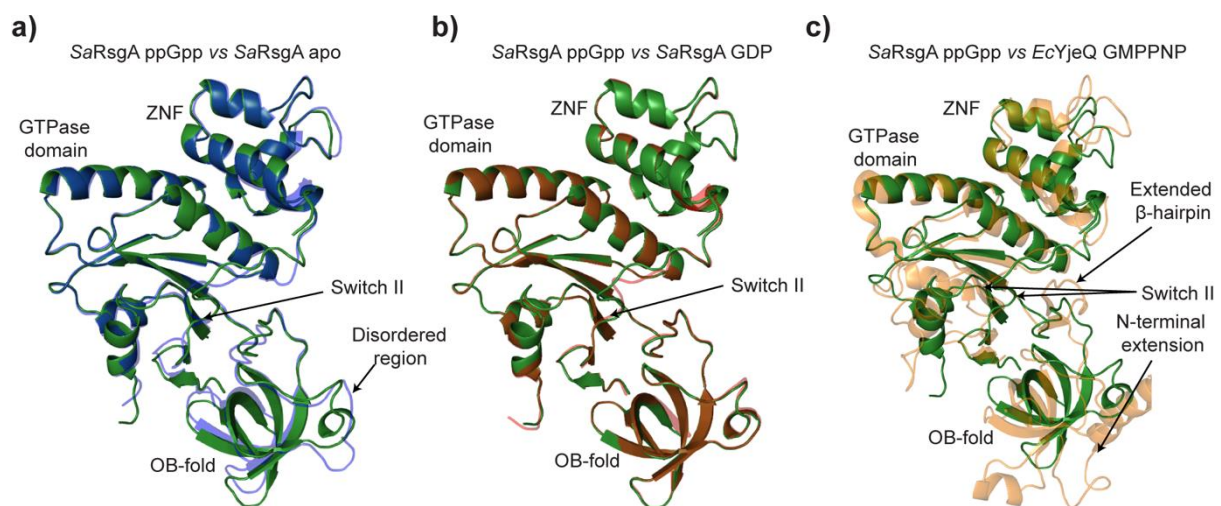
Figure 5.4.2: Structural comparison of *S. aureus* RsgA-ppGpp with the apo and GDP-bound states as well as *E. coli* YjeQ-GMPPNP. Structural alignment of *S. aureus* RsgA-ppGpp (green) (PDB: 6ZHL, this study) with a) *S. aureus* apo RsgA (blue) (PDB:6ZJO, this study), b) *S.aureus* RsgA-GDP (brown) (PDB:6ZHM, this study) and c) *E. coli* YjeQ-GMPPNP (orange) (PDB: 5UZ4, chain Z) (Razi *et al.*, 2017). RsgA molecules are represented as cartoons coloured as specified, with all ligands removed. Key structural aspects are labelled, as well as points of note. Note the alteration in switch II positioning between the ppGpp-bound and GMPPNP-bound structure in part (c).

5.5 Comparison of the ppGpp-bound state to existing ON state and OFF state structures

5.5.1 GTPase domain comparison between the ppGpp-bound RsgA and ON-state homologues

In most canonical Ras-like GTPases, the catalytic glutamine residue stems from the switch II loop, and as such correct rearrangement of this loop correctly positions the glutamine amide group for

activation of a water molecule (Carvalho *et al.*, 2015). A subfamily of the TRAFAC GTPases, the hydrophobic amino acid substituted for catalytic glutamine (HAS)-GTPases, however, contain a hydrophobic substitution at this catalytic site, and as such require either a relocated mechanism of catalysis or the function of an exogenous GTPase activating protein (GAP) (Mishra *et al.*, 2005). In RsgA, this catalytic residue has been identified as a conserved histidine within the switch I loop, H197 in the *S. aureus* homologue, which is correctly positioned upon association with the matured h44 of the 16S rRNA on the 30S subunit (López-Alonso *et al.*, 2017b). It has also been proposed previously that the 3'-diphosphate of (p)ppGpp could sterically inhibit correct switch I docking in RbgA (Pausch *et al.*, 2018), which may account for the inability of this protein to hydrolyse (p)ppGpp.

Localised structural comparisons were carried out between the apo and ppGpp-bound states of our *S. aureus* RsgA models (Figure 5.5.1a-d), and available structures of an OFF state, GDP-bound YjeQ from *A. aeolicus* (PDB: 2YV5, unpublished), and an ON state, GMPPNP-bound YjeQ from *E. coli* (PDB: 5UZ4) (Razi *et al.*, 2017). It is worth noting that two GMPPNP-bound structures exist in the databank, both from the *E. coli* homologue, namely PDB: 5UZ4 (Razi *et al.*, 2017) and PDB: 5NO2 (López-Alonso *et al.*, 2017b). Both exhibit consistent GTPase domain conformation, including switch I and II positioning. However, the bound GMPPNP ligand differs slightly in both cases, with a translocation of 1.5 Å and a rotation of 19° about the longitudinal axis of the molecule seen in 5NO2 relative to 5UZ4, the latter of which almost perfectly reflects the position of the GDP backbone of our GDP and ppGpp-bound structures. Therefore, structural comparisons were carried out using 5UZ4.

Both the GMPPNP-bound and GDP-bound homologue exhibit a partially resolved switch I loop (Figure 5.5.1a, b), enabling us to postulate the loop positioning in the *S. aureus* variants, with both appearing to mimic the OFF conformation (Figure 5.5.1c, d). The overall domain similarity was high, although distinct differences were visible in both the switch I and switch II regions. When bound to GMPPNP, the switch I is docked against the guanosine rings of GMPPNP, enclosing the triphosphate moiety of GMPPNP within the catalytic pocket (Figure 5.5.1a). This docking appears mediated by G2 threonine-Mg^{2+} interactions. The switch II region is positioned as to extend towards the γ-phosphate of GMPPNP and the predicted Mg^{2+} binding site (Figure 5.5.1e), in line with ligand stabilisation through interactions with the conserved glycine residue (Verstraeten *et al.*, 2011). When in the GDP-bound state, however, the switch I loop fails to dock correctly and instead extends towards the solvent, leaving the catalytic pocket uncovered. Furthermore, the switch II loop appears 'flipped' in comparison to the GMPPNP-bound structure, extending away from the predicted sites of the γ-phosphate and Mg^{2+} cofactor (Figure 5.5.1c, e). In both of the *S. aureus* structures presented here, the

switch II loop conformation appears to closely resemble that of the GDP-bound structure, supporting the previous observation that the OFF state of RsgA is maintained in the apo form and when bound to ppGpp. The unresolved switch I loop is therefore postulated to resemble that of the GDP-bound structure (Figure 5.5.1c, d), extending in a distal manner from the nucleotide binding pocket. Interestingly, while in the GMPPNP-bound conformation, the fold of the switch I loop occupies the same space as the 3'-diphosphate moiety of ppGpp would (Figure 5.5.1a, blue oval), which may prevent correct docking of this region while in the (p)ppGpp-bound state and therefore inhibition of Mg^{2+} coordination and GTPase activity.

a) *Ec*YjeQ GMPPNP

b) *Aa*YjeQ GDP

c) *Sa*RsgA Apo

d) *Sa*RsgA ppGpp

e)
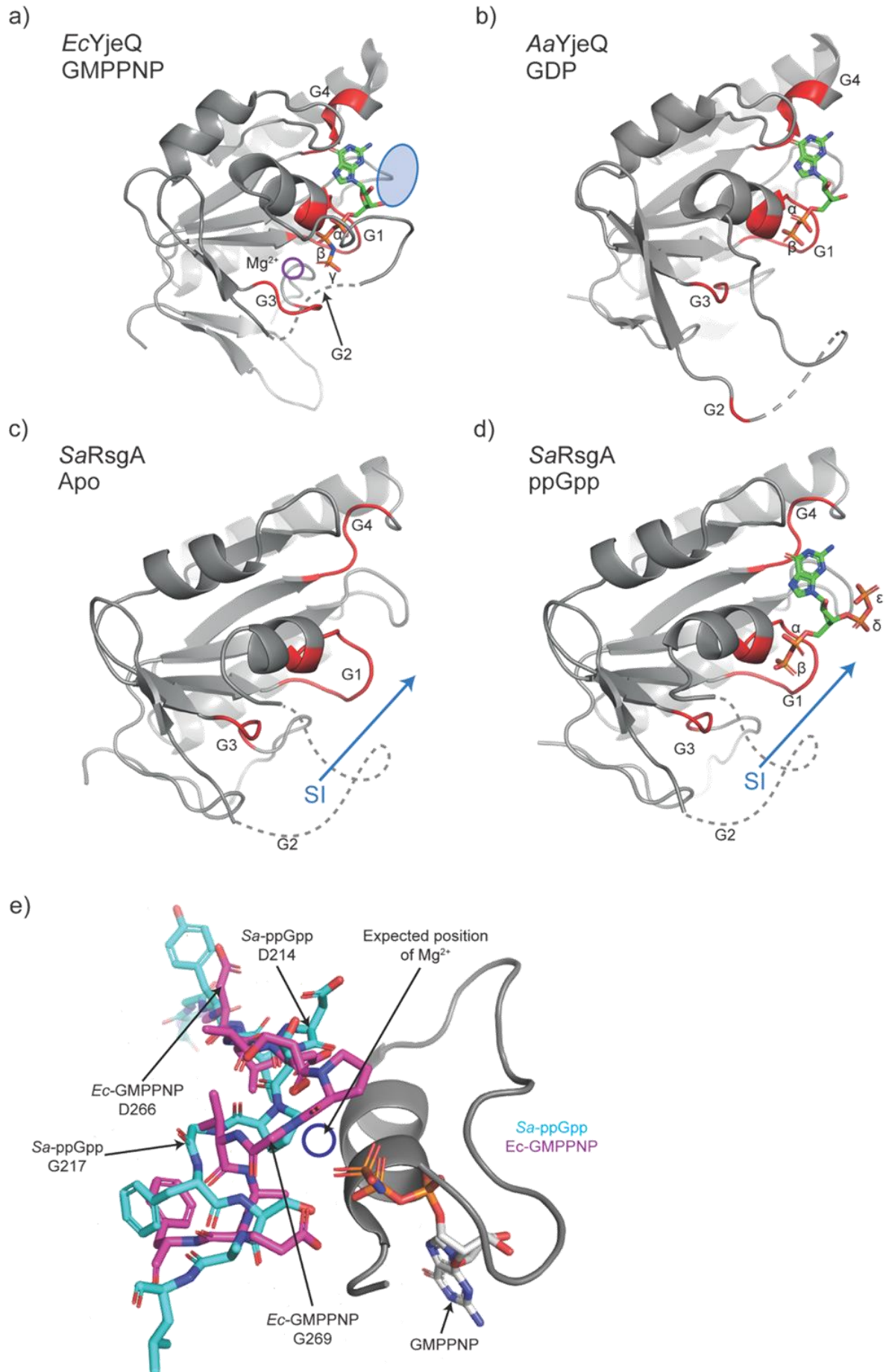
Figure 5.5.1: Comparison between the GTPase domain conformations of RsgA homologues in different nucleotide-bound states. a-d) The GTPase domain of a) *E. coli* YjeQ bound to GMPPNP (PDB: 5UZ4, chain Z) (Razi *et al.*, 2017), b) *A. aeolicus* YjeQ bound to GDP (PDB: 2YV5, unpublished), c) *S. aureus* RsgA in the apo state (PDB: 6ZJO, this study) and d) *S. aureus* RsgA bound to ppGpp (PDB: 6ZHL, this study). The RsgA/YjeQ models are represented by grey cartoons, with the G1, G2, G3 and G4 motifs coloured red where resolved. The proposed position of the switch I loop where unresolved in (c) and (d) is represented by a grey dashed line in accordance with the GDP-bound homologue (b). Switch I rearrangements during the OFF/ON transition represented by a blue arrow. The expected Mg^{2+} binding site is shown by a purple circle, and the expected position of the 3' δ,ε-phosphate of ppGpp is represented in the GMPPNP-bound conformation (a) as a blue oval. Bound nucleotides are coloured by atom as follows: carbon, green; nitrogen, blue; oxygen, red; phosphorous, orange. e) Residue detail of the switch II loops of *E. coli* YjeQ-GMPPNP (magenta, PDB: 5UZ4) (Razi *et al.*, 2017) and *S. aureus* RsgA-ppGpp (cyan, PDB: 6ZHL), with the latter overlaid onto the *E. coli* YjeQ-GMPPNP model. The GMPPNP cofactor is coloured by atom as follows: carbon, white; oxygen, red; nitrogen, blue; phosphorous, orange. The predicted position of the Mg^{2+} binding site is indicated by a blue circle. The positions of the conserved G3 glycine and aspartate residues are indicated. Note that the glycine backbone is extended towards the γ-phosphate of GMPPNP while in the ON-state.

5.5.2 Computational docking of the OFF state GDP- and ppGpp-bound RsgA on the 30S

The ON state structure of RsgA homologues has exclusively been solved while in complex with the 30S subunit, suggesting that these conformations of switch I and II are stabilised during subunit association (López-Alonso *et al.*, 2017b; Razi *et al.*, 2017). This led us to hypothesis that while steric inhibition of switch I docking by the 3'-diphosphate of (p)ppGpp may inhibit hydrolysis, it may also be the underlying cause of the reduced ribosome association characterised in Chapter 4.

In order to investigate the effect of switch I misalignment on the 30S interaction interface, we performed computational superimpositions of the GTPase domains of the available GDP-bound structure (PDB: 2YV5, unpublished) and our ppGpp-bound model with the available GMPPNP-bound YjeQ-30S complex (PDB: 5UZ4) (Razi *et al.*, 2017) (Figure 5.5.2a-c), as well as carrying out primary amino acid alignments between the homologues used. It has been suggested previously that the target rRNA of h44 is clamped between the β$_6$-β$_7$ hairpin loop and the switch I loop, which contact the major and minor groove of h44 respectively while in the GMPPNP-bound state (López-Alonso *et al.*, 2017b; Razi *et al.*, 2017) (Figure 5.5.2a). The switch I loop resolution in this conformation suggests that upon ribosome binding, the docked state is the only conformation of switch I that facilitates stable complex formation. However, when the GDP-bound OFF state structure from *A. aeolicus* is superimposed in place of the GMPPNP-bound ON state *E. coli* structure, it appears that the conformation of the switch I loop would cause steric clashing with the polyphosphate backbone of the 16S h44 (Figure 5.5.2b). Likewise, the prevention of switch I docking in the ppGpp-bound structure would lead to similar steric clashing (Figure 5.5.2c). Primary amino acid identity was around 35% similar for each of the three homologues used (Figure 5.5.2d), namely *S. aureus*, *A. aeolicus* and *E. coli*, however overall structural conservation was high, and the functional motifs were highly similar as expected. All in all, we hypothesise that while bound to (p)ppGpp, inhibition of correct switch I

positioning by the 3'-diphosphate moiety leads to steric clashing between the RA-GTPase and the h44 polyphosphate backbone, preventing stable complex formation.
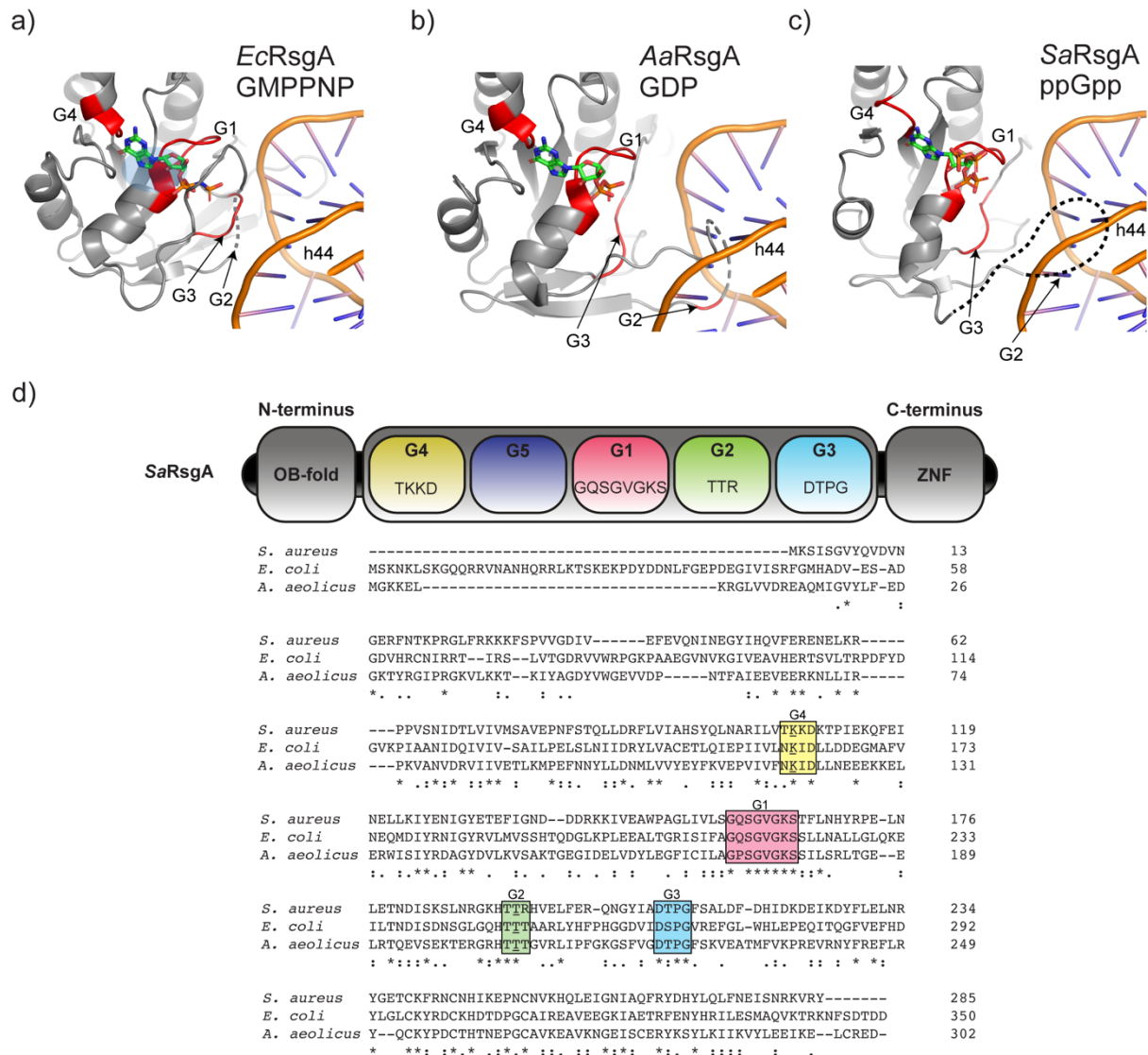
Figure 5.5.2: ppGpp-mediated inhibition of switch I docking leads to steric clashing with the 30S association site. a) The GTPase domain of *E. coli* GMPPNP-bound YjeQ (PDB: 5UZ4, chain Z) and 16S rRNA h44 (Chain A) (Razi *et al.*, 2017). Additional rRNA helices have been removed for clarity. b, c) C_α superimposition of the GTPase domains of b) *A. aeolicus* GDP-bound YjeQ (PDB: 2YV5, chain A, unpublished) and c) *S. aureus* ppGpp-bound RsgA (PDB: 6ZHL, chain A, this study) onto the 16S rRNA h44 (PDB: 5UZ4, chain A). Models of RsgA/YjeQ are represented as grey cartoons, with G1, G2, G3 and G4 motifs coloured red whenever resolved. The 16S rRNA h44 is represented as a carton helix, with the polyphosphate backbone and ribonucleotides coloured orange and blue respectively. Bound GMPPNP, GDP and ppGpp are represented as stick models, with atoms coloured as follows: Carbon, green; nitrogen, blue; oxygen, red; phosporous, orange. The suggested conformation of the unresolved switch I region in the ppGpp-bound structure (c) is represented by a black dashed line. C_α alignments were carried out using PyMOL. d) Clustal Omega Sequence alignment of the RsgA homologues from *S. aureus* (top), *E. coli* (middle) and *A. aeolicus* (bottom). The G1 (pink), G2 (green), G3 (cyan) and G4 (yellow) motifs are indicated, and the target residues for point mutation are underlined. Respective primary amino acid sequence identities between *S. aureus* and *E. coli*, and *S. aureus* and *A. aeolicus* are 33.5% and 34.2% respectively.

160

5.6 Discussion

In this chapter, we aimed to elucidate the consequences of (p)ppGpp binding on the tertiary structure of RA-GTPases, and to better understand the inhibition of ribosome association observed in Chapter 4. We achieved this via crystallographic studies into RsgA in the apo, GDP-bound and ppGpp-bound states, and following comparison of these models both to each other and to available ON and OFF state conformations from *E. coli* and *A. aeolicus*, including a structure of the YjeQ-30S complex, we were able to propose a model for (p)ppGpp-mediated inhibition of ribosome assembly.

We first identified conditions under which RsgA will crystallise while in the OFF state (Figure 5.2, Table 5.2). The use of predefined shotgun screening approaches to crystallising a protein comes with several advantages, namely the high throughput nature and automation of the process, however as with any method of screening, they are entirely trial and error based. In our case, however, these approaches only yielded crystals for one of our four RA-GTPases. In the case of RbgA, Era and HflX, a total of six commercial shotgun screens were utilised, including the three mentioned earlier. Homologues of each of these proteins have been crystallised previously (Pausch *et al.*, 2018; Tu *et al.*, 2009; Wu *et al.*, 2010), and bespoke crystal screens were set up in an attempt to mimic previously successful conditions, however all were unsuccessful. While every attempt was made to mimic these conditions carefully, intangible differences in purification quality, ligand quality, protein concentration and any other condition may affect the outcome of these trials.

Of the three states of RsgA crystallised here, namely the apo, GDP-bound and ppGpp-bound, the apo and GDP-bound states were obtained in a serendipitous manner while incubating RsgA with GMPPNP, suggesting an element of copurification with bound GDP, which is not unfeasible given the comparatively higher affinity for GDP than GTP (Chapter 3.3). A very high level of structural similarity was observed between the three states, however in the case of the GDP and ppGpp-bound states, the two structures were near identical (RMSD of 0.131 Å) (Figure 5.4.2). An interesting observation is that the RsgA-ppGpp and RsgA-GDP states were crystallised using the same conditions from within the Pact premier screen well F11, exhibiting the same space group of $P2_12_12_1$ and the same unit cell dimensions and angles (Table 5.3), implying that the packing of molecules within the crystal matrix is identical between the two samples. On the other hand, the apo crystal contained two monomers per asymmetric unit with a space group of $P12_11$. The physiochemical forces defining the conditions under which any given molecule crystallises are poorly understood, however it is presumed that molecules with similar structures pack similarly under the same conditions (McPherson and Gavira, 2014). As such it would be interesting to investigate the potential of the apo state of RsgA to crystallise under

PACT F11 conditions, and by extension whether any microscale differences in tertiary structure would be observed between apo RsgA in a condition-dependent manner. This could give valuable insight into the effects of artifacts introduced by crystal packing on observed structure. Our complete inability to crystallise RsgA while bound to GMPPNP may be indicative of a macroscale difference in tertiary structure or domain configuration, which may impede the packing of monomers under conditions in which OFF state RsgA could crystallise. Alternatively, the rearrangement of the switch I and switch II loops may be sufficient to prevent crystallisation. It is therefore important to proceed with investigations into the ON state structure of *S. aureus* RsgA, which may require the use of cryo-EM while in complex with the 30S subunit, in order to better understand the conformational consequences of the OFF/ON state transition.

All known homologues of RsgA bind the same site on their cognate 30S subunit, with the accessory OB-fold domain and ZNF interacting with h44 and h29/h30 respectively (Jomaa *et al.*, 2011; López-Alonso *et al.*, 2017b; Nichols *et al.*, 2007; Razi *et al.*, 2017; Thurlow *et al.*, 2016) in order to position the GTPase domain towards the decoding centre. Cryo-EM studies of the *E. coli* homologue have identified seemingly stabilising interactions between the switch I loop and a hairpin loop between β_6 and β_7 of the GTPase domain, clamping the 16S rRNA h44 between the minor and major groove respectively, and therefore suggested that the GTPase domain is responsible for a third specific site of interaction with the 30S subunit (López-Alonso *et al.*, 2017b). This hairpin is also present in the *S. typhimurium* homologue of YjeQ (Nichols *et al.*, 2007) but not in the *S. aureus* (this study) or *B. subtilis* (Levdikov *et al.*, 2004) variants, and as such may be unique amongst the γ-proteobacteria similarly to the 7 Å translation of the OB-fold domain (Nichols *et al.*, 2007; Razi *et al.*, 2017). Extensive sequence alignments of interspecies homologues of RsgA revealed little residue conservation within the switch I region other than the conserved G2 threonine (data not shown), rendering it unlikely that this region is responsible for specific interactions with the 30S rRNA. Instead, we propose that the initial docking of RsgA to the 30S subunit is mediated by OB-fold domain and ZNF interactions, followed by minor electrostatic interactions between the switch I loop and h44 and h45 rRNA which serve to correctly position switch I into a catalytically active conformation while concurrently removing the steric hindrance to association. This proposition is in accordance with our kinetic model (Chapter 4.4), during which an initial interaction (k_1) is followed by a stabilisation step (k_2), which we propose to be initial accessory domain-mediated association, and complex stabilisation via switch I docking respectively. The presence of the 3' diphosphate of (p)ppGpp would sterically prevent this docking, and therefore lead to the complete inhibition of k_2 while in the (p)ppGpp-bound state, preventing stable complex formation and reducing ribosome association. When regarding computational superimposition and

docking of our *S. aureus* models with homologues from *E. coli* (33.5% sequence similarity) and *A. aeolicus* (34.2% sequence similarity) (Figure 5.5.2d), it is crucial to consider that there may be innate structural differences between organisms which may lead to false interpretation, and as such the GMPPNP-bound and 30S-associated models of *S. aureus* RsgA should be solved in order to gain more relevant insight. For this reason, C_α alignment was carried out using only the relatively highly conserved GTPase domain in an attempt to reduce any impact of the less highly conserved accessory domains. Currently, our proposed model requires further biochemical investigation to validate.

It is widely accepted that due to overlap of binding sites on the 30S subunit, binding of Era and RsgA is mutually exclusive (Figure 5.6a, left panel) (Razi *et al.*, 2017; Sharma *et al.*, 2005). Furthermore, the 50S-binding RA-GTPases RbgA and HflX are also deemed mutually exclusive (Figure 5.6a, right panel) (Seffouh *et al.*, 2019; Zhang *et al.*, 2015). Despite the slight differences in these binding sites, rRNA recognition is the major means by which each of these proteins associates with the ribosome. Therefore, it stands to reason that the mechanism of (p)ppGpp-mediated inhibition of association could be consistent throughout. Cryo-EM structures of *B. subtilis* RbgA associated with the 45S intermediate (Seffouh *et al.*, 2019) reveal that the switch I loop docks against the minor groove of h89 in a similar manner to RsgA docking against h44 on the 30S subunit (Figure 5.6b, left panel). The switch I loop of HflX on the other hand makes no contact with either rRNA or r-proteins, with the closest contact being h66, albeit with a separation of over 12 Å compared to around 6 Å in the case of RbgA and RsgA. We observed in Chapter 4 that HflX is capable of associating with the 50S and 30S subunits in the ON state and while in the apo state, whereas both RsgA and RbgA were unable to associate with the 30S while in the apo state, suggesting a difference in dissociation mechanism which may be dependent on switch I positioning. Furthermore, the helical linker domain of HflX undergoes a conformation change upon GTP hydrolysis, leading to dissociation of the 100S complex and subsequent dissociation of HflX from the ribosome (Dey *et al.*, 2018). All in all, this suggests that the dissociation of HflX from the ribosome may be dependent on conformational changes in the helical linker domain as opposed to the switch I region, and that the GDP- or (p)ppGpp-bound OFF-state may hold this domain in a conformation incompatible with ribosome association. Era is also capable of 30S association in the apo state, although the cryo-EM structure available in the case of this protein is too low resolution for molecular detail (Sharma *et al.*, 2005). Further high-quality structural studies of the Era-30S complex would be required to provide insight into the mechanism of dissociation from the ribosome, specifically whether this is switch I mediated or reliant on domain rearrangement. Given the difference in function between HflX and the remaining RA-GTPases, it is likely that this mechanism of association control could be widespread.
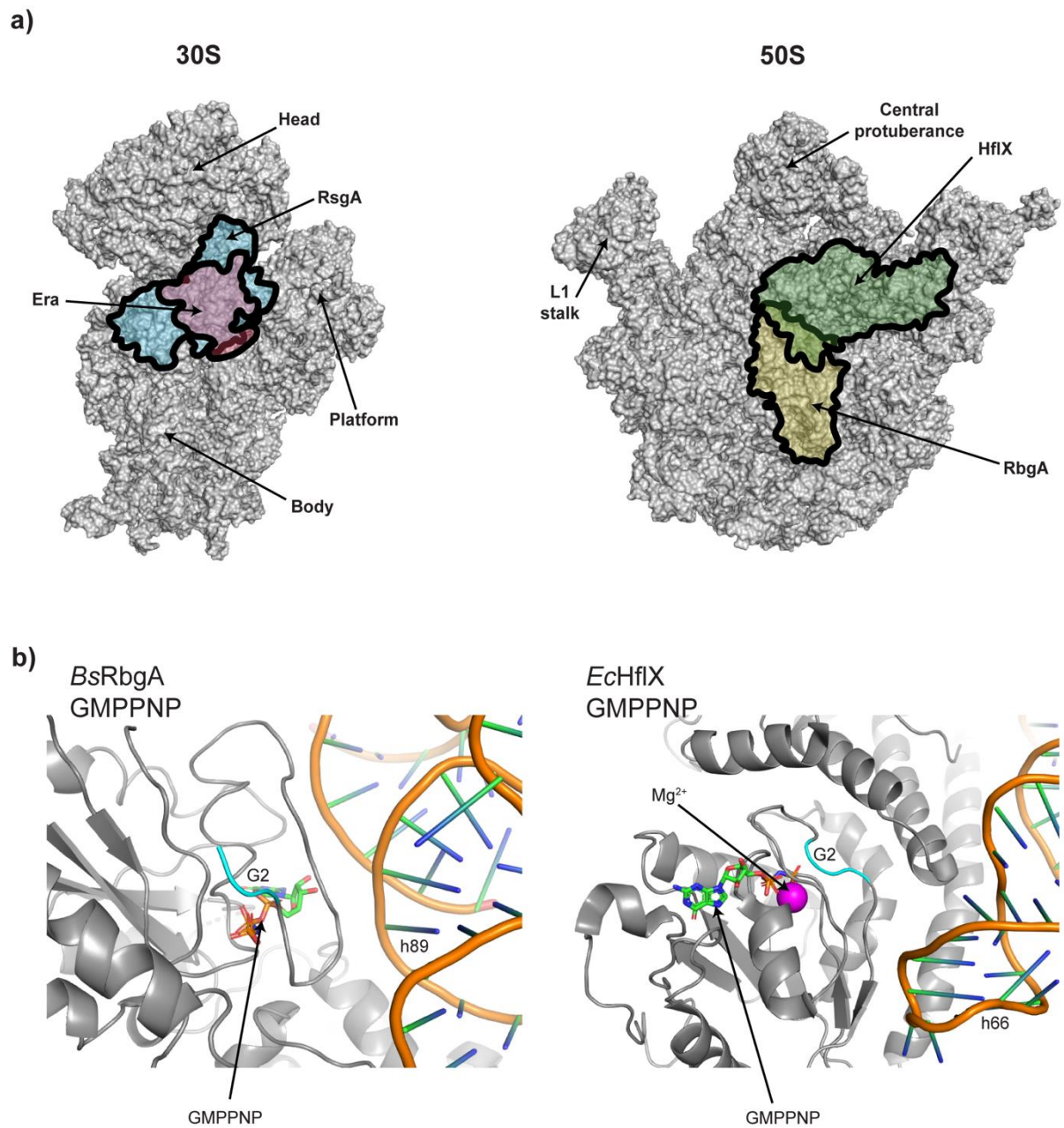
Figure 5.6 Incorrect docking of the switch I loop may lead to steric clashing between the ribosome and RbgA or HflX. a) Schematic representations of the ribosomal binding sites of the 30S binders RsgA and Era (left panel, blue and pink respectively), and the 50S binders RbgA and HflX (right panel, yellow and green respectively). Binding sites interpreted from PDB entries 5UZ4, 1X18, 6PPK and 5ADY respectively (Razi *et al.*, 2017; Seffouh *et al.*, 2019; Sharma *et al.*, 2005; Zhang *et al.*, 2015). The 30S and 50S subunits were modelled using available data from PDB: 5UZ4 and PDB: 5ADY respectively. b) *B. subtilis* RbgA (left panel, PDB: 6PPK) and *E. coli* HflX (right panel, PDB: 5ADY) associated with the 45S and 50S ribosomal particles respectively. Models of RbgA/HflX are shown as grey cartoons, with the G2 motif coloured cyan. The associated GMPPNP ligands are coloured by atom as follows: carbon, green; oxygen, red; nitrogen, blue; phosphorous, orange. The closest rRNA contact to the switch I loop is shown as an orange helix, and ribonucleotides are shown in blue. Distal rRNA removed for clarity.

Previously solved crystal structures of the non-(p)ppGpp-binding TRAFAC GTPase YsxC from the thermophilic bacterium *Thermotoga maritima* have revealed two distinct switch I conformations while in the GDP-bound state (Chan and Wong, 2011), an 'open' conformation in line with the *A. aeolicus* model referred to in this chapter, and a 'closed conformation' in line with the *E. coli* ON state model, which would suggest a stable docking of the switch I loop in the absence of GTP binding. The 'open' conformation of this loop appears to be stabilised by crystal packing and hydrogen bonding between adjacent monomers, which is possibly the reason that the loop is so highly ordered, whereas the 'closed' conformation exhibits extensive backbone H-bonding between the switch I loop and both the P-loop and α-phosphate of GDP. The structure of *B. subtilis* YsxC has been solved in the GMPPNP-bound and GDP-bound state (Ruzheinikov *et al.*, 2004), with a similar 'closed' conformation observed while bound to GMPPPNP. The 'open' structure from *T. maritima* is recapitulated in the *B. subtilis* GDP-bound structure. Interestingly, the α-phosphate H-bonding by S37 described by Chan and Wong is present in the *B. subtilis* structure, however the authors of the latter have not included the cognate H-bond acceptor as part of the flexible region of the switch I loop, instead labelling S37 as the final point of secondary interaction before the loop becomes innately unstable. While it is impossible to dismiss that non-(p)ppGpp-binding GTPases may be regulated in a different manner to (p)ppGpp-binding GTPases, these results suggest that switch I mediated control of ribosome association may be common amongst TRAFAC GTPases.

The absence of electron density corresponding to the switch I loop of RsgA is a recurring theme between the apo, GDP-bound and ppGpp-bound structures, with a 19-21 residue segment unresolved in each structure. This is common among GTPases in general, especially in the case of cpGTPase domains in the YjeQ/YawG/YlqF subfamilies in which the switch I loop is extended to maintain the nucleotide binding pocket following permutation (Anand *et al.*, 2006; Do *et al.*, 2008; Shin *et al.*, 2004). Partial resolution of this loop can be achieved in some cases, particularly in the case of thermophilic bacteria (such as *A. aeolicus*) which are commonly used in structural biology due to the enhanced resistance to proteolysis and (on average) lower B-factors (Vieille and Zeikus, 2001) of thermostable proteins. Partial switch I resolution has also been achieved in complex with the 30S subunit while in the ON state, indicating that switch stability is conferred in this complex (López-Alonso *et al.*, 2017b; Razi *et al.*, 2017). Several techniques have been utilised previously to manipulate the flexible regions of proteins, with two examples being the introduction of proline residues to confer loop rigidity (Matthews *et al.*, 1987) and introduction of targeted disulphide bonds to restrict loop conformations (Meek *et al.*, 2019). Both of these techniques show potential to further the investigation into switch I mechanics in RsgA by manipulating positioning. The property of proline residues to restrict amino acid

phi angles between the backbone nitrogen and C$_\alpha$ could render the loop rigid, and therefore enhance the electron density upon diffraction analysis of crystals. However this could also lock the loop in an unnatural conformation and potentially destabilise any secondary structure into which the proline residue is inserted (Choi and Mayo, 2006). Attempting to introduce cysteine substitutions into RsgA to lock the switch I loop in the docked state in the absence of bound nucleotides could also provide insight into the role of this docking in ribosome association. Rational design of these mutant sites, however, would require knowledge of the precise positioning of each potential target residue in space in order to model bond formation accurately, and in the case of the *S. aureus* homologue of RsgA, the structural data concerning the switch I loop required for this level of planning is currently lacking. The true potential of these techniques lies in coordination, as enhancing loop order through proline introduction could pave the way for rational disulphide bond design.

In conclusion, here we have established that the apo, GDP-bound and ppGpp-bound conformation of *S. aureus* RsgA are highly similar, and as such can all be considered to exist in the OFF state. Comparison of our structures to a GDP-bound OFF state homologue from *A. aeolicus* also shows a high degree of structural similarity, notably in the switch II region. The switch II conformation differs in a GMPPNP-bound ON state homologue from *E. coli*, which also displays stable docking of the switch I loop in such a manner that would sterically clash with the δ,ε-phosphate of (p)ppGpp. Subsequent misalignment of this loop while in the OFF state appears to sterically clash with the polyphosphate backbone of h44, enabling the proposal of a model by which binding of (p)ppGpp inhibits not only the GTPase activity of our RA-GTPases, but also their association to the ribosomal subunits.

Chapter 6 – Functional characterisation of G2, G4 and ΔG2 variants

6.1 Introduction

The capacity of GTPases to cycle between the GTP-bound ON state and the GDP-bound OFF state is responsible for their ability to act as molecular switches and control crucial cellular processes, such as ribosome assembly. Generally, GTPases interact with downstream targets while in the ON state, followed by entry into the GDP-bound OFF state using the free energy released upon GTP hydrolysis, and subsequent dissociation from the binding target. We previously demonstrated that the ppGpp-bound state of RsgA structurally mimics the GDP-bound state (Chapter 5), suggesting that during the stringent response, when GTP levels decrease drastically and the concentration of (p)ppGpp increases (Kriel *et al.*, 2012), RA-GTPases are trapped in the nonfunctional OFF state. This observation is corroborated by our work showing that (p)ppGpp binding disrupts interactions between RA-GTPases and the ribosome (Chapter 4). To examine this in more detail, we sought to generate mutant variants of RsgA, RbgA, Era and HflX which would trap the protein in the OFF state, and to characterise the activity of these variants *in vitro*, including their ability to associate with the ribosomal subunits, and the *in vivo* consequences regarding growth, ribosome biogenesis and translation rate.

The mechanism by which P-loop GTPases bind to and hydrolyse GTP nucleotides is very highly conserved (Figure 6.1), with either four or five motifs (termed G1-G5) conferring functionality (Britton, 2009; Karbstein, 2007; Verstraeten *et al.*, 2011). Briefly, the G1 motif (consensus GxxxxGK[S/T]) is involved in coordinating the α- and β-phosphate of GTP, the G2 motif (consensus xTx) is positioned within a flexible loop region termed Switch I which confers protein activity via conformational changes based on the bound nucleotide. The conserved threonine residue is responsible for coordinating the catalytic Mg^{2+} cofactor, which in turn contacts the β- and γ-phosphate of GTP. The G3 motif (consensus DxxG) is also involved in coordination of the γ-phosphate. The G4 motif (consensus [N/T][K/Q]xD) is responsible for determining nucleotide specificity by forming specific and selective interactions with guanine rings, with the conserved lysine/glutamine exhibiting nonspecific stacking interactions against the plane of the bound guanine. Together, these motifs form a specific and selective binding pocket to not only bind GTP, but also catalyse hydrolysis.

In this chapter, we generate single-site nonconservative point mutations in the conserved G2 and G4 regions of RsgA, RbgA, Era and HflX though inverse PCR, as well as mutant variants of RbgA and Era lacking the entire switch I/G2 loop (ΔG2). For the purposes of this chapter, switch I and the G2 loop are interchangeable, whereas the G2 motif is the single conserved threonine residue within the switch I/G2 loop. We reasoned that mutation of the G2 threonine residue would occlude GTP binding while

allowing GDP/ppGpp binding and result in a perpetually OFF-state protein (Corrigan *et al.*, 2016; Martínez-Vicente *et al.*, 2005), and that the G4 lysine mutation would prevent the binding of all nucleotides by preventing the stable stacking interaction with the guanine base, resulting in a constantly apo protein in the OFF conformation. The switch I region is responsible for a large conformational change upon GTP hydrolysis, which reverts the GTPase from the ON to the OFF conformation and triggers dissociation. The direct interface between the switch I loop and the target rRNA (Guo *et al.*, 2011a; López-Alonso *et al.*, 2017b; Razi *et al.*, 2017) suggests that this loop in intimately involved in governing the GTPase ON/OFF cycle and ribosomal interaction, and so we reasoned that the ΔG2 mutant variants could enable investigation into the role of the switch I loop in the ppGpp-mediated reduction of GTPase-ribosome association. Basic biochemical characterisation of the recombinant mutant proteins was carried out, including nucleotide binding curves and timecourses of GTPase activity. The similarity between the secondary structure of the wild-type and mutant variants was assessed using circular dichroism (CD) spectroscopy, and the impact of these mutations on ribosome binding was investigated *in vitro* using enzyme-linked immunosorbent assays (ELISA). We recreated the G2 and G4 mutant variants of RsgA, Era and HflX in a LAC* Δ*RA-gtpase* background in order to assess the effect on growth rate. Finally, we investigated the effect of the Era T40A and K123T mutation on cellular ribosome content and translation rate. All of this work was carried out with the purpose of better understanding the role of the GTPase activity and nucleotide binding capacity on the function of RA-GTPases both *in vitro* and *in vivo*.
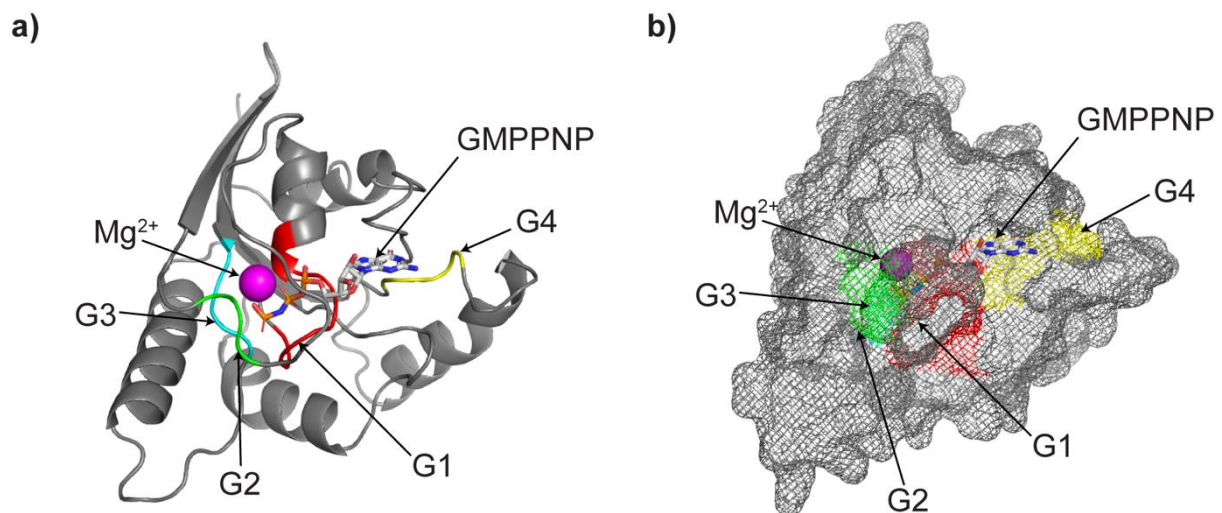
Figure 6.1: Structure of the conserved GTPase domain. a) A cartoon representation of the GTPase domain of *Aquifex aeolicus* Era in the GMPPNP bound state (adapted from PDB: 3R9W). b) Surface mesh structure of the *Aquifex aeolicus* Era in the GMPPNP bound state (adapted from PDB: 3R9W). The conserved motifs G1 (red), G2 (green), G3 (blue, behind G2 in (b)) and G4 (yellow) are highlighted. Note that the G2 region docks onto the bound GMPPNP ligand, forming an enclosed binding pocket. The bound GMPPPNP ligand is coloured by atom as follows: carbon, white; nitrogen, blue; oxygen, red and phosphorous, orange. The bound Mg^{2+} cofactor is shown in magenta.

6.2 Generation of RA-GTPase mutants

Many previous studies have sought to alter the capacity of P-loop GTPases to bind and hydrolyse GTP through mutation of these crucial conserved residues. Here, we aimed to generate two point mutants, targeting the conserved G2 threonine and G4 lysine residue. Based on previous work (Corrigan *et al.*, 2016; Martínez-Vicente *et al.*, 2005), we expected that the former would occlude binding to GTP while enabling binding of GDP and (p)ppGpp, resulting in a perpetually OFF protein, while the latter would occlude all guanine nucleotides from binding and maintain the apo state due to the loss of the stacking interaction. Secondly, we aimed to delete the entire switch I loop to remove not only the functional G2 motif, but also the likely interaction interface between the RA-GTPase and the ribosome, and the major component of the ON/OFF switch. Previous studies regarding *S. aureus* RbgA revealed that in the (p)ppGpp-bound state, the 3'-diphosphate would prevent switch I docking into the active ON conformation. The ΔG2 variants constructed here would enable further insight into the role of this switch on GTPase activity and nucleotide binding, and also as a potential determinant of association with the ribosomal subunit.

6.2.1 Site-directed mutagenesis of the conserved G2 and G4 residues of RsgA, RbgA, Era and HflX – identification and cloning

The first step in generating point mutations in the active site of RA-GTPases was identification of the conserved G2 and G4 residues in question. The primary amino acid sequence which constitutes the G1-G5 motifs is highly conserved, especially in the case of the P-loop (G1). Complete sequence alignments between RsgA, RbgA, Era and HflX were of limited use, as the circularly permuted nature of the RsgA and RbgA GTPase domain led to low apparent sequence identity, rendering identification of key motifs difficult. Instead, separate alignments were carried out for the circularly permuted and the canonical domains, with the RsgA/RbgA and Era/HflX alignments proving much clearer (Figure 6.2.1a). We opted to substitute the G2 threonine and G4 lysine residues (Figure 6.2.1a) nonconservatively, with the former being mutated to alanine and the latter being mutated to threonine.

Overlapping primers were designed to introduce a targeted single nucleotide mutation: in the case of Era, the threonine codon ACA was mutated to the alanine codon GCA and the lysine codon AAA was mutated to the threonine codon ACA (Figure 6.2.1b). Mutagenic inverse PCRs were carried out using a pET28b plasmid template, which contains the coding region of *S. aureus* RsgA, RbgA, Era and HflX, as described in the methods section. PCR products were digested using DpnI to remove any

methylated wild-type plasmids, and transformed into *E. coli* XL1 Blue. Following successful sequencing of the resulting plasmid confirming the presence of the desired mutation, mutant protein variants were transformed into *E. coli* BL21 DE3 for purification.

Figure 6.2.1: Identification and generation of G2 and G4 point mutants. a) Sequence alignments of the canonical GTPase domains of Era and HflX (upper) and the circularly permuted GTPase domains of RsgA and

RbgA (lower). Domain structure and the consensus of conserved G1-G5 sequence motifs are indicated. G1-G4 motifs highlighted as follows: G1, red. G2, green. G3, blue. G4, yellow. Target G2 and G4 residues for mutation are underlined. Alignments were carried out using Clustal Omega using sequences from *S. aureus* strain USA300. b) Primer design and Sanger sequencing analysis of the introduction of the T40A point mutation in Era. Note the mutagenic nucleotide mismatch highlighted in red. Sequencing results alignment was carried out using SnapGene.

6.2.2 Deletion of the switch I loop of RbgA and Era

Upon completion of GTP hydrolysis, a large conformational change in the switch I loop reverts the GTPase into the OFF state, causing dissociation from the binding target. Furthermore, cryo-EM studies of RsgA have shown that the Switch I loop lies directly on the binding interface between RsgA and the 30S ribosomal subunit (López-Alonso *et al.*, 2017b), supported by the fact that the RNA-binding motifs of the N-terminal OB domain and C-terminal Zn^{2+}-finger domain lie on the same face as the switch I region (Guo *et al.*, 2011). This suggests that the switch I region is intimately involved in the GTPase ON/OFF cycle and controlling ribosomal interaction, and is likely involved in the reduction in association seen when bound to (p)ppGpp (Chapter 4).

Work from Shimamoto and Inouye previously deleted a 10 residue segment of the flexible switch I loop of *E. coli* Era, a region which encompasses the conserved G2 threonine residue responsible for coordination of the Mg^{2+} cofactor and binding of the γ-phosphate of GTP (Shimamoto and Inouye, 1996), in order to investigate the role of this region in GTP binding and hydrolysis. We sought to determine the role of the switch I loop on ribosome association, and as such set out to reconstruct this 10 residue deletion in *S. aureus* Era in order to investigate the effect this may have on ribosome interactions. We also generated a parallel 10 residue deletion in the switch I loop of *S. aureus* RbgA, to gain some general perspective of the similarities or differences between the mechanism of action of 30S and 50S binding RA-GTPases. The mutations in question were as follows: Era ΔA38-G47 and RbgA ΔV154-V163 (Figure 6.2.2a), and are referred to as Era ΔG2 and RbgA ΔG2. The segment was deleted via Splicing by Overlap Extension (SOE) PCR (Figure 6.2.2b-d). Resulting fragments were enzymatically digested as specified in the methods section and transformed into *E. coli* XL1 Blue. Plasmids were isolated and validated via Sanger sequencing, before transformation into *E. coli* BL21 DE3 and protein purification.
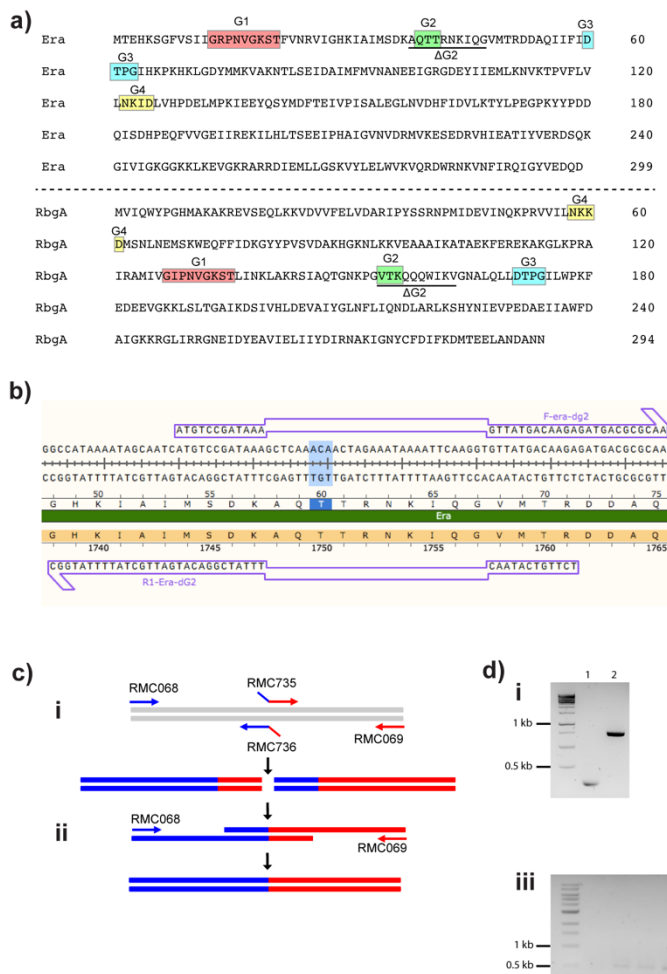
Figure 6.2.2: Generation of the Era ΔG2 mutation via SOE PCR. a) Sequence of *S. aureus* Era and RbgA, highlighting the G1 (red), G2 (green), G3 (blue) and G4 (yellow). The target residues for deletion during construction of the ΔG2 mutation are underlined. b) Primer design for the deletion of the switch I loop. Note the complementarity of the overhang regions to enable downstream splicing of the PCR product. The conserved G2 residue is highlighted. Primer-sequence alignment generated using SnapGene. c) Schematic overview of SOE PCR. ci) Two amplifications are carried out to generate the two fragments to be joined. Internal primers are used to generate 3' or 5' overhangs which are complementary to each other, while occluding the region to be deleted. cii) Complementary overhangs anneal to form a template containing the desired mutation. Forward and reverse primers which span the entire template are used to amplify the region as a whole, which can then be digested and transformed as desired. d) 1% agarose electrophoresis of the PCR products of steps i) and ii) as described for panel (c). di) Lane 1: The forward (129 bp) and Lane 2: reverse (~778 bp) fragment of the Era amplification in lanes 1 and 2 respectively, using primer pairs RMC068 + RMC736, and RMC069 +RMC735. dii) The 897 bp product of splicing the forward and reverse fragments from panel (di) using primer pair RMC068 + RMC069. diii) Colony PCR of transformants following product digestion and ligation into pET28b plasmid using screening primers RMC062 + RMC063. Positive colony with an insert of 1.19 kb indicated in lane 12.

6.3 The ability of RA-GTPase mutants to bind to guanine nucleotides

6.3.1 Binding curves of G2 and G4 mutants

Next we sought to fully assess the ability of these mutants to bind to the four major guanosine nucleotides present within the cell – namely GTP, GDP, ppGpp and pppGpp using DRaCALAs with [α-

[32P] labelled nucleotides (Figure 6.3.1a, b). Doubling dilutions of recombinant protein were mixed with a consistent concentration of radiolabelled nucleotide for 5 mins before spotting onto a nitrocellulose membrane. Binding curves of the wild-type RA-GTPases for comparison can be found in Figure 3.3.1. Fitting of these binding curves with the single exponential functions accounting for an undetermined level of background signal enables binding coefficients to be calculated (Table 6.3.1), specifically the K_d and the B_{max}.

Overall, we found that the G2 threonine mutants of the two circularly permuted RA-GTPases, RsgA and RbgA, demonstrated reduced GTP binding in RsgA and RbgA, while the binding of GTP by Era was unaffected (Table 6.3.1). Each of the G2 mutant variants showed a comparable affinity to GDP, ppGpp and pppGpp as the wild-types. While the K_d of RsgA binding to GTP was only slightly impaired (3.56 $\pm$ 0.41 µM compared to 7.32 $\pm$ 3.46 µM), the K_d of RbgA binding to GTP was not derivable, implying a much greater impact on binding. The ability of Era T40A to bind GTP, unlike the cognate RsgA mutant T199A or RbgA mutant T155A, could be in part due to a compensatory effect of the adjacent T41 residue, as for the *E. coli* GTPase MnmE. Here, mutation of both adjacent threonine residues showed a cooperative decline in activity compared to either single mutation (Martínez-Vicente *et al.*, 2005). It is worth noting that under the conditions used for this investigation, the binding of HflX to GTP and pppGpp was insufficient to determine any binding coefficients, making conclusions regarding the effect of the T239A mutation difficult to draw. In the case of the G4 lysine mutants, binding to all nucleotides is abolished for all four RA-GTPases investigated, and as such no parameters can be calculated for this interaction. Some slight increase in binding is observed at higher protein concentrations, but this is likely due to nonspecific interactions imparted by increasing the quantity of polar molecules (i.e. proteins) within the reaction mixture. Altogether, we have constructed two protein variants for each RA-GTPase. The RsgA T199A and RbgA T155A mutants exhibited a reduced affinity for GTP while their capacity to bind GDP, ppGpp or pppGpp was unaffected, and as such these mutations may maintain the OFF state conformation. The Era T40A mutant appeared able to bind each of the four guanine nucleotides with a similar affinity to the wild-type. The G4 lysine mutants for each of the RA-GTPases were completely unable to bind any guanine nucleotide, and as such may represent the apo conformation of these proteins.
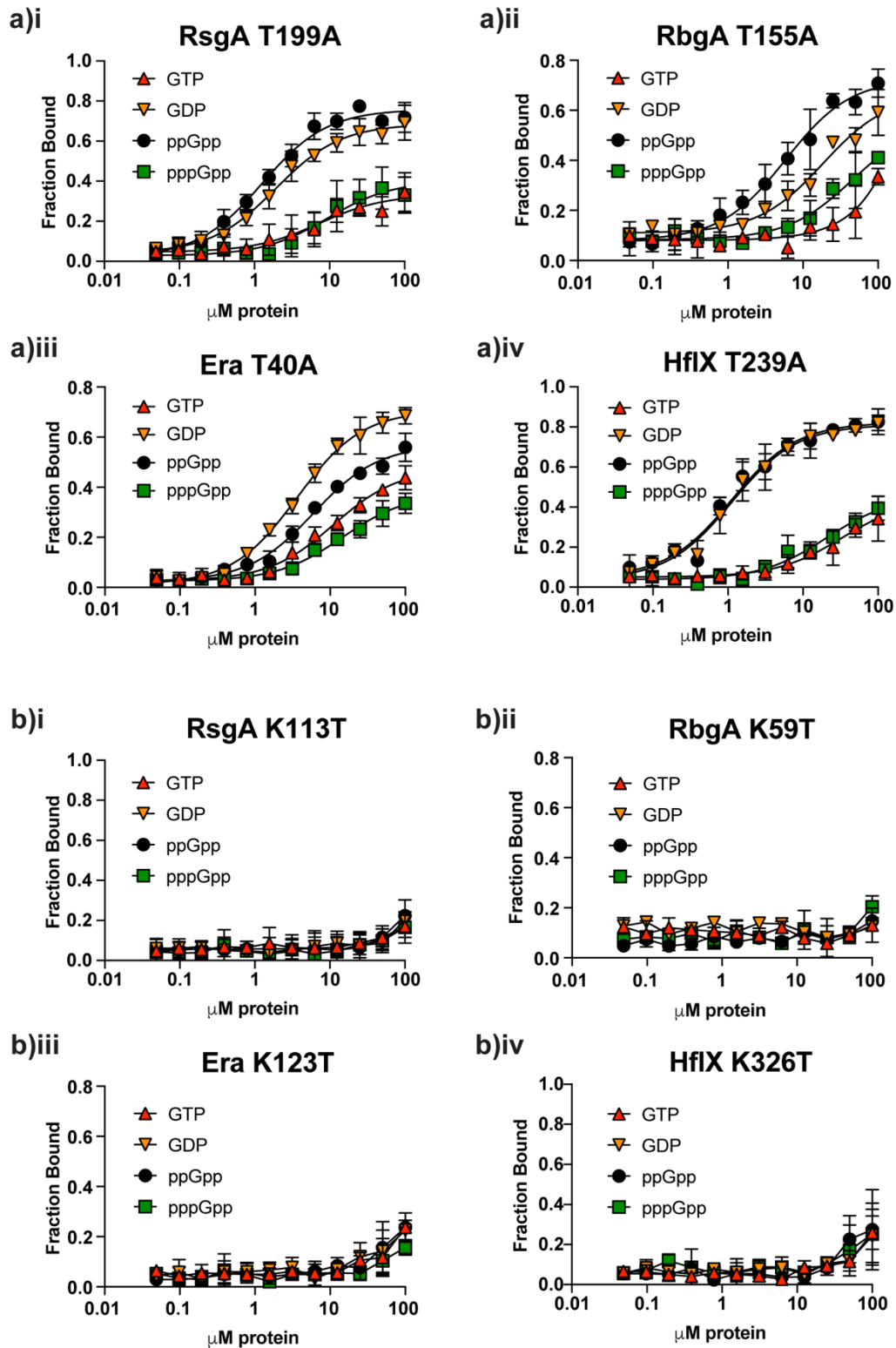
Figure 6.3.1: Nucleotide binding curves of the G2 threonine and G4 lysine mutants of RsgA, RbgA, Era and HflX. Doubling dilutions of a) G2 mutant protein variants or b) G4 mutant protein variants of i) RsgA, ii) RbgA, iii) Era or iv) HflX from an initial 100 μM concentration were incubated with 1.83 nM [α-^{32}P] labelled GTP, GDP, ppGpp or pppGpp. Following a 5 min incubation at room temperature, samples were spotted onto nitrocellulose and visualised using a phosphorimager. Pixel densitometry was carried out as specified in the methods section. Resulting curves were fitted using the One Site Specific Binding model on Prism, amended to include a background signal. Experiments were performed in triplicate, with error bars representing the standard deviation between replicates.

Table 6.3.1: Binding parameters of guanine nucleotides to G2 mutant variants of RsgA, RbgA, Era and HflX

		WT		G2 threonine substitution mutant	
		K_d	B_{max}	K_d	B_{max}
RsgA	**GTP**	3.56 ± 0.41	0.77 ± 0.02	7.32 ± 3.46	0.29 ± 0.03
	GDP	1.83 ± 0.16	0.92 ± 0.02	1.92 ± 0.30	0.65 ± 0.02
	ppGpp	2.17 ± 0.20	0.85 ± 0.02	1.27 ± 0.18	0.74 ± 0.02
	pppGpp	10.06 ± 2.16	0.43 ± 0.03	9.35 ± 4.02	0.37 ± 0.04
RbgA	**GTP**	18.48 ± 5.35	0.40 ± 0.04	ND	ND
	GDP	6.07 ± 1.05	0.52 ± 0.02	18.47 ± 4.33	0.56 ± 0.04
	ppGpp	2.86 ± 0.40	0.56 ± 0.02	5.89 ± 1.16	0.65 ± 0.03
	pppGpp	13.76 ± 4.04	0.41 ± 0.03	45.58 ± 17.14	0.48 ± 0.08
Era	**GTP**	11.50 ± 1.61	0.34 ± 0.02	11.11 ± 1.68	0.45 ± 0.02
	GDP	4.94 ± 0.72	0.54 ± 0.02	3.63 ± 0.36	0.70 ± 0.02
	ppGpp	4.21 ± 0.55	0.42 ± 0.01	5.98 ± 0.68	0.55 ± 0.02
	pppGpp	13.87 ± 4.71	0.20 ± 0.02	14.51 ± 2.65	0.35 ± 0.02
HflX	**GTP**	ND	0.65 ± 0.03	ND	0.39 ± 0.06
	GDP	4.92 ± 0.70	0.68 ± 0.02	1.12 ± 0.18	0.77 ± 0.03
	ppGpp	3.37 ± 0.44	0.62 ± 0.02	1.12 ± 0.20	0.77 ± 0.03
	pppGpp	ND	0.48 ± 0.02	ND	0.42 ± 0.04

ND = Not Determined

6.3.2 DRaCALA of RbgA ΔG2 and Era ΔG2 binding to ^{32}P-nucleotides

End-point binding assays were applied to determine the capacity of Era ΔG2 and RbgA ΔG2 to bind to GTP, GDP, ppGpp and pppGpp. DRaCALAs were carried out using 10 μM protein, which was incubated with [α-^{32}P] labelled nucleotides and fraction bound quantified as above (Figure 6.3.2). Interestingly, no significant difference was observed between the wild-type and ΔG2 mutant for either RbgA or Era. This suggests that the switch I loop is not essential for binding to guanine nucleotides, although it is worthy of note that RbgA T155A, which contains a point mutation at a single site within the switch I loop, demonstrated reduced binding to GTP. One caveat of using an end-point DRaCALA is that this technique does not enable calculation of K_D values or rate constants of this interaction, and as such it is impossible to comment on the relative affinity of the ΔG2 mutants compared to the wild-type. It is possible that the fast-phase binding kinetics of this interaction are affected yet still reach the same equilibrium and hence endpoint level of binding. Structural studies of the ΔG2 ligand binding site would likely be required to fully understand the specifics of GTP binding in the absence of the switch

I region, and any effect on fast-state or dynamic binding which our DRaCALA fails to detect could be determined using kinetic techniques such as stopped-flow using MANT-nucleotides. In conclusion, we show that the Era ΔG2 and RbgA ΔG2 mutant variants are able to bind to guanine nucleotides to a similar degree as the wild-types.
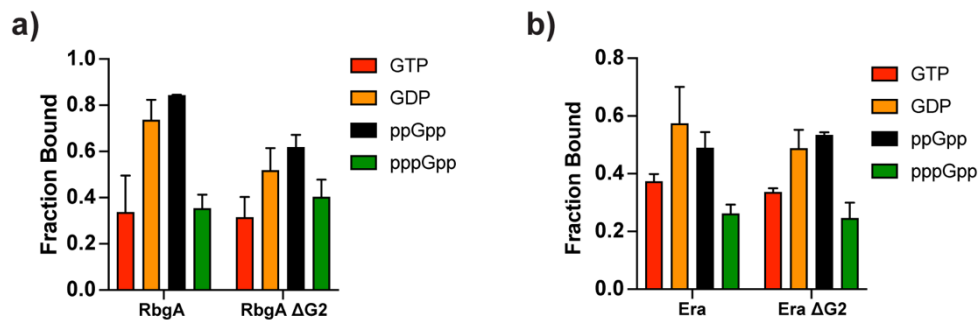
Figure 6.3.2: Deletion of the switch I loop has no impact on nucleotide binding by RbgA or Era. DRaCALAs were carried out as described in the methods section using 10 μM of a) RbgA or RbgA ΔG2, or b) Era or Era ΔG2. The protein was incubated with 1.83 nM [α-^{32}P]-labelled GTP, GDP, ppGpp or pppGpp, and incubated for 5 mins at room temperature before spotting onto nitrocellulose membrane and visualisation using a phosphorimager. Experiments were carried out in triplicate, with error bars showing the standard deviation between each repeat.

6.4 Mutation of the conserved motifs of RA-GTPases abolishes GTPase activity

6.4.1 GTPase activity timecourses of G2 and G4 mutant variants

Following the observation that mutation of the conserved G2 threonine does not seem to drastically affect the nucleotide binding capacity of the four RA-GTPases, we proceeded to investigate the effect of the G2 and G4 mutations on GTPase activity. The mechanism of GTP hydrolysis in RA-GTPases is consistent with all known P-loop NTPases, utilising a coordinate water molecule activated by adjacent divalent metal (in this case Mg^{2+}) cofactors to carry out S$_N$2 nucleophilic attack on the γ-phosphate of GTP (Hamlin *et al.*, 2018; Mishra and Lambright, 2016), resulting in the formation of GDP and the release of inorganic phosphate. In the case of the four RA-GTPases included in this study, this catalytic water molecule is coordinated by a Mg^{2+} cofactor, which in turn is coordinated by the conserved G2 threonine located within the switch I loop. Mutation of this residue to an alanine was expected to remove the capacity of this G2 motif to coordinate the crucial Mg^{2+} cofactor and thus abolish hydrolytic activity. Since the G4 mutants cannot bind to GTP, it was expected that they would also exhibit no GTPase activity.

To test these hypotheses, GTPase activity timecourses were carried out to monitor the enzymatic hydrolysis of GTP into GDP over time (Figure 6.4.1). As mentioned in Chapter 3, 70S ribosomes were included in the mixture to act as the GAP by *in trans* provision of a crucial catalytic moiety. An excess of cold GTP was also included so as not to limit the reaction through ligand depletion, and the mixture

was spiked with [α-^{32}P]-labelled GTP to provide a means of tracking the reaction progress via TLC as described previously (Chapter 3). A GTP-only control was included to rule out any background hydrolysis influenced by the length of incubation, and a 70S control was included to rule out any background hydrolysis due to the ribosomes. In the case of RsgA, RbgA and HflX (Figure 6.4.1 a, b, d), the G2 threonine mutants were completely lacking GTPase activity, in line with the negative GTP-only control. The Era T40A mutant displayed some residual GTPase activity (Figure 6.4.1c), albeit much lower than the wild-type. Alongside the wild-type levels of GTP binding that T40A exhibits, this residual GTPase activity could be attributed to a compensatory effect of the adjacent T41 residue. In all cases (Figure 6.4.1), the G4 lysine mutations exhibit no GTPase activity as expected due to the lack of GTP binding. Thus, with these mutations we have generated variants of RsgA, RbgA, Era and HflX that are either able to bind but not hydrolyse GTP (G2 threonine mutants), or that are unable to bind nor hydrolyse guanine nucleotides (G4 lysine mutants). These will allow further investigation into the role of the ON/OFF cycle in ribosome assembly *in vivo*, by having RA-GTPase G2 variants trapped in either the GTP-bound ON state or G4 variants in the apo OFF state. Furthermore, these mutants may provide insight into the effect of (p)ppGpp-mediated inhibition of RA-GTPase activity, by mimicking the inhibited (OFF) state.
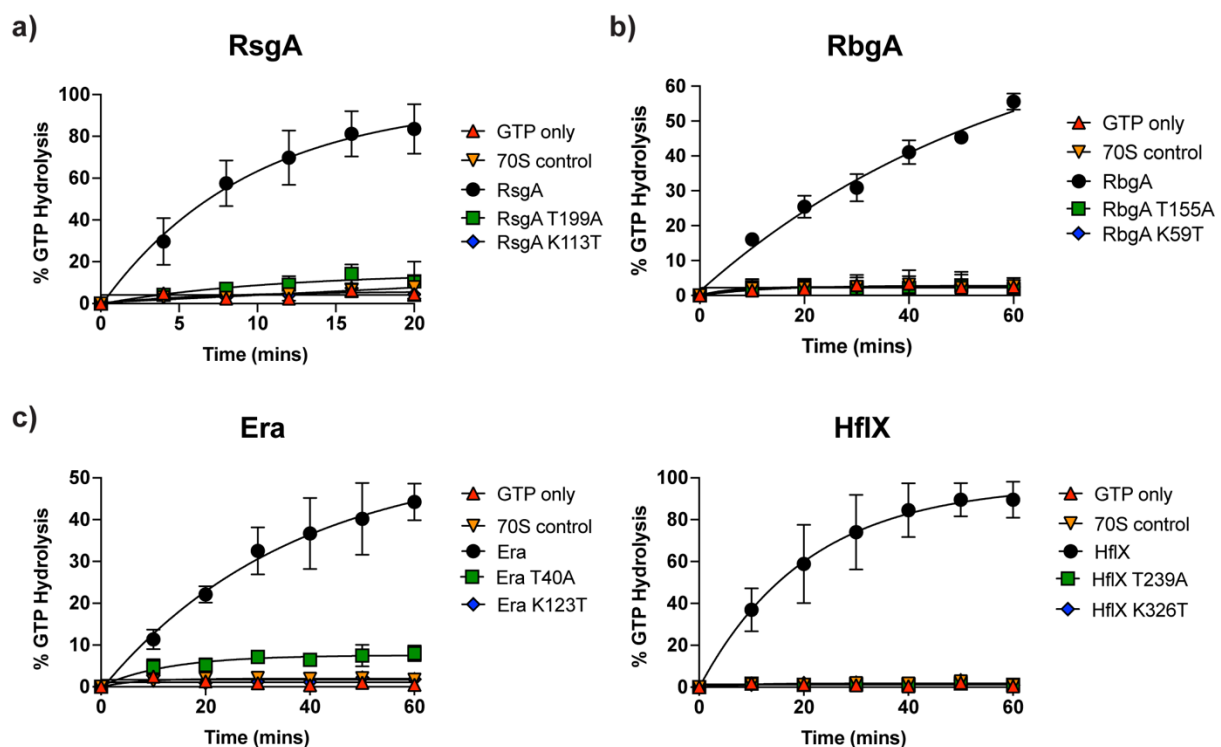
Figure 6.4.1: Mutation of the G2 and G4 residues of RA-GTPases abolishes GTPase activity. 0.1 μM recombinant wild-type or mutant a) RsgA, b) RbgA, c) Era or d) HflX was incubated with 0.1 μM 70S ribosomes and 1 μM cold

GTP spiked with 1.83 nM [α-^{32}P]-labelled GTP, and incubated at 37°C for either 20 mins or 60 mins. Samples were taken every 4 mins over a 20 min timecourse, or every 10 mins over a 60 min timecourse. Percentage hydrolysis was calculated via TLC and pixel densitometry as described in the methods section. Experiments were carried out in triplicate, with error bars representing standard deviation between repeats.

6.4.2 GTPase timecourses of RbgA ΔG2 and Era ΔG2

Structural studies have frequently implicated the switch I loop as a whole in controlling the activity of the GTPase, both in terms of GTP hydrolysis and also secondary target binding. It has been shown that upon binding GTP, switch I repositions in order to adopt the conformation required to correctly orient the catalytic water molecule (Pausch *et al.*, 2018), thus enabling hydrolysis. This is in fitting with our structural models of RsgA in the GDP, ppGpp and apo OFF states (Chapter 5), each of which exhibit a disordered switch I, whereas solved structures of *E. coli* RsgA homologues in the GMPPNP-bound form show increased loop order (López-Alonso *et al.*, 2017b; Razi *et al.*, 2017) while in the 30S-bound ON conformation. As such we expect our ΔG2 variants to lack GTPase activity due to the inability to coordinate the Mg^{2+} cation, and therefore inability to activate the nucleophilic water molecule.

In the previous section we demonstrated that deletion of the Switch I region in RbgA and Era did not affect the nucleotide binding capability of these proteins, so the next step was to investigate the effect of Switch I deletion on the GTPase activity of these protein variants. To this end, timecourses of GTP hydrolysis were carried out (Figure 6.4.2) As for the G2 and G4 point mutants above, recombinant protein was incubated with an excess of cold GTP spiked with [α-^{32}P]-labelled GTP, and samples were taken every 3 mins for RbgA or every 10 mins in the Era timecourses to enable quantification of GTP hydrolysis over time. For both RbgA and Era, deleting the switch I loop completely abolished GTPase activity as expected, as the switch I loop facilitates orientation of the catalytic water molecule. These deletion mutants in the switch I loop of RbgA and Era will enable further investigation into the role of switch I in the activity of RA-GTPases, especially regarding the role of this region within the interaction interface between the RA-GTPase and the ribosomal subunits.
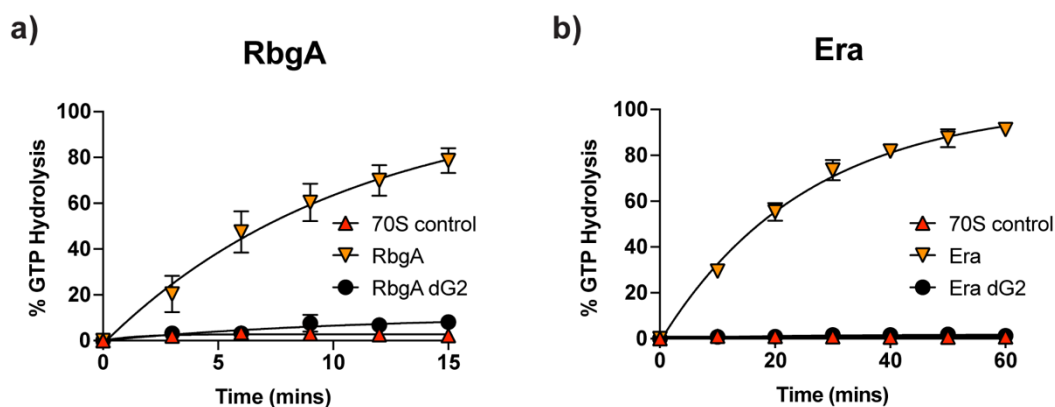
Figure 6.4.2: Deleting the switch I loop of RbgA and Era abolishes GTPase activity. 0.1 µM recombinant wild-type or ΔG2 a) RbgA or b) Era was incubated with 0.1 µM 70S ribosomes and 1 µM cold GTP spiked with 1.83 nM [α-^{32}P]-labelled GTP, and incubated at 37°C for either 15 mins or 60 mins. Samples were taken every 3 mins in the case of RbgA, and every 10 mins in the case of Era, and nucleotides were separated via TLC as described in the methods section. Experiments were carried out in triplicate, with error bars representing standard deviation between repeats.

6.5 Circular Dichroism (CD) spectroscopy of mutant RA-GTPase variants

We showed in Section 5.3 that mutating the conserved G2 threonine of the four RA-GTPases did indeed impact GTP binding in RbgA and RsgA, however it had minimal effect on the binding of other nucleotides or on the binding of GTP by Era and HflX. This in itself suggests a fully structured active site, which retains the tertiary structure necessary to facilitate most ligand binding even if the catalytic residue is lacking. The same can be said in the case of the ΔG2 mutations of RbgA and Era, which retain wild-type levels of nucleotide binding regardless of the absent switch I region. On the other hand, mutation of the conserved G4 lysine residue completely abolishes nucleotide binding of all four RA-GTPases in question. While this could simply indicate that this conserved lysine residue is essential for guanine accommodation in the active site as postulated, another possibility is that the lysine to threonine substitution structurally destabilised the active site, or perhaps even the entire protein. The probable impact of any single mutation on the overall structural integrity of a protein can be estimated *in silico* using a rigidity analysis pipeline (Siderius and Jagodzinski, 2018), or *in vitro* using a variety of techniques such as gel filtration or CD spectroscopy. Here, we employ CD spectroscopy to analyse the overall composition of the protein secondary structure, under the assumption that any sort of structural destabilisation will negatively influence the formation of either α-helices or β-sheets during protein folding.

6.5.1 CD Spectroscopy of G2 and G4 mutant variants of Era

CD spectroscopy is a very sensitive technique, with irregularities between samples leading to distorted data. Prior to carrying out this assay, numerous minimal buffers were tested to check for background

CD signal (data not shown). Sodium Phosphate buffer with added 50 mM NaCl was chosen due to the formulaic simplicity, lack of observed CD signal and suitable ionic strength. After extensive dialysis of the protein samples into the same volume of buffer, some of the dialysis buffer was taken for use as a blank during CD spectroscopy. Protein samples were then normalised to 10 μM through dilution in the dialysis buffer, to maintain exact buffer composition between the blank and samples. Samples were then analysed using SDS-PAGE and band densitometry to confirm equal concentration (Figure 6.5.1a). The different secondary structures that a protein commonly has, α-helices and β-sheets, give different peaks and troughs on the CD spectrum which can give rough information on the secondary structure composition. For α-helices, a peak at 193 nm and troughs at 208 nm and 222 nm are expected, whereas for β-sheets, a peak is expected at 195 nm and a trough at 218 nm (Greenfield, 2006).

For the wild-type and T40A mutant, very comparable spectra were observed with strong troughs at 208 nm and 222 nm, indicating the presence of α-helices, and weak troughs at 218 nm, indicating the presence of β-sheets (Figure 6.5.1b). The strength of the 208 nm trough is expected, as the central GTPase domain of Era is a helical bundle (Anand *et al.*, 2006), with helices also present in the accessory KH domain. The K123T mutant shows a different signal however (Figure 6.5.1b). Less pronounced troughs are still present at 208 nm, 218 nm and 222 nm, however the signal amplitude is much lesser than either the wild-type or the T40A mutant. This could imply several things, namely that there is a large difference in either protein or buffer concentration, or that there is a difference in secondary structure between protein samples. Given that band density on the sample SDS-PAGE (Figure 6.5.1a) was consistent across variant, we conclude that there is a structural difference between the K123T mutant and the wild-type. The high tension (Figure 6.5.1c) also differs in the case of the K123T mutant when compared to the wild type, indicating that the distribution of molecules in solution may be less uniform due to protein aggregation or some other factor, perhaps induced by the disorder among unstructured protein regions. Overall, it appears that the G2 threonine substitution results in a stable and structured protein variant, whereas the G4 substitution results in an unstable or otherwise unreliable protein variant which appears to lose structure within solution.
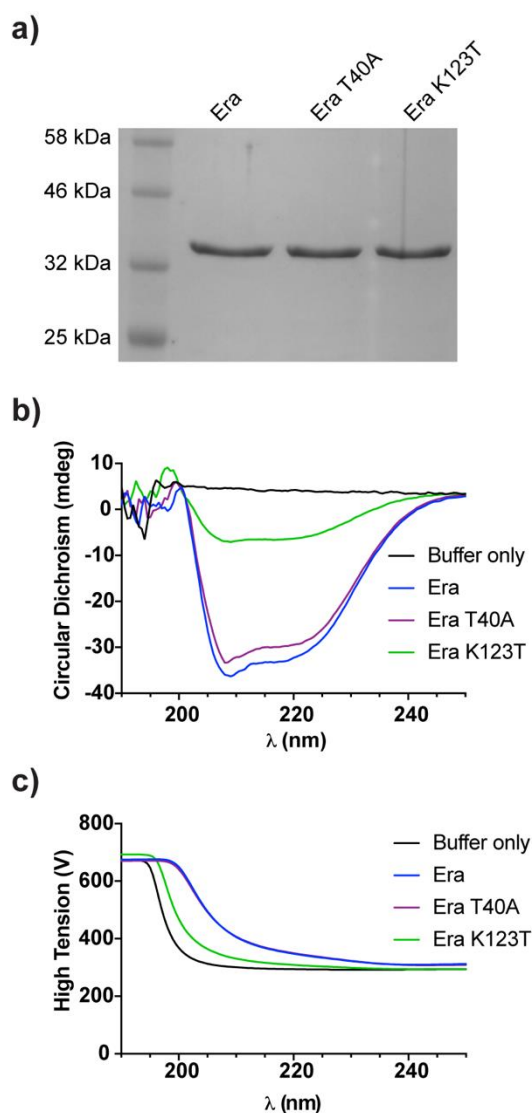
Figure 6.5.1: Analysis of the secondary structure composition of Era T40A and K213T mutant variants. a) SDS-PAGE analysis of Era, Era T40A and Era K123T post dilution to 10 μM in preparation for CD spectroscopy. Protein samples were loaded onto a 12% polyacrylamide gel, then stained using Coomassie Brilliant Blue. Pixel densitometry was carried out using ImageJ (data not shown) to enable comparison of concentrations. b) CD spectroscopy and c) High Tension spectra of buffer background (black), Era (blue), Era T40A (red) and Era K123T (green). 10 μM protein sample was loaded into a Jasco J810 spectropolarimeter was used to scan continuously between 190 nm and 250 nm for each protein, with a sampling interval of 0.5 nm and a scanning speed of 20 nm/min. Each spectrum is the average of at least 5 replicates.

6.5.2 CD Spectroscopy of ΔG2 mutant variants

The tertiary structures of RbgA and Era differ somewhat, with RbgA being a member of the circularly permuted family of TRAFAC GTPases. This means that the G1-G5 motifs within the central GTPase domain are oriented differently, with the canonical G1-G2-G3-G4-G5 arrangement being altered to G4-G5-G1-G2-G3 in RbgA. While in terms of the catalytic and enzymatic mechanism, these GTPases are highly similar to canonical GTPases, this does lead to differences in the GTPase domain arrangement and therefore the accessory domain interface. Both RbgA and Era have two domains,

with the C-terminal domains being ANTAR and KH RNA-binding domains respectively. In RbgA, switch I is extended laterally from the main body of the protein, and swings inwards to contact the outermost face of the nucleotide binding site while in the GTP-bound ON state (Pausch *et al.*, 2018). This implies that switch I is not involved heavily in protein structure, as the N-terminus and C-terminus of the loop are located closely in space. The switch I loop of Era, on the other hand, has a much more involved role at the domain interface (Tu *et al.*, 2009). In the OFF state, the loop is extended towards the posterior of the protein, but upon entry into the ON state, the loop packs against the KH domain and the nucleotide binding site. Furthermore, the N- and C-terminal ends of switch I are distally located in Era. This implies that deletion of switch I, while unlikely to destabilise RbgA, may have a profound impact on protein structure and domain stability in Era. In order to investigate this impact, CD spectroscopy was carried out on the Era and RbgA ΔG2 variants.

As described above, protein samples were extensively dialysed into Sodium Phosphate buffer plus 50 mM NaCl and diluted to 10 μM in post-dialysis buffer. Samples were then assayed for regularity in concentration using SDS-PAGE and band densitometry (data not shown), before carrying out CD spectroscopy. In the case of RbgA (Figure 6.5.2a), the spectra were very similar between the wild-type and the ΔG2 variant (Figure 6.5.2ai), indicating a similarity in secondary structure and potential conservation of tertiary structure. The High Tension was also highly similar, indicating a similarity in molecule arrangement and a lack of aggregation (Figure 6.5.2aii). The CD spectra for Era differed slightly between the wild-type and the ΔG2 variant. While the α-helix troughs were similar at 208 nm, the troughs at 218 nm and 222 nm display a difference in curve shape and amplitude between the wild-type and ΔG2 mutant (Figure 6.5.2bi). In the latter, the troughs are much more pronounced and actually exceed the 208 nm trough in terms of amplitude, which is not seen in the wild-type. One possible explanation for this is an increase in the proportion of β-sheets relative to the overall secondary structure composition, which may indicate a loss of order within the helical GTPase domain. Alternatively, it could be due to the two domains being pulled into closer proximity of each other by the deletion of the flexible loop – which effectively alters the tertiary structure of the protein. It seems unlikely that the former is true, as with any sort of unfolding we expect to see an increase in aggregation and thus a decrease in High Tension, whereas we actually see an increase in High Tension (Figure 6.5.2bii). Thus, we conclude that the Era ΔG2 protein variant is stable albeit altered in some way compared to the wild-type, likely to be in relation to the domain orientation due to deletion of a section of the domain interface in the switch I loop. All in all, the ΔG2 variants appear to be stable and structured, albeit in the case of Era where some innate change in domain configuration or interaction has led to an alteration in secondary structure composition. Despite this, the nucleotide binding

domain appears to remain functional (Figure 6.3.2) and so precise structural studies would be required to elucidate the nature of this alteration.

a)i

a)ii

b)i

b)ii
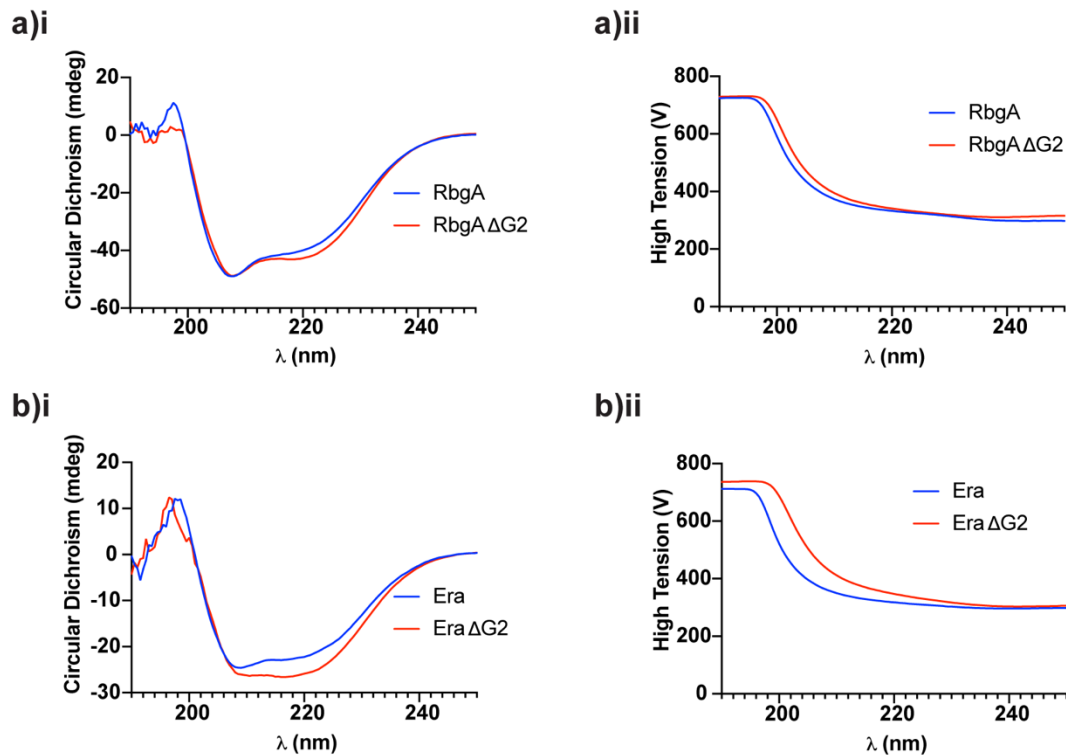
Figure 6.5.2: Deletion of the switch I loop of RbgA and Era does not destabilise the protein. i) CD spectroscopy and ii) High Tension analysis of a) RbgA ΔG2 and b) Era ΔG2. 10 μM protein sample was analysed using a Jasco J810 spectropolarimeter, using continuous scanning between 190 nm and 250 nm. The sampling interval was 0.5 nm, and the scanning speed was 20 nm/min. Each spectrum is the average of at least 5 replicates. Wild-type samples are represented in blue, while ΔG2 variants are represented in red.

6.6 The interaction of mutant RA-GTPase variants with ribosomal subunits

As mentioned previously, switch I undergoes drastic conformational change upon binding to GTP, during which the usually disordered loop docks into an ordered position to coordinate the bound Mg^{2+} cofactor and a non-bridging oxygen atom of the γ-phosphate of GTP (Carvalho *et al.*, 2015). This docking of the switch I loop primes the GTPase to undergo hydrolysis upon receiving the correct stimulus, in the case of RA-GTPases this would be binding of the correctly matured rRNA target motif on the ribosomal subunit. Furthermore, this loop docking is thought to be the defining factor in the switch between the OFF and ON states of P-loop GTPases, which governs the ability of the GTPase to associate with the downstream target protein/rRNA, if applicable. As discussed in Section 4, we have two working hypotheses regarding the mechanism of (p)ppGpp-mediation inhibition of ribosome association: 1) The switch I loop in the docked ON state forms specific interactions with the target binding site, be that rRNA or r-protein, to facilitate interactions with the ribosome which are disrupted

upon (p)ppGpp binding, or 2) The switch I loop forms no specific interactions, and instead docking of this loop in the ON state removes a non-specific steric hindrance to association, a steric hindrance which (p)ppGpp binding maintains. We sought to distinguish between these two hypotheses through investigation of the ribosome binding capacity of our mutant variants, in particular the ΔG2 variant.

Here, we investigate the effect of our Era G2 substitution, G4 substitution and ΔG2 variant on ribosome association, through use of ELISA (Figure 6.6). Doubling dilutions of purified staphylococcal 30S ribosomal subunits were adsorbed overnight onto a 96-well plate. Following washing, 6xHis-tagged, recombinantly expressed and purified wild-type, G2, G4 and ΔG2 protein variants were incubated with the adsorbed ribosomal subunits, and stable association was identified through the use of αHis antibodies developed using 3,3',5,5'-Tetramethylbenzidine (TMB), and quantified using A_{450}. This assay was carried out in the presence of an excess of GMPPNP, to ensure that the RA-GTPases remain trapped in the ON state during which ribosome association can be expected for the wild-type. The wild-type Era, T40A mutant and ΔG2 mutant all show high levels of association to the 30S. The K123T mutant, however, shows no binding. It has been previously suggested that the apo state of Era is capable of binding to the 30S (Sharma *et al.*, 2005; Tu *et al.*, 2009) (Chapter 4), which suggests that the K123T substitution in Era and perhaps the G4 lysine to threonine substitution in general serves to destabilise the protein rather than trap the protein in an apo OFF conformation as initially intended. This assay was also attempted with RbgA, RbgA T155A, RbgA K59T and RbgA ΔG2, using mature *S. aureus* 50S ribosomal subunits during the ELISA. However in the case of all RbgA variants investigated, the signal:noise ratio of the ELISA assay was very low, leading to a lack of high quality data, difficulty observing trends in the data, and low reproducibility between repeats. While the reasons for this greatly decreased signal as compared to the Era variants are unknown, it is possible that the structure of RbgA may lead to protection of the N-terminal hexahistidine tag, which in turn may reduce the capacity of anti-His antibodies to recognise the presence of the protein and lead to low signal intensity.

We next sought to better understand the role of switch I in mediating RA-GTPase association to the ribosomal subunit in the presence of ppGpp. Our structural studies (Chapter 5) led us to hypothesise that the 3'-diphosphate of (p)ppGpp would prevent correct switch 1 docking in RsgA, in line with previous observations in the case of *S. aureus* RbgA (Pausch *et al.*, 2018), which would in turn sterically hinder ribosome association in a nonspecific manner. Here, we utilised our Era ΔG2 mutant variant in order to investigate the role of the switch I loop on ppGpp-mediated inhibition of ribosome assembly (Figure 6.6b). Wild-type and ΔG2 Era was incubated with either GMPPNP or ppGpp to encourage

association or dissociation from the 30S subunit respectively. In the case of the wild-type Era, the K_D of Era binding to the 30S subunit decreased from 15.6 nM to 35.8 nM (Table 6.6) when in the ppGpp-bound state compared to the GMPPNP-bound state. However, this decrease in affinity was abolished in the case of the Era ΔG2 variant, which was similarly capable of 30S association whether bound to GMPPNP or ppGpp, with K_D values of 13.5 nM and 9.4 nM (Table 6.6) respectively. The fact that ppGpp is incapable of reducing the affinity of Era ΔG2 to the 30S suggests that the switch I loop is essential for the alteration in ribosome association observed during the ON/OFF cycle, yet does not specifically contribute to association of the RA-GTPase to the subunit.

Overall, we have shown that GTPase activity and the switch I loop are both nonessential for the association of Era to the 30S ribosomal subunit, and that the switch I loop is an essential mediator of efficient ribosome association between different nucleotide-bound states. While in the associative ON state, docking of the switch I loop removes the steric hindrance to subunit association, however upon entry into the OFF state, loop docking is not possible and as such the steric block returns. This data supports the second hypothesis outlined above, in that switch I makes no specific interactions with the ribosome target site to enable association, and instead could serve as a steric hindrance to association while disordered as a result of being in the GDP- or ppGpp-bound OFF-state.
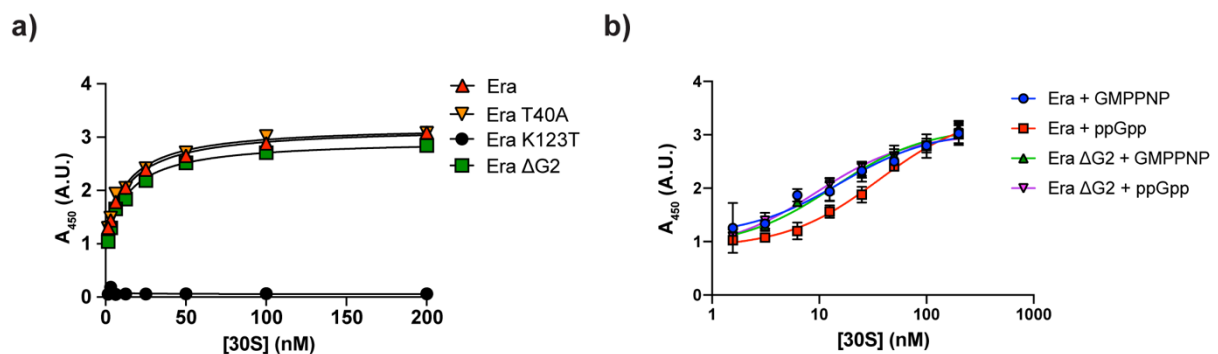
Figure 6.6: The conserved G2 threonine and the switch I loop of Era are not essential for ribosome binding. ELISAs were carried out using constant concentrations of purified recombinant a) Era, Era T40A, K123T and ΔG2 in the presence of GMPPNP or b) Era and Era ΔG2 in the presence of an excess of either GMPPNP or ppGpp. Highly pure 30S ribosomal subunits from *S. aureus* were doubly diluted from an initial 200 nM. Bound proteins were detected using α-His HRP-conjugated antibodies and absorbance was quantified at 450 nm. Experiments were performed in quadruplicate and error bars represent standard deviation.

Table 6.6: The effect of ppGpp on the binding affinity of Era and Era ΔG2 to the 30S ribosomal subunit.

Bound Nucleotide	Era		Era ΔG2	
	K_d (nM)	B_{max} (A_{260})	K_d (nM)	B_{max} (A_{260})
GMPPNP	15.54 ± 5.41	1.99 ± 0.15	13.54 ± 2.84	2.26 ± 0.10
ppGpp	35.84 ± 5.96	2.55 ± 0.10	9.39 ± 1.97	2.20 ± 0.11

Error values shown represent standard error.

6.7 The effect of G2 and G4 RA-GTPase mutant variants in *S. aureus*

Having biochemically characterised the G2 and G4 mutant variants of RsgA, RbgA, Era and HflX *in vitro*, we next sought to better understand the role of the GTPase activity and nucleotide binding capacity of RA-GTPases in a more physiologically representative environment, namely the bacterial cell. To this end, the mutant variants of RsgA, Era and HflX were reconstructed in vectors amenable to replication in *S. aureus*, and introduced into backgrounds lacking the wild-type RA-GTPases in question such that the mutant variant of RsgA, Era or HflX is the only copy of these proteins present in the cell. We employed the multi-copy pCN55iTET plasmid (Charpentier *et al.*, 2004) to enable expression of *era* variants, and the single-copy integrative pCL55iTET shuttle vector in the case of *rsgA* and *hflX* variants (Luong and Lee, 2007). This integrative vector contains the φL54a-encoded *int* integrase and *attP* site, enabling integration into the *attB* site encoded within the *S. aureus geh* gene. Both of these vectors enable anhydrotetracycline (Atet)-inducible expression of the protein of interest. Chromosomal deletion mutants of *rsgA, era* and *hflX* in the *S. aureus* background LAC* were readily available in our lab strain collection, and as such the effect of the mutant variants were assessed following *in trans* complementation of these knockout strains. Seeing as RbgA is an essential protein in Gram-positive bacteria (Seffouh *et al.*, 2019; Uicker *et al.*, 2006), we were unable to generate a chromosomal deletion mutant and as such the *in vivo* implications of RbgA mutant variants were not assessed here.

6.7.1 The effect of the G2 and G4 mutant variants on growth in *S. aureus*

The RA-GTPase Era is thought to be essential in bacteria (Ji, 2016; Tu *et al.*, 2009), and while this is still thought to be true in the case of *E. coli* and others, the *era* gene has been successfully deleted in *S. aureus* (Wood *et al.*, 2019). While viable, the Δ*era* strain has a profound growth defect in line with that observed in the case of *rsg*A deletion (Corrigan *et al.*, 2016) (Figure 6.7.1a, b). Deletion of HflX, however, had no apparent effect on unstressed growth in rich media, as expected due to the proposed role of this protein in ribosome splitting and repair of heat-shocked ribosomes under heat shock conditions rather than exponential phase ribosome assembly (Dey *et al.*, 2018; Zhang *et al.*, 2015) (Figure 6.7.1c).

As previously demonstrated (Figure 6.3, Figure 6.4), mutation of the G2 threonine residue abolishes GTPase activity through disruption the coordination of the Mg^{2+} cofactor. In the case of RsgA, this also reduces the affinity of GTP binding by around 2-fold. The G4 lysine mutation completely abrogates nucleotide binding and GTPase activity of each protein, although CD spectroscopy raises doubts as to the tertiary structure of these variants. Introduction and expression of RsgA T199A and Era T40A could not rescue the growth defect observed in the respective chromosomal deletion mutants (Figure 6.7.1a, b), indicating that the ability to hydrolyse GTP is essential for protein function. The HflX T239A mutant exhibits no growth defect in line with the chromosomal deletion (Figure 6.7.1c), although further investigation into the ability of these strains to survive heat shock are necessary to draw conclusions as to the role of GTPase activity in the rRNA-repair function of HflX. The G4 lysine mutants of RsgA, Era and HflX each exhibit a profound growth defect (Figure 6.7.1a-c). This is expected in the case of RsgA K113T and Era K123T, due to a lack of protein functionality in the absence of GTPase activity, however the K326T mutant of HflX exhibits a defect in growth which is not present in the chromosomal knockout. This could be due to several factors, including intracellular aggregation, or an accumulation of non-functional protein variants. Interestingly, this phenotype is consistent when expressing HflX K326T in a wild-type LAC* background, indicating that this detrimental effect is independent of the GTPase activity or nucleotide-binding capability of HflX. Since HflX is capable of splitting 70S subunits in the presence of any guanine nucleotide (Coatham *et al.*, 2016; Zhang *et al.*, 2015), and capable of associating with the ribosomal subunits in the apo-state (Chapter 4), it is possible that non-productive association of this K326T variant with the ribosomal subunits may be hindering association in some way. Overall, here we have determined that the GTPase activity of the assembly cofactors RsgA and Era are essential for protein function and important for bacteria growth. The GTPase activity of HflX is dispensable during exponential growth, however expression of the K326T variant which is incapable of binding any nucleotides is detrimental to cell growth.
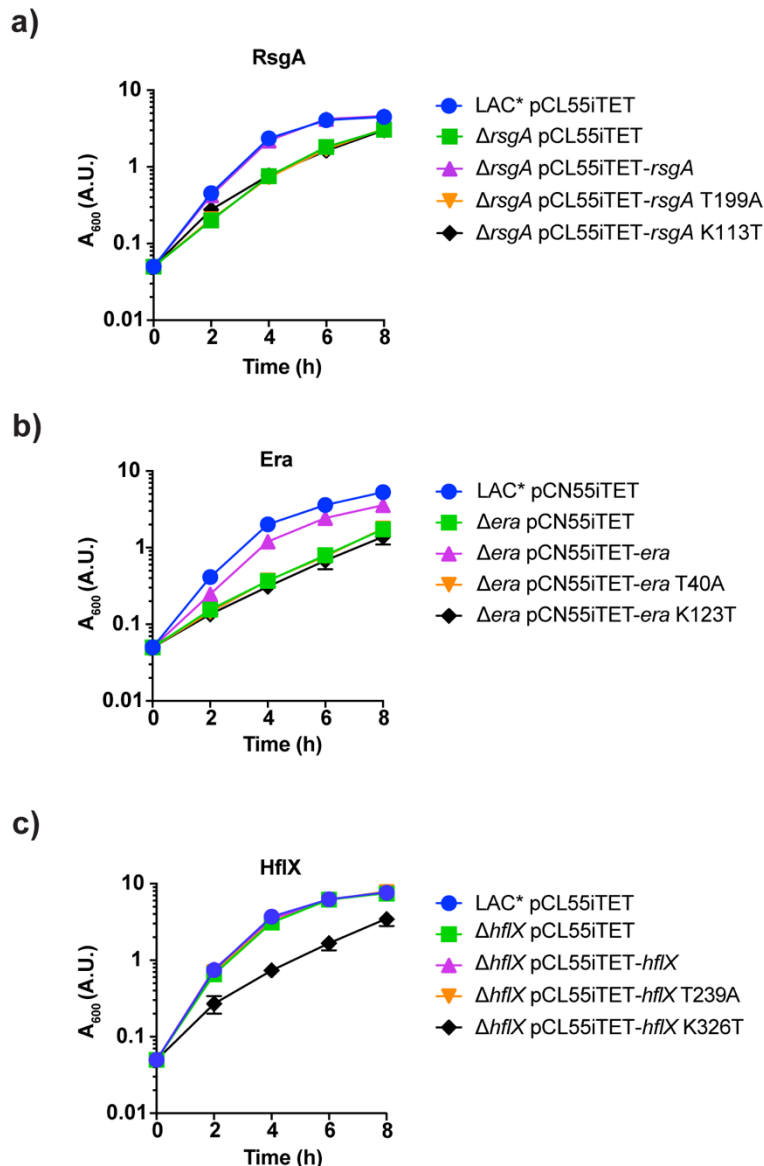
Figure 6.7.1: The effect of mutant RsgA, Era and HflX variants on the growth of *S. aureus*. Growth of *S. aureus* strains a) LAC* pCL55iTET, LAC* Δ*rsgA* pCL55iTET, LAC* Δ*rsgA* pCL55iTET-*rsgA*, LAC* Δ*rsgA* pCL55iTET-*rsgA* T199A and LAC* Δ*rsgA* pCL55iTET-*rsgA* K113T, b) LAC* pCN55iTET, LAC* Δ*era* pCN55iTET, LAC* Δ*era* pCN55iTET-*era*, LAC* Δ*era* pCN55iTET-*era* T40A and LAC* Δ*era* pCN55iTET-*era* K123T, and c) LAC* pCL55iTET, LAC* Δ*hflX* pCL55iTET, LAC* Δ*hflX* pCL55iTET-*hflX*, LAC* Δ*hflX* pCL55iTET-*hflX* T239A and LAC* Δ*hflX* pCL55iTET-*hflX* K326T. Saturated overnight cultures were backdiluted to an A_{600} of 0.05, and grown at 37°C in the presence of 100 ng/ml Atet and the appropriate antibiotics for 8 hrs, with samples taken every 2 hrs and analysed for A_{600}. Experiments were carried out in triplicate, and error bars represent the standard deviation between replicates.

6.7.2 Mutation of the G2 or G4 residues in Era reduced 70S biogenesis

Despite having been implicated in a plethora of cellular functions, including cell cycle control (Gollop and March, 1991), Era is predominantly considered to be a ribosome assembly factor which facilitates maturation of the 30S subunit. Previous studies concerning *era* depletions or knockouts have identified a marked decrease in 70S formation and increase in unprocessed 17S rRNA (Inoue *et al.*, 2003; Wood *et al.*, 2019). We next sought to investigate the role of the GTPase activity of Era in

ribosome assembly by investigating the effect of our T40A and K123T mutants on *S. aureus* ribosome content via sucrose density ultracentrifugation of crude cell lysates. The defect in 70S biosynthesis in the LAC* Δ*era* strain was reasoned to be responsible for the detrimental effect of this deletion on cell growth, and as such we expected that since the G2 and G4 mutants both exhibit a similar slow growth phenotype, they would both also exhibit a reduction in 70S content.

In the wild-type LAC* background containing our empty pCN55iTET expression vector, the ribosome profile (Figure 6.7.2a) shows small 30S and 50S peaks, which may be attributed to *de novo* 30S biogenesis and free subunits following post-elongation splitting of the 70S to enable reformation of the 30S pre-IC. A large 70S peak is observed, with a shoulder representing polysomes, representing the actively translating pool. Consistent with previous observations, deletion of *era* (Figure 6.7.2b) leads to a marked decrease in 70S content, increase in 50S content and a complete absence of 30S and polysome peaks. This excess of free 50S subunits and absence of free 30S subunits ipso facto suggests that biogenesis of the 30S ribosomal subunit is inhibited in the absence of Era, leading to an excess of free 50S. This phenotype is reversed following complementation (Figure 6.7.2c), but is recapitulated upon expression of the G2 T40A (Figure 6.7.2d) and G4 K123T (Figure 6.7.2e) mutants in the Δ*era* background. Interestingly, in the T40A mutant there is a small peak in accordance with 30S content (Figure 6.7.2d, fractions 7-10), suggesting that this mutant may be more able to facilitate ribosome assembly than either the Δ*era* or Era K123T mutant, albeit much less efficiently than the wild-type. Regardless, the slight increase in the 30S pool is insufficient to see even a slight rescue of the slow growth phenotype (Figure 6.7.1b) or indeed the 70S ribosome pool. This indicates that there may also be an issue regarding subunit joining in the GTPase-inactive T40A mutant, which may stem from the ability of this variant to associate with the 30S (Figure 6.6b), but not dissociate in the absence of proper GTPase-driven regulation. This would also support previous observations that Era is involved in what is thought to be the final stage of 30S assembly, prior to 30S pre-IC formation and translation initiation (Chen *et al.*, 2012; Razi *et al.*, 2019; Tu *et al.*, 2011; Tu *et al.*, 2009; Wood *et al.*, 2019). All in all, this data suggests that the GTPase activity of Era is essential for correct 70S formation, however association of Era to the immature 30S subunit in the absence of GTPase activity may be sufficient to increase 30S formation but not 70S formation, likely due to inhibition of subunit association and lack of ON/OFF transitioning following GTP hydrolysis.
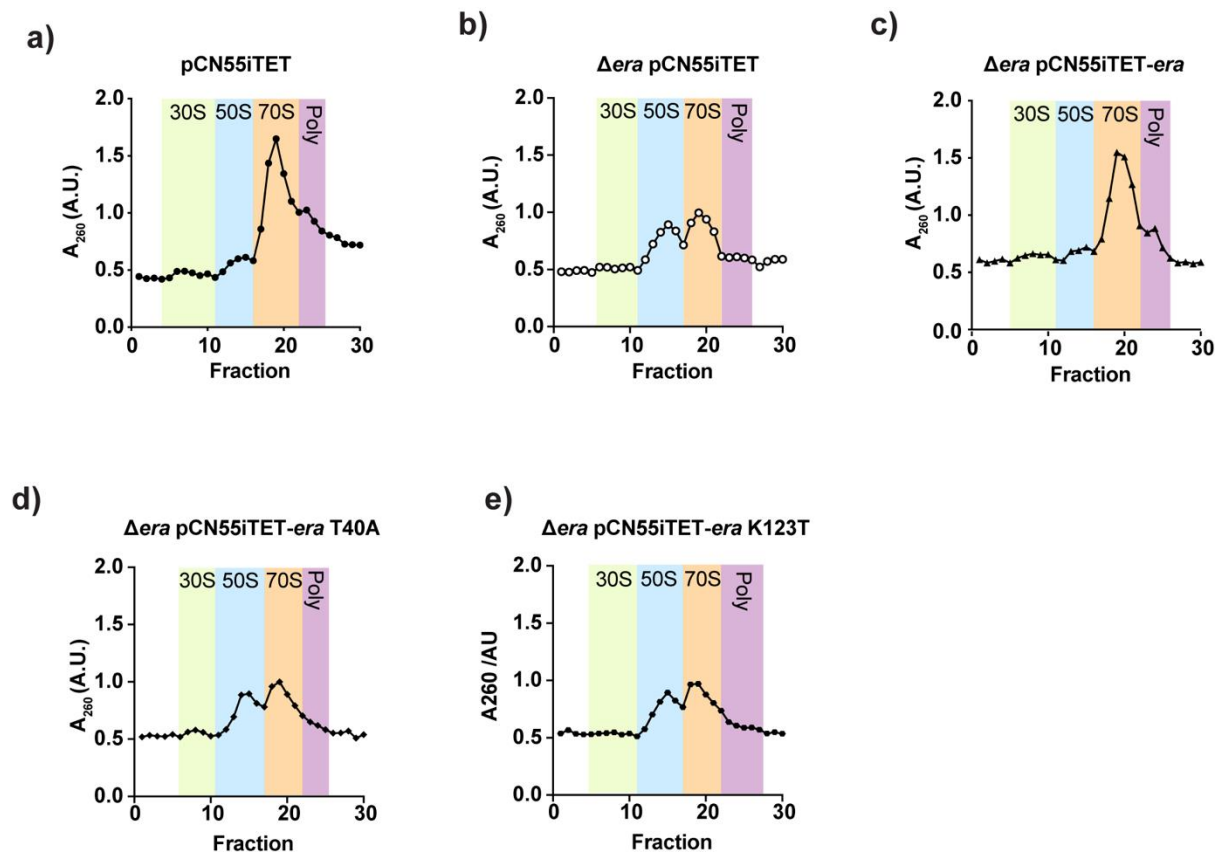
Figure 6.7.2: The effect of Era T40A and K123T mutant variants on cellular ribosome content. Crude ribosome profiles from *S. aureus* strains a) LAC* pCN55iTET, b) LAC* Δ*era* pCN55iTET, c) LAC* Δ*era* pCN55iTET-*era*, d) LAC* Δ*era* pCN55iTET-*era* T40A and e) LAC* Δ*era* pCN55iTET-*era* K123T. Strains were growth to mid exponential phase, and crude cell lysates were applied to a 10%-50% sucrose gradient made up in subunit association buffer, and ribosomal content was assessed following a 7 hr spin at 192,000 × *g*. 250 µl fractions were analysed for RNA content at A_{260}. Expected peaks representing the 30S, 50S, 70S and polysomes are highlighted in green, blue, orange and red respectively.

6.7.3 Inactivation of the GTPase activity of Era reduces translation rate *in vivo*

During the translation elongation cycle, the 30S pre-IC matures into the 30S IC following association of the mature 30S subunit, IF1, IF2, IF3, the mRNA translation initiation region (TIR) and the initiating fMet-tRNA[fMet] (Julián *et al.*, 2011; Vinogradova *et al.*, 2020). The relative complexity of this step makes it the most tightly regulated in the translation elongation cycle, especially when considering the differing affinity of each TIR to the 30S pre-IC while IF2 is in different nucleotide-bound conformations (Vinogradova *et al.*, 2020), and indeed it is the rate of initiation which limits the rate of translation as a whole (Gualerzi and Pon, 2015). While complex, formation of the 30S IC occurs rapidly upon availability of mature 30S subunits due to the presence of an excess of initiation factors, and as such this process is highly dependent on both the efficiency of 30S biogenesis and post-elongation subunit splitting and recycling (Gualerzi and Pon, 2015; Rodnina, 2016). Due to the reduction in 30S biogenesis observed in our Era T40A and K123T mutant variants, we hypothesised that this would reduce the rate of cellular translation, which may account for the slow growth phenotype.

In order to investigate this, we conducted pulse-chase assays using ^{35}S-methionine in order to observe the difference in mid-exponential phase translation rate depending on the presence or absence of Era, Era T40A and Era K123T. This approach was undertaken as a measure of the ability of LAC* strains containing different Era variants to increase their rate of translation in nutrient rich conditions, which stimulates *de novo* ribosome biogenesis (Failmezger *et al.*, 2017) as growth rate increases. Furthermore, culture samples were taken in accordance with A_{600} values rather than following set time periods in order to minimise the effect of different growth rates between mutant strains. Firstly, we tested our experimental system using two antibiotic controls. Chloramphenicol is a known inhibitor of translation through inhibition of the peptidyltransferase centre, and indeed we observe a near complete abrogation of methionine uptake and therefore translation rate following treatment (Figure 6.7.3a), indicating that our system was effective at monitoring changes in the rate of translation. We also examined the effect of a high concentration of mupirocin, a known activator of the stringent response via inhibition of isoleucyl-tRNA synthetase (Reiss *et al.*, 2012), on translation rate. Similar to chloramphenicol, this antibiotic led to a complete loss of translation following treatment, suggesting that translation comes to a near complete halt during the heights of the stringent response. The rate of methionine incorporation in both the wild-type and complement Δ*era* strains (Figure 6.7.3b) increased by around 5-fold upon entry into mid-exponential phase growth, demonstrating the capacity of these strains to carry out efficient *de novo* ribosome biogenesis. The Δ*era*, T40A and K123T strains each exhibited a statistically significant reduction in methionine uptake, with the clean deletion mutant and K123T variant demonstrating similar rates of methionine uptake. The T40A-expressing strain on the other hand did demonstrate a 2.5-fold increase in methionine uptake compared to during stationary phase. This indicates a reduction in translation rate as compared to the wild-type, likely due to a lower capacity for *de novo* ribosome biogenesis in line with our previous observations (Figure 6.7.2). All in all, these data suggest that the lack of Era GTPase activity via mutation of the conserved G2 threonine and G4 lysine residues reduces the translational capacity of the cell in line with a clean deletion of this protein, although translation is not completely inhibited as in the case of chloramphenicol treatment.
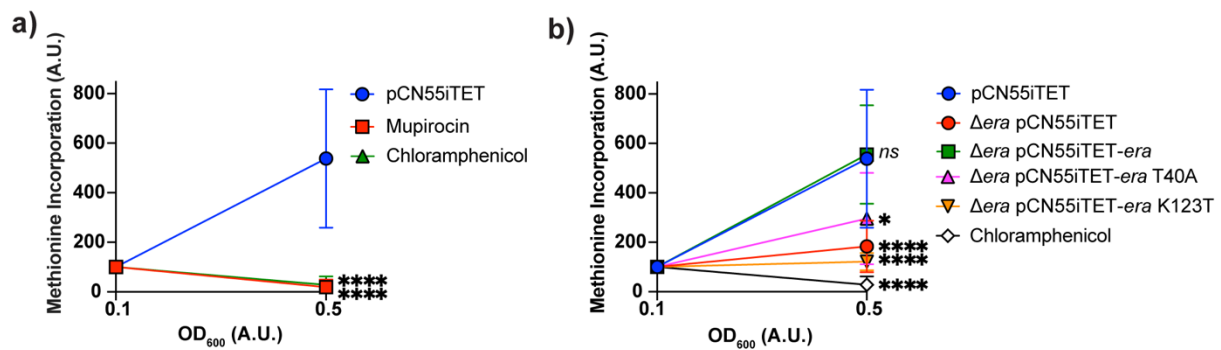
Figure 6.7.3: Era T40A and K123T variants reduce the translational capacity of *S. aureus*. Translation rates of) LAC* pCN55iTET treated with 60 µg/ml mupirocin and b) LAC* pCN55iTET, LAC* Δ*era* pCN55iTET, LAC* Δ*era* pCN55iTET-*era*, LAC* Δ*era* pCN55iTET-*era* T40A and LAC* Δ*era* pCN55iTET-*era* K123T. Cultures treated with 100 µg/ml chloramphenicol were included as a control of inhibition of translation. Points plotted are the average of 5 independent replicates, with error bars representing the standard deviation between individual replicates. Statistical analyses were carried out using two-way ANOVA (mixed-effects analysis), with differences between each sample and the wild-type LAC* pCN55iTET represented by stars as follows: *, $p < 0.05$; ****, $p < 0.0001$.

6.8 Discussion

In this chapter, we aimed to generate and functionally characterise three RA-GTPase mutant variants *in vitro*: a single residue substitution in the highly conserved G2 threonine and G4 lysine residues of each of the four RA-GTPases in question. We then recreated the G2 and G4 mutants of RsgA, Era and HflX *in vivo* using Δ*RA-gtpase* backgrounds in order to assess the impact of these variants on cell growth, and further investigated the effect of these mutant Era variants on cellular ribosome content and translation rate. We also generated a deletion in the switch I of RbgA and Era. The point mutations were generated with the aim of investigating the impact of altering RA-GTPase activity *in vivo* in the native host, namely *S. aureus*, and as such had to be fully characterised prior to this transition. The ΔG2 mutants were generated in order to better understand the role of this intrinsically disordered region on ribosome association, given that in Chapter 5, we hypothesised that suboptimal positioning of switch I is responsible for inhibiting the hydrolytic activity of RA-GTPases while in the (p)ppGpp-bound state. Additionally, in Chapter 4 we hypothesised that this incorrect positioning of the switch I loop is responsible for the reduction in ribosome association observed in the (p)ppGpp-bound state.

Here, we first characterised the ability of the mutant variants of RsgA, RbgA, Era and HflX to bind to the guanine nucleotides GTP, GDP, ppGpp and pppGpp. We observed a decrease in the affinity for GTP in the case of RsgA T199A and RbgA T155A and no change in the affinity for GTP in the case of Era T40A (Figure 6.3.1) The K_d of HflX binding to GTP was not calculable under these conditions. The overall K_D values for the binding of GDP, ppGpp and pppGpp were unaffected in the case of all four RA-GTPase G2 mutants, although it is impossible to rule out any microscale changes in the binding kinetics (k_1, k_{-1}) which may result in a similar binding equilibrium. It was expected that the binding affinity of both

GDP and ppGpp would be unaffected by the G2 mutation, as the presence of a 3' γ-phosphate is an essential requirement of G2 threonine interaction upon switch I docking. We were previously unsure of the effect of the G2 mutation on pppGpp binding, which contains the 3' γ-phosphate but also the 5' diphosphate which prevents stable switch I docking and therefore prevents the interaction between the G2 threonine and 3' γ-phosphate (Pausch *et al.*, 2018), and indeed the pppGpp-binding capacity of the G2 mutant variants appears unaffected. The G4 lysine substitution on the other hand unerringly abolished the nucleotide binding capacity of each RA-GTPase. The ability of the G2 threonine mutation of RsgA to bind GTP with an affinity comparable to wild-type was surprising. Previous work from our lab showed that recombinant MBP-RsgA-T199A had greatly reduced GTP binding capacity (Corrigan *et al.*, 2016), although the precise K_d of this interaction was not calculated and so the fixed-point DRaCALA may have accentuated the difference in affinity. Another possibility is that the presence of the MBP tag may in some way alter the binding of GTP or the flexibility of the switch I loop. Contrary to that, mutation of either one of the adjacent threonine residues in Era has negligible effect on GTP binding (Shimamoto and Inouye, 1996), although mutation of both reduced the GTP-binding capacity of Era. Likewise, mutation of the G2 threonine of the GTPase MnmE has no effect on GTP binding (Martínez-Vicente *et al.*, 2005).

Interestingly, both RsgA and RbgA, which in this study show decreased GTP binding when the G2 threonine is substituted, are members of the circularly permuted family. Within the circularly permuted GTPases, a common feature is that the switch I loop is much longer than the cognate region in canonical GTPases, leading to many difficulties resolving this region through crystallographic studies (Levdikov *et al.*, 2004; Pausch *et al.*, 2018). This disparity is likely due to the structural rearrangement of the GTPase domain, as although the functional motifs form the highly conserved nucleotide binding pocket, the overall domain architecture differs from canonical proteins in order to compensate for this. Thus, the length and relative displacement of the switch I loop from the globular body of the GTPase is larger in the circularly permuted family, leading to more dramatic rearrangements upon GTP binding (Sudhamsu *et al.*, 2008; Vetter *et al.*, 1999). This may be partially responsible for the reduction in GTP binding upon mutation of the G2 threonine residue, due to the stabilisation of the longer switch I loop being more energetically unfavourable than the canonical, non-circularly permuted equivalent and therefore increasing the importance of the G2 threonine-γ-phosphate interaction. It is also possible that due to GTP binding being the initial step of the OFF-ON switch, stabilisation of this interaction by switch I is reduced in RsgA and RbgA which increases the rate of dissociation. A similar model could be applied to the ΔG2 variants, although no difference in binding capacity was observed when compared to the wild-type (Figure 6.3.2).

We have shown here that mutation of either the G2 or G4 residue, or the deletion of the switch I loop (ΔG2) renders the RA-GTPase unable to hydrolyse the bound GTP (Figure 6.4.1, 6.4.2). This was expected, due to the role of the G2 threonine in hydrolysis. Upon initial binding of GTP, switch I coordinates both a non-bridging oxygen of the γ-phosphate of GTP and the crucial Mg^{2+} cofactor. During catalysis, this Mg^{2+} generates an active water molecule which is capable of S_N2 nucleophilic attack on the β-γ-phosphodiester link through a pentavalent intermediate (Carvalho *et al.*, 2015). This coordination relies on H-bonding between the hydroxyl group of the G2 threonine side chain and the Mg^{2+} cofactor, and as such any mutation removing this specific H-bonding potential (i.e. G2 or ΔG2) will render the protein GTPase-null, and indeed this has been shown to be the case multiple times in previous studies (Corrigan *et al.*, 2016; Martínez-Vicente *et al.*, 2005; Shimamoto and Inouye, 1996; Vetter *et al.*, 1999). The G4 lysine mutation however removes all nucleotide binding capacity of the protein, whether by preventing the necessary stacking interaction required to bind the guanine ring, or whether by destabilisation of the GTPase domain as a whole. As such, no activity is expected.

It is worth noting that the wild-type RbgA samples used in Figures 6.4.1b and 6.4.2a were from different preparations, as were the 70S ribosomes included in the reaction. While the concentrations of both were normalised between experiments according to absorbance at 280 nm and 260 nm respectively, differences in the quality of the preparation may be responsible for the different reaction rates observed. In future experiments, the quality of the preparations should be assessed more thoroughly using gel filtration and GTPase timecourse experiments should use a greater excess of nucleotide in order to prevent saturation of the reaction. Not only would this decrease the issue of differences in activity between preparations, it would also enable apparent rate calculation of the linear hydrolysis of GTP, and thus calculation of Michaelis-Menten kinetics such as the V_{max} and K_m. As no specific kinetic parameters were calculated from these assays, they were used purely for arbitrary comparison between the wild-type and mutant variants and since each assay was internally controlled, the results and observations can still be considered valid.

While circular dichroism spectroscopy is a useful technique for providing insight into the secondary structure of protein samples, it is important to bear in mind some of the caveats and limitations associated with this. While useful for estimating the rough overall secondary structure composition of a protein, attempting to gain specific structural information from this technique is nigh impossible. The close proximity and minima and maxima, especially the 218 nm and 222 nm troughs relative to β-sheets and α-helices make them difficult to distinguish. This leads to the issue of determining composition of a protein rich in both α- and β-elements (Khrapunov, 2009). Since the conserved GTPase domain fold consists of α-helices surrounding a central β-sheet, and in the case of the Era, the

C-terminal KH domain is a mix of both α- and β-elements, the signals for each can contribute to adjacent troughs. Here, we applied CD spectroscopy to determine whether mutation of the RA-GTPases destabilised the protein. All RA-GTPases have accessory domains that are spatially distinct from the central GTPase domain, and as such are likely to be unaffected by any mutation in the GTPase domain. It is also likely that in the event of destabilisation of a domain, stochastic formation of secondary structures will still occur due to entropic progression (Bowler, 2012) and thus influence the signal. Tertiary structure is not represented at all during CD spectroscopy, so the differences observed between spectra in Figures 6.5.1 and 6.5.2 may not represent the full extent of any tertiary structure alteration. More accurate insight into protein stability and structure can be obtained through the application of filtration techniques which are influenced by tertiary structure – for example native PAGE or size exclusion chromatography, which would separate structured and unstable protein variants clearly and reliably.

Through use of ELISA, we showed that mutation of the G2 threonine and deletion of the switch I loop in Era had no impact on ribosome association, whereas mutation of the G4 lysine abolished ribosome association. Furthermore, the switch I loop is essential for mediating the lowered affinity of Era to the 30S subunit while in the ppGpp-bound OFF conformation. These data support the hypothesis that the switch I loop acts as a steric block to RA-GTPase-ribosome association while proximal and disordered in the OFF state. Extensive sequence alignments carried out using multiple RA-GTPases and their homologues failed to identify any residue conservation aside from the G2 threonine, which indicates that switch I may not be involved in specific interactions with the ribosome target site. Should this be the case, we would expect to find conservation between the switch I region of RA-GTPase homologues, which are mostly associated with the same target site between organisms. Our structural models of RsgA are lacking order of the switch I loop, and as such no conclusions can be drawn regarding any interactions which may form at the interface. Previously published cryo-EM models of *E. coli* YjeQ-GMPPNP (López-Alonso *et al.*, 2017b; Razi *et al.*, 2017) associated with the 30S subunit show switch I docking into the minor groove of h44. Other than the catalytic histidine residue which facilitates GTP hydrolysis, switch I of RsgA/YjeQ contains no basic or aromatic amino acid residues as would be expected for nucleotide-interacting regions (Baker and Grant, 2007) to form strong interactions with the rRNA backbone. As discussed in Chapter 5, the role of the switch I loop as a mediator of complex formation would fit with our two-step model of RA-GTPase-ribosomal subunit association (Chapter 4), in which case the initial interaction (k_1) would be mediated by the accessory RNA-binding domains, and the secondary slow-phase reaction (k_2) would be mediated by stabilization of the complex following switch I docking.

Finally, we showed that introduction of the Era T40A and K123T mutant variants into a LAC* Δ*era* background failed to rescue the abnormal ribosomal profile present in this background, and that the rate of translation is reduced compared to the wild-type following expression of these variants. The inhibitory effect of (p)ppGpp on RA-GTPases couples both inactivation of the GTPase activity and prevention of stable association of the GTPase to the 30S or 50S subunit. The downstream effect of this may be similar to the G2 and G4 mutants employed here, although neither will perfectly recapitulate the (p)ppGpp-bound OFF state. The G2 mutation appears to trap the protein in the GTP-bound ON state while bound to GTP in energetically favourable conditions, and the G4 appears to produce a completely nonfunctional protein variant which is incapable of ribosomal interaction. In the case of Era, we have shown that Era is capable of 30S association while in the apo state (Chapter 4), whereas the G4 point mutant is not (Figure 6.6), and as such does not represent the apo OFF state as initially intended. Era is thought to be involved in late-stage assembly of the 30S subunit following association to the 3' of the 16S rRNA close to the anti-Shine-Dalgarno sequence (Tu *et al.*, 2011; Tu *et al.*, 2009), with functions including recruitment of late-stage processing factors such as the endoribonuclease YbeY (Vercruysse *et al.*, 2016) and prevention of premature subunit joining (Razi *et al.*, 2019). We have established that the T40A variant of this protein is capable of binding to GTP (Figure 6.3.1a) with a similar affinity to the wild-type, and that this variant remains capable of associating with the 30S subunit (Figure 6.6), with the only apparent effect being a complete loss of GTPase activity. This suggests that the maturation events for which Era is responsible may still occur, and that Era may fail to undergo GTPase-mediated dissociation following this maturation to enable subunit joining and translation initiation – leading to the presence of free 30S subunits and reduction in 70S ribosomes observed in Figure 6.7.2d. This may also account for the increase in translation rate of the T40A mutant relative to the clean deletion and K123T variant, as some stochastic dissociation of Era from the ribosome may occur to yield mature 30S subunits. An interesting continuation of this study would consider the ongoing translation during the stringent response (Vinogradova *et al.*, 2020), and whether this is due to the constant recycling of the extant pool of mature ribosomes in the absence of *de novo* synthesis (Razi *et al.*, 2019) upon inhibition of all (p)ppGpp-binding ribosome assembly factors, or whether *de novo* ribosome biogenesis does occur. Pulse-chase analysis of stringent cells with a detectable isotope, such as ^{15}N would enable identification of nascent ribosomal particles via quantitative mass spectrometry (Chen *et al.*, 2012).

Era-depleted strains of *E. coli* (in which Era is thought to be essential) were found to be completely incapable of producing mature 30S subunits (Razi *et al.*, 2019), instead accumulating a variety of immature subunits ranging from early to late-stage conformations resulting from unusual 16S rRNA

folding patterns. In *S. aureus*, however, Era is nonessential and therefore the ability of this organism to generate 30S subunits in the absence of Era should be investigated further, potentially by quantitative mass spectrometry and high-resolution cryo-EM to identify each 30S intermediate present in the cell, in order to form a rationale for this difference in essentiality. It is worth considering that our hypothesis attributing the growth defect in the Era mutant strains to a reduction in ribosome content and translation rate does not take into account the previous observations concerning the role of Era in the cell division cycle (Britton *et al.*, 1998; Gollop and March, 1991). Depletion of the wild-type Era in *E. coli* has been shown to lead to accumulation of cells in the pre-partitioning two-cell stage via an unknown mechanism (Britton *et al.*, 1998), and so it is possible that the observed growth defect is in fact a compounding effect of the roles of Era in cell growth and partitioning as well as ribosome assembly. In order to clarify this matter, further understanding of the role of Era in cell cycle control is required in order to experimentally separate these two distinct functions of Era.

In conclusion, here we have generated and functionally characterized point mutations of the conserved G2 threonine and G4 lysine in RsgA, RbgA, Era and HflX, and a deletion of the 10 residue switch I loop of RbgA and Era. We have also examined the effect of the G2 and G4 mutations of RsgA, Era and HflX *in vivo*, particularly in the context of the effect of the Era T40A and K123T mutation on ribosome assembly and translation rate, demonstrating that abrogation of the GTPase activity of Era is sufficient to recapitulate the Δ*era* phenotype in most cases. This highlights the importance of GTPase activity and a functional ON/OFF cycle for the function of RA-GTPases, lending further insight into the potential effects of (p)ppGpp-mediated inhibition of these proteins.

Chapter 7 – Discussion

In all known organisms, including both eukaryotes and prokaryotes, ribosome assembly factors play an essential role in facilitating the assembly of the mature ribosome to enable efficient cellular translation and growth (Connolly and Culver, 2009; Hage and Tollervey, 2004; Strunk and Karbstein, 2009). Indeed, the essentiality of many of these proteins, such as RbgA and YsxC (Cooper *et al.*, 2009; Gulati *et al.*, 2013) in *S. aureus* leads to speculation regarding the potential of these proteins as antibiotic targets. A subset of these proteins, central to this study, also function as stringent response effector proteins to facilitate survival of transient stress conditions. The stringent response is a crucial regulator of virulence in many known pathogens (Godfrey *et al.*, 2002), and is essential for survival within the host following the transition from commensalism to pathogenesis as well as following antibiotic treatment (Pokhrel *et al.*, 2020). As such, the stringent response remains an important field of study in light of the emergence of multidrug resistant pathogens. The Gram-negative stringent response directly alters the cellular transcriptome through binding of (p)ppGpp to the RNAP-DksA complex (Sanchez-Vazquez *et al.*, 2019), with 757 target genes identified. In Gram-positive organisms, the transcriptional alteration is highly dependent on the intracellular guanine nucleotide pools, with a reduction of GTP concentration during (p)ppGpp synthesis derepressing the *codY* regulon (Geiger and Wolz, 2014). Despite the differences between the Gram-negative and Gram-positive stringent response, the use of RA-GTPases to reduce ribosome assembly upon direct (p)ppGpp binding is conserved. In this study, we investigated the effect of (p)ppGpp on RA-GTPases both *in vitro* and *in vivo* using *S. aureus*, in order to better understand the specific mechanism of stringent-response-mediated reduction in 70S assembly and growth rate.

We performed biochemical characterisation on the nucleotide binding (Figure 3.3) and GTP hydrolysis (Figure 3.4) activity of the four RA-GTPases RsgA, RbgA, Era and HflX through use of the DRaCALA assay (Roelofs *et al.*, 2011), and confirmed previous observations that (p)ppGpp binds to the nucleotide binding site of these RA-GTPases in a competitive manner (Corrigan *et al.*, 2016; Feng *et al.*, 2014; Pausch *et al.*, 2018). The K_d values calculated were in line with those previously described by our lab (Corrigan *et al.*, 2016), although the new observation that GDP is bound similarly to ppGpp and more strongly than either GTP or pppGpp (Table 3.3) highlights the essentiality of relative intracellular nucleotide concentration (namely the excess of GTP over GDP during proliferative conditions) to drive the binding equilibrium towards the GTP-bound ON state. This also paves the way for further study regarding the binding affinity for 5'-diphosphate vs 5'-triphosphate containing nucleotides, which may be an important consideration if antibiotics targeting ribosome assembly are developed in the future

as hypothesised (Nikolay *et al.*, 2016). The GTPase activity of the four RA-GTPases was shown to be inhibited by ppGpp (Figure 3.4.1a), and despite previous publications only identifying the potential ATPase activity of HflX (Dutta *et al.*, 2009; Shields *et al.*, 2009), RsgA, Era and HflX were all shown to possess innate, ribosome-stimulated ATPase activity which could be inhibited by ppGpp (Figure 3.4.1b), although an excess of ATP was found to be incapable of competing with any guanine nucleotide within the active site (Figure 3.3.2) suggesting that this ATPase activity may be irrelevant under physiological conditions.

The current dogma regarding the effect of (p)ppGpp-mediated inhibition of RA-GTPases centres around the fact that pppGpp-bound RbgA was shown to bind more strongly to the 50S subunit than GMPPNP-bound RbgA in *B. subtilis* (Achila *et al.*, 2012). In an attempt to recapitulate this using *S. aureus* RA-GTPases and ribosomal subunits, it was found that binding of (p)ppGpp or GDP invariably reduced the interaction between the RA-GTPase and ribosomal subunit relative to the GMPPNP-bound state (Figure 4.3), which can be recapitulated *in vivo* (Figure 4.5). Further kinetic study into this enabled us to propose a two-step association mechanism (Equation 2, Figure 4.4.3.2, Table 4.4.3.2), the second step of which was completely inhibited in the presence of ppGpp, although a low signal:noise ratio made accurate quantification of these data difficult. This suggests that the reduction in interaction is due to the inhibition of complex stabilisation. Truncation of the Era GTPase revealed that the accessory rRNA-binding by the KH domain is independent of the bound nucleotide, and requires correct positioning of the GTPase domain on the 30S subunit to stimulate GTPase activity (Figure 4.6.1, Figure 4.6.2, Figure 4.6.3). This differs from the previously suggested substrate assisted activation model (Tu *et al.*, 2011; Tu *et al.*, 2009), which was developed using isolated rRNA for co-crystallisation studies. This implies that the regulation of ribosome association in response to (p)ppGpp or GDP binding may in fact rely on nonspecific GTPase domain conformational changes, with the switch I loop of major interest due to structural observations of incorrect docking during (p)ppGpp-binding by *S. aureus* RbgA (Pausch *et al.*, 2018). While the γ-phosphate of GTP may still act as a general base as suggested in the substrate assisted model (Pasqualato and Cherfils, 2005; Tu *et al.*, 2009), hydrolysis cannot occur without outside influence by the ribosomal subunit. The observations made in Chapter 4 are the antithesis of those observations which defined the current model (Achila *et al.*, 2012), and would suggest that instead of sequestering a pool of immature ribosomal subunits, the stringent response triggers a complete dissociation of RA-GTPases from their binding partners. Speculative possibilities include that this dissociation would enable these proteins to carry out secondary functions while bound to ppGpp. Era, for example, has many proposed effects in cell cycle regulation (Britton *et al.*, 1998; Ji, 2016), and HflX in manganese homeostasis (Kaur *et al.*, 2014;

Sengupta *et al.*, 2018), both of which may be important regulation targets during nutrient limitation. Further interaction screens, for example bacterial two hybrid or pull-down assays, would be required to determine the binding partners of these GTPases while in the (p)ppGpp-bound conformation to further unravel this possibility.

The use of fully mature 30S and 50S subunits in the association assays presented here rather than the more physiologically relevant immature state is an important caveat. The purification of immature ribosomal particles is far from an exact science, with a large degree of heterogeneity in ribosome assembly intermediates leading to an undefined mixture of these intermediates following purification (Razi *et al.*, 2019) which differs in each preparation. This would lead to any analysis being carried out using an undefined system, rendering accurate biochemical characterisation of these systems impossible and leading to potentially complex outcomes with low intrinsic reproducibility, the latter of which is a major point of concern in the current research environment (Baker, 2016). Here, the use of homogeneous preparations of highly pure, mature ribosomal subunits provides a useful, defined and reproducible system for assessing the initial interaction between the RA-GTPases and ribosomal subunits. Specifically, we focus on the mechanistic details from the perspective of the nucleotide-bound state of the RA-GTPases, which are likely to remain consistent regardless of the binding partner. Our experimental system could provide a useful baseline for the development of future research regarding the differences between the effect of immature and mature ribosomal particles on RA-GTPases, when homogeneous preparation of ribosomal subunit maturation intermediates is possible.

We solved the crystal structures of staphylococcal RsgA while in the apo, GDP-bound and ppGpp-bound states (Figure 5.3, PDB: 6ZJO, PDB: 6ZHM and PDB: 6ZHL respectively), in order to better understand the tertiary conformational effects of ppGpp binding on RA-GTPases. It was revealed that in each of the solved forms, the overall conformation of RsgA was unchanged, with the switch II loop adopting the OFF-state conformation in line with our GDP-bound structure (Figure 5.4.2). Innate flexibility in the disordered state led to lack of electron density concerning the switch I loop. Switch II exhibited a conformation in line with previously solved OFF-state homologues, with the G3 motif contacting the core of the GTPase domain rather than the bound Mg^{2+} cofactor as observed in the GMPPNP-bound ON-state (Levdikov *et al.*, 2004; López-Alonso *et al.*, 2017b; Razi *et al.*, 2017), suggesting that while bound to ppGpp, the conformation of RsgA mimics the GDP-bound OFF-state structure. This is in line with our observations in Chapter 4, showing a reduced ribosomal subunit association in the presence of either GDP or ppGpp (Figure 4.3), augmenting our hypothesis that ppGpp encourages dissociation from the ribosome. Binding of (p)ppGpp to RbgA has been previously

shown to prevent correct docking of the switch I loop into the active conformation (Pausch *et al.*, 2018), instead rendering the loop unstructured and distal from the body of the GTPase domain. By comparing the available structures of *E. coli* homologues in the GMPPNP and GDP bound state, we show that the hypothetical disordered position of the switch I loop is incompatible with ribosomal subunit association (Figure 5.5.2), and as such propose a mechanism by which (p)ppGpp-mediated disorder in the switch I region sterically inhibits RA-GTPase-ribosome complex formation (Figure 7.1). Since the association model was generated using RA-GTPases with a single accessory RNA-binding domain, we cannot be certain in the case of RsgA whether both the OB-fold and ZNF contribute to unstable complex formation, or whether initial contact is reliant on a single domain. It is important to bear in mind that despite a sequence identity of 33.5% between the *S. aureus* and *E. coli* homologues, there will be some structural differences. Therefore to gain a better understanding, the structure of *S. aureus* RsgA should be solved in the presence of GMPPNP. Furthermore, the RsgA models are limited by the lack of order within the switch I region. The most revealing solution, however, would be cryo-EM studies of RA-GTPases in the GMPPNP-bound state associated with their cognate ribosomal subunit, in which the switch I loop remains resolved. Comparison between this GMPPNP bound structure and crystallographic (p)ppGpp-bound structures would enable accurate visualisation of the movement and misalignment of this loop in response to (p)ppGpp binding.
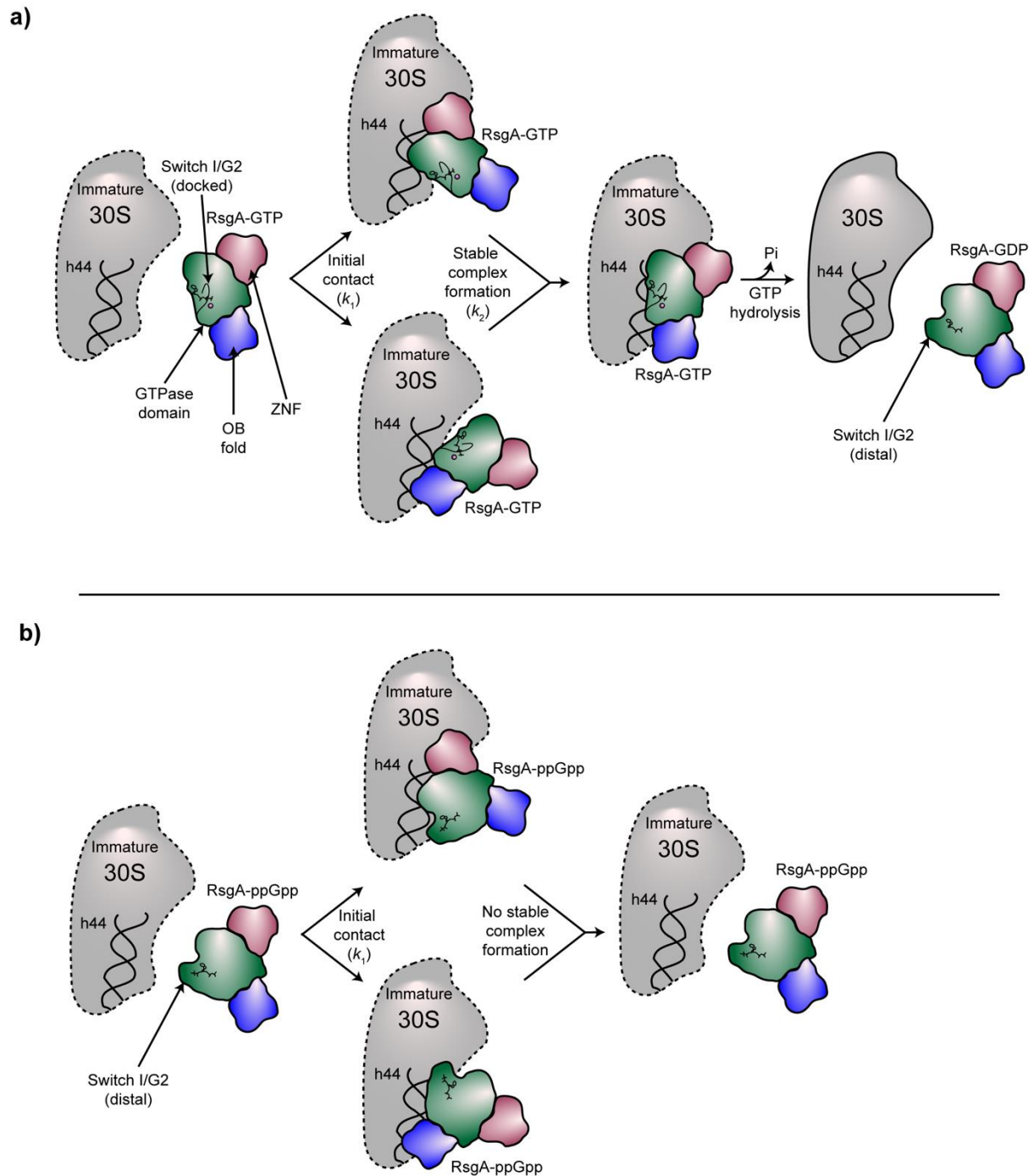
Figure 7.1: A schematic model of (p)ppGpp-mediated reduction in RA-GTPase-ribosome interaction via prevention of docking of the switch I. a) During proliferative conditions, the RA-GTPase nucleotide binding equilibrium will be in favour of the GTP-bound ON state, due to docking of the switch I loop, leading to ribosome association. Initial contact between the RA-GTPase and the ribosomal subunit occurs via one accessory domain (k_1), followed by stable complex formation (k_2). Upon correct ribosomal subunit maturation, the GTPase activity is activated and the bound GTP molecule is hydrolysed to GDP, facilitating entry into the OFF state. The switch I loop adopts the distal conformation, encouraging dissociation of the RA-GTPase from the ribosomal subunit, where the bound GDP can be exchanged for GTP to enable further maturation cycles. b) During the stringent response, (p)ppGpp becomes the dominant guanine nucleotide and the RA-GTPase nucleotide binding equilibrium shifts in favour of (p)ppGpp-binding. The 3'-diphosphate group of (p)ppGpp prevents switch I loop docking and maintains the distal conformation. While initial contact between an accessory domain and the rRNA can still occur (k_1), stable complex formation is sterically inhibited by the switch I loop ($k_2 = 0$ s^{-1}). Therefore dissociation occurs and RA-GTPases remain trapped in the OFF conformation until GTP concentrations rise and

enable re-entry into the ON state. RsgA is used as a model RA-GTPase, and is coloured by domain as follows: OB-fold, blue; GTPase domain, green; ZNF, red. The hypothetical position of the switch I loop is indicated. The associated magnesium ion is represented by a purple sphere, and the bound nucleotide is shown as black lines as described in the panel. The RsgA interaction site of the 30S ribosomal subunit is represented by a grey cartoon, and the 16S h44 RsgA binding site is shown in black.

Finally we carried out site directed mutagenesis in an effort to create mutants which mimic the ppGpp-bound OFF state. We showed that mutation of the highly conserved G2 threonine of RsgA and RbgA decreased the GTP binding affinity while enabling wild-type binding levels of GDP, ppGpp and pppGpp (Figure 6.3.1, Table 6.3.1), as previously suggested (Corrigan *et al.*, 2016). The GTP binding capacity of Era and HflX was unaffected, however, suggesting fundamental differences in the specific residues involved in GTP recognition. The presence of adjacent threonine residues in Era may impart some cooperativity to GTP binding in a similar manner to *E. coli* MnmE (Martínez-Vicente *et al.*, 2005; Shimamoto and Inouye, 1996), and as such in order to generate an Era variant with a pronounced defect in GTP binding both residues should be mutated. Mutation of the conserved G4 lysine completely abrogated the nucleotide binding capacity of the protein (Figure 6.3.1, Table 6.3.1), although CD spectroscopy may indicate that this mutant variant lacks protein structure (Figure 6.5.1). Both the G2 and G4 point mutants were found to be completely GTPase inactive (Figure 6.4.1). When introduced *in vivo*, the G2 and G4 mutant Era variants were unable to even partially rescue the slow growth phenotype of the Δ*era* strain (Figure 6.7.1), which was attributed to a lack of 70S ribosomes and a subsequent reduced translation rate (Figure 6.7.2, Figure 6.7.3), a hallmark phenotype of the stringent response. We also showed that the (p)ppGpp-mediated inhibition of ribosome association of Era is dependent upon the presence of the switch I loop (Figure 6.6), as deletion of this loop removed the inhibitory effect of (p)ppGpp on ribosome association. This further supports our model of steric prevention of complex formation by the switch I loop, and further contrasts the current model of ppGpp-bound RA-GTPases sequestering immature ribosomal subunits (Achila *et al.*, 2012; Pausch *et al.*, 2018). Mutagenesis of some non-catalytic residues in this region could provide insight into the role of specificity in the GTPase domain-ribosome interaction.

Together, our results enable the proposal of a model describing the role of RA-GTPases in the S*. aureus* stringent response (Figure 7.2), as follows: during proliferative growth, the intracellular concentration of GTP is dominant among the guanine nucleotide pool (Varik *et al.*, 2017), and as such skews the binding equilibrium in favour of the GTP-bound ON state of RA-GTPases. In turn, this facilitates efficient ribosome biogenesis and maturation, enabling rapid growth (Failmezger *et al.*, 2017), with GTP hydrolysis causing dissociation from the ribosome following entry into the GDP-bound OFF state. Upon activation of the stringent response following nutrient limitation, cell wall stress or via other

means, the intracellular nucleotide pools shift drastically within 4 mins (Varik *et al.*, 2017), with (p)ppGpp becoming the dominant guanine nucleotide within 5 mins (Patacq *et al.*, 2020) and shift the RA-GTPase binding equilibrium towards the (p)ppGpp-bound OFF state. The 3'-diphosphate of (p)ppGpp sterically prevents correct docking of the switch I loop to complete the nucleotide binding pocket, which also serves to prevent hydrolysis of the β-γ-phosphodiester bond of pppGpp. While the accessory rRNA-binding domain still initiates contact with the ribosomal subunit, stable complex formation is prevented due to the steric contacts between the ribosomal subunit and the distal, protruding switch I, encouraging RA-GTPase dissociation from the ribosomal subunit. This prevents the maturation chaperoning effect of RA-GTPases from taking place, and significantly slows the biogenesis of mature ribosomes, in turn slowing the rate of translation and cell growth rate. Upon re-entry into proliferative conditions, the nucleotide binding equilibrium will shift back in favour of the GTP-bound state, which enables RA-GTPases to enter the ON conformation and resume ribosome assembly and cell growth.
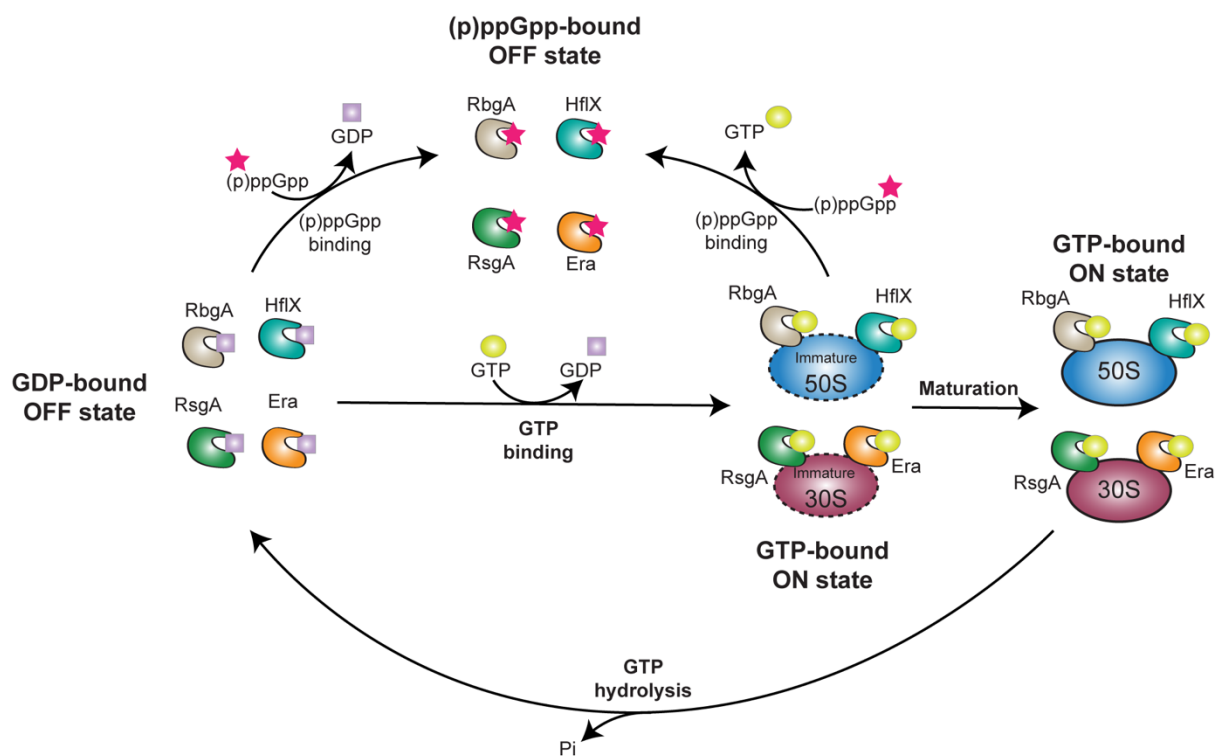
Figure 7.2: A schematic model of the control of ribosome biogenesis by (p)ppGpp-mediated inhibition of RA-GTPases. Under high-nutrient, favourable conditions, GTP binds to the RA-GTPases, enabling association with the immature ribosome subunits and facilitating subunit maturation. The presence of the mature ribosomal subunit triggers GTP hydrolysis, entry into the GDP-bound state and subsequent dissociation of the RA-GTPase. Under conditions of stress, activation of the stringent response causes an accumulation of the effector nucleotide (p)ppGpp and a reduction in intracellular GTP concentration, leading to competitive binding and entry into the (p)ppGpp-bound state. This inhibits RA-GTPase association to the ribosome and reduces ribosome biogenesis, resulting in a pool of immature 30S and 50S subunits. Upon re-entry into favourable conditions, the nucleotide binding equilibrium shifts in favour of GTP as intracellular (p)ppGpp concentration falls, and ribosome subunit maturation can resume.

As with any study investigating the stringent response, one must consider that no single aspect of this multi-faceted signalling network occurs in isolation. While we have shown that (p)ppGpp does indeed inhibit the association of RA-GTPases and the ribosomal subunits, which results in a decrease in the cellular translation rate and growth, this is not the only way by which bacteria regulate their translational machinery during the stringent response. As well as ribosome assembly, the translation process remains a key target, with (p)ppGpp-binding leading to the inhibition of EF-G, EF-Tu, EF-Ts and RF3 (Kihira *et al*., 2012; Milon *et al*., 2006; Mitkevich *et al*., 2010; Vinogradova *et al*., 2020), all of which contribute to the progression of the bacterial elongation cycle. Furthermore, IF2-mediated 30S pre-IC formation is regulated according to whether IF2 contains GTP or ppGpp at the nucleotide binding site, allowing for a selective translation process depending on the pre-IC affinity for any particular mRNA (Vinogradova *et al*., 2020). Additionally, the cellular reduction in GTP concentration downregulates the transcription of genes with a guanine initiator nucleotide at the +1 site (Geiger *et al*., 2012), which includes genes in the rRNA-encoding *rrn* operon in the firmicutes. Perhaps most interesting is that during the stringent response, translation is largely decreased (Bennison *et al*., 2019; Cheng-Guang and Gualerzi, 2020; Christensen *et al*., 2001; Feng *et al*., 2014; Ronneau and Hallez, 2019; Steinchen and Bange, 2016; Wolz *et al*., 2010) yet remains permissive to certain essential mRNAs which are required for cell survival, such as the m*tufA* encoding EF-Tu (Vinogradova *et al*., 2020). The interplay between each of the stringent response targets in order to result in this finely-tuned translational apparatus warrants further investigation to better understand the mechanics of this permissive translation, and to identify the mRNAs preferentially translated under stringent conditions.

In conclusion, here we have provided novel insight into the mechanism by which translation is modulated during the stringent response as a means of slowing cell growth in order to survive transient conditions of stress. We have shown that under proliferative conditions, RA-GTPases bind to GTP and undergo productive GTPase cycling. Under stringent conditions, however, the binding of (p)ppGpp to these proteins inhibits not only GTPase activity but also entry into the ribosome-binding ON conformation, resulting in a slowing of growth due to a reduction in 70S biogenesis and translation rate, potentially representing a widespread mechanism of (p)ppGpp-mediated control of GTPase interactions. We believe that this knowledge may contribute to the rational generation of novel bacteriostatic antimicrobials targeting ribosome assembly and thus provide a foundation for treatment of multidrug-resistant strains of bacteria such as *S. aureus*.

Bibliography

Abeck, D., and Mempel, M. (1998). Staphylococcus aureus colonization in atopic dermatitis and its therapeutic implications. Br J Dermatol *139 Suppl 53*, 13-16. 10.1046/j.1365-2133.1998.1390s3013.x.

Achila, D., Gulati, M., Jain, N., and Britton, R.A. (2012). Biochemical characterization of ribosome assembly GTPase RbgA in *Bacillus subtilis*. J Biol Chem *287*, 8417-8423. 10.1074/jbc.M111.331322.

Adio, S., Sharma, H., Senyushkina, T., Karki, P., Maracci, C., Wohlgemuth, I., Holtkamp, W., Peske, F., and Rodnina, M.V. (2018). Dynamics of ribosomes and release factors during translation termination in *E. coli*. Elife *7*. 10.7554/eLife.34252.

Aedo, S., and Tomasz, A. (2016). Role of the stringent stress response in the antibiotic resistance phenotype of methicillin-resistant *Staphylococcus aureus*. Antimicrob Agents Chemother *60*, 2311-2317. 10.1128/AAC.02697-15.

Agrawal, A., Mohanty, B.K., and Kushner, S.R. (2014). Processing of the seven valine tRNAs in *Escherichia coli* involves novel features of RNase P. Nucleic Acids Res *42*, 11166-11179. 10.1093/nar/gku758.

Ahmad, S., Wang, B., Walker, M.D., Tran, H.R., Stogios, P.J., Savchenko, A., Grant, R.A., McArthur, A.G., Laub, M.T., and Whitney, J.C. (2019). An interbacterial toxin inhibits target cell growth by synthesizing (p)ppApp. Nature *575*, 674-678. 10.1038/s41586-019-1735-9.

Akanuma, G., Kazo, Y., Tagami, K., Hiraoka, H., Yano, K., Suzuki, S., Hanai, R., Nanamiya, H., Kato-Yamada, Y., and Kawamura, F. (2016). Ribosome dimerization is essential for the efficient regrowth of *Bacillus subtilis*. Microbiology (Reading) *162*, 448-458. 10.1099/mic.0.000234.

Anand, B., Verma, S.K., and Prakash, B. (2006). Structural stabilization of GTP-binding domains in circularly permuted GTPases: implications for RNA binding. Nucleic Acids Res *34*, 2196-2205. 10.1093/nar/gkl178.

Andreeva, I., Belardinelli, R., and Rodnina, M.V. (2018). Translation initiation in bacterial polysomes through ribosome loading on a standby site on a highly translated mRNA. Proc Natl Acad Sci U S A *115*, 4411-4416. 10.1073/pnas.1718029115.

Andreson, L., Tenson, T., and Hauryliuk, V. (2016). Cationic bactericidal peptide 1018 does not specifically target the stringent response alarmone (p)ppGpp. Sci Rep *6*. https://doi.org/10.1038/srep36549.

Apirion, D., and Miczak, A. (1993). RNA processing in prokaryotic cells. Bioessays *15*, 113-120. 10.1002/bies.950150207.

Arenz, S., and Wilson, D.N. (2016). Blast from the past: reassessing forgotten translation inhibitors, antibiotic selectivity, and resistance mechanisms to aid drug development. Mol Cell *61*, 3-14. 10.1016/j.molcel.2015.10.019.

Arthur, M., Molinas, C., Depardieu, F., and Courvalin, P. (1993). Characterization of Tn1546, a Tn3-related transposon conferring glycopeptide resistance by synthesis of depsipeptide peptidoglycan precursors in *Enterococcus faecium* BM4147. J Bacteriol *175*, 117-127. 10.1128/jb.175.1.117-127.1993.

Ash, M.R., Maher, M.J., Guss, J.M., and Jormakka, M. (2011). The initiation of GTP hydrolysis by the G-domain of FeoB: insights from a transition-state complex structure. PLoS One *6*, e23355. 10.1371/journal.pone.0023355.

Atkinson, G.C., Tenson, T., and Hauryliuk, V. (2011). The RelA/SpoT homolog (RSH) superfamily: distribution and functional evolution of ppGpp synthetases and hydrolases across the tree of life. PLoS One *6*, e23479. 10.1371/journal.pone.0023479.

Ayyub, S.A., Dobriyal, D., and Varshney, U. (2017). Contributions of the n- and c-terminal domains of initiation factor 3 to its functions in the fidelity of initiation and antiassociation of the ribosomal subunits. J Bacteriol *199*. 10.1128/JB.00051-17.

Baba, T., Takeuchi, F., Kuroda, M., Yuzawa, H., Aoki, K., Oguchi, A., Nagai, Y., Iwama, N., Asano, K., Naimi, T., *et al*. (2002). Genome and virulence determinants of high virulence community-acquired MRSA. Lancet *359*, 1819-1827. 10.1016/s0140-6736(02)08713-5.

Baker, C.M., and Grant, G.H. (2007). Role of aromatic amino acids in protein-nucleic acid recognition. Biopolymers *85*, 456-470. 10.1002/bip.20682.

Baker, M. (2016). 1,500 scientists lift the lid on reproducibility. Nature *533*, 452-454. 10.1038/533452a.

Basu, A., Shields, K.E., and Yap, M.F. (2020). The hibernating 100S complex is a target of ribosome-recycling factor and elongation factor G in *Staphylococcus aureus*. J Biol Chem *295*, 6053-6063. 10.1074/jbc.RA119.012307.

Basu, A., and Yap, M.N. (2016). Ribosome hibernation factor promotes Staphylococcal survival and differentially represses translation. Nucleic Acids Res *44*, 4881-4893. 10.1093/nar/gkw180.

Basu, A., and Yap, M.N. (2017). Disassembly of the *Staphylococcus aureus* hibernating 100S ribosome by an evolutionarily conserved GTPase. Proc Natl Acad Sci U S A *114*, E8165-E8173. 10.1073/pnas.1709588114.

Battesti, A., and Bouveret, E. (2006). Acyl carrier protein/SpoT interaction, the switch linking SpoT-dependent stress response to fatty acid metabolism. Mol Microbiol *62*, 1048-1063. 10.1111/j.1365-2958.2006.05442.x.

Becker, K., Heilmann, C., and Peters, G. (2014). Coagulase-negative staphylococci. Clin Microbiol Rev *27*, 870-926. 10.1128/CMR.00109-13.

Beckert, B., Turk, M., Czech, A., Berninghausen, O., Beckmann, R., Ignatova, Z., Plitzko, J.M., and Wilson, D.N. (2018). Structure of a hibernating 100S ribosome reveals an inactive conformation of the ribosomal protein S1. Nat Microbiol *3*, 1115-1121. 10.1038/s41564-018-0237-0.

Beljantseva, J., Kudrin, P., Jimmy, S., Ehn, M., Pohl, R., Varik, V., Tozawa, Y., Shingler, V., Tenson, T., Rejman, D., and Hauryliuk, V. (2017). Molecular mutagenesis of ppGpp: turning a RelA activator into an inhibitor. Sci Rep *7*, 41839. 10.1038/srep41839.

Bennison, D.J., Irving, S.E., and Corrigan, R.M. (2019). The impact of the stringent response on TRAFAC GTPases and prokaryotic ribosome assembly. Cells *8*. 10.3390/cells8111313.

Benvenuti, M., and Mangani, S. (2007). Crystallization of soluble proteins in vapor diffusion for x-ray crystallography. Nat Protoc *2*, 1633-1651. 10.1038/nprot.2007.198.

Bergman, J.M., Hammarlof, D.L., and Hughes, D. (2014). Reducing ppGpp level rescues an extreme growth defect caused by mutant EF-Tu. PLoS ONE *9*. 10.1371/journal.pone.0090486.

Bernasconi, C.F. (1976). Relaxation kinetics (Academic Press).

Bischoff, M., Entenza, J.M., and Giachino, P. (2001). Influence of a functional *sigB* operon on the global regulators *sar* and *agr* in *Staphylococcus aureus*. J Bacteriol *183*, 5171-5179. 10.1128/jb.183.17.5171-5179.2001.

Blombach, F., Launay, H., Zorraquino, V., Swarts, D.C., Cabrita, L.D., Benelli, D., Christodoulou, J., Londei, P., and van der Oost, J. (2011). An HflX-type GTPase from *Sulfolobus solfataricus* binds to the 50S ribosomal subunit in all nucleotide-bound states. J Bacteriol *193*, 2861-2867. 10.1128/JB.01552-10.

Boisset, S., Geissmann, T., Huntzinger, E., Fechter, P., Bendridi, N., Possedko, M., Chevalier, C., Helfer, A.C., Benito, Y., Jacquier, A., *et al*. (2007). *Staphylococcus aureus* RNAIII coordinately represses the synthesis of virulence factors and the transcription regulator Rot by an antisense mechanism. Genes Dev *21*, 1353-1366. 10.1101/gad.423507.

Boles, B.R., Thoendel, M., Roth, A.J., and Horswill, A.R. (2010). Identification of genes involved in polysaccharide-independent *Staphylococcus aureus* biofilm formation. PLoS One *5*, e10146. 10.1371/journal.pone.0010146.

Borg, A., Pavlov, M., and Ehrenberg, M. (2016). Complete kinetic mechanism for recycling of the bacterial ribosome. RNA *22*, 10-21. 10.1261/rna.053157.115.

Bosdriesz, E., Molenaar, D., Teusink, B., and Bruggeman, F.J. (2015). How fast-growing bacteria robustly tune their ribosome concentration to approximate growth-rate maximization. FEBS J *282*, 2029-2044. 10.1111/febs.13258.

Bowler, B.E. (2012). Residual structure in unfolded proteins. Curr Opin Struct Biol *22*, 4-13. 10.1016/j.sbi.2011.09.002.

Brandt, F., Etchells, S.A., Ortiz, J.O., Elcock, A.H., Hartl, F.U., and Baumeister, W. (2009). The native 3D organization of bacterial polysomes. Cell *136*, 261-271. 10.1016/j.cell.2008.11.016.

Bremer, H., and Dennis, P.P. (2008). Modulation of chemical composition and other parameters of the cell at different exponential growth rates. EcoSal Plus *3*. 10.1128/ecosal.5.2.3.

Britton, R.A. (2009). Role of GTPases in bacterial ribosome assembly. Annu Rev Microbiol *63*, 155--176. 10.1146/annurev.micro.091208.073225.

Britton, R.A., Powell, B.S., Dasgupta, S., Sun, Q., Margolin, W., Lupski, J.R., and Court, D.L. (1998). Cell cycle arrest in Era GTPase mutants: a potential growth rate-regulated checkpoint in *Escherichia coli*. Mol Microbiol *27*, 739-750. 10.1046/j.1365-2958.1998.00719.x.

Bronner, S., Monteil, H., and Prévost, G. (2004). Regulation of virulence determinants in *Staphylococcus aureus*: complexity and applications. FEMS Microbiol Rev *28*, 183-200. 10.1016/j.femsre.2003.09.003.

Brown, A., Fernández, I.S., Gordiyenko, Y., and Ramakrishnan, V. (2016). Ribosome-dependent activation of stringent control. Nature *534*, 277-280. 10.1038/nature17675.

Brumshtein, B., Greenblatt, H.M., Futerman, A.H., Silman, I., and Sussman, J.L. (2008). Control of the rate of evaporation in protein crystallization by the 'microbatch under oil' method. J Appl Crystallogr *41*, 969-971. 10.1107/S0021889808024667.

Bubeck Wardenburg, J., Palazzolo-Ballance, A.M., Otto, M., Schneewind, O., and DeLeo, F.R. (2008). Panton-Valentine leukocidin is not a virulence determinant in murine models of community-associated methicillin-resistant *Staphylococcus aureus* disease. J Infect Dis *198*, 1166-1170. 10.1086/592053.

Buglino, J., Shen, V., Hakimian, P., and Lima, C.D. (2002). Structural and biochemical analysis of the Obg GTP binding protein. Structure *10*, 1581-1592. 10.1016/s0969-2126(02)00882-1.

Carvalho, A.T., Szeler, K., Vavitsas, K., Åqvist, J., and Kamerlin, S.C. (2015). Modeling the mechanisms of biological GTP hydrolysis. Arch Biochem Biophys *582*, 80-90. 10.1016/j.abb.2015.02.027.

Cashel, M. (1969). The control of ribonucleic acid synthesis in *Escherichia coli*. IV. Relevance of unusual phosphorylated compounds from amino acid-starved stringent strains. J Biol Chem *244*, 3133-3141.

Cashel, M. (1975). Regulation of bacterial ppGpp and pppGpp. Annu Rev Microbiol *29*, 301-318. 10.1146/annurev.mi.29.100175.001505.

CDC (2002). *Staphylococcus aureus* resistant to vancomycin--United States, 2002. MMWR Morb Mortal Wkly Rep *51*, 565-567.

Chalmers, S.J., and Wylam, M.E. (2020). Methicillin-resistant *Staphylococcus aureus* infection and treatment options. Methods Mol Biol *2069*, 229-251. 10.1007/978-1-4939-9849-4_16.

Chambers, H.F. (1997). Methicillin resistance in staphylococci: molecular and biochemical basis and clinical implications. Clin Microbiol Rev *10*, 781-791. 10.1128/CMR.10.4.781-791.1997.

Chambers, H.F., and Deleo, F.R. (2009). Waves of resistance: *Staphylococcus aureus* in the antibiotic era. Nat Rev Microbiol *7*, 629-641. 10.1038/nrmicro2200.

Chan, K.H., and Wong, K.B. (2011). Structure of an essential GTPase, YsxC, from *Thermotoga maritima*. Acta Crystallogr Sect F Struct Biol Cryst Commun *67*, 640-646. 10.1107/S1744309111011651.

Charpentier, E., Anton, A.I., Barry, P., Alfonso, B., Fang, Y., and Novick, R.P. (2004). Novel cassette-based shuttle vector system for Gram-positive bacteria. Appl Environ Microbiol *70*, 6076-6085. 10.1128/AEM.70.10.6076-6085.2004.

Chen, C., Cui, X., Beausang, J.F., Zhang, H., Farrell, I., Cooperman, B.S., and Goldman, Y.E. (2016). Elongation factor G initiates translocation through a power stroke. Proc Natl Acad Sci U S A *113*, 7515-7520. 10.1073/pnas.1602668113.

Chen, S.S., Sperling, E., Silverman, J.M., Davis, J.H., and Williamson, J.R. (2012). Measuring the dynamics of *E. coli* ribosome biogenesis using pulse-labeling and quantitative mass spectrometry. Mol Biosyst *8*, 3325-3334. 10.1039/c2mb25310k.

Cheng-Guang, H., and Gualerzi, C.O. (2020). The ribosome as a switchboard for bacterial stress response. Front Microbiol *11*, 619038. 10.3389/fmicb.2020.619038.

Ching, C.B., Hidajat, K., and Uddin, M.S. (1989). Evaluation of equilibrium and kinetic parameters of smaller molecular size amino acids on KX zeolite crystals via liquid chromatographic techniques. Separ Sci and Tech *24*, 581-597.

Choi, E.J., and Mayo, S.L. (2006). Generation and analysis of proline mutants in protein G. Protein Eng Des Sel *19*, 285-289. 10.1093/protein/gzl007.

Choi, J., Rieke, E.L., Moorman, T.B., Soupir, M.L., Allen, H.K., Smith, S.D., and Howe, A. (2018). Practical implications of erythromycin resistance gene diversity on surveillance and monitoring of resistance. FEMS Microbiol Ecol *94*. 10.1093/femsec/fiy006.

Christensen, S.K., Mikkelsen, M., Pedersen, K., and Gerdes, K. (2001). RelE, a global inhibitor of translation, is activated during nutritional stress. Proc Natl Acad Sci U S A *98*, 14328--14333. 10.1073/pnas.251327898.

Chulluncuy, R., Espiche, C., Nakamoto, J.A., Fabbretti, A., and Milón, P. (2016). Conformational response of 30s-bound IF3 to A-site binders streptomycin and kanamycin. Antibiotics (Basel) *5*. 10.3390/antibiotics5040038.

Clauditz, A., Resch, A., Wieland, K.P., Peschel, A., and Götz, F. (2006). Staphyloxanthin plays a role in the fitness of *Staphylococcus aureus* and its ability to cope with oxidative stress. Infect Immun *74*, 4950-4953. 10.1128/IAI.00204-06.

Clouet-d'Orval, B., Batista, M., Bouvier, M., Quentin, Y., Fichant, G., Marchfelder, A., and Maier, L.K. (2018). Insights into RNA-processing pathways and associated RNA-degrading enzymes in Archaea. FEMS Microbiol Rev *42*, 579-613. 10.1093/femsre/fuy016.

Coates-Brown, R., Moran, J.C., Pongchaikul, P., Darby, A.C., and Horsburgh, M.J. (2018). Comparative genomics of S*taphylococcus* reveals determinants of speciation and diversification of antimicrobial defense. Front Microbiol *9*, 2753. 10.3389/fmicb.2018.02753.

Coatham, M.L., Brandon, H.E., Fischer, J.J., Schümmer, T., and Wieden, H.J. (2016). The conserved GTPase HflX is a ribosome splitting factor that binds to the E-site of the bacterial ribosome. Nucleic Acids Res *44*, 1952-1961. 10.1093/nar/gkv1524.

Coleman, G. (1983). The effect of glucose on the differential rates of extracellular protein and alpha-toxin formation by *Staphylococcus aureus* (Wood 46). Arch Microbiol *134*, 208-211. 10.1007/BF00407759.

Collart, M.A., and Weiss, B. (2020). Ribosome pausing, a dangerous necessity for co-translational events. Nucleic Acids Res *48*, 1043-1055. 10.1093/nar/gkz763.

Connolly, K., and Culver, G. (2009). Deconstructing ribosome construction. Trends Biochem Sci *34*, 256-263. 10.1016/j.tibs.2009.01.011.

Cooper, E.L., García-Lara, J., and Foster, S.J. (2009). YsxC, an essential protein in *Staphylococcus aureus* crucial for ribosome assembly/stability. BMC Microbiol *9*, 266. 10.1186/1471-2180-9-266.

Corrigan, R.M., Bellows, L.E., Wood, A., and Gründling, A. (2016). ppGpp negatively impacts ribosome assembly affecting growth and antimicrobial tolerance in Gram-positive bacteria. Proc Natl Acad Sci U S A *113*, E1710-E1719. 10.1073/pnas.1522179113.

Cosgrove, S.E., Sakoulas, G., Perencevich, E.N., Schwaber, M.J., Karchmer, A.W., and Carmeli, Y. (2003). Comparison of mortality associated with methicillin-resistant and methicillin-susceptible *Staphylococcus aureus* bacteremia: a meta-analysis. Clin Infect Dis *36*, 53-59. 10.1086/345476.

Cuervo, G., Camoez, M., Shaw, E., Dominguez, M., Gasch, O., Padilla, B., Pintado, V., Almirante, B., Molina, J., López-Medrano, F., *et al.* (2015). Methicillin-resistant *Staphylococcus aureus* (MRSA) catheter-related bacteraemia in haemodialysis patients. BMC Infect Dis *15*, 484. 10.1186/s12879-015-1227-y.

Cui, L., Neoh, H.M., Iwamoto, A., and Hiramatsu, K. (2012). Coordinated phenotype switching with large-scale chromosome flip-flop inversion observed in bacteria. Proc Natl Acad Sci U S A *109*, E1647-1656. 10.1073/pnas.1204307109.

Dago, A.E., Schug, A., Procaccini, A., Hoch, J.A., Weigt, M., and Szurmant, H. (2012). Structural basis of histidine kinase autophosphorylation deduced by integrating genomics, molecular dynamics, and mutagenesis. Proc Natl Acad Sci U S A *109*, E1733-1742. 10.1073/pnas.1201301109.

Dai, X., Zhu, M., Warren, M., Balakrishnan, R., Patsalo, V., Okano, H., Williamson, J.R., Fredrick, K., Wang, Y.P., and Hwa, T. (2016). Reduction of translating ribosomes enables *Escherichia coli* to maintain elongation rates during slow growth. Nat Microbiol *2*, 16231. 10.1038/nmicrobiol.2016.231.

Daigle, D.M., and Brown, E.D. (2004). Studies of the interaction of *Escherichia coli* YjeQ with the ribosome *in vitro*. J Bacteriol *186*, 1381-1387. 10.1128/JB.186.5.1381-1387.2004.

Dalebroux, Z.D., and Swanson, M.S. (2012). ppGpp: magic beyond RNA polymerase. Nat Rev Microbiol *10*, 203-212. 10.1038/nrmicro2720.

Dallas, A., and Noller, H.F. (2001). Interaction of translation initiation factor 3 with the 30S ribosomal subunit. Mol Cell *8*, 855-864. 10.1016/s1097-2765(01)00356-2.

Dasgupta, S., Basu, P., Pal, R.R., Bag, S., and Bhadra, R.K. (2014). Genetic and mutational characterization of the small alarmone synthetase gene relV of *Vibrio cholerae*. Microbiology (Reading) *160*, 1855-1866. 10.1099/mic.0.079319-0.

Datta, P.P., Wilson, D.N., Kawazoe, M., Swami, N.K., Kaminishi, T., Sharma, M.R., Booth, T.M., Takemoto, C., Fucini, P., Yokoyama, S., and Agrawal, R.K. (2007). Structural aspects of RbfA action during small ribosomal subunit assembly. Mol Cell *28*, 434-445. 10.1016/j.molcel.2007.08.026.

Daum, R.S., and Spellberg, B. (2012). Progress toward a *Staphylococcus aureus* vaccine. Clin Infect Dis *54*, 560-567. 10.1093/cid/cir828.

Daumke, O., and Praefcke, G.J.K. (2016). Invited review: Mechanisms of GTP hydrolysis and conformational transitions in the dynamin superfamily. Biopolymers *105*, 580--593. 10.1002/bip.22855.

Davies, B.W., Khrer, C., Jacob, A.I., Simmons, L.A., Zhu, J., Aleman, L.M., RajBhandary, U.L., and Walker, G.C. (2010). Role of *Escherichia coli* YbeY, a highly conserved protein, in rRNA processing. Mol Microbiol *78*, 506--518. 10.1111/j.1365-2958.2010.07351.x.

Davis, J.H., Tan, Y.Z., Carragher, B., Potter, C.S., Lyumkis, D., and Williamson, J.R. (2016). Modular assembly of the bacterial large ribosomal subunit. Cell *167*, 1610-1622. 10.1016/j.cell.2016.11.020.

Davis, J.H., and Williamson, J.R. (2017). Structure and dynamics of bacterial ribosome biogenesis. Philos Trans R Soc Lond B Biol Sci *372*. 10.1098/rstb.2016.0181.

Day, R.N., and Davidson, M.W. (2009). The fluorescent protein palette: tools for cellular imaging. Chem Soc Rev *38*, 2887-2921. 10.1039/b901966a.

Dayan, G.H., Mohamed, N., Scully, I.L., Cooper, D., Begier, E., Eiden, J., Jansen, K.U., Gurtman, A., and Anderson, A.S. (2016). *Staphylococcus aureus*: the current state of disease, pathophysiology and strategies for prevention. Expert Rev Vaccines *15*, 1373-1392. 10.1080/14760584.2016.1179583.

de la Fuente-Núñez, C., Reffuveille, F., Haney, E.F., Straus, S.K., and Hancock, R.E. (2014). Broad-spectrum anti-biofilm peptide that targets a cellular stress response. PLoS Pathog *10*, e1004152. 10.1371/journal.ppat.1004152.

Deltoro, D., Ortiz, D., Ordyan, M., Sippy, J., Oh, C.S., Keller, N., Feiss, M., Catalano, C.E., and Smith, D.E. (2016). Walker-A motif acts to coordinate ATP hydrolysis with motor output in viral DNA packaging. Journal of Molecular Biology *428*, 2709--2729. 10.1016/j.jmb.2016.04.029.

Dennis, P.P., Ehrenberg, M., and Bremer, H. (2004). Control of rRNA synthesis in *Escherichia coli*: a systems biology approach. Microbiol Mol Biol Rev *68*, 639-668. 10.1128/MMBR.68.4.639-668.2004.

Deora, R., and Misra, T.K. (1996). Characterization of the primary Sigma factor of *Staphylococcus aureus*. J Biol Chem *271*, 21828-21834. 10.1074/jbc.271.36.21828.

Dey, S., Biswas, C., and Sengupta, J. (2018). The universally conserved GTPase HflX is an RNA helicase that restores heat-damaged *Escherichia coli* ribosomes. J Cell Biol *217*, 2519-2529. 10.1083/jcb.201711131.

Ding, C.C., Rose, J., Sun, T., Wu, J., Chen, P.H., Lin, C.C., Yang, W.H., Chen, K.Y., Lee, H., Xu, E., *et al*. (2020). MESH1 is a cytosolic NADPH phosphatase that regulates ferroptosis. Nat Metab *2*, 270-277. 10.1038/s42255-020-0181-1.

Do, J.K., Jun, Y.J., Yoon, H.J., and Se, W.S. (2008). Crystal structure of YlqF, a circularly permuted GTPase: Implications for its GTPase activation in 50S ribosomal subunit assembly. Proteins: Structure, Function and Genetics *72*, 1363-1370. 10.1002/prot.22112.

Doniselli, N., Rodriguez-Aliaga, P., Amidani, D., Bardales, J.A., Bustamante, C., Guerra, D.G., and Rivetti, C. (2015). New insights into the regulatory mechanisms of ppGpp and DksA on *Escherichia coli* RNA polymerase-promoter complex. Nucleic Acids Res *43*, 5249-5262. 10.1093/nar/gkv391.

Doris, S.M., Smith, D.R., Beamesderfer, J.N., Raphael, B.J., Nathanson, J.A., and Gerbi, S.A. (2015). Universal and domain-specific sequences in 23S-28S ribosomal RNA identified by computational phylogenetics. RNA *21*, 1719-1730. 10.1261/rna.051144.115.

Dorneanu, O.S., Luncă, C., Năstase, E.V., Tuchiluş, C.G., Vremeră, T., and Iancu, L.S. (2016). Detection of aminoglycoside and macrolide resistance mechanisms in methicillin-resistant S*taphylococcus aureus*. Rev Med Chir Soc Med Nat Iasi *120*, 886-891.

Dunman, P.M., Murphy, E., Haney, S., Palacios, D., Tucker-Kellogg, G., Wu, S., Brown, E.L., Zagursky, R.J., Shlaes, D., and Projan, S.J. (2001). Transcription profiling-based identification of *Staphylococcus aureus* genes regulated by the agr and/or sarA loci. J Bacteriol *183*, 7341-7353. 10.1128/JB.183.24.7341-7353.2001.

Durfee, T., Hansen, A.M., Zhi, H., Blattner, F.R., and Ding, J.J. (2008). Transcription profiling of the stringent response in *Escherichia coli*. J Bacteriol *190*, 1084--1096. 10.1128/JB.01092-07.

Dutta, D., Bandyopadhyay, K., Datta, A.B., Sardesai, A.A., and Parrack, P. (2009). Properties of HflX, an enigmatic protein from *Escherichia coli*. J Bacteriol *191*, 2307-2314. 10.1128/JB.01353-08.

Dzyubak, E., and Yap, M.N. (2016). The expression of antibiotic resistance methyltransferase correlates with mrna stability independently of ribosome stalling. Antimicrob Agents Chemother *60*, 7178-7188. 10.1128/AAC.01806-16.

Eiamphungporn, W., and Helmann, J.D. (2008). The *Bacillus subtilis* σM regulon and its contribution to cell envelope stress responses. Mol Microbiol. 10.1111/j.1365-2958.2007.06090.x.

Elvekrog, M.M., and Gonzalez, R.L. (2013). Conformational selection of translation initiation factor 3 signals proper substrate selection. Nat Struct Mol Biol *20*, 628-633. 10.1038/nsmb.2554.

Emsley, P., and Cowtan, K. (2004). Coot: model-building tools for molecular graphics. Acta Crystallogr D Biol Crystallogr *60*, 2126-2132. 10.1107/S0907444904019158.

Emsley, P., Lohkamp, B., Scott, W.G., and Cowtan, K. (2010). Features and development of Coot. Acta Crystallogr D Biol Crystallogr *66*, 486-501. 10.1107/S0907444910007493.

Enright, M.C., Day, N.P., Davies, C.E., Peacock, S.J., and Spratt, B.G. (2000). Multilocus sequence typing for characterization of methicillin-resistant and methicillin-susceptible clones of *Staphylococcus aureus*. J Clin Microbiol *38*, 1008-1015. 10.1128/JCM.38.3.1008-1015.2000.

Failmezger, J., Ludwig, J., Nieß, A., and Siemann-Herzberg, M. (2017). Quantifying ribosome dynamics in *Escherichia coli* using fluorescence. FEMS Microbiol Lett *364*. 10.1093/femsle/fnx055.

Falugi, F., Kim, H.K., Missiakas, D.M., and Schneewind, O. (2013). Role of protein A in the evasion of host adaptive immune responses by *Staphylococcus aureus*. mBio *4*, e00575-00513. 10.1128/mBio.00575-13.

Fan, H., Hahm, J., Diggs, S., Perry, J.J., and Blaha, G. (2015). Structural and functional analysis of BipA, a regulator of virulence in enteropathogenic *Escherichia coli.* J Biol Chem *290*, 20856-20864. 10.1074/jbc.M115.659136.

Farrelly, V., Rainey, F.A., and Stackebrandt, E. (1995). Effect of genome size and rrn gene copy number on PCR amplification of 16S rRNA genes from a mixture of bacterial species. Appl Environ Microbiol *61*, 2798-2801. 10.1128/AEM.61.7.2798-2801.1995.

Fauvart, M., De Groote, V.N., and Michiels, J. (2011). Role of persister cells in chronic infections: clinical relevance and perspectives on anti-persister therapies. J Med Microbiol *60*, 699-709. 10.1099/jmm.0.030932-0.

Feaga, H.A., Kopylov, M., Kim, J.K., Jovanovic, M., and Dworkin, J. (2020). Ribosome Dimerization Protects the Small Subunit. J Bacteriol *202*. 10.1128/JB.00009-20.

Feil, E.J., Li, B.C., Aanensen, D.M., Hanage, W.P., and Spratt, B.G. (2004). eBURST: inferring patterns of evolutionary descent among clusters of related bacterial genotypes from multilocus sequence typing data. J Bacteriol *186*, 1518-1530. 10.1128/jb.186.5.1518-1530.2004.

Feng, B., Mandava, C.S., Guo, Q., Wang, J., Cao, W., Li, N., Zhang, Y., Wang, Z., Wu, J., Sanyal, S., *et al*. (2014). Structural and functional insights into the mode of action of a universally conserved Obg GTPase. PLoS Biol *12*, e1001866. 10.1371/journal.pbio.1001866.

Feng, Y., Chen, C.J., Su, L.H., Hu, S., Yu, J., and Chiu, C.H. (2008). Evolution and pathogenesis of *Staphylococcus aureus*: lessons learned from genotyping and comparative genomics. FEMS Microbiol Rev *32*, 23-37. 10.1111/j.1574-6976.2007.00086.x.

Fischer, J.J., Coatham, M.L., Bear, S.E., Brandon, H.E., De Laurentiis, E.I., Shields, M.J., and Wieden, H.J. (2012). The ribosome modulates the structural dynamics of the conserved GTPase HflX and triggers tight nucleotide binding. Biochimie *94*, 1647-1659. 10.1016/j.biochi.2012.04.016.

Fleischer, B., and Schrezenmeier, H. (1988). T cell stimulation by staphylococcal enterotoxins. Clonally variable response and requirement for major histocompatibility complex class II molecules on accessory or target cells. J Exp Med *167*, 1697-1707. 10.1084/jem.167.5.1697.

Fluit, A.C., Jansen, M.D., Bosch, T., Jansen, W.T., Schouls, L., Jonker, M.J., and Boel, C.H. (2016). rRNA Operon Copy Number Can Explain the Distinct Epidemiology of Hospital-Associated Methicillin-Resistant Staphylococcus aureus. Antimicrob Agents Chemother *60*, 7313-7320. 10.1128/AAC.01613-16.

Flynn, R.L., and Zou, L. (2010). Oligonucleotide/oligosaccharide-binding fold proteins: a growing family of genome guardians. Crit Rev Biochem Mol Biol *45*, 266-275. 10.3109/10409238.2010.488216.

Forchhammer, K., Leinfelder, W., and Böck, A. (1989). Identification of a novel translation factor necessary for the incorporation of selenocysteine into protein. Nature *342*, 453-456. 10.1038/342453a0.

Foster, T. (1996). Medical Microbiology 4th Edition, Chapter 12- Staphylococcus (University of Texas Medical Branch at Galveston).

Foster, T.J., Geoghegan, J.A., Ganesh, V.K., and Höök, M. (2014). Adhesion, invasion and evasion: the many functions of the surface proteins of *Staphylococcus aureus*. Nat Rev Microbiol *12*, 49-62. 10.1038/nrmicro3161.

Fowler, V.G., Allen, K.B., Moreira, E.D., Moustafa, M., Isgro, F., Boucher, H.W., Corey, G.R., Carmeli, Y., Betts, R., Hartzel, J.S., *et al*. (2013). Effect of an investigational vaccine for preventing *Staphylococcus aureus* infections after cardiothoracic surgery: a randomized trial. JAMA *309*, 1368-1378. 10.1001/jama.2013.3010.

Francisco-Velilla, R., Fernandez-Chamorro, J., Ramajo, J., and Martinez-Salas, E. (2016). The RNA-binding protein Gemin5 binds directly to the ribosome and regulates global translation. Nucleic Acids Res *44*, 8335-8351. 10.1093/nar/gkw702.

Freymann, D.M., Keenan, R.J., Stroud, R.M., and Walter, P. (1997). Structure of the conserved GTPase domain of the signal recognition particle. Nature *385*, 361-364. 10.1038/385361a0.

Fujishima, K., and Kanai, A. (2014). tRNA gene diversity in the three domains of life. Front Genet *5*, 142. 10.3389/fgene.2014.00142.

Gaca, A.O., Kudrin, P., Colomer-Winter, C., Beljantseva, J., Liu, K., Anderson, B., Wang, J.D., Rejman, D., Potrykus, K., Cashel, M., *et al*. (2015). From (p)ppGpp to (pp)pGpp: Characterization of regulatory

effects of pGpp synthesized by the small alarmone synthetase of *Enterococcus faecalis*. J Bacteriol *197*, 2908-2919. 10.1128/JB.00324-15.

Galbán, J., Mateos, E., Cebolla, V., Domínguez, A., Delgado-Camón, A., de Marcos, S., Sanz-Vicente, I., and Sanz, V. (2009). The environmental effect on the fluorescence intensity in solution. An analytical model. Analyst *134*, 2286-2292. 10.1039/b912063g.

Gao, N., Zavialov, A.V., Li, W., Sengupta, J., Valle, M., Gursky, R.P., Ehrenberg, M., and Frank, J. (2005). Mechanism for the disassembly of the posttermination complex inferred from cryo-EM studies. Mol Cell *18*, 663-674. 10.1016/j.molcel.2005.05.005.

Gao, W., Chua, K., Davies, J.K., Newton, H.J., Seemann, T., Harrison, P.F., Holmes, N.E., Rhee, H.W., Hong, J.I., Hartland, E.L., *et al*. (2010). Two novel point mutations in clinical *Staphylococcus aureus* reduce linezolid susceptibility and switch on the stringent response to promote persistent infection. PLoS Pathog *6*, e1000944. 10.1371/journal.ppat.1000944.

Garvey, M.I., Wilkinson, M.A.C., Bradley, C.W., Holden, K.L., and Holden, E. (2018). Wiping out MRSA: effect of introducing a universal disinfection wipe in a large UK teaching hospital. Antimicrob Resist Infect Control *7*, 155. 10.1186/s13756-018-0445-7.

Ge, X., Cai, Y., Chen, Z., Gao, S., Geng, X., Li, Y., Jia, J., and Sun, Y. (2018). Bifunctional Enzyme SpoT Is Involved in Biofilm Formation of *Helicobacter pylori* with Multidrug Resistance by Upregulating Efflux Pump Hp1174 (*gluP*). Antimicrob Agents Chemother *62*. 10.1128/AAC.00957-18.

Geiger, T., Francois, P., Liebeke, M., Fraunholz, M., Goerke, C., Krismer, B., Schrenzel, J., Lalk, M., and Wolz, C. (2012). The stringent response of *Staphylococcus aureus* and its impact on survival after phagocytosis through the induction of intracellular PSMs expression. PLoS Path *8*. 10.1371/journal.ppat.1003016.

Geiger, T., Goerke, C., Fritz, M., Schfer, T., Ohlsen, K., Liebeke, M., Lalk, M., and Wolz, C. (2010). Role of the (p)ppGpp synthase RSH, a RelA/SpoT homolog, in stringent response and virulence of *Staphylococcus aureus*. Infect Immun *78*, 1873--1883. 10.1128/IAI.01439-09.

Geiger, T., Kästle, B., Gratani, F.L., Goerke, C., and Wolz, C. (2014). Two small (p)ppGpp synthases in *Staphylococcus aureus* mediate tolerance against cell envelope stress conditions. J Bacteriol *196*, 894-902. 10.1128/JB.01201-13.

Geiger, T., and Wolz, C. (2014). Intersection of the stringent response and the CodY regulon in low GC Gram-positive bacteria. Int J Med Microbiol *304*, 150--155. 10.1016/j.ijmm.2013.11.013.

Germain, E., Guiraud, P., Byrne, D., Douzi, B., Djendli, M., and Maisonneuve, E. (2019). YtfK activates the stringent response by triggering the alarmone synthetase SpoT in *Escherichia coli*. Nat Commun *10*, 5763. 10.1038/s41467-019-13764-4.

Gillet, Y., Issartel, B., Vanhems, P., Fournet, J.C., Lina, G., Bes, M., Vandenesch, F., Piémont, Y., Brousse, N., Floret, D., and Etienne, J. (2002). Association between *Staphylococcus aureus* strains carrying gene for Panton-Valentine leukocidin and highly lethal necrotising pneumonia in young immunocompetent patients. Lancet *359*, 753-759. 10.1016/S0140-6736(02)07877-7.

Giraud, C., Hausmann, S., Lemeille, S., Prados, J., Redder, P., and Linder, P. (2015). The C-terminal region of the RNA helicase CshA is required for the interaction with the degradosome and turnover of bulk RNA in the opportunistic pathogen *Staphylococcus aureus*. RNA Biol *12*, 658-674. 10.1080/15476286.2015.1035505.

Godfrey, H.P., Bugrysheva, J.V., and Cabello, F.C. (2002). The role of the stringent response in the pathogenesis of bacterial infections. Trends Microbiol *10*, 349-351. 10.1016/s0966-842x(02)02403-4.

Goerke, C., Fluckiger, U., Steinhuber, A., Zimmerli, W., and Wolz, C. (2001). Impact of the regulatory loci agr, sarA and sae of *Staphylococcus aureus* on the induction of alpha-toxin during device-related infection resolved by direct quantitative transcript analysis. Mol Microbiol *40*, 1439-1447. 10.1046/j.1365-2958.2001.02494.x.

Gollop, N., and March, P.E. (1991). A GTP-binding protein (Era) has an essential role in growth rate and cell cycle control in *Escherichia coli*. J Bacteriol *173*, 2265-2270. 10.1128/jb.173.7.2265-2270.1991.

Gomez, J.E., Kaufmann-Malaga, B.B., Wivagg, C.N., Kim, P.B., Silvis, M.R., Renedo, N., Ioerger, T.R., Ahmad, R., Livny, J., Fishbein, S., *et al.* (2017). Ribosomal mutations promote the evolution of antibiotic resistance in a multidrug environment. Elife *6*. 10.7554/eLife.20420.

Goto, S., Kato, S., Kimura, T., Muto, A., and Himeno, H. (2011). RsgA releases RbfA from 30S ribosome during a late stage of ribosome biosynthesis. EMBO Journal *30*, 104--114. 10.1038/emboj.2010.291.

Greenfield, N.J. (2006). Using circular dichroism spectra to estimate protein secondary structure. Nat Protoc *1*, 2876-2890. 10.1038/nprot.2006.202.

Groaz, E., and De Jonghe, S. (2020). Overview of biologically active nucleoside phosphonates. Front Chem *8*, 616863. 10.3389/fchem.2020.616863.

Grondek, J.F., and Culver, G.M. (2004). Assembly of the 30S ribosomal subunit: positioning ribosomal protein S13 in the S7 assembly branch. RNA *10*, 1861-1866. 10.1261/rna.7130504.

Grundling, A., and Schneewind, O. (2007). Genes required for glycolipid synthesis and lipoteichoic acid anchoring in *Staphylococcus aureus*. J Bacteriol *189*, 2521-2530. 10.1128/JB.01683-06.

Gualerzi, C., Pon, C.L., and Kaji, A. (1971). Initiation factor dependent release of aminoacyl-tRNAs from complexes of 30S ribosomal subunits, synthetic polynucleotide and aminoacyl tRNA. Biochem Biophys Res Commun *45*, 1312-1319. 10.1016/0006-291x(71)90162-8.

Gualerzi, C.O., and Pon, C.L. (2015). Initiation of mRNA translation in bacteria: structural and dynamic aspects. Cell Mol Life Sci *72*, 4341-4367. 10.1007/s00018-015-2010-3.

Gulati, M., Jain, N., Anand, B., Prakash, B., and Britton, R.A. (2013). Mutational analysis of the ribosome assembly GTPase RbgA provides insight into ribosome interaction and ribosome-stimulated GTPase activation. Nuc Acid Res *41*, 3217--3227. 10.1093/nar/gks1475.

Gulati, M., Nikhil, J., Davis, J.H., Williamson, J.R., Britton, R.A. (2014). Functional interaction between ribosomal protein L6 and RbgA during ribosome assembly. PLoS Gen *10*. 10.1371/journal.pgen.1004694.

Guo, Q., Yuan, Y., Xu, Y., Feng, B., Liu, L., Chen, K., Sun, M., Yang, Z., Lei, J., and Gao, N. (2011). Structural basis for the function of a small GTPase RsgA on the 30S ribosomal subunit maturation revealed by cryoelectron microscopy. Proc Natl Acad Sci U S A *108*, 13100-13105. 10.1073/pnas.1104645108.

Gupta, P., Sothiselvam, S., Vázquez-Laslop, N., and Mankin, A.S. (2013). Deregulation of translation due to post-transcriptional modification of rRNA explains why erm genes are inducible. Nat Commun *4*, 1984. 10.1038/ncomms2984.

Hage, A.E., and Tollervey, D. (2004). A surfeit of factors: why is ribosome assembly so much more complicated in eukaryotes than bacteria? RNA Biol *1*, 10-15.

Hall, D.C., Król, J.E., Cahill, J.P., Ji, H.F., and Ehrlich, G.D. (2020). The development of a pipeline for the identification and validation of small-molecule RelA inhibitors for use as anti-biofilm drugs. Microorganisms *8*. 10.3390/microorganisms8091310.

Hamilton, S., Odili, J., Pacifico, M.D., Wilson, G.D., and Kupsch, J.M. (2003). Effect of imidazole on the solubility of a his-tagged antibody fragment. Hybrid Hybridomics *22*, 347-355. 10.1089/153685903771797048.

Hamlin, T.A., Swart, M., and Bickelhaupt, F.M. (2018). Nucleophilic substitution (S$_N$2): dependence on nucleophile, leaving group, central atom, substituents and solvent. Chemphyschem *19*, 1315-1330. 10.1002/cphc.201701363.

Han, C., Liu, Y., Dai, R., Ismail, N., Su, W., and Li, B. (2020). Ferroptosis and its potential role in human diseases. Front Pharmacol *11*, 239. 10.3389/fphar.2020.00239.

Haugen, S.P., Ross, W., Manrique, M., and Gourse, R.L. (2008). Fine structure of the promoter-sigma region 1.2 interaction. Proc Natl Acad Sci U S A *105*, 3292-3297. 10.1073/pnas.0709513105.

Hauryliuk, V., Atkinson, G.C., Murakami, K.S., Tenson, T., and Gerdes, K. (2015). Recent functional insights into the role of (p)ppGpp in bacterial physiology. Nat Revs Microbiol *13*, 298--309. 10.1038/nrmicro3448.

Hauryliuk, V., Mitkevich, V.A., Eliseeva, N.A., Petrushanko, I.Y., Ehrenberg, M., and Makarov, A.A. (2008). The pretranslocation ribosome is targeted by GTP-bound EF-G in partially activated form. Proc Natl Acad Sci U S A *105*, 15678-15683. 10.1073/pnas.0807912105.

Held, W.A., Ballou, B., Mizushima, S., and Nomura, M. (1974). Assembly mapping of 30 S ribosomal proteins from *Escherichia coli*. Further studies. J Biol Chem *249*, 3103-3111.

Henderson, R. (1990). Cryo-Protection of protein crystals against radiation damage in electron and X-ray diffraction. Proceedings: Natural Sciences *241*, 6-8.

Herold, M., and Nierhaus, K.H. (1987). Incorporation of six additional proteins to complete the assembly map of the 50 S subunit from *Escherichia coli* ribosomes. J Biol Chem *262*, 8826-8833.

Himeno, H., Hanawa-Suetsugu, K., Kimura, T., Takagi, K., Sugiyama, W., Shirata, S., Mikami, T., Odagiri, F., Osanai, Y., Watanabe, D., *et al*. (2004). A novel GTPase activated by the small subunit of ribosome. Nucleic Acids Res *32*, 5303-5309. 10.1093/nar/gkh861.

Hiramatsu, K., Hanaki, H., Ino, T., Yabuta, K., Oguri, T., and Tenover, F.C. (1997). Methicillin-resistant *Staphylococcus aureus* clinical strain with reduced vancomycin susceptibility. J Antimicrob Chemother *40*, 135-136. 10.1093/jac/40.1.135.

Hisatsune, J., Hirakawa, H., Yamaguchi, T., Fudaba, Y., Oshima, K., Hattori, M., Kato, F., Kayama, S., and Sugai, M. (2013). Emergence of *Staphylococcus aureus* carrying multiple drug resistance genes on

a plasmid encoding exfoliative toxin B. Antimicrob Agents Chemother *57*, 6131-6140. 10.1128/AAC.01062-13.

Hobbs, J.K., and Boraston, A.B. (2019). (p)ppGpp and the stringent response: an emerging threat to antibiotic therapy. ACS Infectious Diseases *5*, 1505--1517. 10.1021/acsinfecdis.9b00204.

Holtfreter, S., Roschack, K., Eichler, P., Eske, K., Holtfreter, B., Kohler, C., Engelmann, S., Hecker, M., Greinacher, A., and Broker, B.M. (2006). *Staphylococcus aureus* carriers neutralize superantigens by antibodies specific for their colonizing strain: a potential explanation for their improved prognosis in severe sepsis. J Infect Dis *193*, 1275-1278. 10.1086/503048.

Hood, R.D., Higgins, S.A., Flamholz, A., Nichols, R.J., and Savage, D.F. (2016). The stringent response regulates adaptation to darkness in the cyanobacterium *Synechococcus elongatus*. Proc Natl Acad Sci U S A *113*, E4867-4876. 10.1073/pnas.1524915113.

Howden, B.P., Davies, J.K., Johnson, P.D., Stinear, T.P., and Grayson, M.L. (2010). Reduced vancomycin susceptibility in *Staphylococcus aureus*, including vancomycin-intermediate and heterogeneous vancomycin-intermediate strains: resistance mechanisms, laboratory detection, and clinical implications. Clin Microbiol Rev *23*, 99-139. 10.1128/CMR.00042-09.

Hu, X.P., Dourado, H., Schubert, P., and Lercher, M.J. (2020). The protein translation machinery is expressed for maximal efficiency in *Escherichia coli*. Nat Commun *11*, 5260. 10.1038/s41467-020-18948-x.

Huntzinger, E., Boisset, S., Saveanu, C., Benito, Y., Geissmann, T., Namane, A., Lina, G., Etienne, J., Ehresmann, B., Ehresmann, C., *et al*. (2005). *Staphylococcus aureus* RNAIII and the endoribonuclease III coordinately regulate *spa* gene expression. EMBO J *24*, 824-835. 10.1038/sj.emboj.7600572.

Hwang, J., and Inouye, M. (2006). The tandem GTPase, Der, is essential for the biogenesis of 50S ribosomal subunits in *Escherichia coli*. Mol Microbiol *61*, 1660-1672. 10.1111/j.1365-2958.2006.05348.x.

Hwang, J., and Inouye, M. (2010). Interaction of an essential *Escherichia coli* GTPase, Der, with the 50S ribosome via the KH-like domain. J Bacteriol *192*, 2277-2283. 10.1128/JB.00045-10.

Ingle, S., Chhabra, S., Laspina, D., Salvo, E., Liu, B., and Bechhofer, D.H. (2020). Polynucleotide phosphorylase and RNA helicase CshA cooperate in *Bacillus subtilis* mRNA decay. RNA Biol, 1-10. 10.1080/15476286.2020.1864183.

Inoue, K., Alsina, J., Chen, J., and Inouye, M. (2003). Suppression of defective ribosome assembly in a *rbfA* deletion mutant by overexpression of Era, an essential GTPase in *Escherichia coli*. Mol Microbiol *48*, 1005-1016. 10.1046/j.1365-2958.2003.03475.x.

Irving, S.E., Choudhury, N.R., and Corrigan, R.M. (2020). The stringent response and physiological roles of (pp)pGpp in bacteria. Nat Rev Microbiol *19*, 256-271. 10.1038/s41579-020-00470-y.

Irving, S.E., and Corrigan, R.M. (2018). Triggering the stringent response: Signals responsible for activating (p)ppGpp synthesis in bacteria. Microbiology (United Kingdom) *164*, 268--276. 10.1099/mic.0.000621.

Ito, T., Katayama, Y., Asada, K., Mori, N., Tsutsumimoto, K., Tiensasitorn, C., and Hiramatsu, K. (2001). Structural comparison of three types of staphylococcal cassette chromosome mec integrated in the

chromosome in methicillin-resistant *Staphylococcus aureus*. Antimicrob Agents Chemother *45*, 1323-1336. 10.1128/AAC.45.5.1323-1336.2001.

Ito, T., Katayama, Y., and Hiramatsu, K. (1999). Cloning and nucleotide sequence determination of the entire *mec* DNA of pre-methicillin-resistant *Staphylococcus aureus* N315. Antimicrob Agents Chemother *43*, 1449-1458. 10.1128/AAC.43.6.1449.

Jacob, A.I., Khrer, C., Davies, B.W., RajBhandary, U.L., and Walker, G.C. (2013). Conserved bacterial RNase YbeY plays key roles in 70S ribosome quality control and 16S rRNA maturation. Mol Cell *49*, 427--438. 10.1016/j.molcel.2012.11.025.

Jain, N., Dhimole, N., Khan, A.R., De, D., Tomar, S.K., Sajish, M., Dutta, D., Parrack, P., and Prakash, B. (2009). *E. coli* HflX interacts with 50S ribosomal subunits in presence of nucleotides. Biochem Biophys Res Commun *379*, 201-205. 10.1016/j.bbrc.2008.12.072.

Jain, N., Vithani, N., Rafay, A., and Prakash, B. (2013). Identification and characterization of a hitherto unknown nucleotide-binding domain and an intricate interdomain regulation in HflX-a ribosome binding GTPase. Nucleic Acids Res *41*, 9557-9569. 10.1093/nar/gkt705.

Jaishankar, J., and Srivastava, P. (2017). Molecular basis of stationary phase survival and applications. Front Microbiol *8*, 2000. 10.3389/fmicb.2017.02000.

Jenkins, J., Mantell, J., Neal, C., Gholinia, A., Verkade, P., Nobbs, A.H., and Su, B. (2020). Antibacterial effects of nanopillar surfaces are mediated by cell impedance, penetration and induction of oxidative stress. Nat Commun *11*, 1626. 10.1038/s41467-020-15471-x.

Jenner, L., Romby, P., Rees, B., Schulze-Briese, C., Springer, M., Ehresmann, C., Ehresmann, B., Moras, D., Yusupova, G., and Yusupov, M. (2005). Translational operator of mRNA on the ribosome: how repressor proteins exclude ribosome binding. Science *308*, 120-123. 10.1126/science.1105639.

Ji, X. (2016). Structural insights into cell cycle control by essential GTPase Era. Postepy Biochem *62*, 335-342.

Jiale, Z., Jian, J., Xinyi, T., Haoji, X., Xueqin, H., and Xiao, W. (2021). Design of a novel antimicrobial peptide 1018M targeted ppGpp to inhibit MRSA biofilm formation. AMB Express *11*, 49. 10.1186/s13568-021-01208-6.

Jimmy, S., Saha, C.K., Kurata, T., Stavropoulos, C., Oliveira, S.R.A., Koh, A., Cepauskas, A., Takada, H., Rejman, D., Tenson, T., *et al*. (2020). A widespread toxin-antitoxin system exploiting growth control via alarmone signaling. Proc Natl Acad Sci U S A *117*, 10500-10510. 10.1073/pnas.1916617117.

Jomaa, A., Stewart Geordie, Martin-Benito, J., Zielke Ryszard, Campbell Tracey L., Maddock Janine R., Brown Eric D., and Joaquin, O. (2011). Understanding ribosome assembly: The structure of *in vivo* assembled immature 30S subunits revealed by cryo-electron microscopy. RNA *17*, 697--709. 10.1261/rna.2509811.

Julián, P., Milon, P., Agirrezabala, X., Lasso, G., Gil, D., Rodnina, M.V., and Valle, M. (2011). The Cryo-EM structure of a complete 30S translation initiation complex from *Escherichia coli*. PLoS Biol *9*, e1001095. 10.1371/journal.pbio.1001095.

Kaczanowska, M., and Ryden-Aulin, M. (2007). Ribosome biogenesis and the translation process in *Escherichia coli*. Microbiol Mol Biol Revs *71*, 477-494. 10.1128/mmbr.00013-07.

Kapust, R.B., and Waugh, D.S. (1999). *Escherichia coli* maltose-binding protein is uncommonly effective at promoting the solubility of polypeptides to which it is fused. Protein Sci *8*, 1668-1674. 10.1110/ps.8.8.1668.

Karbstein, K. (2007). Role of GTPases in ribosome assembly. Biopolymers *87*, 1-11. 10.1002/bip.20762.

Kaur, G., Sengupta, S., Kumar, V., Kumari, A., Ghosh, A., Parrack, P., and Dutta, D. (2014). Novel MntR-independent mechanism of manganese homeostasis in *Escherichia coli* by the ribosome-associated protein HflX. J Bacteriol *196*, 2587-2597. 10.1128/JB.01717-14.

Kavčič, B., Tkačik, G., and Bollenbach, T. (2020). Mechanisms of drug interactions between translation-inhibiting antibiotics. Nat Commun *11*, 4013. 10.1038/s41467-020-17734-z.

Kelley, L.A., Mezulis, S., Yates, C.M., Wass, M.N., and Sternberg, M.J. (2015). The Phyre2 web portal for protein modeling, prediction and analysis. Nat Protoc *10*, 845-858. 10.1038/nprot.2015.053.

Khemici, V., Prados, J., Petrignani, B., Di Nolfi, B., Bergé, E., Manzano, C., Giraud, C., and Linder, P. (2020). The DEAD-box RNA helicase CshA is required for fatty acid homeostasis in *Staphylococcus aureus*. PLoS Genet *16*, e1008779. 10.1371/journal.pgen.1008779.

Khrapunov, S. (2009). Circular dichroism spectroscopy has intrinsic limitations for protein secondary structure analysis. Anal Biochem *389*, 174-176. 10.1016/j.ab.2009.03.036.

Kihira, K., Shimizu, Y., Shomura, Y., Shibata, N., Kitamura, M., Nakagawa, A., Ueda, T., Ochi, K., and Higuchi, Y. (2012). Crystal structure analysis of the translation factor RF3 (release factor 3). FEBS Lett *586*, 3705-3709. 10.1016/j.febslet.2012.08.029.

Kim, C., Mwangi, M., Chung, M., Milheiriço, C., Milheirço, C., de Lencastre, H., and Tomasz, A. (2013). The mechanism of heterogeneous beta-lactam resistance in MRSA: key role of the stringent stress response. PLoS One *8*, e82814. 10.1371/journal.pone.0082814.

Kluska, K., Adamczyk, J., and Krężel, A. (2017). Metal binding properties, stability and reactivity of zinc fingers. Coordination Chemistry Reviews *367*, 18-64.

Kluska, K., Adamczyk, J., and Krężel, A. (2018). Metal binding properties of zinc fingers with a naturally altered metal binding site. Metallomics *10*, 248-263. 10.1039/c7mt00256d.

Kobayashi, S.D., and DeLeo, F.R. (2013). *Staphylococcus aureus* protein A promotes immune suppression. mBio *4*, e00764-00713. 10.1128/mBio.00764-13.

Koenig, R.L., Ray, J.L., Maleki, S.J., Smeltzer, M.S., and Hurlburt, B.K. (2004). *Staphylococcus aureus* AgrA binding to the RNAIII-agr regulatory region. J Bacteriol *186*, 7549-7555. 10.1128/JB.186.22.7549-7555.2004.

Kourtis, A.P., Hatfield, K., Baggs, J., Mu, Y., See, I., Epson, E., Nadle, J., Kainer, M.A., Dumyati, G., Petit, S., *et al*. (2019). Vital signs: epidemiology and recent trends in methicillin-resistant and in methicillin-susceptible *Staphylococcus aureus* bloodstream infections - United States. MMWR Morb Mortal Wkly Rep *68*, 214-219. 10.15585/mmwr.mm6809e1.

Krasny, L., and Gourse, R.L. (2004). An alternative strategy for bacterial ribosome synthesis: *Bacillus subtilis* rRNA transcription regulation. Embo J *23*, 4473-4483. 10.1038/sj.emboj.7600423.

Kriel, A., Bittner, A.N., Kim, S.H., Liu, K., Tehranchi, A.K., Zou, W.Y., Rendon, S., Chen, R., Tu, B.P., and Wang, J.D. (2012). Direct regulation of GTP homeostasis by (p)ppGpp: a critical component of viability and stress resistance. Mol Cell *48*, 231-241. 10.1016/j.molcel.2012.08.009.

Kudva, R., Tian, P., Pardo-Avila, F., Carroni, M., Best, R.B., Bernstein, H.D., and von Heijne, G. (2018). The shape of the bacterial ribosome exit tunnel affects cotranslational protein folding. eLife *7*. 10.7554/eLife.36326.

Kullik, I., Giachino, P., and Fuchs, T. (1998). Deletion of the alternative sigma factor sigmaB in *Staphylococcus aureus* reveals its function as a global regulator of virulence genes. J Bacteriol *180*, 4814-4820. 10.1128/JB.180.18.4814-4820.1998.

Kumar, V., Chen, Y., Ero, R., Ahmed, T., Tan, J., Li, Z., Wong, A.S., Bhushan, S., and Gao, Y.G. (2015). Structure of BipA in GTP form bound to the ratcheted ribosome. Proc Natl Acad Sci U S A *112*, 10944-10949. 10.1073/pnas.1513216112.

Kuroda, A., Murphy, H., Cashel, M., and Kornberg, A. (1997). Guanosine tetra- and pentaphosphate promote accumulation of inorganic polyphosphate in *Escherichia coli*. J Biol Chem *272*, 21240-21243. 10.1074/jbc.272.34.21240.

Kuwahara-Arai, K., Kondo, N., Hori, S., Tateda-Suzuki, E., and Hiramatsu, K. (1996). Suppression of methicillin resistance in a *mecA*-containing pre-methicillin-resistant *Staphylococcus aureus* strain is caused by the mecI-mediated repression of PBP 2' production. Antimicrob Agents Chemother *40*, 2680-2685. 10.1128/AAC.40.12.2680.

Kwon, N.H., Park, K.T., Moon, J.S., Jung, W.K., Kim, S.H., Kim, J.M., Hong, S.K., Koo, H.C., Joo, Y.S., and Park, Y.H. (2005). Staphylococcal cassette chromosome *mec* (SCC*mec*) characterization and molecular analysis for methicillin-resistant *Staphylococcus aureus* and novel SCC*mec* subtype IVg isolated from bovine milk in Korea. J Antimicrob Chemother *56*, 624-632. 10.1093/jac/dki306.

Kycia, J.H., Biou, V., Shu, F., Gerchman, S.E., Graziano, V., and Ramakrishnan, V. (1995). Prokaryotic translation initiation factor IF3 is an elongated protein consisting of two crystallizable domains. Biochemistry *34*, 6183-6187. 10.1021/bi00018a022.

Kästle, B., Geiger, T., Gratani, F.L., Reisinger, R., Goerke, C., Borisova, M., Mayer, C., and Wolz, C. (2015). rRNA regulation during growth and under stringent conditions in *Staphylococcus aureus*. Envir Microbiol *17*, 4394-4405. 10.1111/1462-2920.12867.

La Teana, A., Pon, C.L., and Gualerzi, C.O. (1993). Translation of mRNAs with degenerate initiation triplet AUU displays high initiation factor 2 dependence and is subject to initiation factor 3 repression. Proc Natl Acad Sci U S A *90*, 4161-4165. 10.1073/pnas.90.9.4161.

Lacey, K.A., Geoghegan, J.A., and McLoughlin, R.M. (2016). The role of *Staphylococcus aureus* virulence factors in skin infection and their potential as vaccine antigens. Pathogens *5*. 10.3390/pathogens5010022.

LaMarre, J., Mendes, R.E., Szal, T., Schwarz, S., Jones, R.N., and Mankin, A.S. (2013). The genetic environment of the cfr gene and the presence of other mechanisms account for the very high linezolid resistance of *Staphylococcus epidermidis* isolate 426-3147L. Antimicrob Agents Chemother *57*, 1173-1179. 10.1128/AAC.02047-12.

Lareau, L.F., Hite, D.H., Hogan, G.J., and Brown, P.O. (2014). Distinct stages of the translation elongation cycle revealed by sequencing ribosome-protected mRNA fragments. Elife *3*, e01257. 10.7554/eLife.01257.

Laurino, P., Tóth-Petróczy, Á., Meana-Pañeda, R., Lin, W., Truhlar, D.G., and Tawfik, D.S. (2016). An ancient fingerprint indicates the common ancestry of Rossmann-fold enzymes utilizing different ribose-based cofactors. PLoS Biol *14*, e1002396. 10.1371/journal.pbio.1002396.

Layne, E. (1957). [73] Spectrophotometric and turbidimetric methods for measuring proteins (Academic Press). https://doi.org/10.1016/S0076-6879(57)03413-8.

Le, K.Y., and Otto, M. (2015). Quorum-sensing regulation in *staphylococci*-an overview. Front Microbiol *6*, 1174. 10.3389/fmicb.2015.01174.

Lee, C.Y., Schmidt, J.J., Johnson-Winegar, A.D., Spero, L., and Iandolo, J.J. (1987). Sequence determination and comparison of the exfoliative toxin A and toxin B genes from *Staphylococcus aureus*. J Bacteriol *169*, 3904-3909. 10.1128/jb.169.9.3904-3909.1987.

Lee, J.W., Park, Y.H., and Seok, Y.J. (2018). Rsd balances (p)ppGpp level by stimulating the hydrolase activity of SpoT during carbon source downshift in *Escherichia coli*. Proc Natl Acad Sci U S A *115*, E6845-E6854. 10.1073/pnas.1722514115.

Lee, S.M., Ender, M., Adhikari, R., Smith, J.M., Berger-Bächi, B., and Cook, G.M. (2007). Fitness cost of staphylococcal cassette chromosome *mec* in methicillin-resistant *Staphylococcus aureus* by way of continuous culture. Antimicrob Agents Chemother *51*, 1497-1499. 10.1128/AAC.01239-06.

Leipe, D.D., Wolf, Y.I., Koonin, E.V., and Aravind, L. (2002). Classification and evolution of P-loop GTPases and related ATPases. Journal of Molecular Biology *317*, 41--72. 10.1006/jmbi.2001.5378.

Leung, E.K., Suslov, N., Tuttle, N., Sengupta, R., and Piccirilli, J.A. (2011). The mechanism of peptidyl transfer catalysis by the ribosome. Annu Rev Biochem *80*, 527-555. 10.1146/annurev-biochem-082108-165150.

Levdikov, V.M., Blagova, E.V., Brannigan, J.A., Cladière, L., Antson, A.A., Isupov, M.N., Séror, S.J., and Wilkinson, A.J. (2004). The crystal structure of YloQ, a circularly permuted GTPase essential for *Bacillus subtilis* viability. Journal of Molecular Biology *340*, 767-782. 10.1016/j.jmb.2004.05.029.

Li, G., Xie, F., Zhang, Y., Bossé, J.T., Langford, P.R., and Wang, C. (2015). Role of (p)ppGpp in Viability and Biofilm Formation of *Actinobacillus pleuropneumoniae* S8. PLoS One *10*, e0141501. 10.1371/journal.pone.0141501.

Li, Z., and Deutscher, M.P. (1996). Maturation pathways for *E. coli* tRNA precursors: a random multienzyme process *in vivo*. Cell *86*, 503-512. 10.1016/s0092-8674(00)80123-3.

Li, Z., Zhuang, H., Wang, G., Wang, H., and Dong, Y. (2021). Prevalence, predictors, and mortality of bloodstream infections due to methicillin-resistant *Staphylococcus aureus* in patients with malignancy: systemic review and meta-analysis. BMC Infect Dis *21*, 74. 10.1186/s12879-021-05763-y.

Lin, J., Zhou, D., Steitz, T.A., Polikanov, Y.S., and Gagnon, M.G. (2018). Ribosome-targeting antibiotics: modes of action, mechanisms of resistance, and implications for drug design. Annu Rev Biochem *87*, 451-478. 10.1146/annurev-biochem-062917-011942.

Lina, G., Piémont, Y., Godail-Gamot, F., Bes, M., Peter, M.O., Gauduchon, V., Vandenesch, F., and Etienne, J. (1999). Involvement of Panton-Valentine leukocidin-producing *Staphylococcus aureus* in primary skin infections and pneumonia. Clin Infect Dis *29*, 1128-1132. 10.1086/313461.

Liu, C., Chen, Z.J., Sun, Z., Feng, X., Zou, M., Cao, W., Wang, S., Zeng, J., Wang, Y., and Sun, M. (2015a). Molecular characteristics and virulence factors in methicillin-susceptible, resistant, and heterogeneous vancomycin-intermediate *Staphylococcus aureus* from central-southern China. J Microbiol Immunol Infect *48*, 490-496. 10.1016/j.jmii.2014.03.003.

Liu, K., Myers, A.R., Pisithkul, T., Claas, K.R., Satyshur, K.A., Amador-Noguez, D., Keck, J.L., and Wang, J.D. (2015b). Molecular mechanism and evolution of guanylate kinase regulation by (p)ppGpp. Mol Cell *57*, 735-749. 10.1016/j.molcel.2014.12.037.

Liu, Q., and Fredrick, K. (2015). Roles of helix H69 of 23S rRNA in translation initiation. Proc Natl Acad Sci U S A *112*, 11559-11564. 10.1073/pnas.1507703112.

Liu, Q., Yeo, W.S., and Bae, T. (2016). The SaeRS Two-Component System of *Staphylococcus aureus*. Genes (Basel) *7*. 10.3390/genes7100081.

Los, F.C., Randis, T.M., Aroian, R.V., and Ratner, A.J. (2013). Role of pore-forming toxins in bacterial infectious diseases. Microbiol Mol Biol Rev *77*, 173-207. 10.1128/MMBR.00052-12.

Loveland, A.B., Bah, E., Madireddy, R., Zhang, Y., Brilot, A.F., Grigorieff, N., and Korostelev, A.A. (2016). Ribosome•RelA structures reveal the mechanism of stringent response activation. Elife *5*. 10.7554/eLife.17029.

L**uong, T.T.**, and Lee, C.Y. (2007). Improved single-copy integration vectors for *Staphylococcus aureus*. J Microbiol Methods *70*, 186-190. 10.1016/j.mimet.2007.04.007.

López-Alonso, J.P., Fabbretti, A., Kaminishi, T., Iturrioz, I., Brandi, L., Gil-Carton, D., Gualerzi, C.O., Fucini, P., and Connell, S.R. (2017a). Structure of a 30S pre-initiation complex stalled by GE81112 reveals structural parallels in bacterial and eukaryotic protein synthesis initiation pathways. Nucleic Acids Res *45*, 2179-2187. 10.1093/nar/gkw1251.

López-Alonso, J.P., Kaminishi, T., Kikuchi, T., Hirata, Y., Iturrioz, I., Dhimole, N., Schedlbauer, A., Hase, Y., Goto, S., Kurita, D., *et al*. (2017b). RsgA couples the maturation state of the 30S ribosomal decoding center to activation of its GTPase pocket. Nucleic Acids Res *45*, 6945-6959. 10.1093/nar/gkx324.

Ma, C., Kurita, D., Li, N., Chen, Y., Himeno, H., and Gao, N. (2017). Mechanistic insights into the alternative translation termination by ArfA and RF2. Nature *541*, 550-553. 10.1038/nature20822.

Maciag, M., Kochanowska, M., Lyzeń, R., Wegrzyn, G., and Szalewska-Pałasz, A. (2010). ppGpp inhibits the activity of *Escherichia coli* DnaG primase. Plasmid *63*, 61-67. 10.1016/j.plasmid.2009.11.002.

Majerczyk, C.D., Sadykov, M.R., Luong, T.T., Lee, C., Somerville, G.A., and Sonenshein, A.L. (2008). *Staphylococcus aureus* CodY negatively regulates virulence gene expression. J Bacteriol *190*, 2257-2265. 10.1128/JB.01545-07.

Manav, M.C., Beljantseva, J., Bojer, M.S., Tenson, T., Ingmer, H., Hauryliuk, V., and Brodersen, D.E. (2018). Structural basis for (p)ppGpp synthesis by the *Staphylococcus aureus* small alarmone synthetase RelP. J Biol Chem *293*, 3254-3264. 10.1074/jbc.RA117.001374.

Martin, R., Hearn, M., Jenny, P., and Gallant, J. (1988). Release factor competition is equivalent at strong and weakly suppressed nonsense codons. Mol Gen Genet *213*, 144-149. 10.1007/BF00333411.

Martin, R., Straub, A.U., Doebele, C., and Bohnsack, M.T. (2013). DExD/H-box RNA helicases in ribosome biogenesis. RNA Biol *10*, 4-18. 10.4161/rna.21879.

Martínez-Vicente, M., Yim, L., Villarroya, M., Mellado, M., Pérez-Payá, E., Björk, G.R., and Armengod, M.E. (2005). Effects of mutagenesis in the switch I region and conserved arginines of *Escherichia coli* MnmE protein, a GTPase involved in tRNA modification. J Biol Chem *280*, 30660-30670. 10.1074/jbc.M503223200.

Matsuo, Y., Morimoto, T., Kuwano, M., Loh, P.C., Oshima, T., and Ogasawara, N. (2006). The GTP-binding protein YlqF participates in the late step of 50 S ribosomal subunit assembly in *Bacillus subtilis*. J Biol Chem *281*, 8110-8117. 10.1074/jbc.M512556200.

Matsuo, Y., Oshima, T., Loh, P.C., Morimoto, T., and Ogasawara, N. (2007). Isolation and characterization of a dominant negative mutant of *Bacillus subtilis* GTP-binding protein, YlqF, essential for biogenesis and maintenance of the 50 S ribosomal subunit. J Biol Chem *282*, 25270-25277. 10.1074/jbc.M703894200.

Matthews, B.W., Nicholson, H., and Becktel, W.J. (1987). Enhanced protein thermostability from site-directed mutations that decrease the entropy of unfolding. Proc Natl Acad Sci U S A *84*, 6663-6667. 10.1073/pnas.84.19.6663.

Matthews, K.R., Roberson, J., Gillespie, B.E., Luther, D.A., and Oliver, S.P. (1997). Identification and differentiation of coagulase-negative *Staphylococcus aureus* by polymerase chain reaction. J Food Prot *60*, 686-688. 10.4315/0362-028X-60.6.686.

Matzov, D., Aibara, S., Basu, A., Zimmerman, E., Bashan, A., Yap, M.F., Amunts, A., and Yonath, A.E. (2017). The cryo-EM structure of hibernating 100S ribosome dimer from pathogenic *Staphylococcus aureus*. Nat Commun *8*, 723. 10.1038/s41467-017-00753-8.

Mazmanian, S.K., Liu, G., Jensen, E.R., Lenoy, E., and Schneewind, O. (2000). *Staphylococcus aureus* sortase mutants defective in the display of surface proteins and in the pathogenesis of animal infections. Proc Natl Acad Sci U S A *97*, 5510-5515. 10.1073/pnas.080520697.

Mazmanian, S.K., Liu, G., Ton-That, H., and Schneewind, O. (1999). *Staphylococcus aureus* sortase, an enzyme that anchors surface proteins to the cell wall. Science *285*, 760-763. 10.1126/science.285.5428.760.

McAdow, M., Missiakas, D.M., and Schneewind, O. (2012). *Staphylococcus aureus* secretes coagulase and von Willebrand factor binding protein to modify the coagulation cascade and establish host infections. J Innate Immun *4*, 141-148. 10.1159/000333447.

McClendon, C.L., Kornev, A.P., Gilson, M.K., and Taylor, S.S. (2014). Dynamic architecture of a protein kinase. Proc Natl Acad Sci U S A *111*, E4623-4631. 10.1073/pnas.1418402111.

McCoy, A.J., Grosse-Kunstleve, R.W., Adams, P.D., Winn, M.D., Storoni, L.C., and Read, R.J. (2007). Phaser crystallographic software. J Appl Crystallogr *40*, 658-674. 10.1107/S0021889807021206.

McLaughlin, J.R., Murray, C.L., and Rabinowitz, J.C. (1981). Unique features in the ribosome binding site sequence of the Gram-positive *Staphylococcus aureus* beta-lactamase gene. J Biol Chem *256*, 11283-11291.

McPherson, A. (2001). A comparison of salts for the crystallization of macromolecules. Protein Sci *10*, 418-422. 10.1110/ps.32001.

McPherson, A., and Gavira, J.A. (2014). Introduction to protein crystallization. Acta Crystallogr F Struct Biol Commun *70*, 2-20. 10.1107/S2053230X13033141.

Mechold, U., Potrykus, K., Murphy, H., Murakami, K.S., and Cashel, M. (2013). Differential regulation by ppGpp versus pppGpp in *Escherichia coli*. Nucleic Acids Res *41*, 6175-6189. 10.1093/nar/gkt302.

Meek, R.W., Cadby, I.T., Moynihan, P.J., and Lovering, A.L. (2019). Structural basis for activation of a diguanylate cyclase required for bacterial predation in *Bdellovibrio*. Nat Commun *10*, 4086. 10.1038/s41467-019-12051-6.

Mestrom, L., Marsden, S.R., Dieters, M., Achterberg, P., Stolk, L., Bento, I., Hanefeld, U., and Hagedoorn, P.L. (2019). Artificial fusion of mCherry enhances trehalose transferase solubility and stability. Appl Environ Microbiol *85*. 10.1128/AEM.03084-18.

Miller, H.K., Carroll, R.K., Burda, W.N., Krute, C.N., Davenport, J.E., and Shaw, L.N. (2012). The extracytoplasmic function sigma factor σS protects against both intracellular and extracytoplasmic stresses in *Staphylococcus aureus*. J Bacteriol *194*, 4342-4354. 10.1128/JB.00484-12.

Milon, P., Tischenko, E., Tomsic, J., Caserta, E., Folkers, G., La Teana, A., Rodnina, M.V., Pon, C.L., Boelens, R., and Gualerzi, C.O. (2006). The nucleotide-binding site of bacterial translation initiation factor 2 (IF2) as a metabolic sensor. Proc Natl Acad Sci U S A *103*, 13962-13967. 10.1073/pnas.0606384103.

Mishra, A.K., and Lambright, D.G. (2016). Invited review: Small GTPases and their GAPs. Biopolymers *105*, 431-448. 10.1002/bip.22833.

Mishra, R., Gara, S.K., Mishra, S., and Prakash, B. (2005). Analysis of GTPases carrying hydrophobic amino acid substitutions in lieu of the catalytic glutamine: implications for GTP hydrolysis. Proteins *59*, 332-338. 10.1002/prot.20413.

Mitkevich, V.A., Ermakov, A., Kulikova, A.A., Tankov, S., Shyp, V., Soosaar, A., Tenson, T., Makarov, A.A., Ehrenberg, M., and Hauryliuk, V. (2010). Thermodynamic characterization of ppGpp binding to EF-G or IF2 and of initiator tRNA binding to free IF2 in the presence of GDP, GTP, or ppGpp. J Mol Biol *402*, 838-846. 10.1016/j.jmb.2010.08.016.

Mittenhuber, G. (2001). Comparative genomics and evolution of genes encoding bacterial (p)ppGpp synthetases/hydrolases (the Rel, RelA and SpoT proteins). J Mol Microbiol Biotechnol *3*, 585-600.

Mizushima, S., and Nomura, M. (1970). Assembly mapping of 30S ribosomal proteins from *E. coli*. Nature *226*, 1214. 10.1038/2261214a0.

Moazed, D., and Noller, H.F. (1989). Intermediate states in the movement of transfer RNA in the ribosome. Nature *342*, 142-148. 10.1038/342142a0.

Molodtsov, V., Sineva, E., Zhang, L., Huang, X., Cashel, M., Ades, S.E., and Murakami, K.S. (2018). Allosteric Effector ppGpp Potentiates the Inhibition of Transcript Initiation by DksA. Mol Cell *69*, 828-839.e825. 10.1016/j.molcel.2018.01.035.

Montgomery, C.P., Boyle-Vavra, S., Roux, A., Ebine, K., Sonenshein, A.L., and Daum, R.S. (2012). CodY deletion enhances in vivo virulence of community-associated methicillin-resistant *Staphylococcus aureus* clone USA300. Infect Immun *80*, 2382-2389. 10.1128/IAI.06172-11.

Moore, P. (2005). The GTPase switch in ribosomal translocation. J Biol *4*, 7. 10.1186/jbiol28.

Moosavian, M., Shahin, M., Navidifar, T., and Torabipour, M. (2018). Typing of staphylococcal cassette chromosome m*ec* encoding methicillin resistance in S*taphylococcus aureus* isolates in Ahvaz, Iran. New Microbes New Infect *21*, 90-94. 10.1016/j.nmni.2017.11.006.

Morroni, G., Brenciani, A., Brescini, L., Fioriti, S., Simoni, S., Pocognoli, A., Mingoia, M., Giovanetti, E., Barchiesi, F., Giacometti, A., and Cirioni, O. (2018). High Rate of ceftobiprole resistance among clinical methicillin-resistant S*taphylococcus aureus* isolates from a hospital in central italy. Antimicrob Agents Chemother *62*. 10.1128/AAC.01663-18.

Mougey, E.B., O'Reilly, M., Osheim, Y., Miller, O.L., Beyer, A., and Sollner-Webb, B. (1993). The terminal balls characteristic of eukaryotic rRNA transcription units in chromatin spreads are rRNA processing complexes. Genes Dev *7*, 1609-1619. 10.1101/gad.7.8.1609.

Murshudov, G.N., Vagin, A.A., and Dodson, E.J. (1997). Refinement of macromolecular structures by the maximum-likelihood method. Acta Crystallogr D Biol Crystallogr *53*, 240-255. 10.1107/S0907444996012255.

Murzin, A.G. (1993). OB(oligonucleotide/oligosaccharide binding)-fold: common structural and functional solution for non-homologous sequences. EMBO J *12*, 861-867.

Młynarczyk, A., Młynarczyk, G., and Jeljaszewicz, J. (1998). The genome of *Staphylococcus aureus*: a review. Zentralbl Bakteriol *287*, 277-314. 10.1016/s0934-8840(98)80165-5.

Naimi, T.S., LeDell, K.H., Como-Sabetti, K., Borchardt, S.M., Boxrud, D.J., Etienne, J., Johnson, S.K., Vandenesch, F., Fridkin, S., O'Boyle, C., *et al*. (2003). Comparison of community- and health care-associated methicillin-resistant *Staphylococcus aureus* infection. JAMA *290*, 2976-2984. 10.1001/jama.290.22.2976.

Najmanovich, R.J. (2017). Evolutionary studies of ligand binding sites in proteins. Curr Opin Struct Biol *45*, 85-90. 10.1016/j.sbi.2016.11.024.

Napper, N., and Culver, G.M. (2015). Analysis of r-protein and RNA conformation of 30S subunit intermediates in bacteria. RNA *21*, 1323-1334. 10.1261/rna.048918.114.

Newman, J., Egan, D., Walter, T.S., Meged, R., Berry, I., Ben Jelloul, M., Sussman, J.L., Stuart, D.I., and Perrakis, A. (2005). Towards rationalization of crystallization screening for small- to medium-sized academic laboratories: the PACT/JCSG+ strategy. Acta Crystallogr D Biol Crystallogr *61*, 1426-1431. 10.1107/S0907444905024984.

Ngan, J.Y.G., Pasunooti, S., Tse, W., Meng, W., Ngan, S.F.C., Jia, H., Lin, J.Q., Ng, S.W., Jaafa, M.T., Cho, S.L.S., *et al*. (2021). HflX is a GTPase that controls hypoxia-induced replication arrest in slow-growing mycobacteria. Proc Natl Acad Sci U S A *118*. 10.1073/pnas.2006717118.

Nichols, C.E., Johnson, C., Lamb, H.K., Lockyer, M., Charles, I.G., Hawkins, A.R., and Stammers, D.K. (2007). Structure of the ribosomal interacting GTPase YjeQ from the enterobacterial species *Salmonella typhimurium*. Acta Crystallogr Sect F Struct Biol Cryst Commun *63*, 922-928. 10.1107/S1744309107048609.

Nierhaus, K.H. (2014). Mg^{2+}, K^+, and the ribosome. J Bacteriol *196*, 3817-3819. 10.1128/JB.02297-14.

Nikolay, R., Schloemer, R., Mueller, S., and Deuerling, E. (2015). Fluorescence-based monitoring of ribosome assembly landscapes. BMC Mol Biol *16*, 3. 10.1186/s12867-015-0031-y.

Nikolay, R., Schmidt, S., Schlmer, R., Deuerling, E., and Nierhaus, K. (2016). Ribosome assembly as antimicrobial target. Antibiotics *5*, 18. 10.3390/antibiotics5020018.

Noller, H.F. (1984). Structure of ribosomal RNA. Annu Rev Biochem *53*, 119-162. 10.1146/annurev.bi.53.070184.001003.

Noller, H.F., Lancaster, L., Zhou, J., and Mohan, S. (2017). The ribosome moves: RNA mechanics and translocation. Nat Struct Mol Biol *24*, 1021-1027. 10.1038/nsmb.3505.

Nürenberg-Goloub, E., and Tampé, R. (2019). Ribosome recycling in mRNA translation, quality control, and homeostasis. Biol Chem *401*, 47-61. 10.1515/hsz-2019-0279.

O'Brien, E.C., and McLoughlin, R.M. (2019). Considering the 'alternatives' for next-generation anti-*Staphylococcus aureus* vaccine development. Trends Mol Med *25*, 171-184. 10.1016/j.molmed.2018.12.010.

Ogston, A. (1881). Report upon micro-organisms in surgical diseases. Br Med J *1*, 369.b362-375. 10.1136/bmj.1.1054.369.

Ogston, A. (1882). *Micrococcus* Poisoning. J Anat Physiol *17*, 24-58.

Oh, Y.T., Park, Y., Yoon, M.Y., Bari, W., Go, J., Min, K.B., Raskin, D.M., Lee, K.M., and Yoon, S.S. (2014). Cholera toxin production during anaerobic trimethylamine N-oxide respiration is mediated by stringent response in *Vibrio cholerae*. J Biol Chem *289*, 13232-13242. 10.1074/jbc.M113.540088.

Oliveira, D., Borges, A., and Simões, M. (2018). *Staphylococcus aureus* toxins and their molecular activity in infectious diseases. Toxins (Basel) *10*. 10.3390/toxins10060252.

Oliveira, D.C., Milheiriço, C., and de Lencastre, H. (2006). Redefining a structural variant of staphylococcal cassette chromosome *mec*, SCC*mec* type VI. Antimicrob Agents Chemother *50*, 3457-3459. 10.1128/AAC.00629-06.

Olsen, R.J., Kobayashi, S.D., Ayeras, A.A., Ashraf, M., Graves, S.F., Ragasa, W., Humbird, T., Greaver, J.L., Cantu, C., Swain, J.L., *et al*. (2010). Lack of a major role of *Staphylococcus aureus* Panton-Valentine leukocidin in lower respiratory tract infection in nonhuman primates. Am J Pathol *176*, 1346-1354. 10.2353/ajpath.2010.090960.

Ooga, T., Ohashi, Y., Kuramitsu, S., Koyama, Y., Tomita, M., Soga, T., and Masui, R. (2009). Degradation of ppGpp by nudix pyrophosphatase modulates the transition of growth phase in the bacterium *Thermus thermophilus*. J Biol Chem *284*, 15549-15556. 10.1074/jbc.M900582200.

Otto, M. (2010). Basis of virulence in community-associated methicillin-resistant *Staphylococcus aureus*. Annu Rev Microbiol *64*, 143-162. 10.1146/annurev.micro.112408.134309.

Pace, N.J., and Weerapana, E. (2014). Zinc-binding cysteines: diverse functions and structural motifs. Biomolecules *4*, 419-434. 10.3390/biom4020419.

Pader, V., Hakim, S., Painter, K.L., Wigneshweraraj, S., Clarke, T.B., and Edwards, A.M. (2016). *Staphylococcus aureus* inactivates daptomycin by releasing membrane phospholipids. Nat Microbiol *2*, 16194. 10.1038/nmicrobiol.2016.194.

Page, R., Grzechnik, S.K., Canaves, J.M., Spraggon, G., Kreusch, A., Kuhn, P., Stevens, R.C., and Lesley, S.A. (2003). Shotgun crystallization strategy for structural genomics: an optimized two-tiered crystallization screen against the *Thermotoga maritima* proteome. Acta Crystallogr D Biol Crystallogr *59*, 1028-1037. 10.1107/s0907444903007790.

Pando, J.M., Pfeltz, R.F., Cuaron, J.A., Nagarajan, V., Mishra, M.N., Torres, N.J., Elasri, M.O., Wilkinson, B.J., and Gustafson, J.E. (2017). Ethanol-induced stress response of *Staphylococcus aureus*. Can J Microbiol *63*, 745-757. 10.1139/cjm-2017-0221.

Parvizi, J., Saleh, K.J., Ragland, P.S., Pour, A.E., and Mont, M.A. (2008). Efficacy of antibiotic-impregnated cement in total hip replacement. Acta Orthop *79*, 335-341. 10.1080/17453670710015229.

Pasqualato, S., and Cherfils, J. (2005). Crystallographic evidence for substrate-assisted GTP hydrolysis by a small GTP binding protein. Structure *13*, 533-540. 10.1016/j.str.2005.01.014.

Pasquina-Lemonche, L., Burns, J., Turner, R.D., Kumar, S., Tank, R., Mullin, N., Wilson, J.S., Chakrabarti, B., Bullough, P.A., Foster, S.J., and Hobbs, J.K. (2020). The architecture of the Gram-positive bacterial cell wall. Nature *582*, 294-297. 10.1038/s41586-020-2236-6.

Patacq, C., Chaudet, N., and Létisse, F. (2020). Crucial Role of ppGpp in the resilience of *Escherichia coli* to growth disruption. mSphere *5*. 10.1128/mSphere.01132-20.

Pausch, P., Steinchen, W., Wieland, M., Klaus, T., Freibert, S.A., Altegoer, F., Wilson, D.N., and Bange, G. (2018). Structural basis for (p)ppGpp-mediated inhibition of the GTPase RbgA. J Biol Chem *293*, 19699-19709. 10.1074/jbc.RA118.003070.

Peske, F., Kuhlenkoetter, S., Rodnina, M.V., and Wintermeyer, W. (2014). Timing of GTP binding and hydrolysis by translation termination factor RF3. Nucleic Acids Res *42*, 1812-1820. 10.1093/nar/gkt1095.

Peyrusson, F., Varet, H., Nguyen, T.K., Legendre, R., Sismeiro, O., Coppée, J.Y., Wolz, C., Tenson, T., and Van Bambeke, F. (2020). Intracellular *Staphylococcus aureus* persisters upon antibiotic exposure. Nat Commun *11*, 2200. 10.1038/s41467-020-15966-7.

Piir, K., Paier, A., Liiv, A., Tenson, T., and Maiväli, U. (2011). Ribosome degradation in growing bacteria. EMBO Rep *12*, 458-462. 10.1038/embor.2011.47.

Pioletti, M., Schlünzen, F., Harms, J., Zarivach, R., Glühmann, M., Avila, H., Bashan, A., Bartels, H., Auerbach, T., Jacobi, C., *et al*. (2001). Crystal structures of complexes of the small ribosomal subunit with tetracycline, edeine and IF3. EMBO J *20*, 1829-1839. 10.1093/emboj/20.8.1829.

Pizarro-Cerdá, J., and Tedin, K. (2004). The bacterial signal molecule, ppGpp, regulates *Salmonella* virulence gene expression. Mol Microbiol *52*, 1827-1844. 10.1111/j.1365-2958.2004.04122.x.

Pletnev, P., Guseva, E., Zanina, A., Evfratov, S., Dzama, M., Treshin, V., Pogorel'skaya, A., Osterman, I., Golovina, A., Rubtsova, M., *et al*. (2020). Comprehensive functional analysis of *Escherichia coli* ribosomal rna methyltransferases. Front Genet *11*, 97. 10.3389/fgene.2020.00097.

Pletzer, D., Wolfmeier, H., Bains, M., and Hancock, R.E.W. (2017). Synthetic peptides to target stringent response-controlled virulence in a *Pseudomonas aeruginosa* murine cutaneous infection model. Front Microbiol *8*, 1867. 10.3389/fmicb.2017.01867.

Pohl, K., Francois, P., Stenz, L., Schlink, F., Geiger, T., Herbert, S., Goerke, C., Schrenzel, J., and Wolz, C. (2009). CodY in *Staphylococcus aureus*: a regulatory link between metabolism and virulence gene expression. J Bacteriol *191*, 2953-2963. 10.1128/JB.01492-08.

Pokhrel, A., Poudel, A., Castro, K.B., Celestine, M.J., Oludiran, A., Rinehold, A.J., Resek, A.M., Mhanna, M.A., and Purcell, E.B. (2020). The (p)ppGpp synthetase RSH mediates stationary-phase onset and antibiotic stress survival in *Clostridioides difficile*. J Bacteriol *202*. 10.1128/JB.00377-20.

Potrykus, K., and Cashel, M. (2008). (p)ppGpp: still magical? Annu Rev Microbiol *62*, 35--51. 10.1146/annurev.micro.62.081307.162903.

Queck, S.Y., Jameson-Lee, M., Villaruz, A.E., Bach, T.H., Khan, B.A., Sturdevant, D.E., Ricklefs, S.M., Li, M., and Otto, M. (2008). RNAIII-independent target gene control by the agr quorum-sensing system: insight into the evolution of virulence regulation in *Staphylococcus aureus*. Mol Cell *32*, 150-158. 10.1016/j.molcel.2008.08.005.

Quintero-Quiroz, C., Botero, L.E., Zárate-Triviño, D., Acevedo-Yepes, N., Escobar, J.S., Pérez, V.Z., and Cruz Riano, L.J. (2020). Synthesis and characterization of a silver nanoparticle-containing polymer composite with antimicrobial abilities for application in prosthetic and orthotic devices. Biomater Res *24*, 13. 10.1186/s40824-020-00191-6.

Radaev, S., Li, S., and Sun, P.D. (2006). A survey of protein-protein complex crystallizations. Acta Crystallogr D Biol Crystallogr *62*, 605-612. 10.1107/S0907444906011735.

Ramakrishnan, V. (1986). Distribution of protein and RNA in the 30S ribosomal subunit. Science *231*, 1562-1564. 10.1126/science.3513310.

Ramsay, R.R., and Tipton, K.F. (2017). Assessment of Enzyme Inhibition: A Review with Examples from the Development of Monoamine Oxidase and Cholinesterase Inhibitory Drugs. Molecules *22*. 10.3390/molecules22071192.

Rao, N., Cannella, B., Crossett, L.S., Yates, A.J., and McGough, R. (2008). A preoperative decolonization protocol for S*taphylococcus aureus* prevents orthopaedic infections. Clin Orthop Relat Res *466*, 1343-1348. 10.1007/s11999-008-0225-4.

Razi, A., Davis, J.H., Hao, Y., Jahagirdar, D., Thurlow, B., Basu, K., Jain, N., Gomez-Blanco, J., Britton, R.A., Vargas, J., *et al*. (2019). Role of Era in assembly and homeostasis of the ribosomal small subunit. Nucleic Acids Res *47*, 8301-8317. 10.1093/nar/gkz571.

Razi, A., Guarné, A., and Ortega, J. (2017). The cryo-EM structure of YjeQ bound to the 30S subunit suggests a fidelity checkpoint function for this protein in ribosome assembly. Proc Natl Acad Sci U S A *114*, E3396-E3403. 10.1073/pnas.1618016114.

Reiss, S., Pane-Farre, J., Fuchs, S., Francois, P., Liebeke, M., Schrenzel, J., Lindequist, U., Lalk, M., Wolz, C., Hecker, M., and Engelmann, S. (2012). Global analysis of the *Staphylococcus aureus* response to mupirocin. Antimicrob Agents Chemother *56*, 787-804. 10.1128/AAC.05363-11.

Rishishwar, L., Petit, R.A., Kraft, C.S., and Jordan, I.K. (2014). Genome sequence-based discriminator for vancomycin-intermediate *Staphylococcus aureus*. J Bacteriol *196*, 940-948. 10.1128/JB.01410-13.

Rodnina, M.V. (2016). The ribosome in action: Tuning of translational efficiency and protein folding. Protein Sci *25*, 1390-1406. 10.1002/pro.2950.

Rodnina, M.V. (2018). Translation in Prokaryotes. Cold Spring Harb Perspect Biol *10*. 10.1101/cshperspect.a032664.

Rodnina, M.V., and Wintermeyer, W. (2009). Recent mechanistic insights into eukaryotic ribosomes. Curr Opin Cell Biol *21*, 435-443. 10.1016/j.ceb.2009.01.023.

Roelofs, K.G., Wang, J., Sintim, H.O., and Lee, V.T. (2011). Differential radial capillary action of ligand assay for high-throughput detection of protein-metabolite interactions. Proc Natl Acad Sci U S A *108*, 15528-15533. 10.1073/pnas.1018949108.

Rogne, P., Dulko-Smith, B., Goodman, J., Rosselin, M., Grundström, C., Hedberg, C., Nam, K., Sauer-Eriksson, A.E., and Wolf-Watz, M. (2020). Structural Basis for GTP versus ATP Selectivity in the NMP Kinase AK3. Biochemistry *59*, 3570-3581. 10.1021/acs.biochem.0c00549.

Rogne, P., Rosselin, M., Grundström, C., Hedberg, C., Sauer, U.H., and Wolf-Watz, M. (2018). Molecular mechanism of ATP versus GTP selectivity of adenylate kinase. Proc Natl Acad Sci U S A *115*, 3012-3017. 10.1073/pnas.1721508115.

Rojas, A.M., Ehrenberg, M., Andersson, S.G., and Kurland, C.G. (1984). ppGpp inhibition of elongation factors Tu, G and Ts during polypeptide synthesis. Mol Gen Genet *197*, 36-45. 10.1007/bf00327920.

Romanò, C.L., Tsuchiya, H., Morelli, I., Battaglia, A.G., and Drago, L. (2019). Antibacterial coating of implants: are we missing something? Bone Joint Res *8*, 199-206. 10.1302/2046-3758.85.BJR-2018-0316.

Romero Romero, M.L., Yang, F., Lin, Y.R., Toth-Petroczy, A., Berezovsky, I.N., Goncearenco, A., Yang, W., Wellner, A., Kumar-Deshmukh, F., Sharon, M., *et al*. (2018). Simple yet functional phosphate-loop proteins. Proc Natl Acad Sci U S A *115*, E11943-E11950. 10.1073/pnas.1812400115.

Ronneau, S., and Hallez, R. (2019). Make and break the alarmone: Regulation of (p)ppGpp synthetase/hydrolase enzymes in bacteria. FEMS Microbiology Reviews *43*, 389--400. 10.1093/femsre/fuz009.

Root-Bernstein, M., and Root-Bernstein, R. (2015). The ribosome as a missing link in the evolution of life. J Theor Biol *367*, 130-158. 10.1016/j.jtbi.2014.11.025.

Rosato, A., Vicarini, H., and Leclercq, R. (1999). Inducible or constitutive expression of resistance in clinical isolates of streptococci and enterococci cross-resistant to erythromycin and lincomycin. J Antimicrob Chemother *43*, 559-562. 10.1093/jac/43.4.559.

Ross, W., Sanchez-Vazquez, P., Chen, A.Y., Lee, J.H., Burgos, H.L., and Gourse, R.L. (2016). ppGpp binding to a site at the RNAP-DksA interface accounts for its dramatic effects on transcription initiation during the stringent response. Mol Cell *62*, 811-823. 10.1016/j.molcel.2016.04.029.

Roy-Chaudhuri, B., Kirthi, N., and Culver, G.M. (2010). Appropriate maturation and folding of 16S rRNA during 30S subunit biogenesis are critical for translational fidelity. Proc Natl Acad Sci U S A *107*, 4567-4572. 10.1073/pnas.0912305107.

Russo Krauss, I., Merlino, A., Vergara, A., and Sica, F. (2013). An overview of biological macromolecule crystallization. Int J Mol Sci *14*, 11643-11691. 10.3390/ijms140611643.

Ruwe, M., Rückert, C., Kalinowski, J., and Persicke, M. (2018). Functional characterization of a small alarmone hydrolase in *Corynebacterium glutamicum*. Front Microbiol *9*, 916. 10.3389/fmicb.2018.00916.

Ruzheinikov, S.N., Das, S.K., Sedelnikova, S.E., Baker, P.J., Artymiuk, P.J., García-Lara, J., Foster, S.J., and Rice, D.W. (2004). Analysis of the open and closed conformations of the GTP-binding protein YsxC from *Bacillus subtilis*. J Mol Biol *339*, 265-278. 10.1016/j.jmb.2004.03.043.

Rymer, R.U., Solorio, F.A., Tehranchi, A.K., Chu, C., Corn, J.E., Keck, J.L., Wang, J.D., and Berger, J.M. (2012). Binding mechanism of metalNTP substrates and stringent-response alarmones to bacterial DnaG-type primases. Structure *20*, 1478-1489. 10.1016/j.str.2012.05.017.

Röhl, R., and Nierhaus, K.H. (1982). Assembly map of the large subunit (50S) of *Escherichia coli* ribosomes. Proc Natl Acad Sci U S A *79*, 729-733. 10.1073/pnas.79.3.729.

Sabat, A.J., Tinelli, M., Grundmann, H., Akkerboom, V., Monaco, M., Del Grosso, M., Errico, G., Pantosti, A., and Friedrich, A.W. (2018). Daptomycin resistant S*taphylococcus aureus* clinical strain with novel non-synonymous mutations in the *mprF* and *vraS* genes: a new insight into daptomycin resistance. Front Microbiol *9*, 2705. 10.3389/fmicb.2018.02705.

Saito, K., Green, R., and Buskirk, A.R. (2020). Ribosome recycling is not critical for translational coupling in *Escherichia coli*. Elife *9*. 10.7554/eLife.59974.

Sajish, M., Tiwari, D., Rananaware, D., Nandicoori, V.K., and Prakash, B. (2007). A charge reversal differentiates (p)ppGpp synthesis by monofunctional and bifunctional Rel proteins. J Biol Chem *282*, 34977-34983. 10.1074/jbc.M704828200.

Sakakibara, Y., and Chow, C.S. (2011). Probing conformational states of modified helix 69 in 50S ribosomes. J Am Chem Soc *133*, 8396-8399. 10.1021/ja2005658.

Sakakibara, Y., and Chow, C.S. (2012). Role of pseudouridine in structural rearrangements of helix 69 during bacterial ribosome assembly. ACS Chem Biol *7*, 871-878. 10.1021/cb200497q.

Salgado-Pabón, W., and Schlievert, P.M. (2014). Models matter: the search for an effective *Staphylococcus aureus* vaccine. Nat Rev Microbiol *12*, 585-591. 10.1038/nrmicro3308.

Sanchez-Vazquez, P., Dewey, C.N., Kitten, N., Ross, W., and Gourse, R.L. (2019). Genome-wide effects on *Escherichia coli* transcription from ppGpp binding to its two sites on RNA polymerase. Proc Natl Acad Sci USA *116*, 8310-8319. 10.1073/pnas.1819682116.

Saravolatz, L.D., Stein, G.E., and Johnson, L.B. (2011). Ceftaroline: a novel cephalosporin with activity against methicillin-resistant *Staphylococcus aureus*. Clin Infect Dis *52*, 1156-1163. 10.1093/cid/cir147.

Schmidt, K.A., Manna, A.C., Gill, S., and Cheung, A.L. (2001). SarT, a repressor of alpha-hemolysin in *Staphylococcus aureus*. Infect Immun *69*, 4749-4758. 10.1128/IAI.69.8.4749-4758.2001.

Schümmer, T., Gromadski, K.B., and Rodnina, M.V. (2007). Mechanism of EF-Ts-catalyzed guanine nucleotide exchange in EF-Tu: contribution of interactions mediated by helix B of EF-Tu. Biochemistry *46*, 4977-4984. 10.1021/bi602486c.

Scrima, A., and Wittinghofer, A. (2006). Dimerisation-dependent GTPase reaction of MnmE: how potassium acts as GTPase-activating element. EMBO J *25*, 2940-2951. 10.1038/sj.emboj.7601171.

Sebastián, M., Estrany, M., Ruiz-González, C., Forn, I., Sala, M.M., Gasol, J.M., and Marrasé, C. (2019). High growth potential of long-term starved deep ocean opportunistic heterotrophic bacteria. Front Microbiol *10*, 760. 10.3389/fmicb.2019.00760.

Seffouh, A., Jain, N., Jahagirdar, D., Basu, K., Razi, A., Ni, X., Guarné, A., Britton, R.A., and Ortega, J. (2019). Structural consequences of the interaction of RbgA with a 50S ribosomal subunit assembly intermediate. Nucleic Acids Res *47*, 10414-10425. 10.1093/nar/gkz770.

Sengupta, S., Mondal, A., Dutta, D., and Parrack, P. (2018). HflX protein protects *Escherichia coli* from manganese stress. J Biosci *43*, 1001-1013.

Seyfzadeh, M., Keener, J., and Nomura, M. (1993). *spoT*-dependent accumulation of guanosine tetraphosphate in response to fatty acid starvation in *Escherichia coli*. Proc Natl Acad Sci U S A *90*, 11004-11008. 10.1073/pnas.90.23.11004.

Shan, Y., Brown Gandt, A., Rowe, S.E., Deisinger, J.P., Conlon, B.P., and Lewis, K. (2017). ATP-dependent persister formation in *Escherichia coli*. mBio *8*. 10.1128/mBio.02267-16.

Shaner, N.C., Campbell, R.E., Steinbach, P.A., Giepmans, B.N., Palmer, A.E., and Tsien, R.Y. (2004). Improved monomeric red, orange and yellow fluorescent proteins derived from *Discosoma* sp. red fluorescent protein. Nat Biotechnol *22*, 1567-1572. 10.1038/nbt1037.

Shariati, A., Dadashi, M., Moghadam, M.T., van Belkum, A., Yaslianifard, S., and Darban-Sarokhalil, D. (2020). Global prevalence and distribution of vancomycin resistant, vancomycin intermediate and heterogeneously vancomycin intermediate *Staphylococcus aureus* clinical isolates: a systematic review and meta-analysis. Sci Rep *10*, 12689. 10.1038/s41598-020-69058-z.

Sharma, I.M., and Woodson, S.A. (2020). RbfA and IF3 couple ribosome biogenesis and translation initiation to increase stress tolerance. Nucleic Acids Res *48*, 359-372. 10.1093/nar/gkz1065.

Sharma, M.R., Barat, C., Wilson, D.N., Booth, T.M., Kawazoe, M., Hori-Takemoto, C., Shirouzu, M., Yokoyama, S., Fucini, P., and Agrawal, R.K. (2005). Interaction of Era with the 30S ribosomal subunit implications for 30S subunit assembly. Mol Cell *18*, 319-329. 10.1016/j.molcel.2005.03.028.

Shaw, L.N., Aish, J., Davenport, J.E., Brown, M.C., Lithgow, J.K., Simmonite, K., Crossley, H., Travis, J., Potempa, J., and Foster, S.J. (2006). Investigations into sigmaB-modulated regulatory pathways governing extracellular virulence determinant production in *Staphylococcus aureus*. J Bacteriol *188*, 6070-6080. 10.1128/JB.00551-06.

Sherlock, M.E., Sudarsan, N., and Breaker, R.R. (2018). Riboswitches for the alarmone ppGpp expand the collection of RNA-based signaling systems. Proc Natl Acad Sci U S A *115*, 6052-6057. 10.1073/pnas.1720406115.

Shields, M.J., Fischer, J.J., and Wieden, H.J. (2009). Toward understanding the function of the universally conserved GTPase HflX from *Escherichia coli*: a kinetic approach. Biochemistry *48*, 10793-10802. 10.1021/bi901074h.

Shimamoto, T., and Inouye, M. (1996). Mutational analysis of Era, an essential GTP-binding protein of *Escherichia coli*. FEMS Microbiol Lett *136*, 57-62. 10.1111/j.1574-6968.1996.tb08025.x.

Shin, D.H., Lou, Y., Jancarik, J., Yokota, H., Kim, R., and Kim, S.H. (2004). Crystal structure of YjeQ from *Thermotoga maritima* contains a circularly permuted GTPase domain. Proc Natl Acad Sci U S A *101*, 13198-13203. 10.1073/pnas.0405202101.

Shine, J., and Dalgarno, L. (1974). The 3'-terminal sequence of Escherichia coli 16S ribosomal RNA: complementarity to nonsense triplets and ribosome binding sites. Proc Natl Acad Sci U S A *71*, 1342-1346. 10.1073/pnas.71.4.1342.

Shore, A.C., and Coleman, D.C. (2013). Staphylococcal cassette chromosome *mec*: recent advances and new insights. Int J Med Microbiol *303*, 350-359. 10.1016/j.ijmm.2013.02.002.

Shu, X., Shaner, N.C., Yarbrough, C.A., Tsien, R.Y., and Remington, S.J. (2006). Novel chromophores and buried charges control color in mFruits. Biochemistry *45*, 9639-9647. 10.1021/bi060773l.

Siderius, M., and Jagodzinski, F. (2018). Mutation Sensitivity Maps: Identifying residue substitutions that impact protein structure via a rigidity analysis *in silico* mutation approach. J Comput Biol *25*, 89-102. 10.1089/cmb.2017.0165.

Singh-Moodley, A., Strasheim, W., Mogokotleng, R., Ismail, H., and Perovic, O. (2019). Unconventional SCC*mec* types and low prevalence of the Panton-Valentine Leukocidin exotoxin in South African blood culture *Staphylococcus aureus* surveillance isolates, 2013-2016. PLoS One *14*, e0225726. 10.1371/journal.pone.0225726.

Sinha, A.K., and Winther, K.S. (2021). The RelA hydrolase domain acts as a molecular switch for (p)ppGpp synthesis. Commun Biol *4*, 434. 10.1038/s42003-021-01963-z.

Sivaramakrishnan, P., Sepúlveda, L.A., Halliday, J.A., Liu, J., Núñez, M.A.B., Golding, I., Rosenberg, S.M., and Herman, C. (2017). The transcription fidelity factor GreA impedes DNA break repair. Nature *550*, 214-218. 10.1038/nature23907.

Smith, W.P., Tai, P.C., and Davis, B.D. (1978). Nascent peptide as sole attachment of polysomes to membranes in bacteria. Proc Natl Acad Sci U S A *75*, 814-817. 10.1073/pnas.75.2.814.

Srisuknimit, V., Qiao, Y., Schaefer, K., Kahne, D., and Walker, S. (2017). Peptidoglycan cross-linking preferences of S*taphylococcus aureus* penicillin-binding proteins have implications for treating MRSA infections. J Am Chem Soc *139*, 9791-9794. 10.1021/jacs.7b04881.

Stapleton, P.D., and Taylor, P.W. (2002). Methicillin resistance in *Staphylococcus aureus*: mechanisms and modulation. Sci Prog *85*, 57-72. 10.3184/003685002783238870.

Stark, H., Mueller, F., Orlova, E.V., Schatz, M., Dube, P., Erdemir, T., Zemlin, F., Brimacombe, R., and van Heel, M. (1995). The 70S *Escherichia coli* ribosome at 23 A resolution: fitting the ribosomal RNA. Structure *3*, 815-821. 10.1016/s0969-2126(01)00216-7.

Steinchen, W., and Bange, G. (2016). The magic dance of the alarmones (p)ppGpp. Mol Microbiol *101*, 531-544. 10.1111/mmi.13412.

Steinchen, W., Schuhmacher, J.S., Altegoer, F., Fage, C.D., Srinivasan, V., Linne, U., Marahiel, M.A., and Bange, G. (2015). Catalytic mechanism and allosteric regulation of an oligomeric (p)ppGpp synthetase by an alarmone. Proc Natl Acad Sci U S A *112*, 13348-13353. 10.1073/pnas.1505271112.

Steinchen, W., Vogt, M.S., Altegoer, F., Giammarinaro, P.I., Horvatek, P., Wolz, C., and Bange, G. (2018). Structural and mechanistic divergence of the small (p)ppGpp synthetases RelP and RelQ. Sci Rep *8*, 2195. 10.1038/s41598-018-20634-4.

Steinchen, W., Zegarra, V., and Bange, G. (2020). (p)ppGpp: magic modulators of bacterial physiology and metabolism. Front Microbiol *11*, 2072. 10.3389/fmicb.2020.02072.

Strauß, L., Stegger, M., Akpaka, P.E., Alabi, A., Breurec, S., Coombs, G., Egyir, B., Larsen, A.R., Laurent, F., Monecke, S., *et al.* (2017). Origin, evolution, and global transmission of community-acquired *Staphylococcus aureus* ST-8. Proc Natl Acad Sci U S A *114*, E10596-E10604. 10.1073/pnas.1702472114.

Strunk, B.S., and Karbstein, K. (2009). Powering through ribosome assembly. RNA *15*, 2083-2104. 10.1261/rna.1792109.

Su, W.W. (2005). Fluorescent proteins as tools to aid protein production. Microb Cell Fact *4*, 12. 10.1186/1475-2859-4-12.

Sudhamsu, J., Lee, G.I., Klessig, D.F., and Crane, B.R. (2008). The structure of YqeH. An AtNOS1/AtNOA1 ortholog that couples GTP hydrolysis to molecular recognition. J Biol Chem *283*, 32968-32976. 10.1074/jbc.M804837200.

Sukhithasri, V., Nisha, N., Biswas, L., Anil Kumar, V., and Biswas, R. (2013). Innate immune recognition of microbial cell wall components and microbial strategies to evade such recognitions. Microbiol Res *168*, 396-406. 10.1016/j.micres.2013.02.005.

Sun, D., Lee, G., Lee, J.H., Kim, H.Y., Rhee, H.W., Park, S.Y., Kim, K.J., Kim, Y., Kim, B.Y., Hong, J.I., *et al*. (2010). A metazoan ortholog of SpoT hydrolyzes ppGpp and functions in starvation responses. Nat Struct Mol Biol *17*, 1188-1194. 10.1038/nsmb.1906.

Syal, K., Flentie, K., Bhardwaj, N., Maiti, K., Jayaraman, N., Stallings, C.L., and Chatterji, D. (2017). Synthetic (p)ppGpp analogue is an inhibitor of stringent response in mycobacteria. Antimicrob Agents Chemother *61*. 10.1128/AAC.00443-17.

Talkington, M.W., Siuzdak, G., and Williamson, J.R. (2005). An assembly landscape for the 30S ribosomal subunit. Nature *438*, 628-632. 10.1038/nature04261.

Tamaru, D., Amikura, K., Shimizu, Y., Nierhaus, K.H., and Ueda, T. (2018). Reconstitution of 30S ribosomal subunits *in vitro* using ribosome biogenesis factors. RNA *24*, 1512-1519. 10.1261/rna.065615.118.

Tamman, H., Van Nerom, K., Takada, H., Vandenberk, N., Scholl, D., Polikanov, Y., Hofkens, J., Talavera, A., Hauryliuk, V., Hendrix, J., and Garcia-Pino, A. (2020). A nucleotide-switch mechanism mediates opposing catalytic activities of Rel enzymes. Nat Chem Biol *16*, 834-840. 10.1038/s41589-020-0520-2.

Tao, L., Wu, X., and Sun, B. (2010). Alternative sigma factor sigmaH modulates prophage integration and excision in *Staphylococcus aureus*. PLoS Pathog *6*, e1000888. 10.1371/journal.ppat.1000888.

Thackray, P.D., and Moir, A. (2003). SigM, an extracytoplasmic function sigma factor of *Bacillus subtilis*, is activated in response to cell wall antibiotics, ethanol, heat, acid, and superoxide stress. J Bacteriol *185*, 3491-3498. 10.1128/JB.185.12.3491-3498.2003.

Thurlow, B., Davis, J.H., Leong, V., Moraes, T.F., Williamson, J.R., and Ortega, J. (2016). Binding properties of YjeQ (RsgA), RbfA, RimM and Era to assembly intermediates of the 30S subunit. Nucleic Acids Research *44*, 9918--9932. 10.1093/nar/gkw613.

Tiwari, S., Jamal, S.B., Hassan, S.S., Carvalho, P.V.S.D., Almeida, S., Barh, D., Ghosh, P., Silva, A., Castro, T.L.P., and Azevedo, V. (2017). Two-component signal transduction systems of pathogenic bacteria as targets for antimicrobial therapy: an overview. Front Microbiol *8*, 1878. 10.3389/fmicb.2017.01878.

Toma-Fukai, S., and Shimizu, T. (2019). Structural insights into the regulation mechanism of small GTPases by GEFs. Molecules *24*. 10.3390/molecules24183308.

Tomczak, H., Wróbel, J., Jenerowicz, D., Sadowska-Przytocka, A., Wachal, M., Adamski, Z., and Czarnecka-Operacz, M.M. (2019). The role of *Staphylococcus aureus* in atopic dermatitis: microbiological and immunological implications. Postepy Dermatol Alergol *36*, 485-491. 10.5114/ada.2018.77056.

Tomsic, J., Vitali, L.A., Daviter, T., Savelsbergh, A., Spurio, R., Striebeck, P., Wintermeyer, W., Rodnina, M.V., and Gualerzi, C.O. (2000). Late events of translation initiation in bacteria: a kinetic analysis. EMBO J *19*, 2127-2136. 10.1093/emboj/19.9.2127.

Tong, S.Y., Davis, J.S., Eichenberger, E., Holland, T.L., and Fowler, V.G. (2015). *Staphylococcus aureus* infections: epidemiology, pathophysiology, clinical manifestations, and management. Clin Microbiol Rev *28*, 603-661. 10.1128/CMR.00134-14.

Traut, T.W. (1994). Physiological concentrations of purines and pyrimidines. Mol Cell Biochem *140*, 1-22. 10.1007/bf00928361.

Tsui, H.C., Feng, G., and Winkler, M.E. (1996). Transcription of the mutL repair, miaA tRNA modification, hfq pleiotropic regulator, and hflA region protease genes of *Escherichia coli* K-12 from clustered Esigma32-specific promoters during heat shock. J Bacteriol *178*, 5719-5731. 10.1128/jb.178.19.5719-5731.1996.

Tu, C., Zhou, X., Tarasov, S.G., Tropea, J.E., Austin, B.P., Waugh, D.S., Court, D.L., and Ji, X. (2011). The Era GTPase recognizes the GAUCACCUCC sequence and binds helix 45 near the 3' end of 16S rRNA. Proc Natl Acad Sci U S A *108*, 10156-10161. 10.1073/pnas.1017679108.

Tu, C., Zhou, X., Tropea, J.E., Austin, B.P., Waugh, D.S., Court, D.L., and Ji, X. (2009). Structure of ERA in complex with the 3' end of 16S rRNA: implications for ribosome biogenesis. Proc Natl Acad Sci U S A *106*, 14843-14848. 10.1073/pnas.0904032106.

Tuchscherr, L., Bischoff, M., Lattar, S.M., Noto Llana, M., Pförtner, H., Niemann, S., Geraci, J., Van de Vyver, H., Fraunholz, M.J., Cheung, A.L., *et al*. (2015). Sigma factor sigb is crucial to mediate *Staphylococcus aureus* adaptation during chronic infections. PLoS Pathog *11*, e1004870. 10.1371/journal.ppat.1004870.

Uebele, J., Habenicht, K., Ticha, O., and Bekeredjian-Ding, I. (2020). Protein A induces human regulatory T cells through interaction with antigen-presenting cells. Front Immunol *11*, 581713. 10.3389/fimmu.2020.581713.

Ueta, M., Wada, C., Daifuku, T., Sako, Y., Bessho, Y., Kitamura, A., Ohniwa, R.L., Morikawa, K., Yoshida, H., Kato, T., *et al*. (2013). Conservation of two distinct types of 100S ribosome in bacteria. Genes Cells *18*, 554-574. 10.1111/gtc.12057.

Uicker, W.C., Schaefer, L., and Britton, R.A. (2006). The essential GTPase RbgA (YlqF) is required for 50S ribosome assembly in *Bacillus subtilis*. Mol Microbiol *59*, 528-540. 10.1111/j.1365-2958.2005.04948.x.

Vaara, M. (1993). Outer membrane permeability barrier to azithromycin, clarithromycin, and roxithromycin in Gram-negative enteric bacteria. Antimicrob Agents Chemother *37*, 354-356. 10.1128/aac.37.2.354.

van der Aart, L.T., Lemmens, N., van Wamel, W.J., and van Wezel, G.P. (2016). Substrate inhibition of VanA by d-alanine reduces vancomycin resistance in a VanX-dependent manner. Antimicrob Agents Chemother *60*, 4930-4939. 10.1128/AAC.00276-16.

van Veen, H.W. (2010). Structural biology: Last of the multidrug transporters. Nature *467*, 926-927. 10.1038/467926a.

Varik, V., Oliveira, S.R.A., Hauryliuk, V., and Tenson, T. (2017). HPLC-based quantification of bacterial housekeeping nucleotides and alarmone messengers ppGpp and pppGpp. Sci Rep *7*, 11022. 10.1038/s41598-017-10988-6.

V**ercruysse, M.**, Köhrer, C., Shen, Y., Proulx, S., Ghosal, A., Davies, B.W., RajBhandary, U.L., and Walker, G.C. (2016). Identification of YbeY-protein interactions involved in 16S rRNA maturation and stress regulation in *Escherichia coli*. mBio *7*, e01785-01716. 10.1128/mBio.01785-16.

Verma, P., Gandhi, S., Lata, K., and Chattopadhyay, K. (2021). Pore-forming toxins in infection and immunity. Biochem Soc Trans *49*, 455-465. 10.1042/BST20200836.

Verstraeten, N., Fauvart, M., Versees, W., and Michiels, J. (2011). The Universally Conserved Prokaryotic GTPases. Microbiology and Molecular Biology Reviews *75*, 507-542. 10.1128/mmbr.00009-11.

Vetter, I.R., Nowak, C., Nishimoto, T., Kuhlmann, J., and Wittinghofer, A. (1999). Structure of a Ran-binding domain complexed with Ran bound to a GTP analogue: implications for nuclear transport. Nature *398*, 39-46. 10.1038/17969.

Vieille, C., and Zeikus, G.J. (2001). Hyperthermophilic enzymes: sources, uses, and molecular mechanisms for thermostability. Microbiol Mol Biol Rev *65*, 1-43. 10.1128/MMBR.65.1.1-43.2001.

Vinogradova, D.S., Zegarra, V., Maksimova, E., Nakamoto, J.A., Kasatsky, P., Paleskava, A., Konevega, A.L., and Milon, P. (2020). How the initiating ribosome copes with ppGpp to translate mRNAs. PLoS Biol *18*, e3000593. 10.1371/journal.pbio.3000593.

Vogt, S.L., Green, C., Stevens, K.M., Day, B., Erickson, D.L., Woods, D.E., and Storey, D.G. (2011). The stringent response is essential for *Pseudomonas aeruginosa* virulence in the rat lung agar bead and *Drosophila melanogaster* feeding models of infection. Infect Immun *79*, 4094-4104. 10.1128/IAI.00193-11.

Voráčková, I., Suchanová, S., Ulbrich, P., Diehl, W.E., and Ruml, T. (2011). Purification of proteins containing zinc finger domains using immobilized metal ion affinity chromatography. Protein Expr Purif *79*, 88-95. 10.1016/j.pep.2011.04.022.

Voyich, J.M., Braughton, K.R., Sturdevant, D.E., Whitney, A.R., Saïd-Salim, B., Porcella, S.F., Long, R.D., Dorward, D.W., Gardner, D.J., Kreiswirth, B.N., *et al*. (2005). Insights into mechanisms used by *Staphylococcus aureus* to avoid destruction by human neutrophils. J Immunol *175*, 3907-3919. 10.4049/jimmunol.175.6.3907.

Wallace, A.C., Laskowski, R.A., and Thornton, J.M. (1995). LIGPLOT: a program to generate schematic diagrams of protein-ligand interactions. Protein Eng *8*, 127-134. 10.1093/protein/8.2.127.

Wang, B., Dai, P., Ding, D., Del Rosario, A., Grant, R.A., Pentelute, B.L., and Laub, M.T. (2018). Affinity-based capture and identification of protein effectors of the growth regulator ppGpp. Nat Chem Biol *15*, 141-150. 10.1038/s41589-018-0183-4.

Watkins, D., and Arya, D. (2019). Regulatory roles of small RNAs in prokaryotes: parallels and contrast with eukaryotic miRNA. Non-coding RNA Investig *3*. 10.21037/ncri.2019.10.02.

Wexselblatt, E., Kaspy, I., Glaser, G., Katzhendler, J., and Yavin, E. (2013). Design, synthesis and structure-activity relationship of novel Relacin analogs as inhibitors of Rel proteins. Eur J Med Chem *70*, 497-504. 10.1016/j.ejmech.2013.10.036.

Wexselblatt, E., Oppenheimer-Shaanan, Y., Kaspy, I., London, N., Schueler-Furman, O., Yavin, E., Glaser, G., Katzhendler, J., and Ben-Yehuda, S. (2012). Relacin, a novel antibacterial agent targeting the Stringent Response. PLoS Pathog *8*, e1002925. 10.1371/journal.ppat.1002925.

Williams, C.J., Headd, J.J., Moriarty, N.W., Prisant, M.G., Videau, L.L., Deis, L.N., Verma, V., Keedy, D.A., Hintze, B.J., Chen, V.B., *et al*. (2018). MolProbity: More and better reference data for improved all-atom structure validation. Protein Sci *27*, 293-315. 10.1002/pro.3330.

Wilson, D.N. (2014). Ribosome-targeting antibiotics and mechanisms of bacterial resistance. Nat Rev Microbiol *12*, 35-48. 10.1038/nrmicro3155.

Wilson, D.N., Hauryliuk, V., Atkinson, G.C., and O'Neill, A.J. (2020). Target protection as a key antibiotic resistance mechanism. Nat Rev Microbiol *18*, 637-648. 10.1038/s41579-020-0386-z.

Winn, M.D., Ballard, C.C., Cowtan, K.D., Dodson, E.J., Emsley, P., Evans, P.R., Keegan, R.M., Krissinel, E.B., Leslie, A.G., McCoy, A., *et al*. (2011). Overview of the CCP4 suite and current developments. Acta Crystallogr D Biol Crystallogr *67*, 235-242. 10.1107/S0907444910045749.

Winter, G. (2010). xia2: an expert system for macromolecular crystallography data reduction. J App Crystall *43*, 186-190. doi:10.1107/S0021889809045701.

Winther, J.R., and Thorpe, C. (2014). Quantification of thiols and disulfides. Biochim Biophys Acta *1840*, 838-846. 10.1016/j.bbagen.2013.03.031.

Winther, K.S., Roghanian, M., and Gerdes, K. (2018). Activation of the stringent response by loading of RelA-tRNA complexes at the ribosomal A-Site. Mol Cell *70*, 95-105.e104. 10.1016/j.molcel.2018.02.033.

Wolz, C., Geiger, T., and Goerke, C. (2010). The synthesis and function of the alarmone (p)ppGpp in Firmicutes. International Journal of Medical Microbiology *300*, 142--147. 10.1016/j.ijmm.2009.08.017.

Wood, A., Irving, S.E., Bennison, D.J., and Corrigan, R.M. (2019). The (p)ppGpp-binding GTPase Era promotes rRNA processing and cold adaptation in *Staphylococcus aureus*. PLoS Genetics *15*, e1008346. 10.1371/journal.pgen.1008346.

Wu, H., Sun, L., Blombach, F., Brouns, S.J., Snijders, A.P., Lorenzen, K., van den Heuvel, R.H., Heck, A.J., Fu, S., Li, X., *et al*. (2010). Structure of the ribosome associating GTPase HflX. Proteins *78*, 705-713. 10.1002/prot.22599.

Wuichet, K., and Søgaard-Andersen, L. (2014). Evolution and diversity of the Ras superfamily of small GTPases in prokaryotes. Genome Biol Evol *7*, 57-70. 10.1093/gbe/evu264.

Xu, S.X., and McCormick, J.K. (2012). Staphylococcal superantigens in colonization and disease. Front Cell Infect Microbiol *2*, 52. 10.3389/fcimb.2012.00052.

Yang, J., Anderson, B.W., Turdiev, A., Turdiev, H., Stevenson, D.M., Amador-Noguez, D., Lee, V.T., and Wang, J.D. (2020). The nucleotide pGpp acts as a third alarmone in *Bacillus*, with functions distinct from those of (p) ppGpp. Nat Commun *11*, 5388. 10.1038/s41467-020-19166-1.

Yang, N., Xie, S., Tang, N.Y., Choi, M.Y., Wang, Y., and Watt, R.M. (2019). The Ps and Qs of alarmone synthesis in *Staphylococcus aureus*. PLoS One *14*, e0213630. 10.1371/journal.pone.0213630.

Yang, X., and Ishiguro, E.E. (2001). Dimerization of the RelA protein of *Escherichia coli*. Biochem Cell Biol *79*, 729-736. 10.1139/o01-144.

Yanling, C., Hongyan, L., Xi, W., Wim, C., and Dongmei, D. (2018). Efficacy of relacin combined with sodium hypochlorite against *Enterococcus faecalis* biofilms. J Appl Oral Sci *26*, e20160608. 10.1590/1678-7757-2016-0608.

Ying, H., Shen, Z., Wang, J., and Zhou, B. (2021). Role of iron homeostasis in the heart: heart failure, cardiomyopathy, and ischemia-reperfusion injury. Herz. 10.1007/s00059-021-05039-w.

Zhang, K., McClure, J.A., Elsayed, S., and Conly, J.M. (2009a). Novel staphylococcal cassette chromosome *mec* type, tentatively designated type VIII, harboring class A *mec* and type 4 *ccr* gene complexes in a Canadian epidemic strain of methicillin-resistant *Staphylococcus aureus*. Antimicrob Agents Chemother *53*, 531-540. 10.1128/AAC.01118-08.

Zhang, W., Dunkle, J.A., and Cate, J.H. (2009b). Structures of the ribosome in intermediate states of ratcheting. Science *325*, 1014-1017. 10.1126/science.1175275.

Zhang, Y., Mandava, C.S., Cao, W., Li, X., Zhang, D., Li, N., Zhang, X., Qin, Y., Mi, K., Lei, J., *et al*. (2015). HflX is a ribosome-splitting factor rescuing stalled ribosomes under stress conditions. Nat Struct Mol Biol *22*, 906-913. 10.1038/nsmb.3103.

Zhang, Y., Zborníková, E., Rejman, D., and Gerdes, K. (2018). Novel (p)ppGpp binding and metabolizing proteins of *Escherichia coli*. mBio *9*. 10.1128/mBio.02188-17.

Zhao, T., Chen, Y.M., Li, Y., Wang, J., Chen, S., Gao, N., and Qian, W. (2021). Disome-seq reveals widespread ribosome collisions that promote cotranslational protein folding. Genome Biol *22*, 16. 10.1186/s13059-020-02256-0.

Zschiedrich, C.P., Keidel, V., and Szurmant, H. (2016). Molecular mechanisms of two-component signal transduction. J Mol Biol *428*, 3752-3775. 10.1016/j.jmb.2016.08.003.